IITRI

304

N71-34365

MAGNETIC HEAD/TAPE INTERFACE STUDY FOR SATELLITE TAPE RECORDERS

Technical Report
Volume II

IITRI Project No. E6134
Contract No. NAS5-11622

Goddard Space Flight Center
Greenbelt, Maryland

IIT RESEARCH INSTITUTE

MAGNETIC HEAD/TAPE INTERFACE STUDY FOR SATELLITE TAPE RECORDERS

Technical Report

Volume II
Test Program and Results

IITRI Project No. E6134
Contract No. NAS5-11622

Prepared by

Robert J. Owen

Submitted by

IIT RESEARCH INSTITUTE
10 West 35th Street
Chicago, Illinois 60616

to

National Aeronautics and Space Administration
Goddard Space Flight Center
Greenbelt, Maryland

February 1971

IIT RESEARCH INSTITUTE

NOTICE

THIS REPORT CONTAINS THE RESULTS OF TESTS DESIGNED TO ISOLATE THE EFFECTS OF HEAD, TAPE, AND OPERATIONAL PARAMETERS ON THE PERFORMANCE OF SATELLITE TAPE RECORDERS. BECAUSE OF CERTAIN UNIQUE REQUIREMENTS FOR SATELLITE RECORDERS, THE RESULTS ARE NOT DIRECTLY APPLICABLE TO CONVENTIONAL, GROUND BASED, COMMERCIAL OR HOME RECORDING SYSTEMS. THE INTENT OF THE PROGRAM WAS TO DEVELOP SOUND ENGINEERING TECHNIQUES FOR SELECTING AND USING TAPE IN SATELLITE APPLICATIONS IRRESPECTIVE OF MANUFACTURER, BRAND NAME, CATALOG NUMBER, OR THE APPLICATION FOR WHICH THE TAPES WERE DESIGNED. THE TEST RESULTS REPORTED SHALL BE CONSIDERED VALID FOR THE INDIVIDUAL REELS OF TAPE EVALUATED. NO PORTION OF THE TEXT OR DATA SHOULD BE INTERPRETED AS AN ENDORSEMENT OR CRITICISM BY IITRI OR NASA OF ANY COMMERCIAL PRODUCT OR MANUFACTURING ORGANIZATION.

FOREWORD

This is a Technical Report on IIT Research Institute Project No. E6134, entitled "Magnetic Head/Tape Interface Study for Satellite Tape Recorders." This study and research effort are being performed for the National Aeronautics and Space Administration, Goddard Space Flight Center, under Contract No. NAS5-11622. The work, performed during the period from 1 December 1968 through 31 December 1970, was monitored by Mr. Carl Powell of GSFC.

The assistance and candor of those organizations visited during the Phase I survey was extremely helpful and most appreciated. We also gratefully acknowledge the work of Mr. Karl Plitt of the National Bureau of Standards, Washington, D.C., who performed the tape surface hardness measurements.

Personnel who made major contributions to this project include K. Gutfreund, Senior Chemist; Dr. R.L. Eshleman, Senior Research Engineer-Mechanical Systems; Dr. E.E. Hahn, Senior Research Engineer-Mechanical Systems; T.M. Scopelite, Manager-Mechanical Systems; G.S.L. Benn, Research Engineer-Electronics; and J.R. Pokorny, formerly Technical Assistant-Electronics. Valuable assistance was provided by I.J. Lesevicius-Chemistry; E. Swider-Mechanical Systems; W.J. Swistek-Model Maker; and I. Corvin, Research Metallurgist. Special acknowledgment is due to M.E. Anderson, Assistant Director of Research-Electronics; G.T. Jacobi, Assistant Director of Research-Electronics; H.G. Tobin, Manager-Instrumentation and Recording; and Dr. M. Camras, Senior Scientific Advisor; for their participation and consultation.

Respectfully submitted,

IIT RESEARCH INSTITUTE

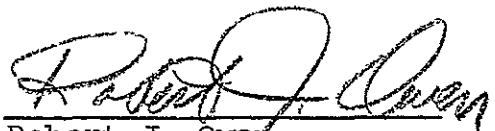

Robert J. Owen
Research Engineer

Approved:

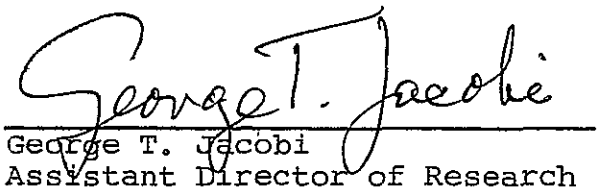

George T. Jacobi
Assistant Director of Research
Electronics Division

TABLE OF CONTENTS

TABLE OF CONTENTS (cont.)

TABLE OF CONTENTS (cont.)

TABLE OF CONTENTS (cont.)

LIST OF ILLUSTRATIONS

LIST OF ILLUSTRATIONS (cont.)

LIST OF ILLUSTRATIONS (cont.)

LIST OF ILLUSTRATIONS (cont.)

LIST OF ILLUSTRATIONS (cont.)

LIST OF ILLUSTRATIONS (cont.)

LIST OF TABLES

LIST OF TABLES (cont.)

TEST PROGRAM AND RESULTS

SECTION I

INTRODUCTION

Magnetic tape recorders have been used in many earth orbiting satellites as the primary means of data storage. The choice of recorders for these applications was correctly based upon the large data storage capacity obtainable in a small volume. However, a number of failures have occurred at the critical head-to-tape interface rendering these systems inoperative. These problems have been related to the deterioration of the magnetic tape on the recorders, and the generation of excessive head-to-tape friction. Although these problems are not unique to satellite systems, the inability to change tape or clean heads has focused attention on failures that have occurred. Therefore, this program was undertaken to obtain an understanding of the chemical and physical forces existing at the interface between the heads and the magnetic tape. Its goal was to derive a magnetic tape and head combination which will function without impairment for a period of one year in satellite tape recorders.

A two-phase program was carried out. Phase I was a survey of appropriate manufacturers and users in the satellite recording industry. The purpose of the survey was to isolate and identify the underlying causes of tape failures due to the dynamics of the chemical and physical forces acting on the tape in satellite recorders. Included in the survey was a determination of the extent to which problems have occurred, the nature of the failures, and what, if any, corrective actions have been taken.

As a result of the survey, a study plan was prepared to investigate experimentally and analytically the problem areas identified during Phase I. The object of the study was to isolate a number of factors attendant to the head/tape interaction, and

to establish correlations between these parameters and the failure modes identified. Included was a classification of tapes and heads and testing under a variety of operating conditions with variations in speed, temperature, and atmosphere.

This volume of the technical report contains a description of the various tests conducted to correlate the operating parameters to the failure mechanisms. It also includes the conclusions drawn from the test program. The results of this test program have been used in the preparation of the guidelines of head and tape selection, given in Volume I of this technical report. Detailed descriptions of the test methods and procedures employed during the test program are contained in Volume III.

SECTION II

PHASE I SURVEY

The first phase of this program was a survey of the appropriate manufacturers and users in the satellite recorder industry. The purpose of this survey was to determine the extent to which problems have occurred, the nature of the failure, and what, if any, corrective actions have been taken. In general, it was found that, although difficulties associated with the head/tape interface were very widespread, little had been accomplished in actually describing the failure mechanisms or resolving the problems.

The majority of the problems reported during the survey could be grouped into three general categories. These include (1) the difficulty in obtaining uniform tape motion, resulting in a stick-slip phenomenon or, in the catastrophic case, actual adhesion of the tape to the head; (2) the generation of frictional wear products and subsequent tape-to-head separation; and (3) a lack of consistency between components or repeatability between tests.

The survey also disclosed a lack of a systematic initial design approach prevalent throughout the industry, and this had resulted in excessive qualification difficulties. The consequence was increased costs and time delays on a number of programs. When compounded with the operational degradation or failures that occurred in orbit, it became evident that a clearer understanding of the head and tape relationship was necessary to obtain the reliability required for long duration satellite recording systems.

Interviews were conducted with a broad range of organizations involved in fields relating to satellite recording. A list of these appears in Appendix I. These included tape, head, and transport manufacturers, prime contractors, and other users, and

suppliers of tape coating equipment and iron oxide. Because the companies visited were assured that the information discussed would be considered proprietary, the details of the interviews will not be presented in this report. In general, it was found that the problems of excessive tape debris, head varnish, layer-to-layer adhesion, reel-to-reel inconsistency in tape, and head-to-tape stiction or adhesion were very widespread and generally not resolved.

At the conclusion of the Phase I survey, which lasted three months, the information obtained was organized by failure characteristic. From this, a test plan evolved describing seven basic problem areas being commonly experienced. A program of analysis and experimentation designed to establish relationships between the problem areas and the applicable head and tape parameters was formulated. The Phase II Test Plan, described in the following section, was submitted to NASA and approved. That Plan became the organizational foundation for the remainder of the program.

SECTION III

PHASE II TEST PROGRAM

The plan of the Phase II Test Program was to conduct a systematic analytical and experimental study to derive correlations between various operating parameters and failures at the head/tape interface. Such relationships would be used to establish design and selection procedures for heads and tapes, as well as constraints on transport operating conditions and environment. Specifically the program had eight objectives. These were:

1. Description of the failure mechanisms occurring
2. Guidelines for tape selection
3. Guidelines for head material selection
4. Recommendations on head/tape interface conditions
5. Environmental constraints
6. Tape transport constraints
7. Procedures for tape evaluation
8. Procedures for tape preconditioning

The organization of the test plan was based upon the classification of the seven distinct problem areas identified during Phase I. By orienting the program toward the investigation of each of the observed effects, it was anticipated that the factors perpetrating these failures could be independently isolated through exhaustive experimental testing augmented by predictive and descriptive analysis of the physical and chemical mechanisms taking place. The seven areas investigated were:

1. Head-to-Tape Adhesion
2. Oxide Binder Debris
3. Substrate Debris
4. Head Varnish

5. Tape Pack Damage
6. Improper Mechanical Tape Handling
7. Detrimental Head/Tape Dynamics

The general format of the study plan for each of these problem areas is shown in Fig. 1. For each investigation, the initial step was to establish a set of conditions within which the actual failure would occur. Having once achieved the desired degradation in operational performance, a concerted effort was placed upon determining the mechanism occurring. This effort was concentrated upon chemical, microscopic, and mathematical analysis of the potential interactions, with emphasis placed upon the physical identification of by-products, parameter changes, and modeling of the expected operational characteristics.

Two basic approaches were then employed in studying the seven areas. Detrimental Tape-to-Head Dynamics, Improper Mechanical Tape Handling, and Tape Pack Damage were viewed mathematically. However, the Tape-to-Head Adhesion, Oxide/Binder Debris, Substrate Debris, and Head Varnish investigations largely consisted of experimental testing supported by chemical-microscopic analysis. The majority of emphasis during the testing program was directed toward the Adhesion and Oxide/Binder Debris characteristics.

Analysis of each of the failure modes dictated a series of failure tests to isolate the significant parameters contributing to the particular problem area under examination. These tests were organized by establishing a series of hypotheses regarding each of the failure areas. A systematic series of tests was then conducted to isolate the effects of each factor hypothesized. Following determination of the significant parameters, a set of testing and conditioning procedures, or guidelines, were established for use in selecting tape, heads, and operational conditions.

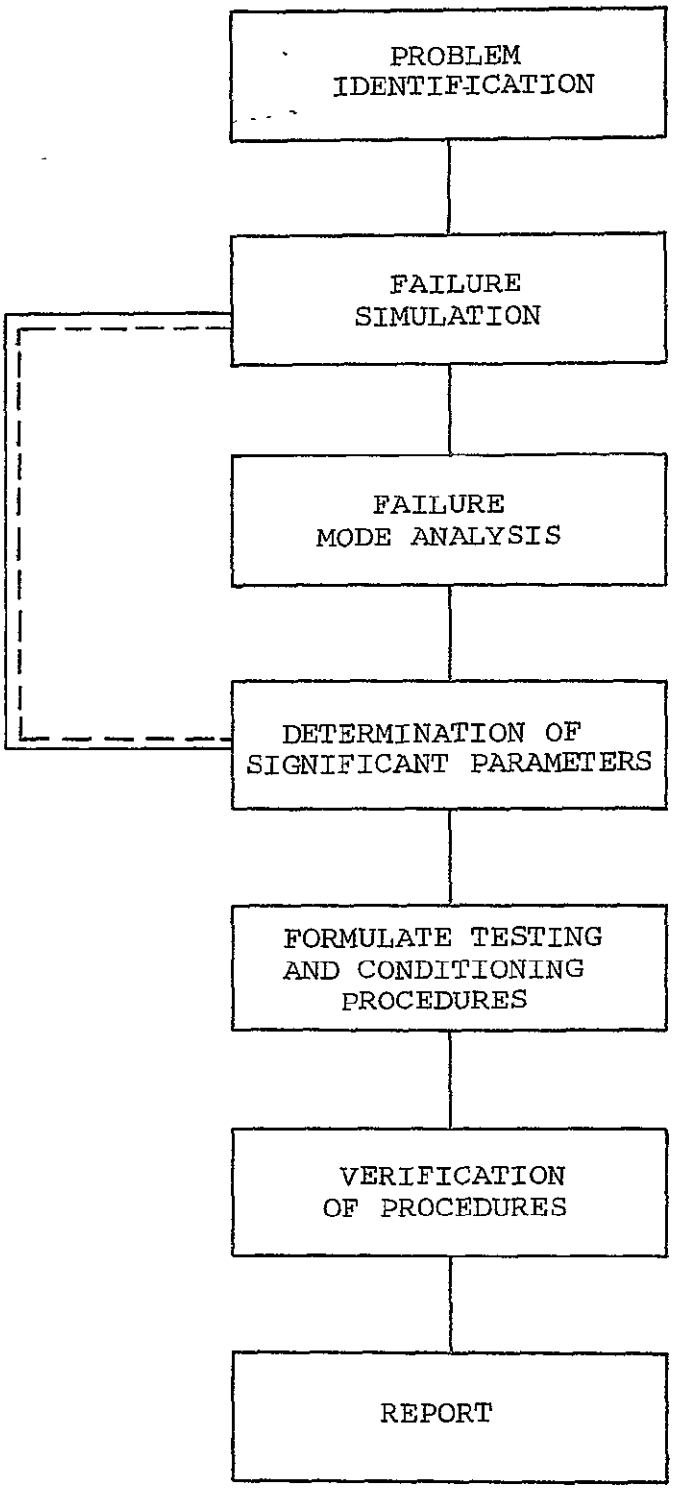

Fig. 1 GENERAL FORMAT, STUDY PROGRAM

Very early in the program, it was recognized that a large number of parameters were potentially applicable. Because the number of combinations of these factors could have become unwieldy, certain general performance limitations were established. These were:

Temperature	20°C to 65°C
Relative Humidity	0 to 45%
Atmosphere	Air and Nitrogen
Tape Speed	0.1 ips to 60 ips, bidirectional
Tape Tension	Nominal 1 to 12 ounces for 1/2-inch tape
Wrap Angle	2° to 15° per side of head
Operating Life	10,000 Passes

The number of tape types evaluated was selected so as to allow types with a variety of physical and electromagnetic characteristics to be tested. At the same time, it was necessary to limit the number to insure that sufficient tests would be carried out and analyzed within the time limitations of the program. In addition, the tapes were selected so as to be representative of those commonly used on both ground-based and satellite recorders. Table I gives the listing of the primary types used and the reason for their selection. Although these nine tape types were tested extensively throughout the program, the intent was to isolate specific parameters inherent in the binder systems rather than brand. Therefore, the conclusions of the program were based upon the binder constituents found to be significant, independent of brand designation. To verify these conclusions, several other tape types from other manufacturers were tested near the end of the program. Appendix VII includes a list of all tape types examined during the program.

Table I

List of Tape Types Evaluated

Manufacturer	Type	Reason for Selection
3M	351	Video tape designed for high head-to-tape speed
3M	777	Thicker substrate and oxide coating
3M	871	Reportedly made for low speed operation
3M	888	Commonly used instrumentation tape
Memorex	63L	Commonly used instrumentation tape
Memorex	79L	Video tape designed for high head-to-tape speed
Memorex	Quantum	Thicker substrate and oxide coating
RCA	617*	Previous use in satellite applications
DuPont	Crolyn	Unique oxide and binder system

*RCA 617 is a tape formulated for a particular satellite recording application and is not commercially available.

A basic objective of this program was to extend the operational lifetime of a satellite tape recorder to one year. Considering that a year consists of nearly 9,000 hours, this design goal was translated into 10,000 passes of tape over the head. In order to accumulate this number of passes throughout a large number of tests, it was necessary to reduce the lengths of tape being tested. Therefore, a number of endless loop tape transports were designed and fabricated. These transports are shown in Fig. 2, and described more fully in Appendix II. Since they accommodated tape lengths up to 64 inches, a large number of passes could be accumulated rapidly.

The tests on the endless loop transports were complemented by additional studies on a reel-to-reel transport using longer lengths of tape. The transports are shown in Fig. 3 and also described in Appendix II. While the endless loop transports facilitated the investigation of tape related problems, the reel-to-reel machines allowed the analysis of head and debris related problems. In addition, the reel-to-reel transports were used to confirm trends initially observed using shorter lengths of tape. Additionally, correlation between the results of accelerated testing on the loop transports and those found on the reel-to-reel transport gave confidence that the tests on the loop machines could be used to determine guidelines for satellite operation.

A commercial tape splicer was used to weld the ends of the tape together under conditions of high temperature and pressure. This gave a continuous loop with no mechanical discontinuities, insuring that the weld itself did not influence the test results.

The two types of special test equipment described above were employed extensively in the experimental testing portion of the program. This work, directed primarily at head-to-tape adhesion and oxide/binder debris, is described in the following two sections of the report. This volume also includes the details of the analytical studies performed in the areas of mechanical tape

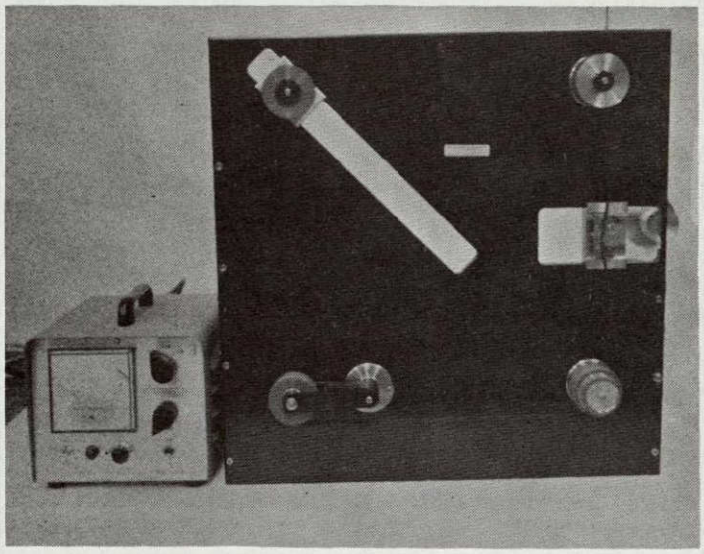

Fig. 2 ENDLESS LOOP TRANSPORT AND MOTOR SERVO ELECTRONICS

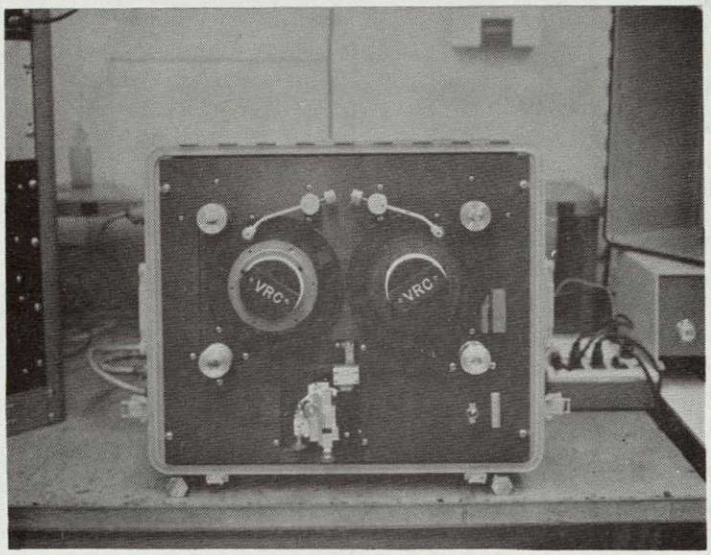

a. Transport

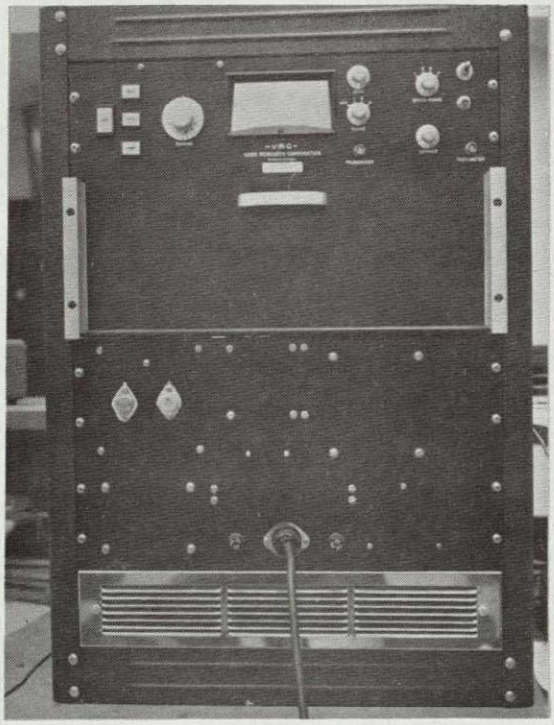

b. Electronic Control Unit

Fig. 3 REEL-TO-REEL TAPE TRANSPORT

handling, tape pack design, and head-to-tape dynamics. Finally, a section is included describing the development of guideline tests given in Volume I. This section also includes the results of tests run to verify the selection procedures imposed in the guidelines.

A. Head/Tape Adhesion

The basic functions common to nearly all tape recorder transports are generation of uniform head-to-tape velocity and intimate head-to-tape contact. The inevitable result of these two factors is frictional drag. Drag has not traditionally been considered a serious limitation in most instrumentation recorder designs, where the principal consideration has been minimizing head-to-tape separation losses. Increases in drag have often only implied greater power consumption. In fact, increased drag has been occasionally welcomed on digital tape decks where rapid stop times were required.

However, transports designed to be employed in satellite or deep space applications have been required to meet limited power consumption specifications. This has led to marginal capstan motor torque capabilities, and resultant concern over the amount of frictional drag developed. Further, increases in drag were observed following repeated usage of the same reel of tape. These increases were occasionally sufficient to overcome the maximum available torque of the transport creating a catastrophic failure. Thus the second unique requirement of a satellite recorder, unattended operation which excluded changing tape or heads, also contributed to the motivation for achieving an understanding and control of the parameters ultimately affecting friction.

1. Analysis of Adhesion Failure Mechanisms

The initial emphasis of the testing program was to simulate adhesion failures. This was done to assess the underlying causes as well as to establish potentially significant head, tape, and environmental parameters. To promote such failures, the endless loop transport was used in an environmental chamber at high temperature. Other parameters such as tape tension and wrap angle were also deliberately set higher than would normally be encountered to accelerate failures.

During the preliminary period of testing, complete calibration procedures and tentative operational methods were established. These include calibration of both the tape speed and the motor starting and running torques. Also, during many of the preliminary tests conducted to establish procedures and and calibration, the tape was only run in one direction. However, a typical satellite application involved recording in one direction at low speed and playing back in reverse at high speed. Therefore, it was decided to modify the procedures by including two tape speeds, 1 ips and 30 ips, and operation in both directions. These changes led directly to several occurrences of head-to-tape adhesion.

The first of several instances of adhesion failures could be determined by the presence of oxide and binder physically transferred to the head surface. The most severe case of tape sticking to the head (and possibly the only true adhesion), occurred while running the DuPont Crolyn tape at 65°C in an atmosphere containing 45% relative humidity.

After approximately 3,700 passes, the capstan torque was no longer capable of pulling the tape over the brass dummy head used. Applying 64 ounces of force in the direction of tape motion was not sufficient to break the head/tape bond, and the tape was finally peeled away.

Following this test, the surfaces of both the tape and head were examined at high magnification using a scanning electron microscope. From the results shown in Fig. 4, total transfer of the oxide and binder from the Mylar to the brass head surface occurred within much of the contact area. In the top picture, Fig. 4a, the dark areas are oxide which remained on the head surface following removal of the tape; in the bottom picture, Fig. 4b, the dark areas are the exposed Mylar seen while looking at the oxide surface of the tape. Further close examination of the surface of the tape, again using the scanning electron microscope, showed distinct areas of softening or melting, as seen in Fig. 5.

The second type of stick observed did not involve an actual transfer of oxide or binder to the head. In fact, there was no evidence of any build-up on the head. The problem was observed only as an increase in frictional drag since, when the head was pulled back or tape tension removed, the tape simply fell away from the head. The definition of failure was not as obvious for this test as in the case of more complete bonding. Therefore, an increase in frictional drag of 10 ounces was arbitrarily defined as failure. Such an increase was beyond the torque capability of most satellite transports.

Two distinct physical changes found on the 3M 888 tape contributed to the observed increase in frictional forces. The first was a physical deformation of the oxide surface caused by the head. In Fig. 6, a concave deformation, corresponding to the length of the contact area, can be seen on the oxide surface. In addition, Fig. 7 shows oxide surface of tape which had been stationary with the Mylar backing against a tape guide. The surface of this roller, although polished, was sufficiently rough to imprint a pattern through the Mylar at the 65°C temperatures. Similar effects were observed at temperatures down to 25°C. The horizontal lines in this photograph show a wear pattern commonly found in used tape.

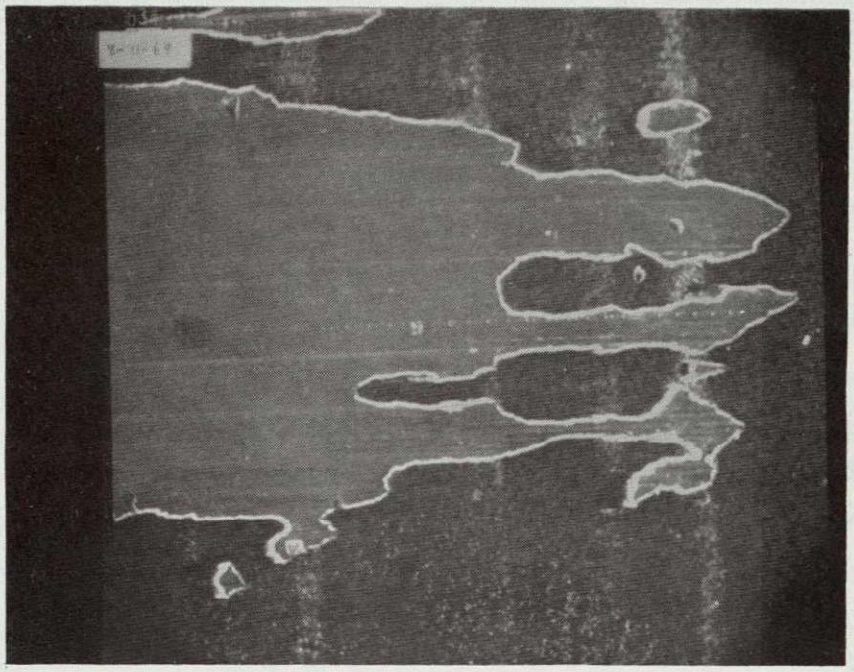

a. Head Surface

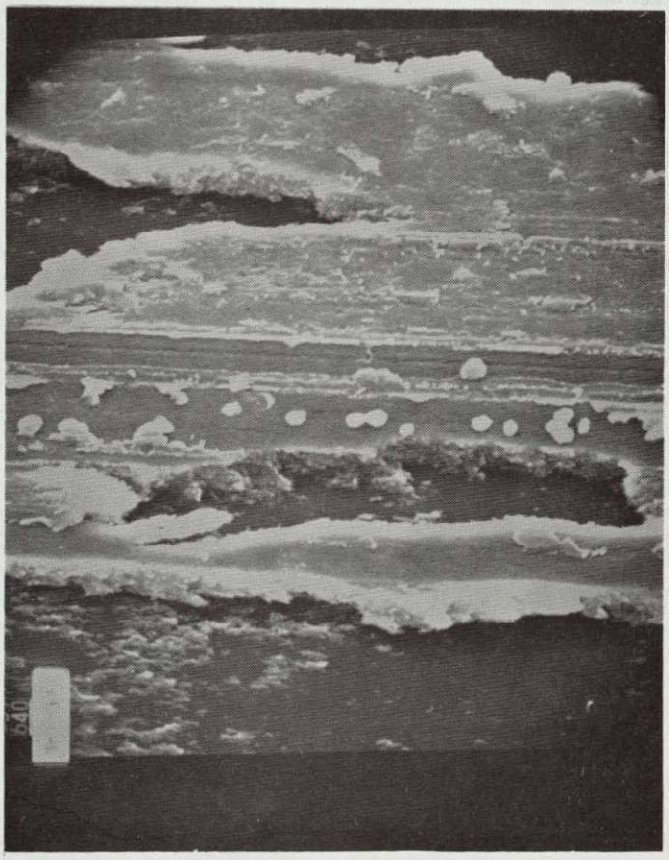

b. Tape Surface

Fig. 4 EXAMINATION OF OXIDE TRANSFER

Fig. 5 SOFTENING OF TAPE SURFACE

Fig. 6 DEFORMATION OF 3M 888 SURFACE

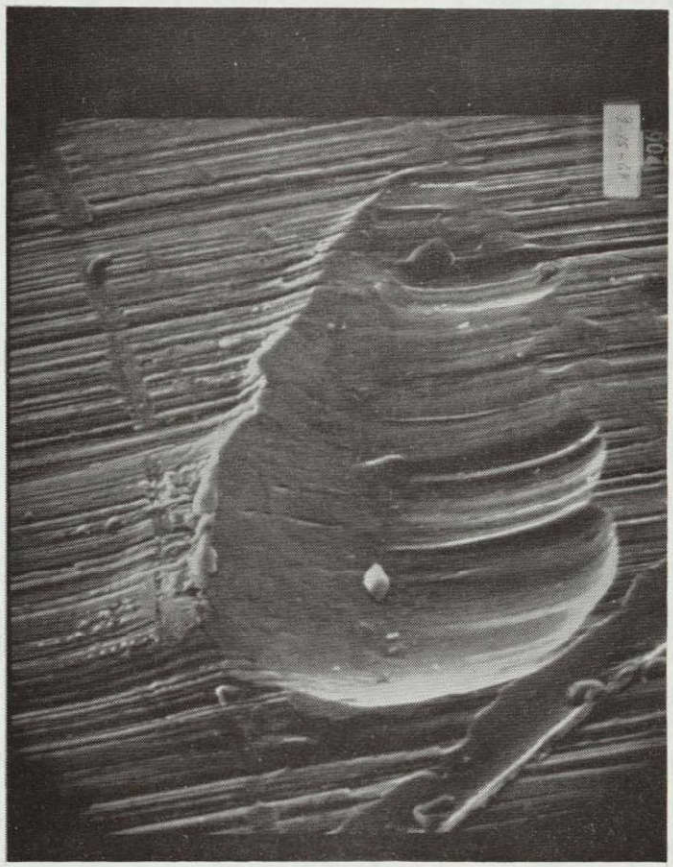

Fig. 7 CAPSTAN IMPRINT ON 3M SURFACE

Another physical change found on the surface of certain tapes examined was the appearance of microscopic ramps that resulted in a fish scale effect. The tape became very direction sensitive, and eventually failed in localized areas. These ramps, most easily observed using a stereo pair of photomicrographs, not only caused an increase in frictional force, but also tended to be transferred to the head in an adhesion failure. Such localized failures can be seen in Fig. 8. The top photograph, Fig. 8a shows the failure areas to be small, but numerous and widespread across the contact area. Fig. 8b shows the corresponding area of the tape, specifically Memorex Type 79L. However, as seen in Fig. 9, which greatly magnifies one of the localized failure areas, the transfer of material was due to lack of binder cohesion rather than lack of adhesion to the Mylar.

The other major failure mechanism identified during the initial tests was a general softening and smoothing of the tape surface. Figure 10 shows the surface of RCA 617 tape following a failure.* The tape to the left of the contact area was representative of a relatively normal surface finish, while the tape in contact with the head had been clearly smoothed.

The interpretation of the results obtained from these preliminary tests relate to both frictional and chemical effects. However, in neither area is the actual mechanism involved fully understood or at least reported throughout the literature. For example, increases observed in running torque were very likely a function of sliding friction phenomena resulting from the initimate head to tape contact and changes in the surface finished. But various theories have been advanced on the nature of friction for surfaces in sliding contact. One, proposed by Schnurmann,[2] is based on the concept of clusters of electrical charges of opposite polarity on adjoining surfaces. The electrostatic force field thus developed is believed to resist slippage of contacting surfaces until a tangential force sufficient to separate the

*The definition of failure throughout these tests was 10 oz of drag.

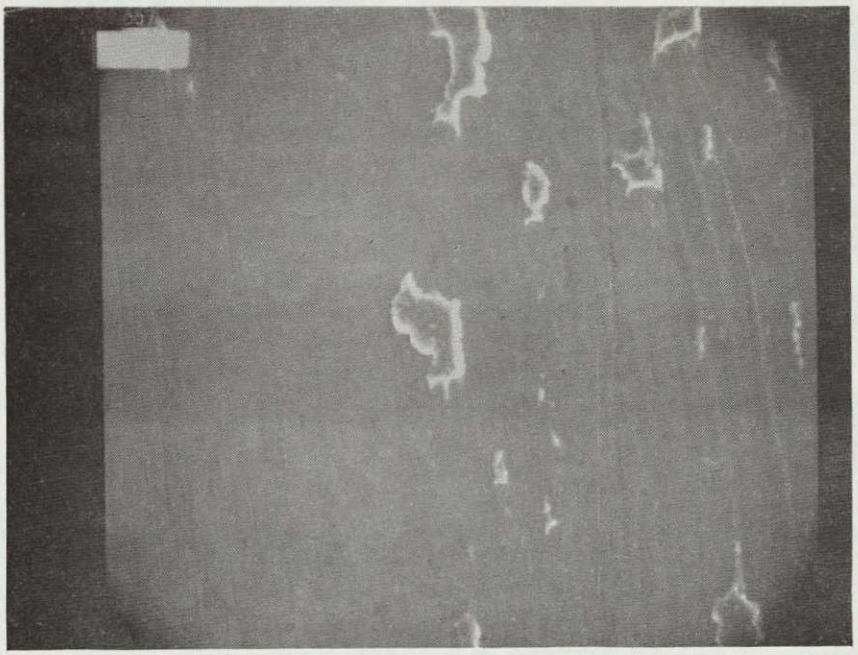

a. Head Surface

b. Tape Surface

Fig. 8 LOCALIZED FAILURE, MEMOREX 79L

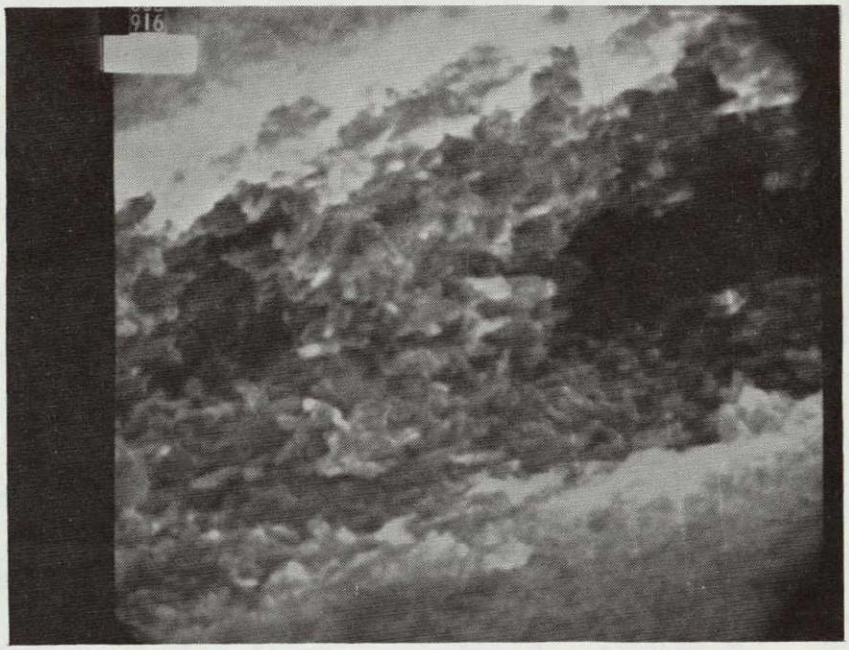

Fig. 9 LOCALIZED COHESION FAILURE (10,000X)

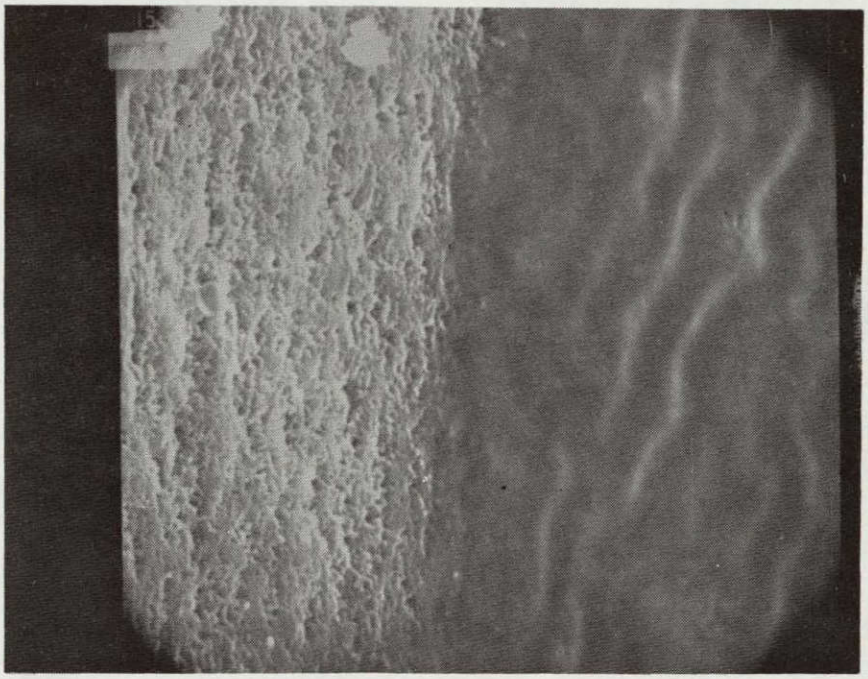

Fig. 10 SOFTENING OF RCA 617 TAPE SURFACE

charges to the breakdown potential is applied. When the local attraction at the interface is overcome, relative movement of the adjoining surfaces occurs in a macroslip process.

Another theory of friction, based on molecular concepts[3] ascribes the presence of restrictive forces between surfaces in contact to interactions of molecules at a separation distance near the minimum of the potential energy curve. The spatial distribution of these effectively interacting entities is such that the majority of them approaches the field of attraction, while a remainder assumes positions in the region of mutual repulsion. The energy expended in severing molecular associations at the interface is represented in the frictional resistance, while the load carrying capacity of the substrate is attributed to the restoring force developed as a result of negative interaction of those molecules which enter into the repulsion field.

For high-molecular-weight organic materials, a welding-shearing theory of friction, proposed by Bowden and Tabor,[4] has gained wide acceptance. This theory explains the mechanism of friction in macroscopic terms, without essentially disagreeing with the previously advanced concepts. It postulates the dependence of frictional resistance to sliding on two main factors: (1) the force required to shear off irregularities at points of contact between two surfaces; and (2) the energy expended in plowing grooves in one material by the asperities of the other.

The overall frictional force F is thus represented by the sum of the shearing and plowing contribution:

$$F = A\ s + P \qquad \text{(A-1)}$$

where the plowing force P for a spherical asperity of radius r can be given by:

$$P = 1/12\ (C^3\ p'/r) \qquad \text{(A-2)}$$

where A = the area supporting the load, s = the shear strength of the asperities, C = the chord length of the segment of the asperity engaged in plowing, and p' = the yield pressure of the material. Equations A-1 and A-2 suggest that the plowing term could dominate the frictional behavior of relatively soft and and deformable plastics for which the depth of indentation by asperities (chord length) would become significant.

A corresponding set of theories have been proposed for the mechanisms of chemical bonding to either metals or the accumulation of organic materials on the head surface resulting from wear. These are discussed in Volume III of this report. To actually determine which of these interactions was the dominant contributor to the adhesion failures simulated was not considered to be the primary objective of this program. Therefore, the emphasis of the program was directed towards the establishment of relationships between the observed frictional performance and the head, tape, and operational parameters involved. The organization of these parameters is shown in Fig. 11.

A set of 24 hypotheses was generated to describe the possible relationships between tape-to-head adhesion performance and the various parameters involved. An extensive series of tests was then performed to determine the validity of each of these factors. The hypotheses tested were stated as follows:

ENVIRONMENT

A-1 _____ Adhesion increases with increased temperature

A-2 _____ Adhesion increases with increased humidity

A-3 _____ Adhesion increases with lack of oxygen

SPEED AND DIRECTION

A-4 _____ Adhesion increases at lower speed

A-5 _____ Adhesion increases with bi-directional operation

A-6 _____ Adhesion varies with direction of coating application

HEAD PRESSURES

A-7 _____ Adhesion increases with increased head pressure

A-8 _____ Adhesion increases with increased tension at constant head pressure

TAPE WEAR

A-9 _____ Adhesion increases with tape wear

A-10 _____ Adhesion increases with a decrease in time between successive passes

TAPE FORMULATION

A-11 _____ Adhesion more likely occurs with epoxy based than with polyurethane based binders

A-12 _____ Adhesion increases with decreased lubrication

A-13 _____ Adhesion increases with halogen content

A-14 _____ Adhesion increases with oxide loading

A-15 _____ Adhesion increases with polymer polarity

A-16 _____ Adhesion increases with decreased resistivity

A-17 _____ Adhesion increases with poor oxide orientation

A-18 _____ Adhesion increases with poor oxide dispersion

SURFACE FINISH

A-19 _____ Adhesion varies with initial tape roughness

HARDNESS

A-20 ____ Adhesion increases with softer tape binders

HEAD MATERIAL

A-21 ____ Adhesion varies with head material

HEAD VARNISH

A-22 ____ Adhesion increases with presence of head varnish

The remainder of this section is a presentation of the results obtained from tests designed to isolate and either confirm or disprove each of these hypotheses. Those factors found to correlate most strongly with performance were then established as the guidelines presented in Volume I.

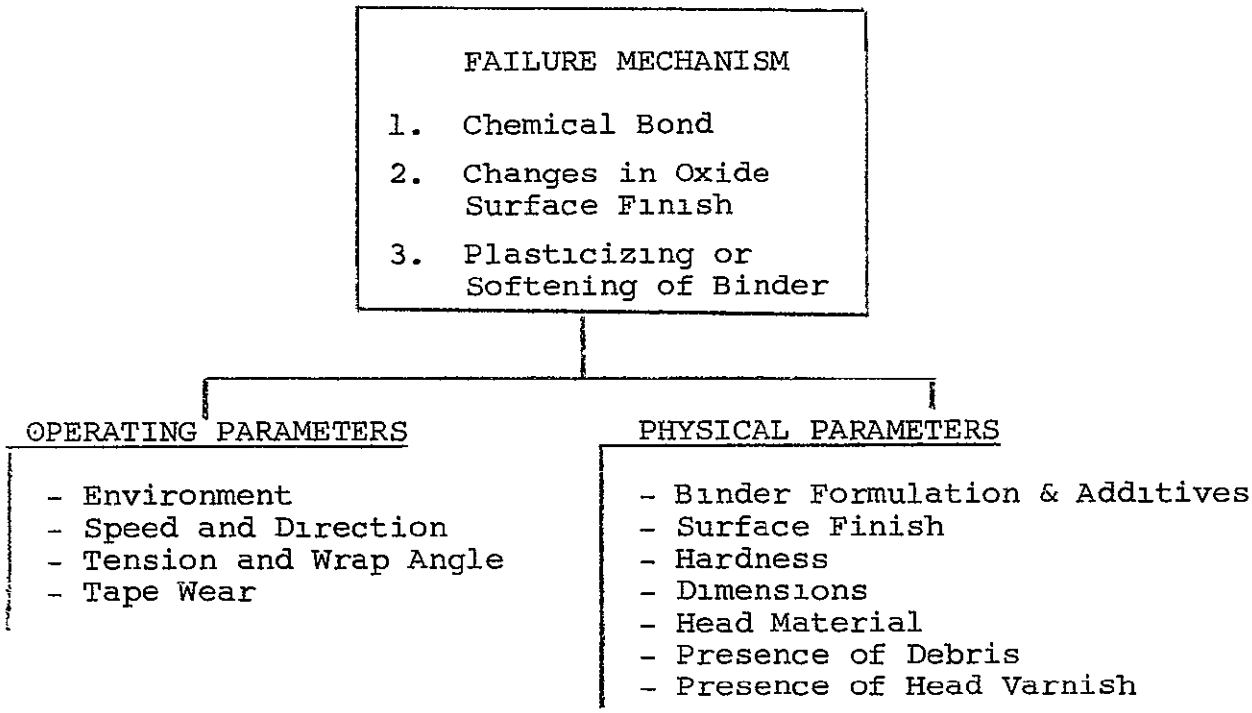

Fig. 11 ORGANIZATION OF VARIABLES

2. Ambient Temperature

It was apparent throughout Phase I and the preliminary tests to simulate adhesion failures that temperature was a significant factor in the determination of both frictional drag and tape degradation. One early change in the procedure used to promote or accelerate adhesion failures was to increase the operating temperature to 65°C. It was found that most tapes would eventually fail at this temperature when run at the relatively high tensions and wrap angles incorporated. Therefore, the first hypothesis that adhesion increases at increased temperatures was verified.

It is well known that the kinetic energy of the tape, when in contact with one or more heads, diminishes with time because of friction. This loss of kinetic energy is dissipated as heat, resulting in a temperature rise in the tape or heads. However, the irregular surface and the nonhomogeneity of the oxide binder coating on the tape make this anticipated temperature rise difficult either to compute or measure. Therefore, temperature throughout this program refers only to the ambient environment of the transport, tape, and heads. Actually, substantial differences in frictional performance were observed between 45°C and 65°C, indicating that the friction generated heat was not the dominant factor in the tests.

In order to isolate the effects of temperature, a series of tests was run on the endless loop transports at 25°C, 45°C, and 65°C. Three relative humidities were used at each of the temperatures. In each test a 52-inch-long loop of tape was run over a brass dummy head at the designated environment. The tape tension was 12 ounces, and the wrap angle was 15°. The dummy heads were constructed of half-hard commercial brass, having a low porosity and a contour radius of 0.25 inches. The general procedure, described in detail in Volume III, was to alternate the tape speed between 1 ips in the forward direction

and 30 ips in the reverse direction at intervals of approximately 1,000 passes. Starting and running torque at the capstan was measured in inch-ounces at the beginning and end of each interval. After subtracting motor and bearing losses, this reading was representative frictional drag at the head. The tests were limited to 10,000 passes, and the previous definition for failure of 10 ounce-inches was maintained.

Table I I is representative of the data taken for each of the tapes at each of the environmental conditions. The torque measurements shown were converted from the servoed dc motor current measurements actually performed. Correction for motor and bearing losses was obtained by running the tape out of contact with the head. It can be seen that the starting torques were somewhat higher than the running torques and were also subject to more variation. However, the starting torques for both the 1 ips and 30 ips intervals show increasing trends throughout the test, until a reading of 12.5 ounce-inch was reached at 10,000 passes.

The differences in starting torque between 1 ips and 30 ips were due to the direction in which the tape was run. When the tape was being pulled over the head towards the capstan, the frictional drag was added to the tape tension on one side of the head. However, in the reverse direction the high tension side was mechanically controlled and such an increase did not occur.

The results of this matrix of tests showed that the coefficient of friction increased at higher temperatures for every tape type examined. Figure 12 shows the relationship between starting torque and tape usage for 3M type 871 tape at three different temperatures. The increasing trend with temperature was typical of all the tapes measured, although the degree and rate of degradation varied considerably. Figure 13 shows the results obtained under the same conditions with Memorex 63L. In this case, the starting torque exceeded our

Table II

SAMPLE TEST RESULTS - ENVIRONMENTAL TESTS

Tape Type Memorex 79L

Temperature 45°C Relative Humidity 15%

Tension 12 oz. Wrap Angle 15°

Brass Head No. N9

Number of Passes	New Tape Speed	Starting Torque	Running Torque	
			Beginning	End
0	30 ips	1.0 oz-in	0.7 oz-in	0.8 oz-in
1040	1	3.4	1.4	1.3
2110	30	2.0	0.4	0.3
3670	1	3.7	1.4	1.2
3720	30	4.2	0.2	0.3
5800	1	3.2	1.5	1.0
5870	30	4.8	0.1	0.1
7950	1	8.3	2.0	1.1
8020	30	6.1	0.1	0.3
10,100	1	12.5	2.0	- -

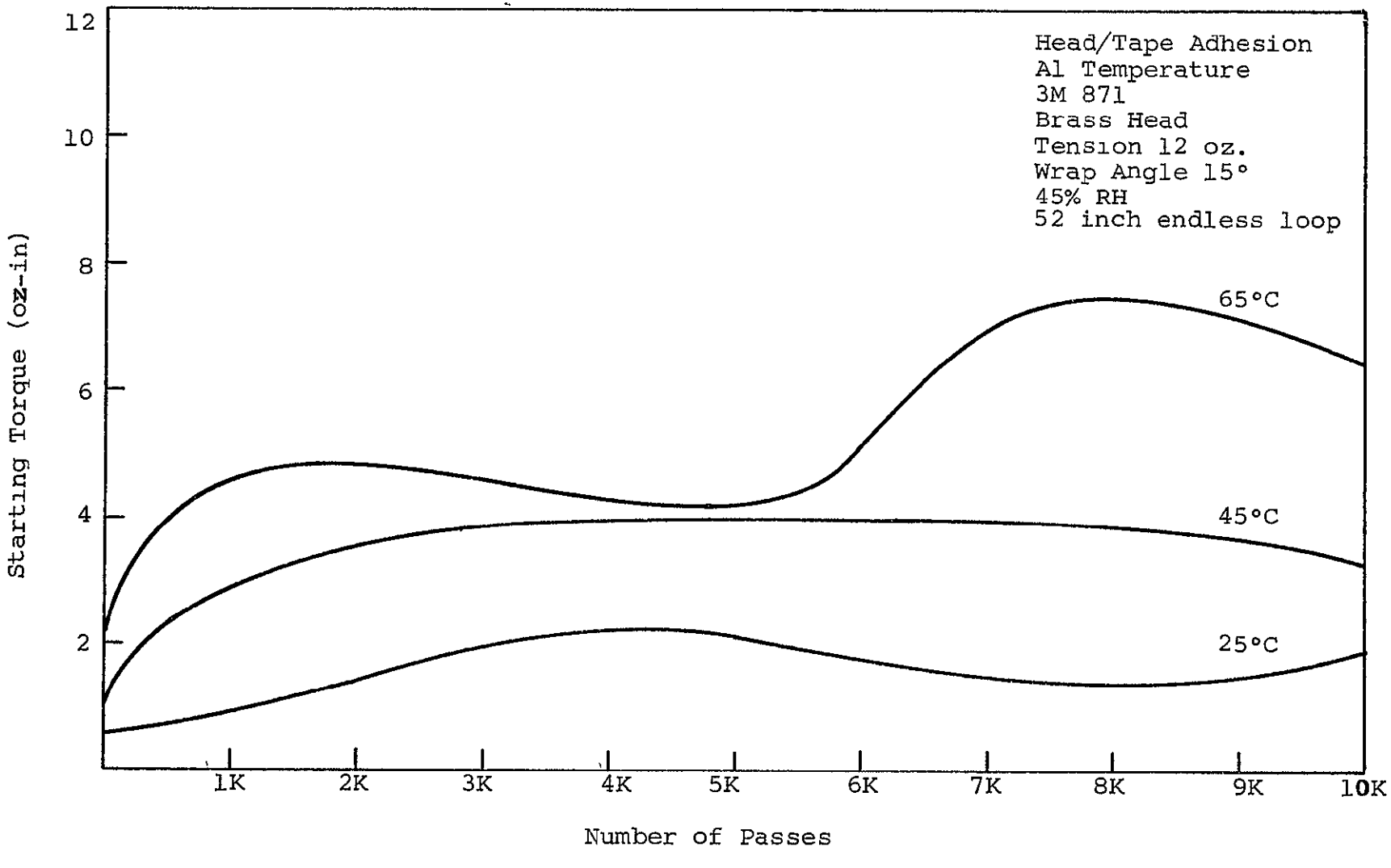

Fig. 12 EFFECT OF TEMPERATURE, 3M 871

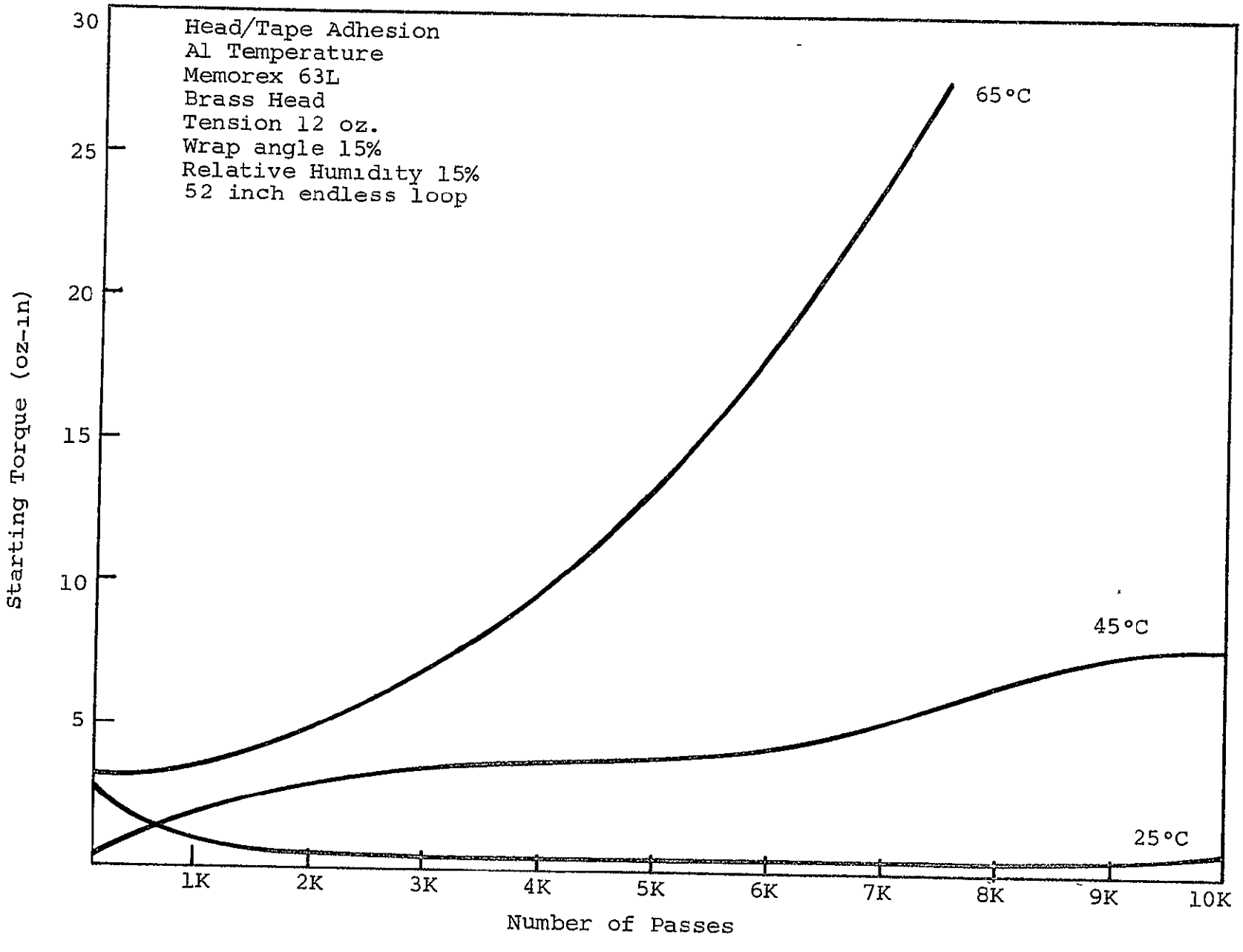

Fig. 13 EFFECT OF TEMPERATURE, MEMOREX 63L

10 ounce-inch limitation well before 10,000 passes had been accumulated at the two higher temperatures.

The two types shown were composed of chemically very different binder systems.* Type 3M 871 tested was a polyurethane based polymer, while the Memorex 63L was an epoxy.* A third general class of polymer, the polyamides, was the basic constituent of DuPont's Crolyn Tape. The corresponding results of starting torque versus number of passes for this tape are shown in Fig. A-14. Again, there is a strong dependence upon ambient temperature. As mentioned in the previous section on failure mode analysis, the failure occuring at 65°C was the most severe example of adhesion encountered during the program.

The RCA 617 tape, also a polyurethane based tape, was included in the tests. It represented a fourth manufacturer and has been used in satellite systems. Figure 15 indicates that, even through the test conditions imposed were too severe for this tape, a temperature dependence is observed.

A total of four 3M tapes -- types 351, 777, 871, and 888 -- were incorporated in these tests. Figure 16 shows the general trend for the dependence of these tapes upon temperature by averaging the values of measured starting torque. At 65°C the 888 tape failed before 10,000 passes, thereby obliterating an upper limit on the range at this temperature.

A similar trend was observed for the three Memorex tapes tested, shown in Fig. 17. The tapes used were types 63L, 79L, and Quantum.

There were two reasons for separating the data by manufacturer. First, similarities were found in the basic binder polymers used in various tape types from the same manufacturer. Also, the general types of failure observed were consistent for each manufacturer. The two 3M tapes that failed at 65°C and

---

* See Volume III for details of the chemical analysis performed.

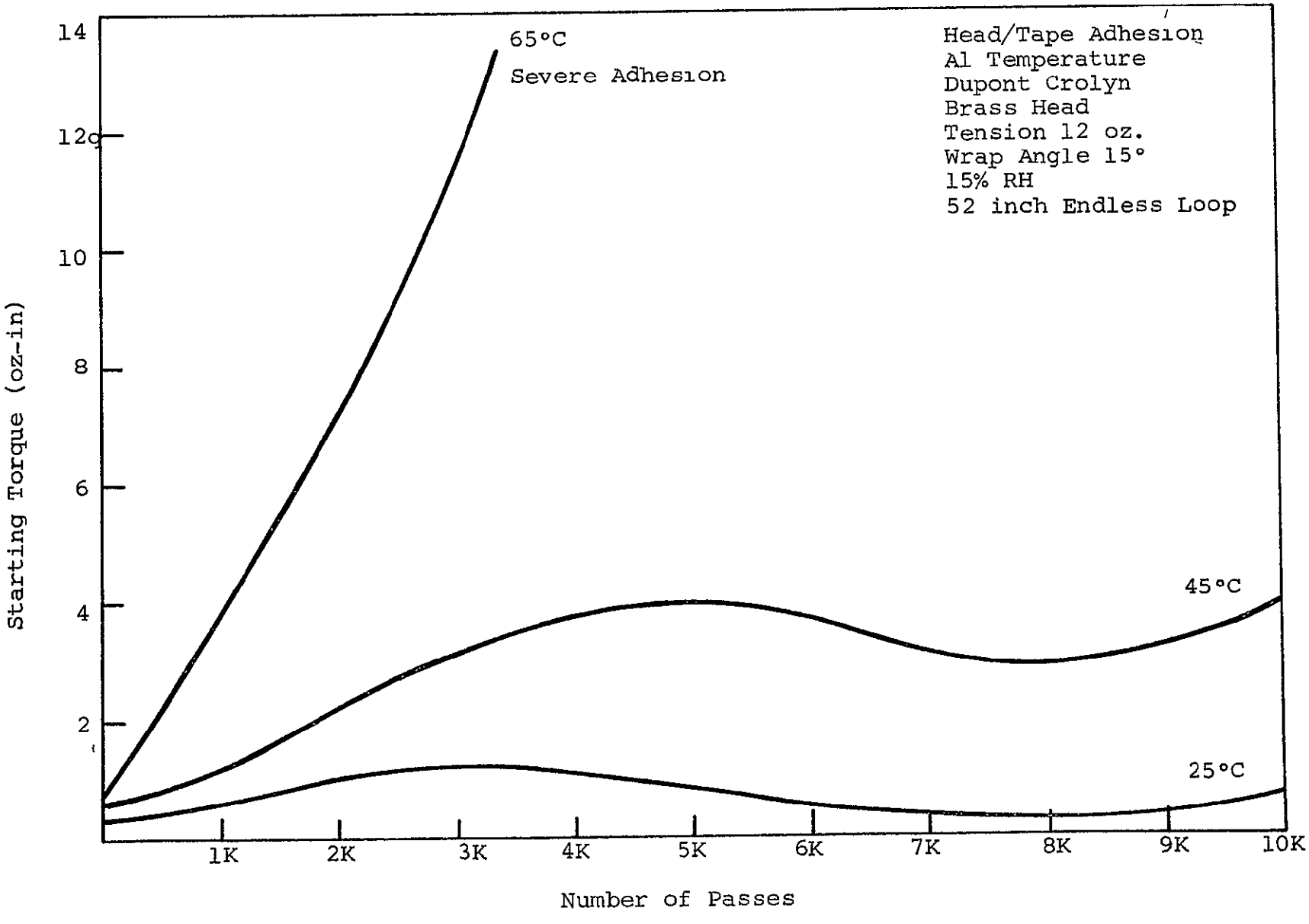

Fig. 14 EFFECT OF TEMPERATURE, DUPONT CROLYN

Head/Tape Adhesion
Al Temperature
RCA 617, Endless Loop
Brass Head
Tension 12 oz
Wrap Angle 15°

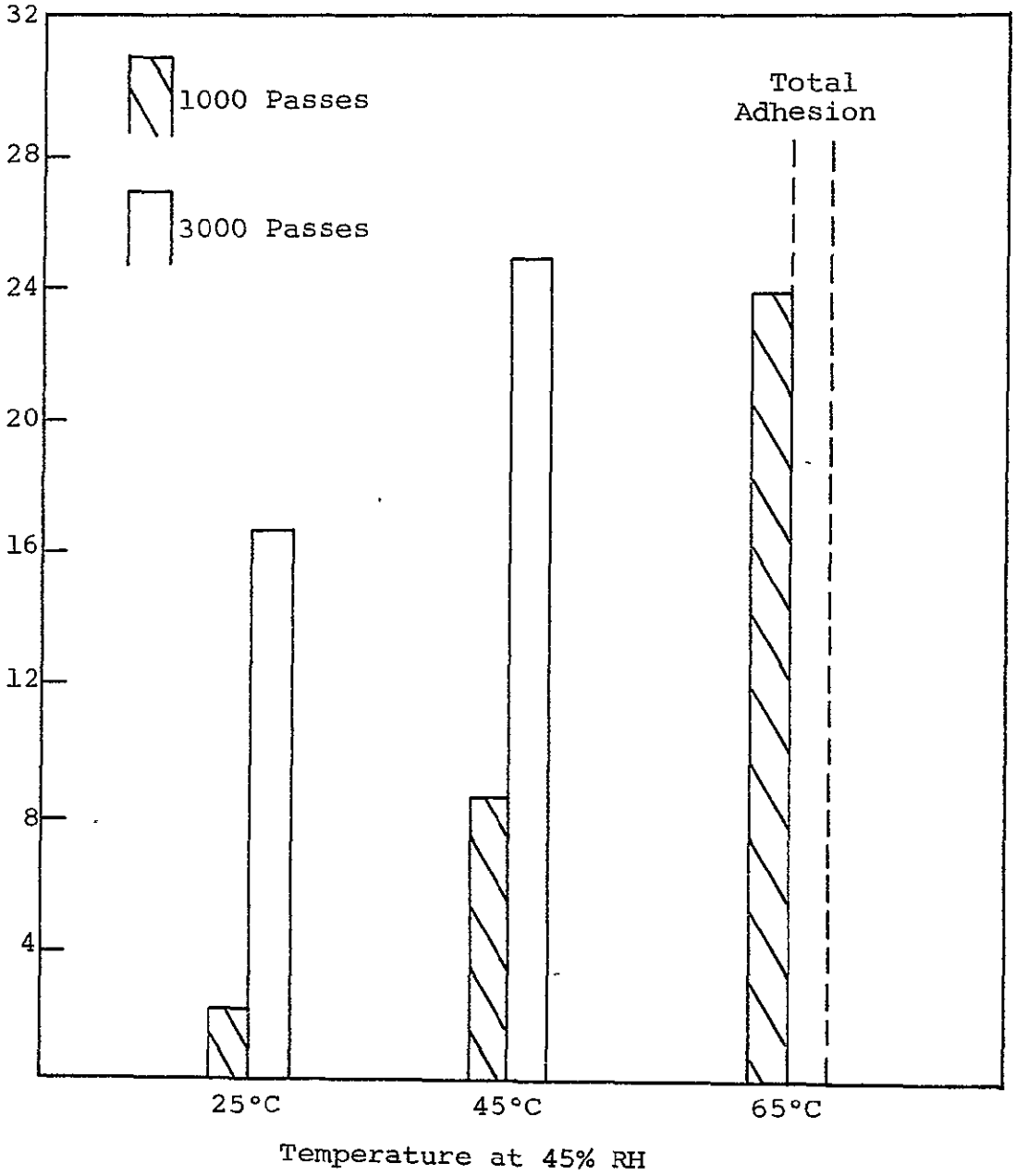

Fig. 15 EFFECT OF TEMPERATURE, RCA 617

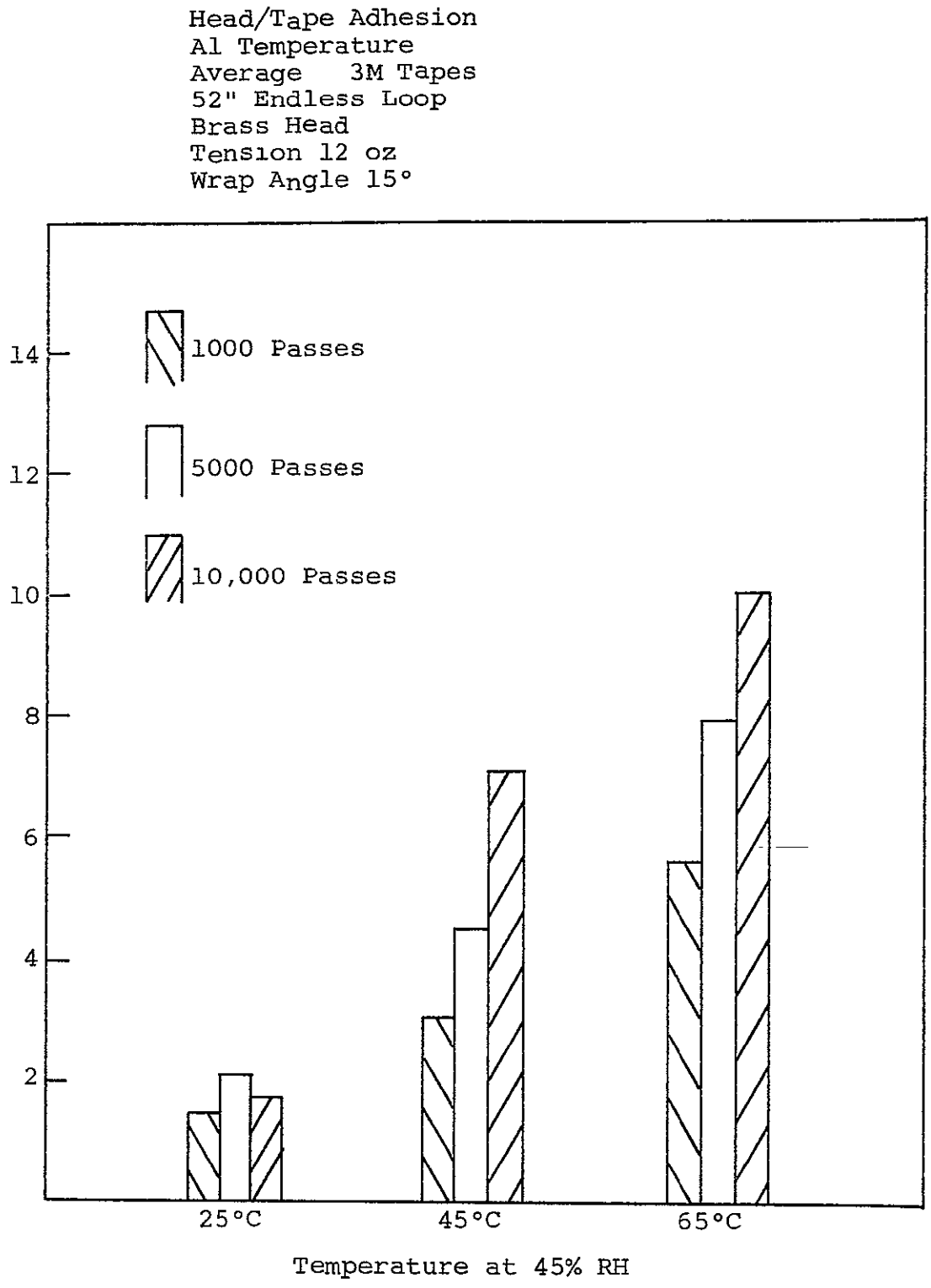

Fig. 16 EFFECT OF TEMPERATURE, 3M TAPES

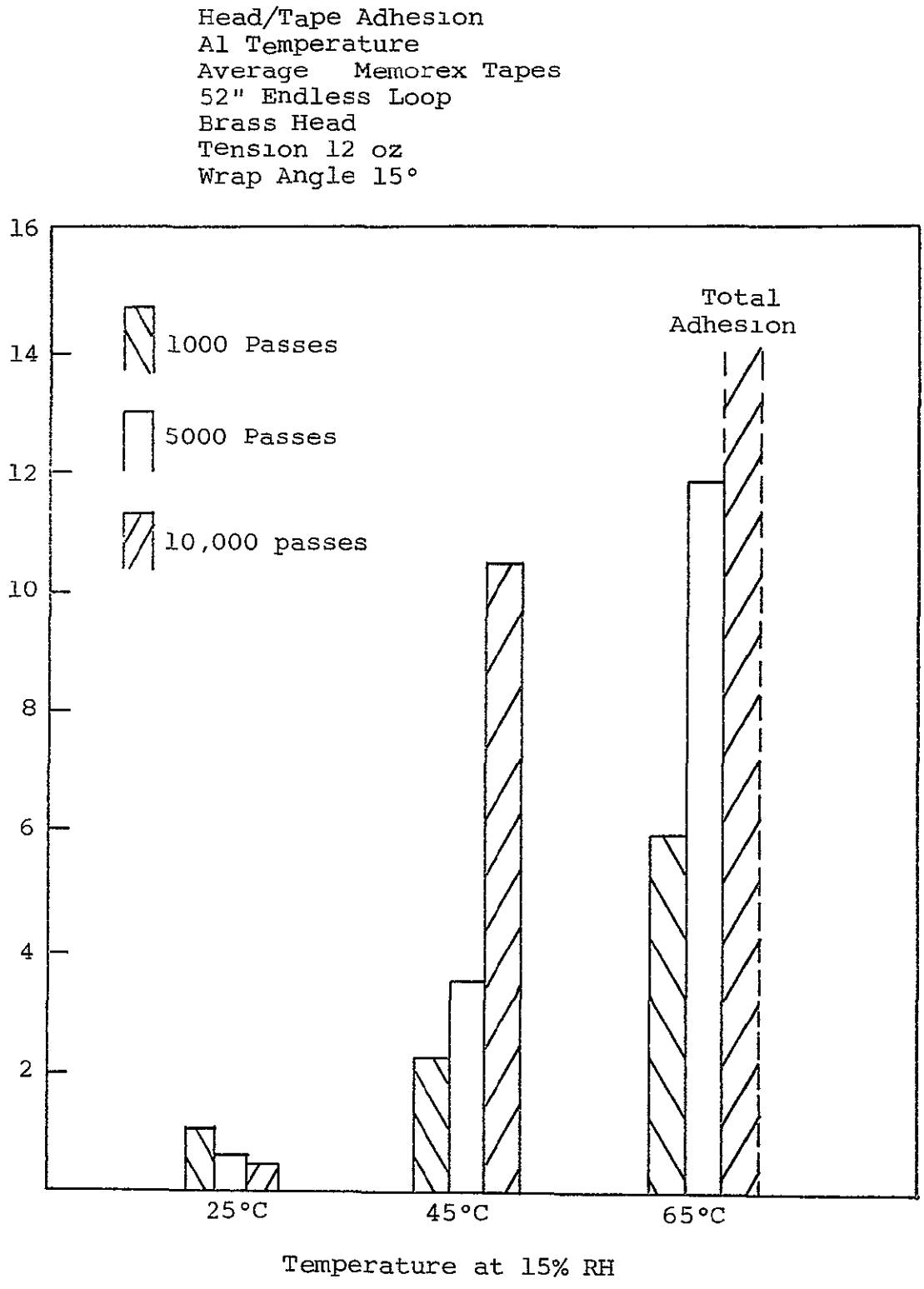

Fig. 17 EFFECT OF TEMPERATURE, MEMOREX TAPES

45% RH left little debris on the heads. In general, the heads, found to be in reasonable condition, had only moderate wear or scratching. Further, there was practically no permanent adhesion bond between the tape and head, and the tape generally would fall away from the head if the tension was removed.

The Memorex tapes, however, developed strong directional preferences, and usually failed while running at the low speed. As mentioned earlier, this was traced to changes in the surface finish of the tape. Further, the bond developed between the tape and head, at least in localized areas, was adhesive. When the tape was peeled off, many dots of oxide binder remained on the head, covering up to 75% of the contact area.

The DuPont Crolyn tape also failed while running, and the test was terminated because the capstan was slipping. The tape and head were removed from the chamber, and an attempt was made to remove the tape by pulling in the direction of travel with a spring scale. However, over 64 ounces of force was insufficient to break the bond, and the tape was finally peeled off. Most of the oxide binder in the contact area remained on the head surface.

The fourth type of failure was observed with the RCA 617 tape. In general, excessively large quantities of debris accumulated on the heads, and the tape, on occasion, appeared to be completely out of contact with the head material itself. Adhesion in these cases appeared to be caused by the binder sticking to the debris previously deposited on the head.

The series of tests conducted on the endless loop transports as specifically intended to produce high frictional forces and adhesion failures by operating at high tensions and wrap angles. In this manner, the differences in performance between tapes was easily distinguishable, and isolation of certain perameters was more readily attained. In addition, the use of an endless loop accelerated the accumulation of 10,000

passes. Finally, the degradation of any segment of the tape was felt to be somewhat independent of the overall tape length.

In order to overcome some of the potential shortcomings of tests using an endless loop, further temperature tests were run on a reel-to-reel transport using longer lengths of tape. Although these tests were run in controlled environments up to 65°C, the values for tension and wrap angle were generally lower.

The reel-to-reel transports employed a head mounting system, supported by a cantilever beam. Strain gages, attached to the beam, allowed a direct measurement of drag force. After amplification, drag measurements were read directly from a meter while the tape was running. A strip chart recorder was used to measure starting force.

The drag forces measured, while running 3M type 888 tape over a brass head, are shown in Fig. 18. This test was run at 65°C and 45% RH using 300 feet of tape. The tape was shuttled back and forth at 60 ips, although measurements were made at various speeds. The drag while running remained approximately constant between 2.0 and 2.25 ounces for the first 2,000 passes. This compared reasonably well with the 1.8 to 2.0 ounce measurements made on the loop transport. At 2247 passes the test was terminated because of severe tape squeal, a marked increase in running drag, and an increase in starting force to 14 ounces. On the endless loop transport, the tape failed while running at 1 ips after 3,500 passes. Starting torque at this point was over 19.5 ounce inches.

Following these two tests an inspection of the heads indicated that considerably more debris had been generated by the longer length of tape. This probably contributed to the premature failure. However, it was concluded that trends and relationships could be established on the endless transports and verified with longer lengths of tape.

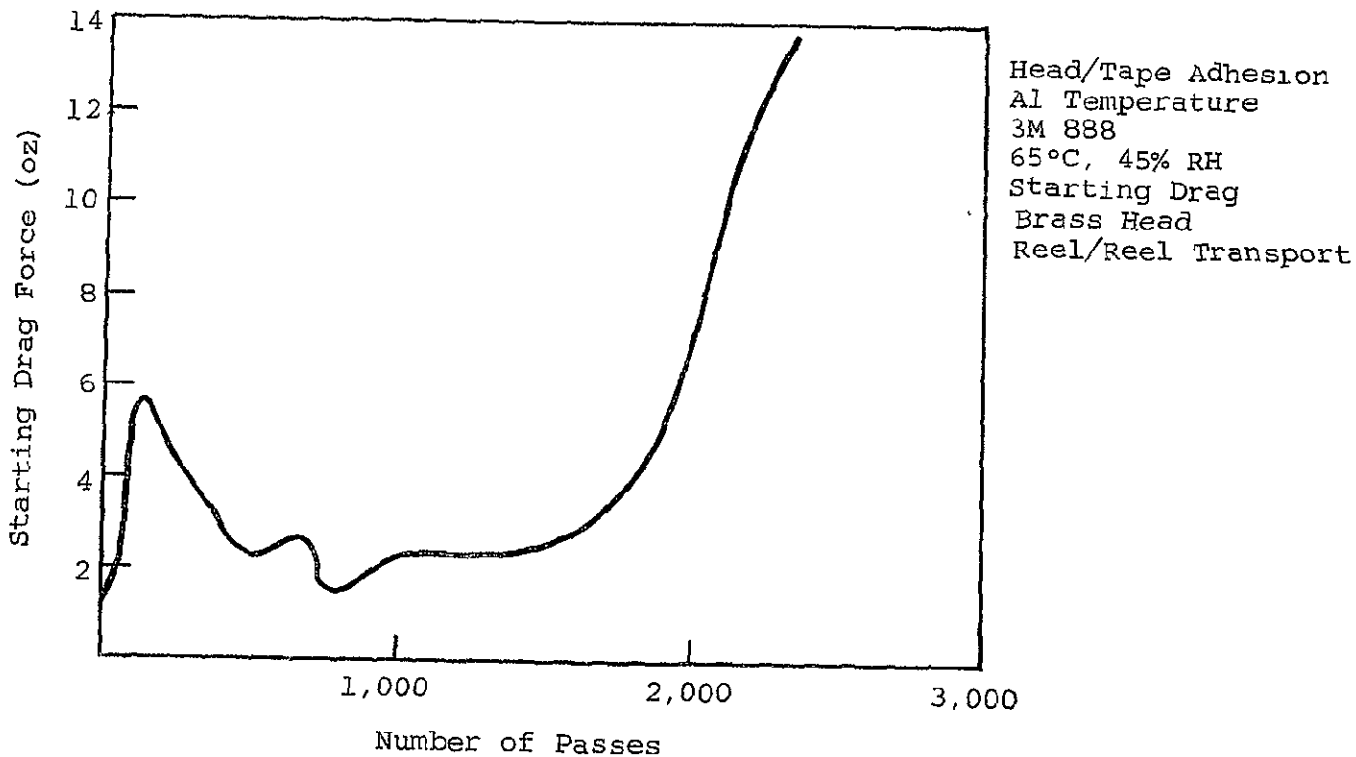

Fig. 18 HIGH TEMPERATURE AND HUMDIITY, 3M 888

The conclusion that trends observed using the loop transports were also representative reel to reel performance was substantiated throughout the program. For example, the tape types successfully completing 10,000 passes at 45°C (ref. Figs. 12, 13, 14, and 16) also performed satisfactorily on the reel to reel configuration. Further verification of the applicability of loop tests was observed in the comparisons of head materials and debris characteristics reported later in this volume.

Using both endless loop and reel to reel transports, the tests indicated a strong relationship between frictional performance and temperature. Under the conditions imposed, most tapes could not be operated for 10,000 passes at 65°C.

3. Relative Humidity

The second hypothesis to determine failure mechanisms was that frictional drag or adhesion increases with increased relative humidity. This relationship with humidity was important to satellite recorder manufacturers because it can generally be adjusted within the closed atmosphere of the recorder container. The hypothesis was verified throughout the program since very low humidities were preferable from a frictional point of view.

Three levels of relative humidity -- 15, 30, and 45% were used at each temperature in the endless loop tests previously described. The results of these tests clearly showed superior performance at the lower humidities when the tapes were run at a high temperature. The most dramatic example of this occured with the Memorex tapes, shown in Fig. 19 for type 63L. The measured starting torques for those tapes run at 30 and 45% relative humidity were considerably above the 10 ounce-inch limitation by the time only 3,000 passes had been accumulated. However, at 15% RH the tape did not exceed this level for the entire 10,000 passes. Similar results were obtained with Memorex 79L, shown in Fig. 20.

These tests suggested that frictional drag may be further reduced by operating at very low relative humidities; therefore, a test was run on the reel-to-reel transport at 65°C and as dry an atmosphere as possible. This atmosphere was obtained by placing a desiccant, $CaSO_4$, in the heated container. The measured humidity throughout the test was 0%, although instrument error could have been as high as 1.5%. The measured drag, while running at 1 ips, is shown in Fig. 21. The drag forces of 1.0 to 1.5 ounces were considered to be well within tolerable limits, particularly considering the 65°C temperature and 12° wrap angle.

The drag force during start for this tape was essentially the same as the running drag for the first 250 passes. At this point, the drag at start became measurable and was

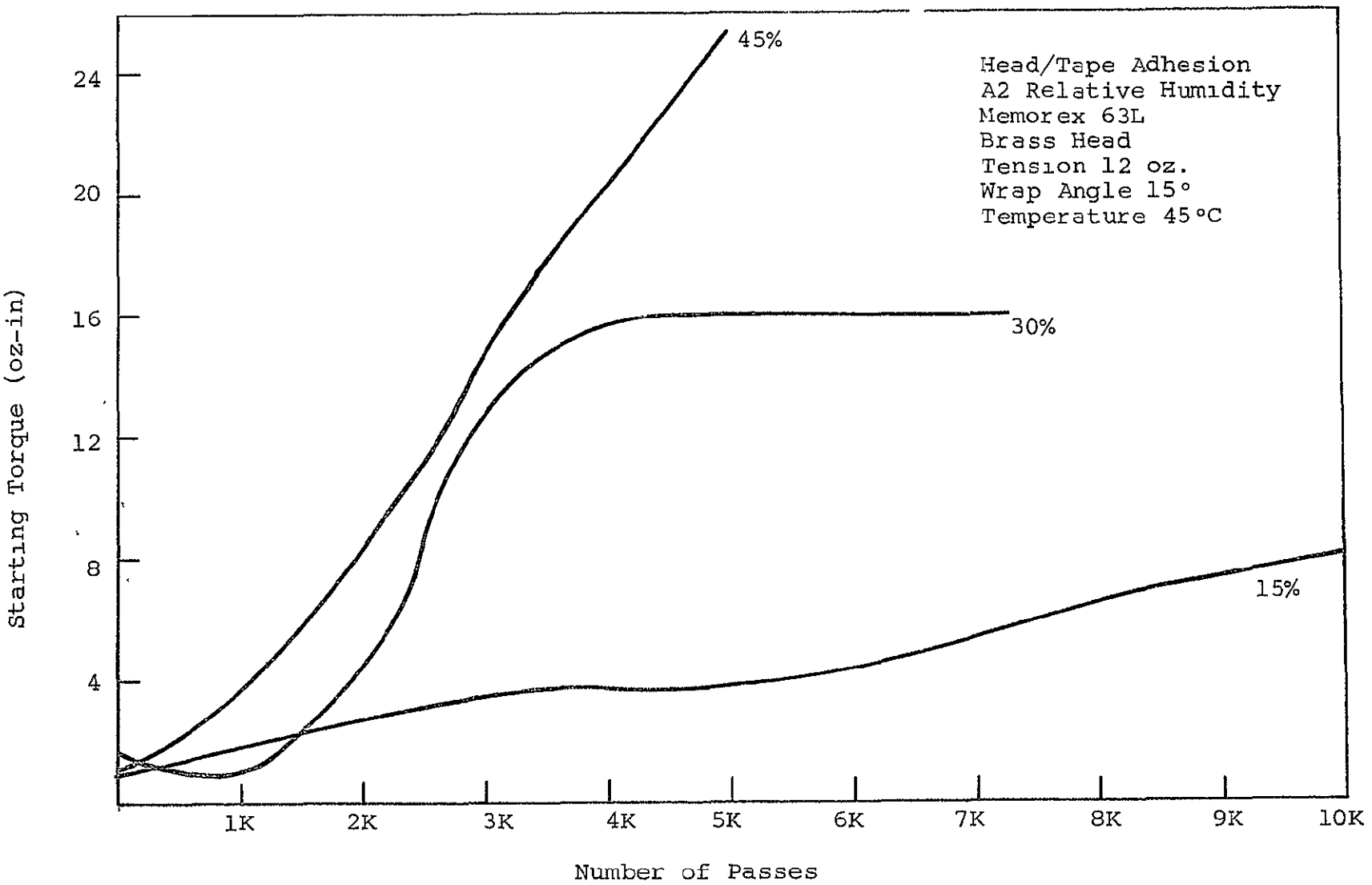

Fig. 19 EFFECT OF RELATIVE HUMIDITY, MEMOREX 63L

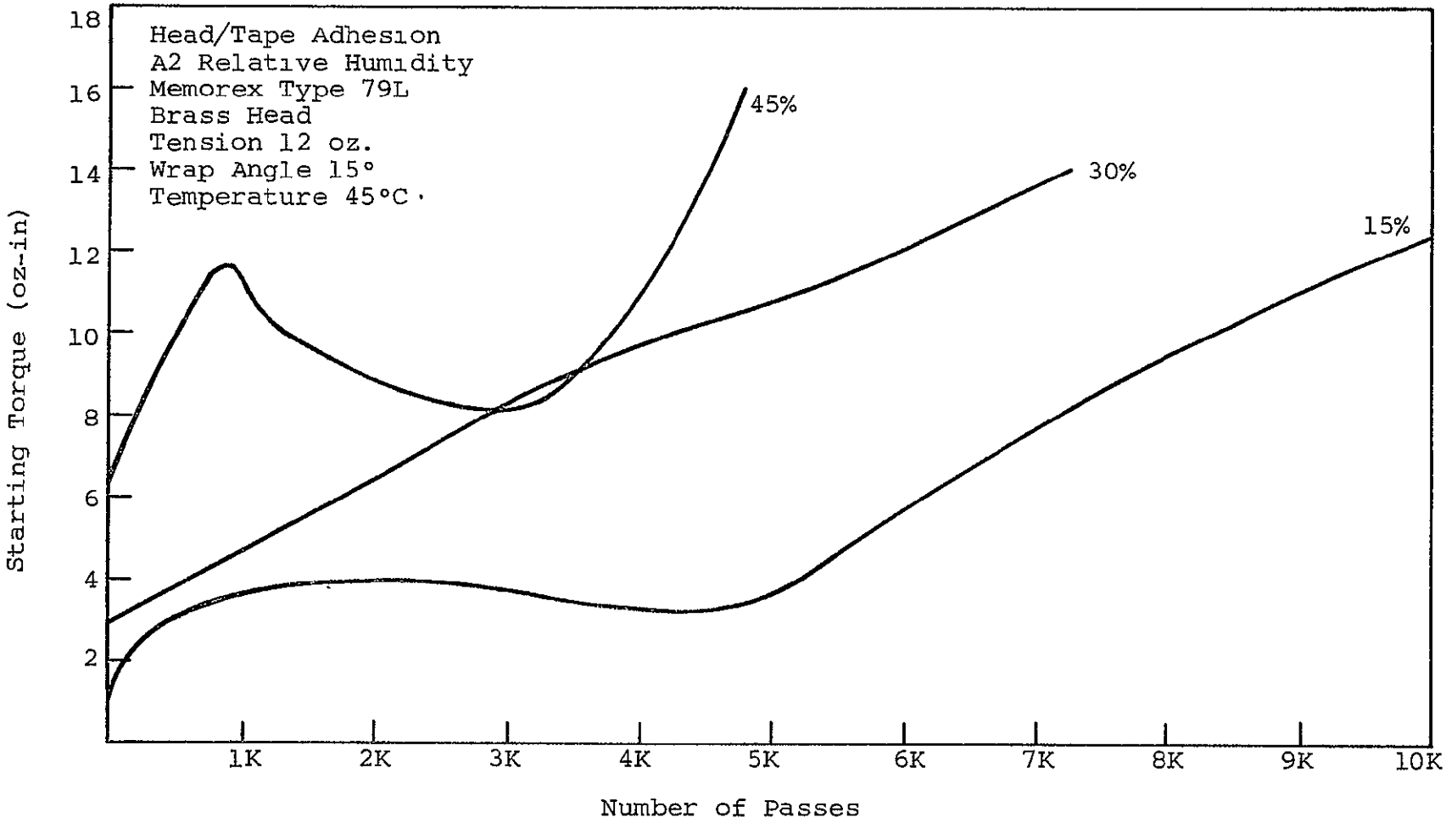

Fig. 20 EFFECT OF RELATIVE HUMIDITY, MEMOREX 79L

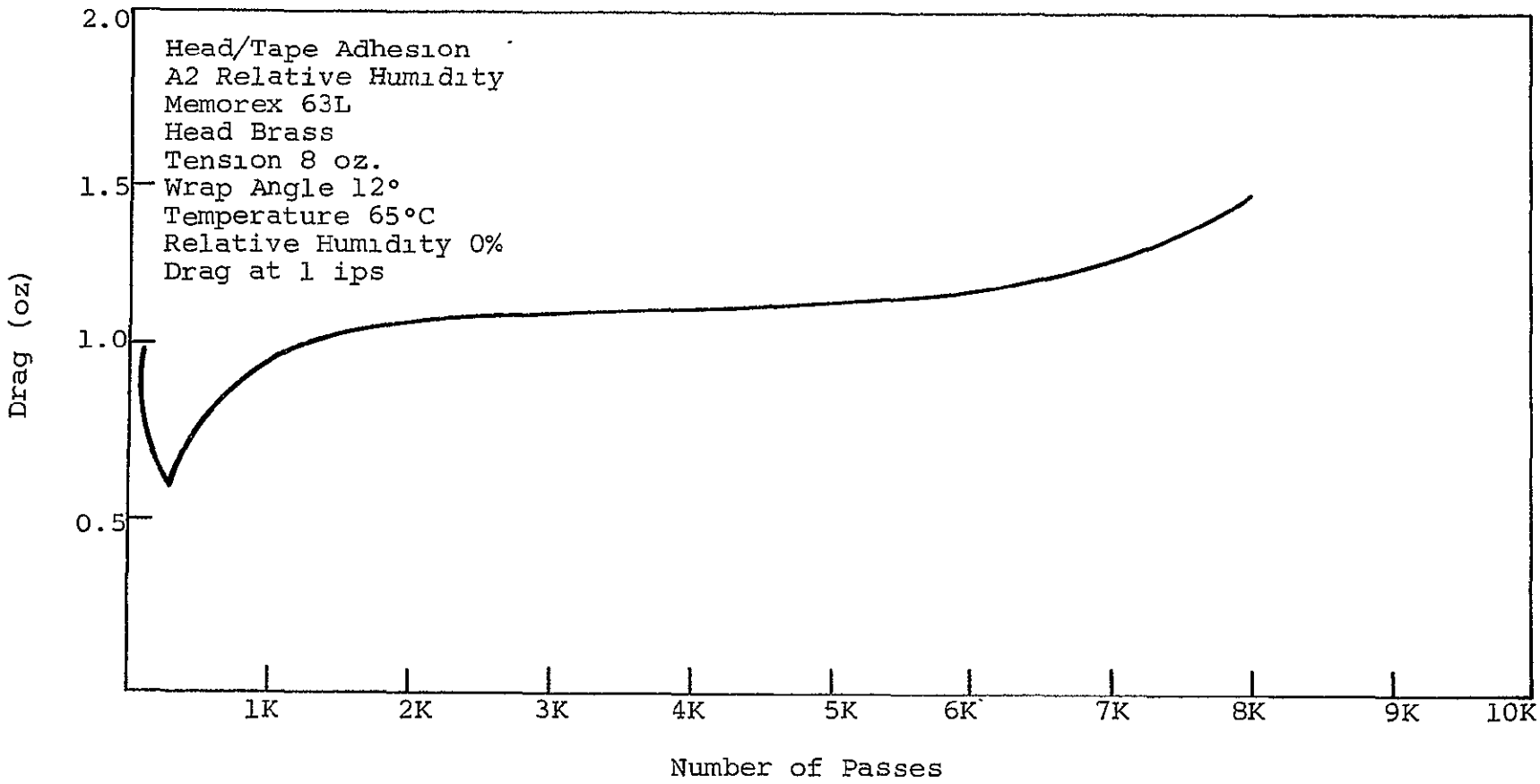

Fig. 21 MEMOREX 63L RUN AT VERY LOW HUMIDITY

approximately 30% higher than the running drag. This ratio was then mentioned throughout the remainder of the test.

The 3M tapes tested showed a similar, though not as pronounced, improvement when operated in lower humidity environments. The endless loop tests at 65°C indicated that the lowest frictional drag occurred at 15% RH, shown in Fig. 22 for 3M 888. Similar results, obtained for 3M 777, are shown in Fig. 23.

At lower temperatures the 3M tapes were less sensitive to changes in humidity, particularly 15 and 30%. Figure 24 shows the average for types 888 and 871 at 45°C. After 10,000 passes both tapes exhibited lower drag at 30% than at 15%.

Tests were also run on the reel-to-reel transport at 65°C and approximately 0% RH. As in the case of the Memorex 63L, the results showed, Fig. 25, low frictional drag at all speeds throughout the 10,000 passes, and in addition, only negligible starting forces were obtained. Typical strip chart recordings of the drag are shown in Fig. 26 for three speeds at the conclusion of 10,000 passes of the tape over the head. Note the lack of a peak at the inception of tape motion, indicating a small difference between the static and dynamic coefficient of friction.

The effects of humidity on the DuPont Crolyn tape were similar to those of the 3M tapes. An increase in humidity at the high temperature (65°C) caused a more pronounced increase in the coefficient of friction; at 45°C the performance became less dependent upon humidity. These results are shown in Figs. 27 and 28.

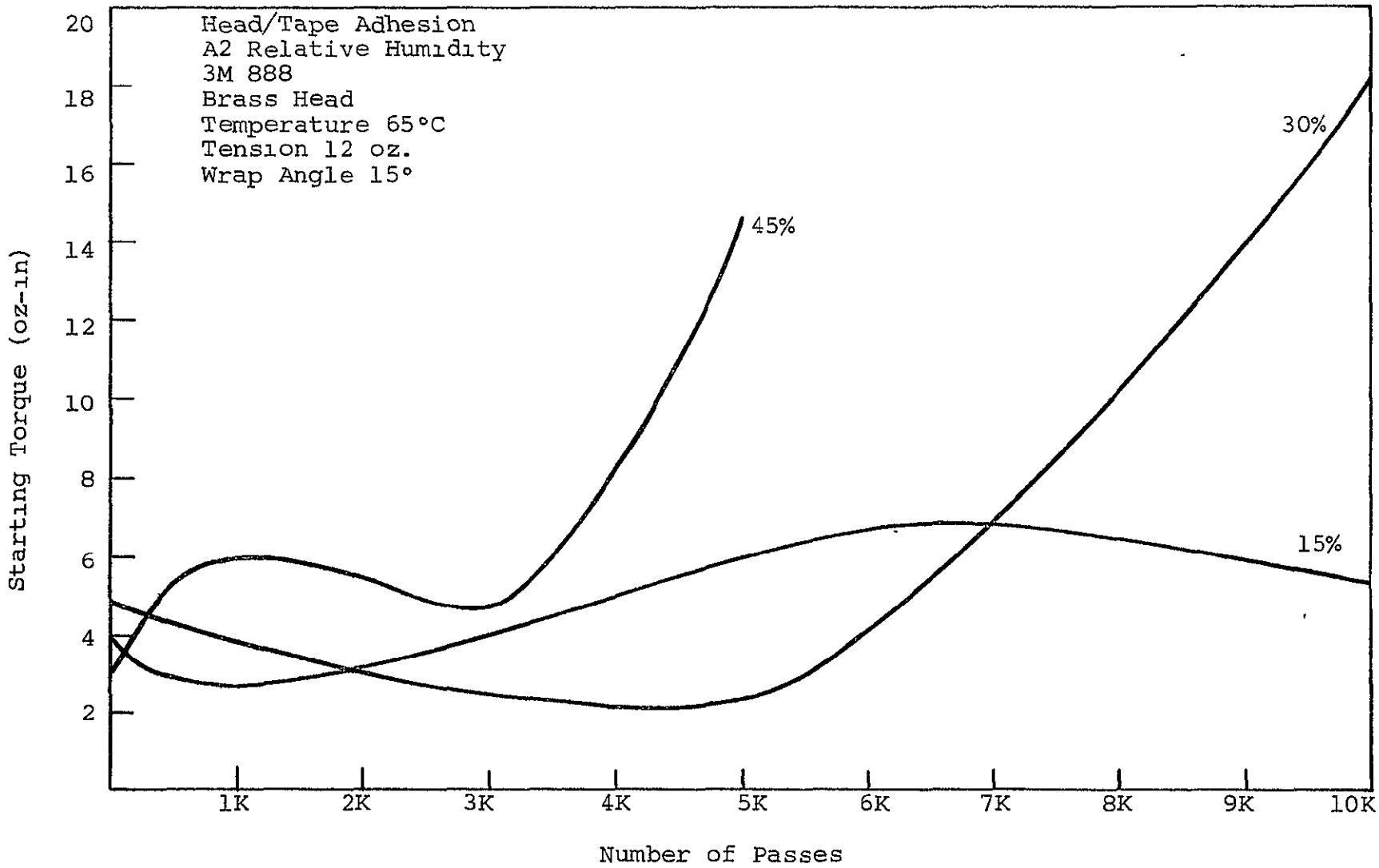

Fig. 22 EFFECT OF RELATIVE HUMIDITY, 3M 888

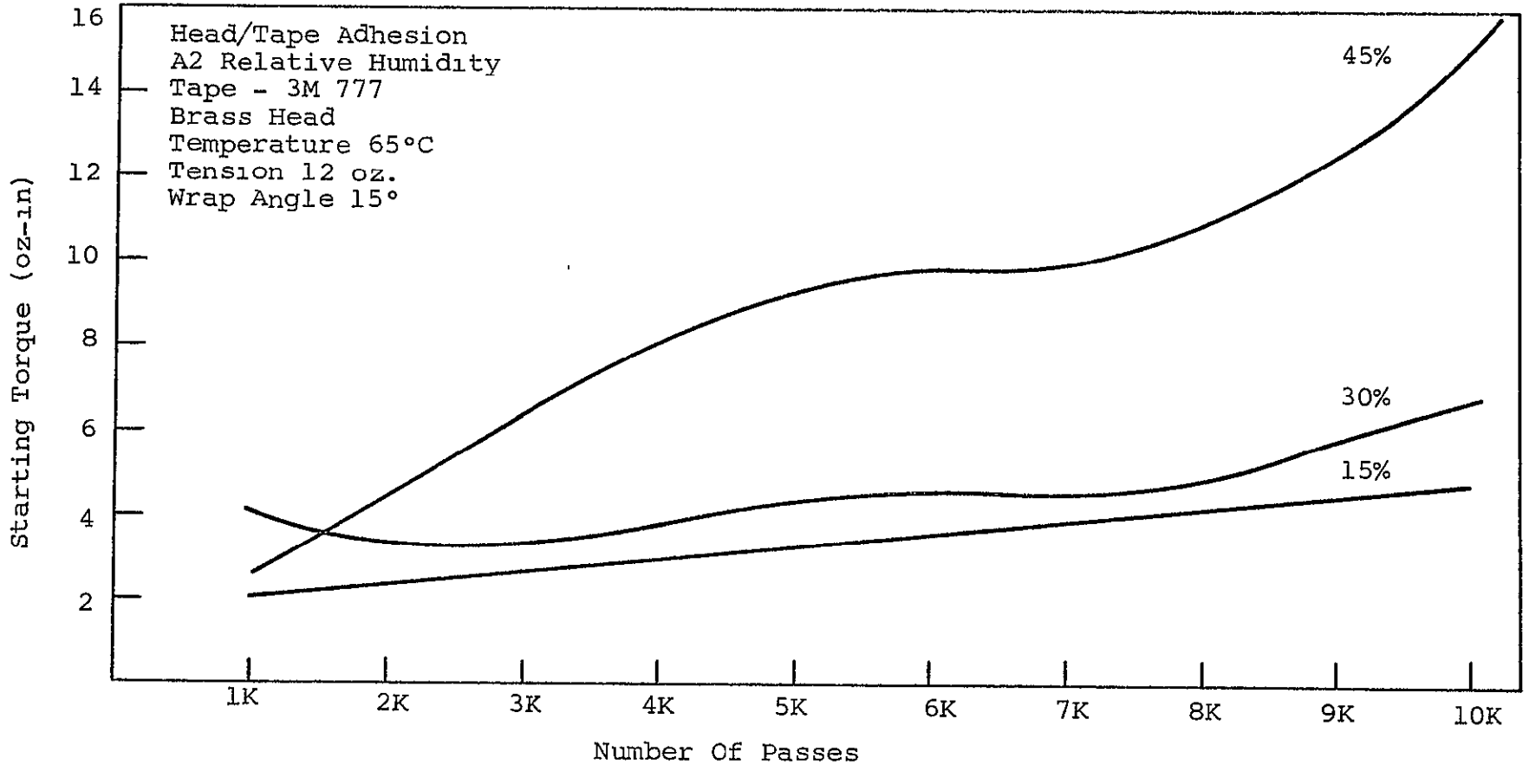

Fig. 23 EFFECT OF HUMIDITY, 3M 777

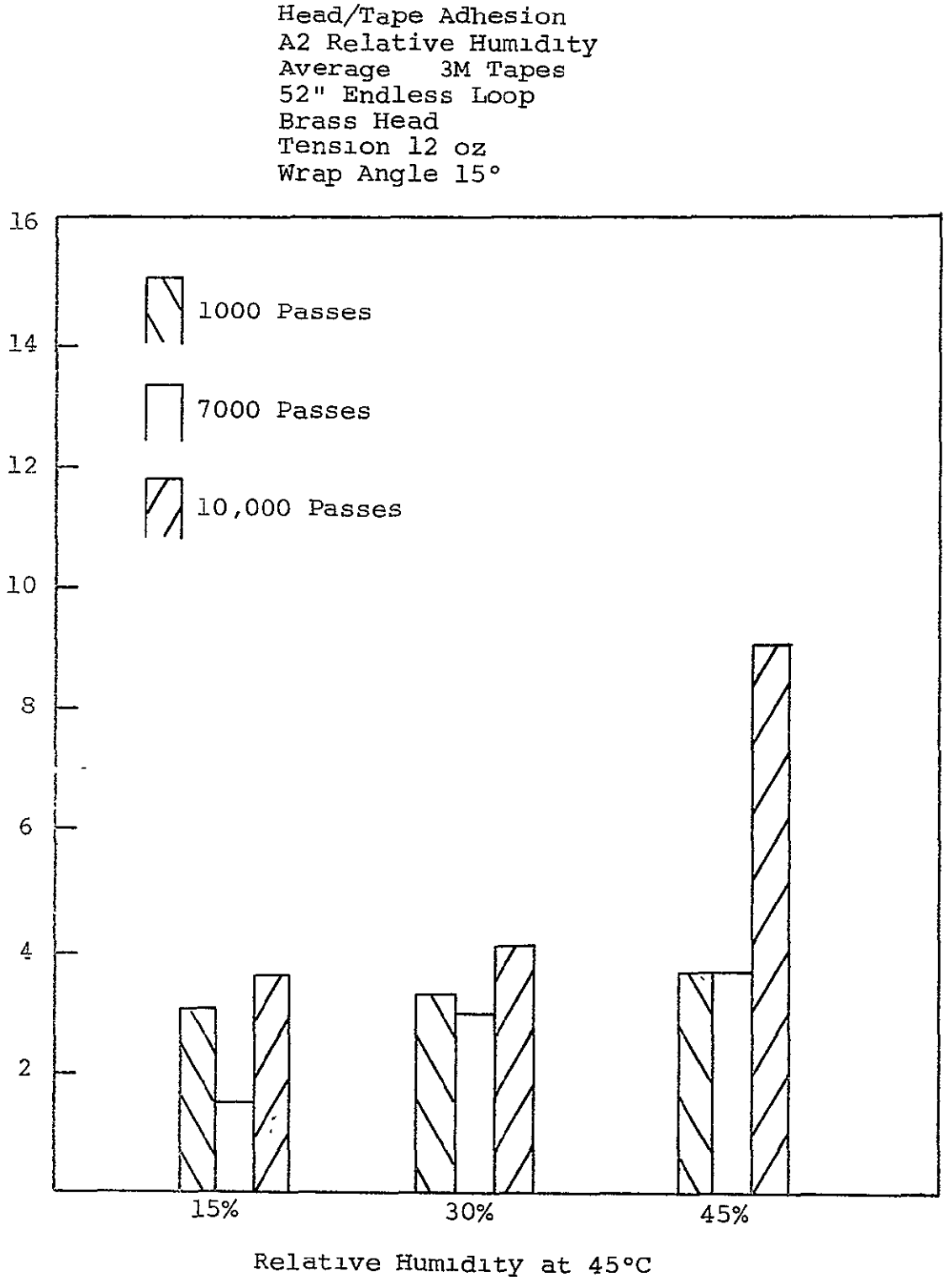

Fig. 24 EFFECT OF RELATIVE HUMIDITY, 3M TAPES

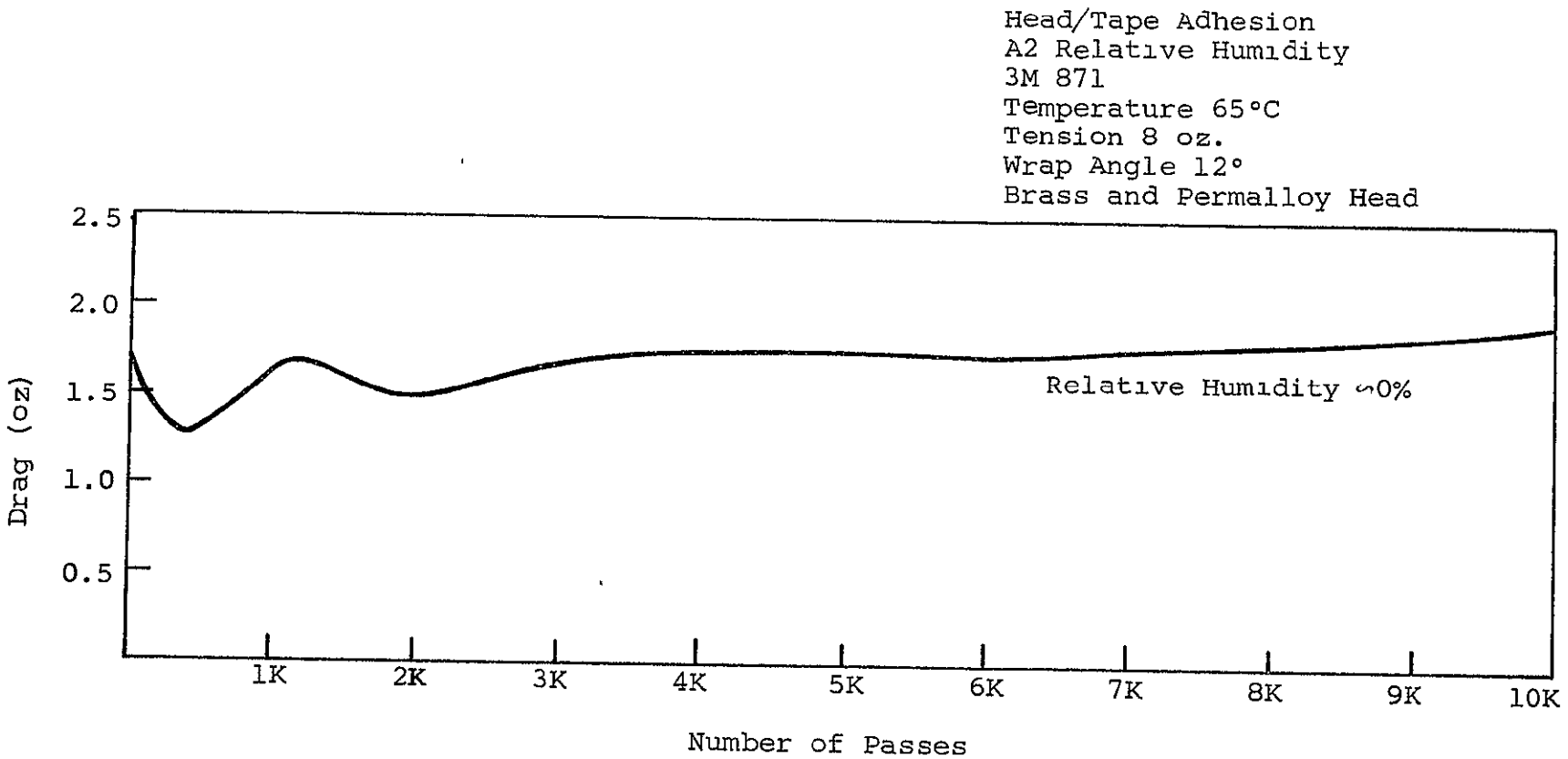

Fig. 25 OPERATION AT LOW HUMIDITY, 3M 871

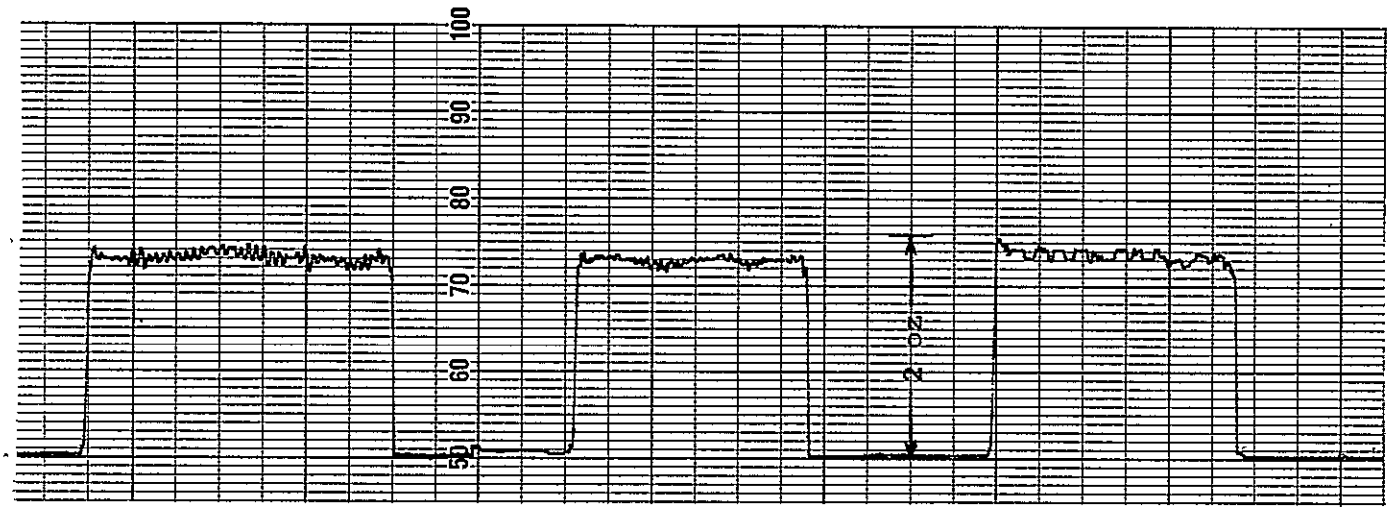

Starting and Running Drag
3M 871
Brass Head
65°C, 0% RH
10,000 Passes

Fig. 26 OPERATION AT LOW RELATIVE HUMIDITY

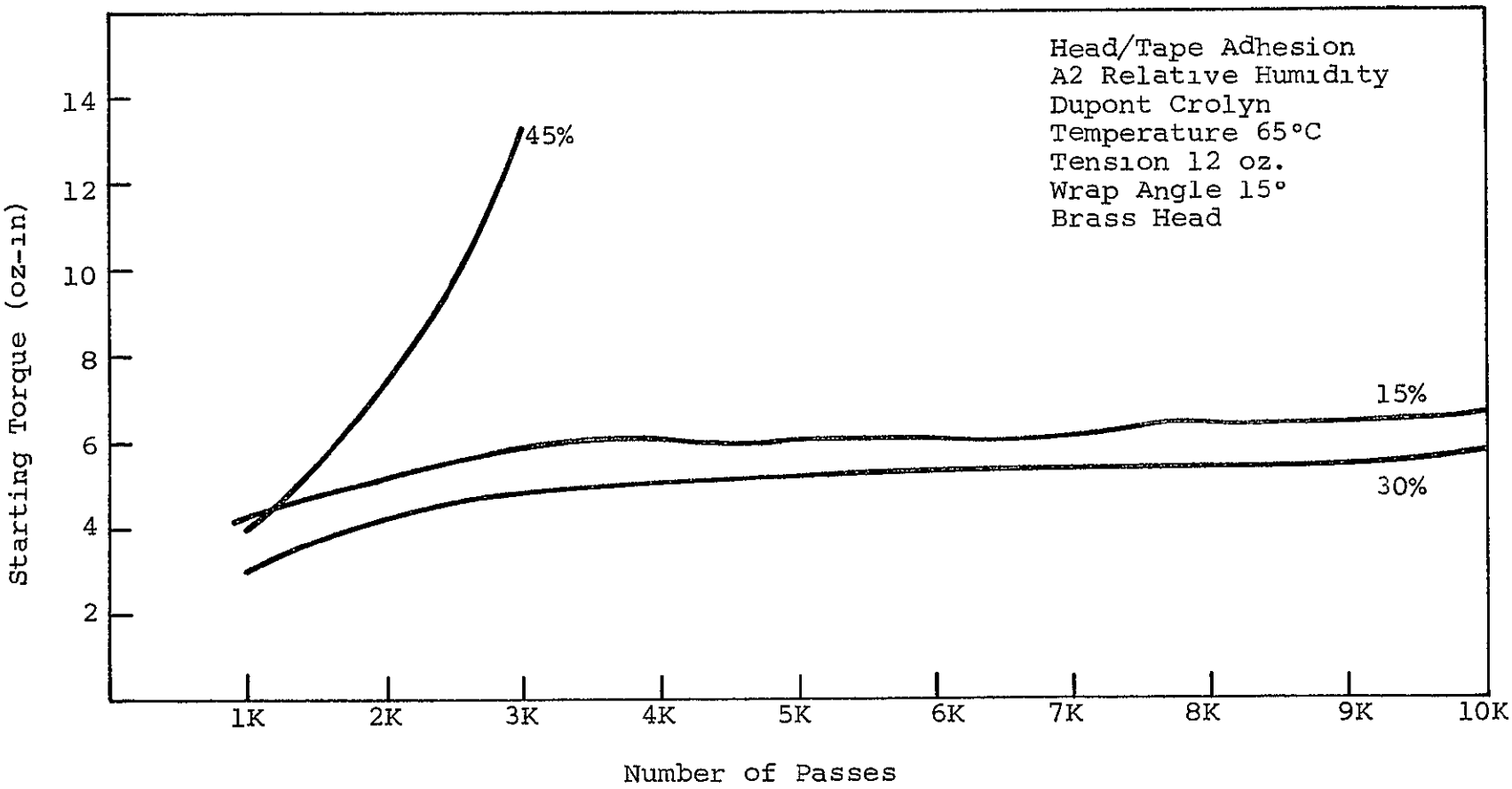

Fig. 27 EFFECT OF HUMIDITY AT 65°C, CROLYN

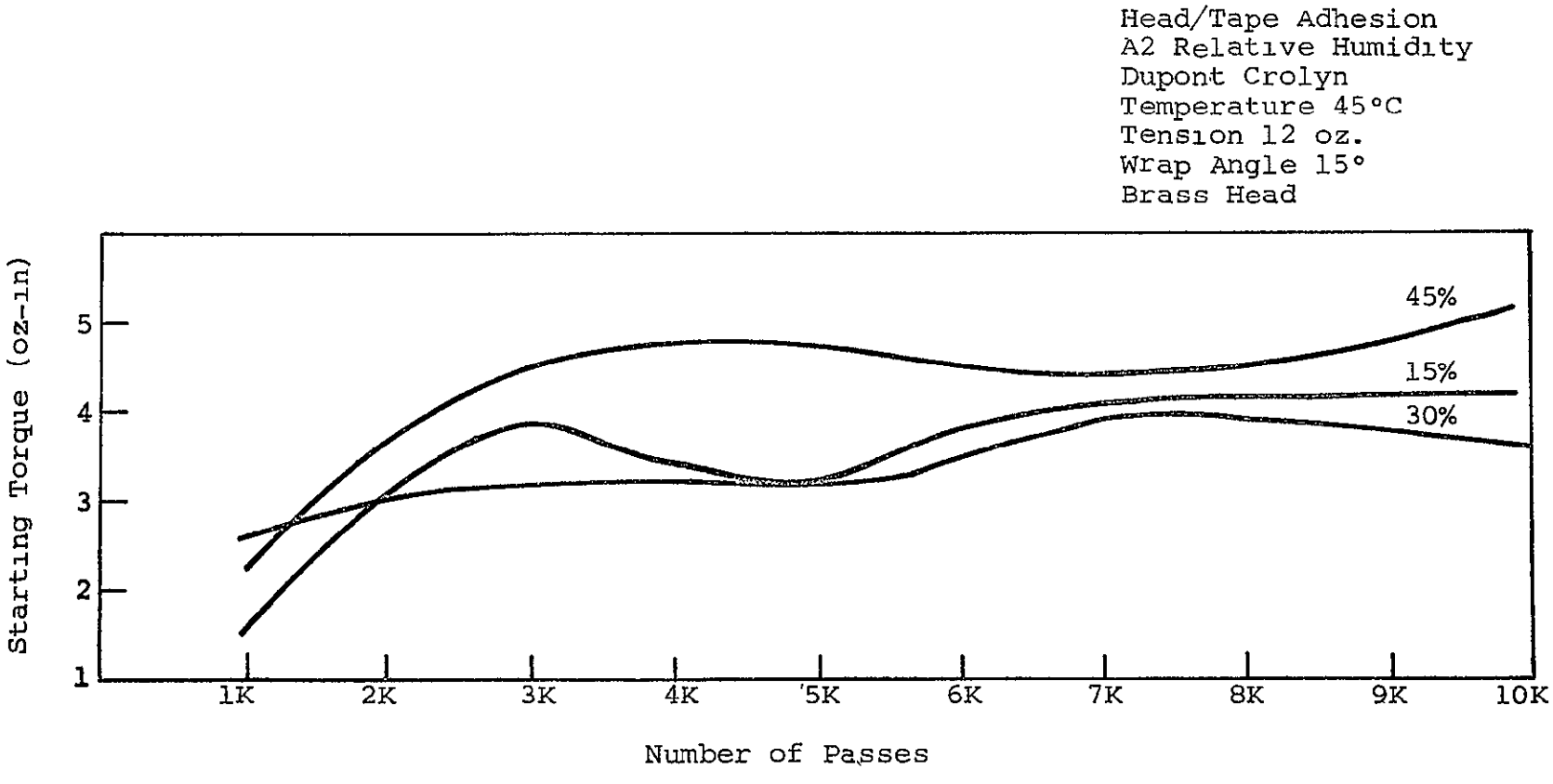

Fig. 28 EFFECT OF HUMIDITY, 45°C, CROLYN

4. Atmosphere

Since most satellite recorders operate in sealed containers, it is unnecessary to run the tape in air. In fact, several manufacturers have traditionally purged the container of air, replacing it with an inert gas, such as nitrogen or argon. Several suggestions were made to improve performance in an inert atmosphere. These mainly center upon the oxidation of either the abraded head surface or the polymeric chain structure of the tape binder system. However, these effects have not conclusively shown to determine head/tape performance, at least on a macroscopic basis. During the testing of this program, very little difference was noted in the frictional drag when various tapes were run in either air or nitrogen environments.

The results of thermal analytical tests run on 3M 888 tape early in the program indicated that the binder system was significantly more stable in an oxygen free atmosphere. Even though the reduced thermal stability observed could be partially attributed to the oxidation of the carbon additive, the relatively good stability in argon suggested the use of an inert atmosphere. This is discussed more thoroughly in Volume III.

However, when tapes were actually run on a reel-to-reel transport in both dry air and nitrogen atmospheres, the frictional drag was only slightly higher for the tape run in air. The differences in performance were not considered large enough to recommend operating air or oxygenated environments. Figure 29 shows the drag measured at 1 ips with Memorex 63L tape and a brass dummy head; ambient temperature of 65°C, tape tension of 8 ounces, and wrap angle of 12° were used for both tests. Following some initial fluctuation in drag during the first 250 passes, relatively constant performance was maintained for several thousand passes. The drag then increased for both tapes, as debris deposited on the heads.

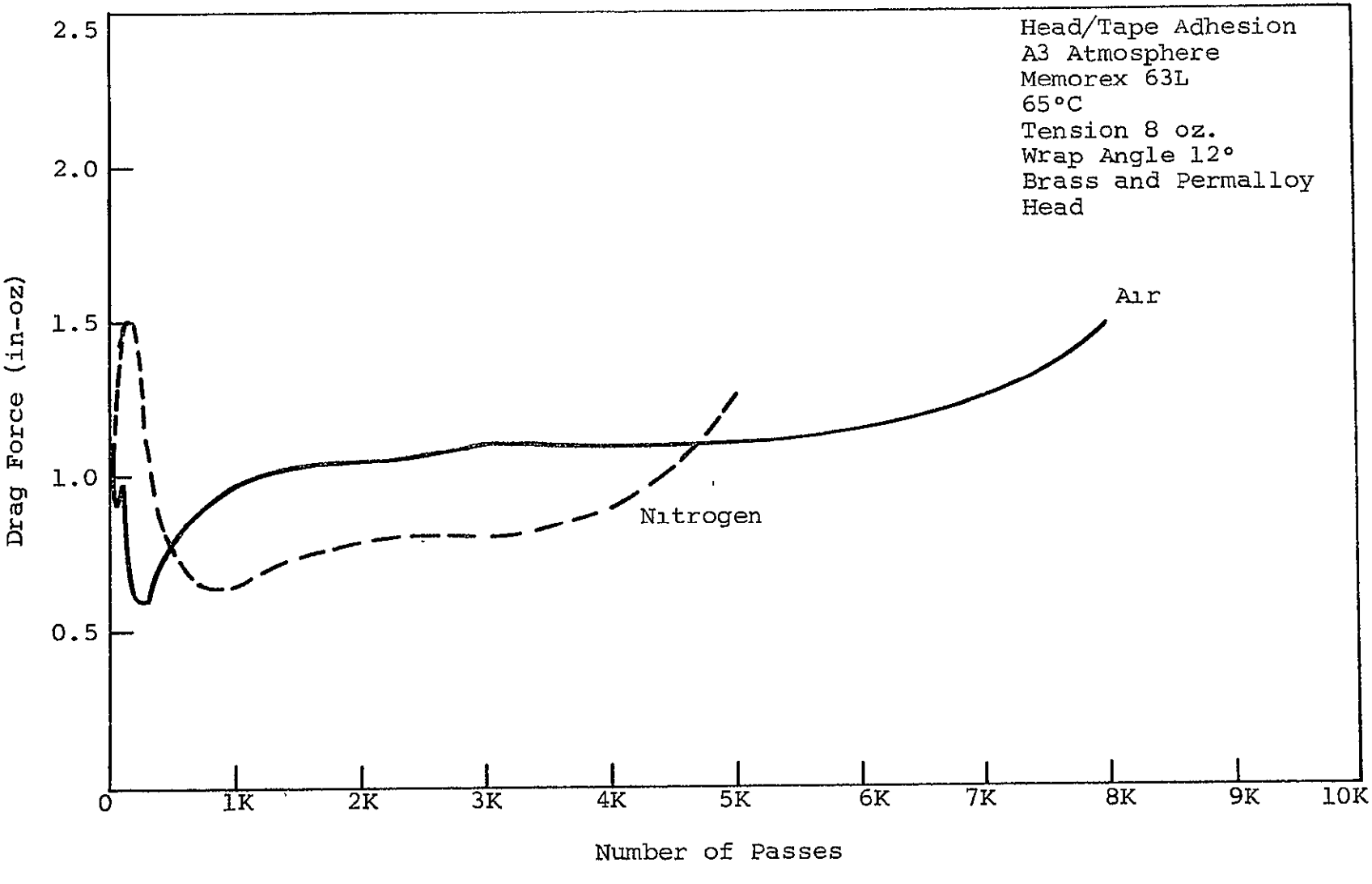

Fig. 29 EFFECT OF ATMOSPHERE, MEMOREX 63L

Similar results were observed with the 3M 351, a polyurethane tape, using an aluminum and alfenol head under the same operational and environmental conditions. The drag force measured were also slightly lower in nitrogen.

Therefore, although the chemical stability measurements indicated a preference for operating in an inert atmosphere, this was not confirmed during the actual tests. In fact, the frictional drag at all tape speeds was slightly better in air. It can only be concluded that no distinct advantage at the head/tape interface was observed by running in nitrogen.

5. Tape Speed

A common operating mode for a satellite recorder has been to record data at a low tape speed for the duration of one orbit, and then to dump that data while passing over a ground receiving station. In the reproduce mode, the tape is often run in reverse at a much higher speed, with a record-to-playback ratio of as high as 64:1.

A variety of effects occur at the head/tape interface with the speed range that has been used, and difficulties have been experienced at both extremes. Because many transports have a mechanical transmission or speed reduction system, less torque is available at the capstan during high speed operation. Further, more energy is imparted to the tape at high speed, although this is not necessarily reflected in head/tape interface problems because of existing air bearings. For cylindrical head profiles, the separation due to air bearings can be approximated by:

$$d = 4.1 \times 10^{-6} \quad R \left(\frac{V}{T} \right)^{2/3}$$

where d = separation in inches

R = head radius

V = velocity in inches persecond

T = tape tension in ounces per inch

This results in approximately 10 microinches of separation with 9 ounces of tension on 1/2-inch tape running at 60 ips.

At low speeds, however, more intimate head-to-tape contact was acheived, and each tape particle was in contact with the head for longer periods of time. Therefore, low speed operation throughout the adhesion portion of the program was emphasized.

One low speed phenomenon commonly known as stick-slip, has been described by Steinhorst[5] as a relationship between the tension and wrap angle, the difference between the static and dynamic coefficient of friction, and the elastic properties of the tape. From these parameters, he computes a critical speed above which stick slip should not be observed. However, his results indicate critical speeds higher than expected from the successful operation of numerous low speed transports.

Although stick-slip was not studied extensively during the program, it was occasionally observed at the low tape speeds, usually in conjunction with tape squeal. The principal factor monitored throughout the program was the variation in frictional drag with tape speed. It was found that, under certain operational conditions, drag did not increase at the very low speeds as had been hypothesized. For example, only small variations in drag were observed between 0.05 and 1.0 ips tape speeds using the 3M 888 and an aluminum head (Fig. 30).

The variation in drag with tape speed for 3M 351 tape run for 10,000 passes at 65°C is shown in Fig. 31. Between 0.2 ips and 20 ips there was little difference in the amount of drag measured, certainly not the increase at the very low speeds that had been hypothesized. However, this test was run after the temperature had been reduced to 25°C. At the elevated temperature, the 0.2 ips drag was 30% above the 1 ips drag.

The overall results of the tape speed tests indicated that several interactions were occuring. In general, increases in drag at the low speeds occurred most often while using brass heads at elevated temperatures. The detrimental effects of brass heads was observed with several tape types, including the Epoch IV tape made by Graham Magnetics, shown in Fig. 32.

Similar results were observed with the 3M 888 tape. Comparing the performance of this tape using brass to aluminum heads, Fig. 33, it was confirmed that the brass head material should be avoided in recorders designed to run a very low tape speeds.

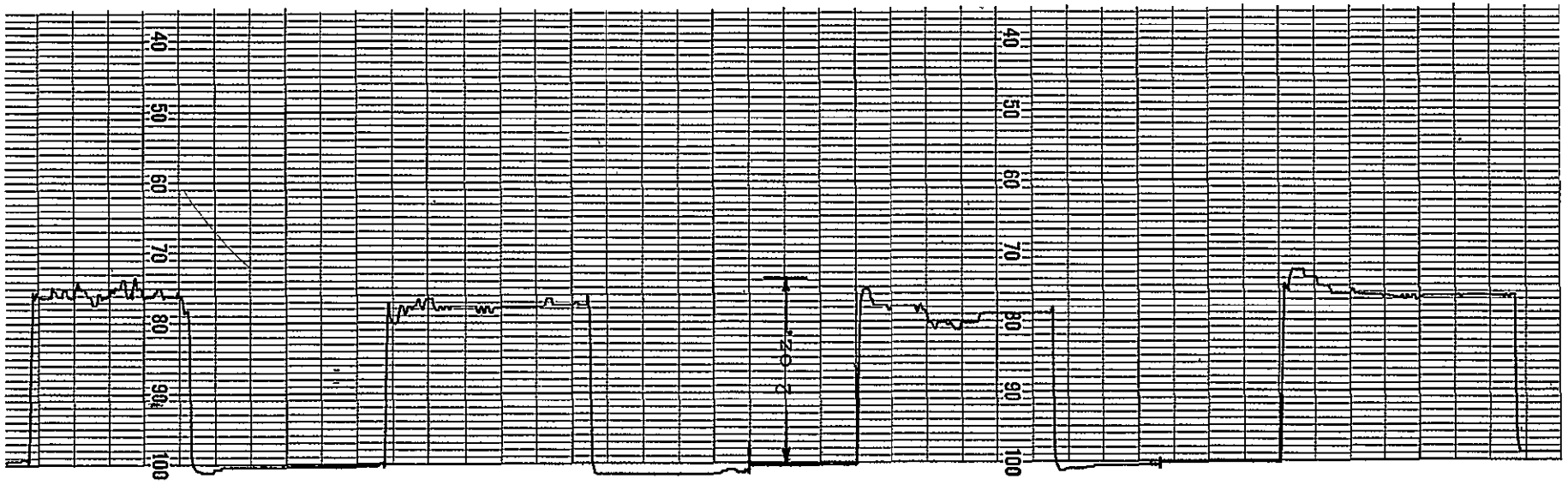

Head/Tape Adhesion
A4 Tape Speed
3M 888
2700 Passes
65°C, 45% RH
Tape Length - 300 Feet

Fig. 30 LACK OF VARIATION IN DRAG WITH TAPE SPEED, 3M 888

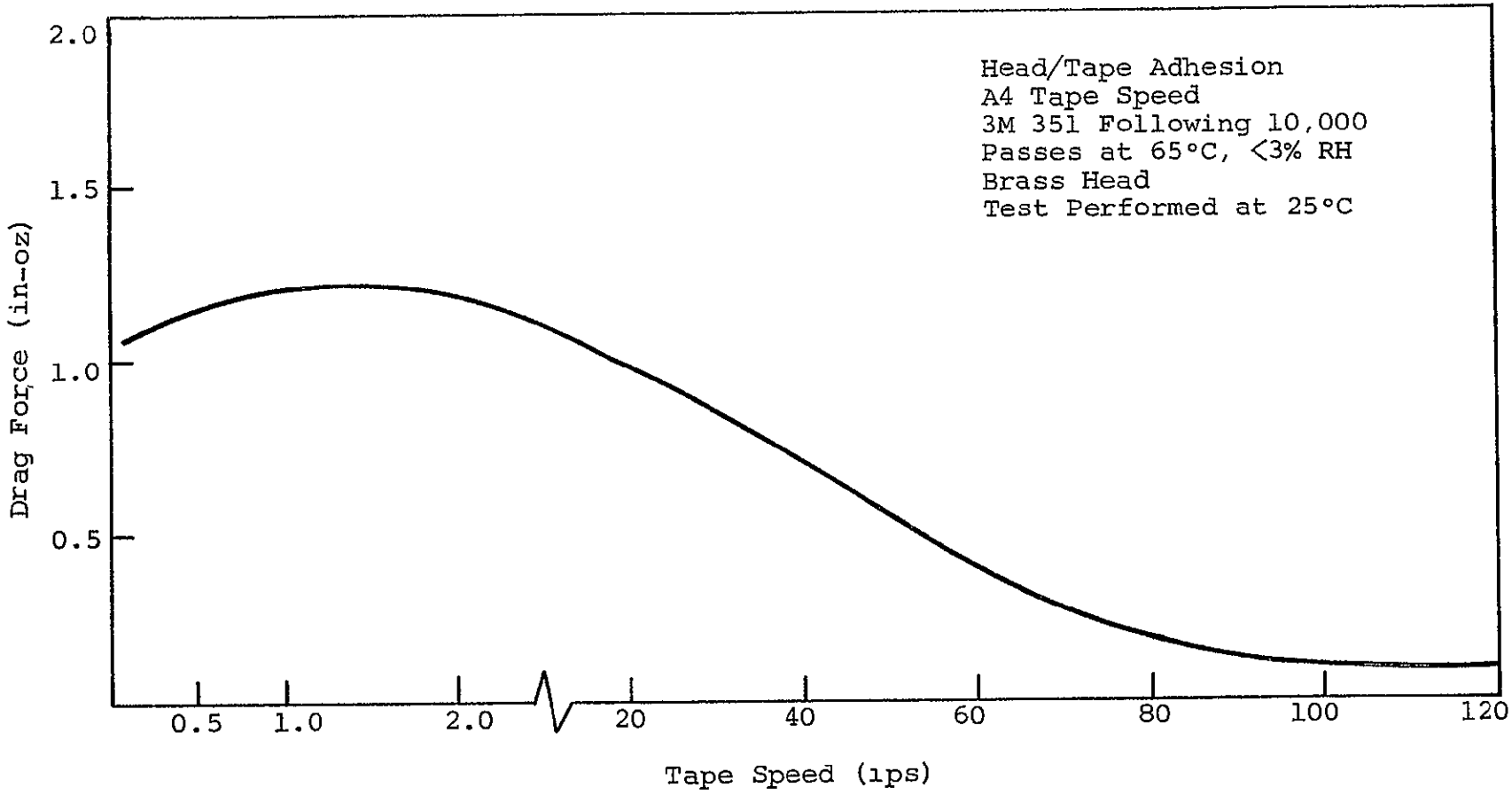

Fig. 31 EFFECT OF TAPE SPEED, 3M 351

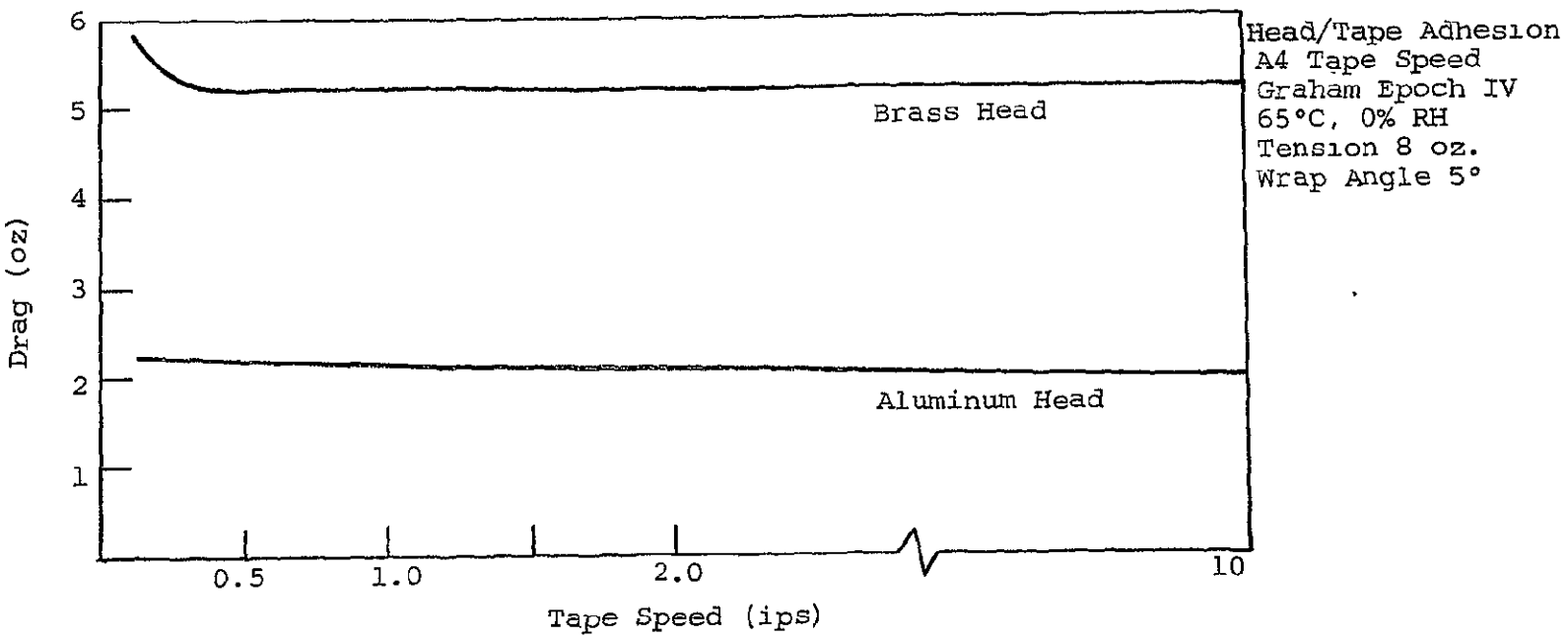

Fig. 32 EFFECT OF HEAD MATERIAL ON LOW SPEED OPERATION

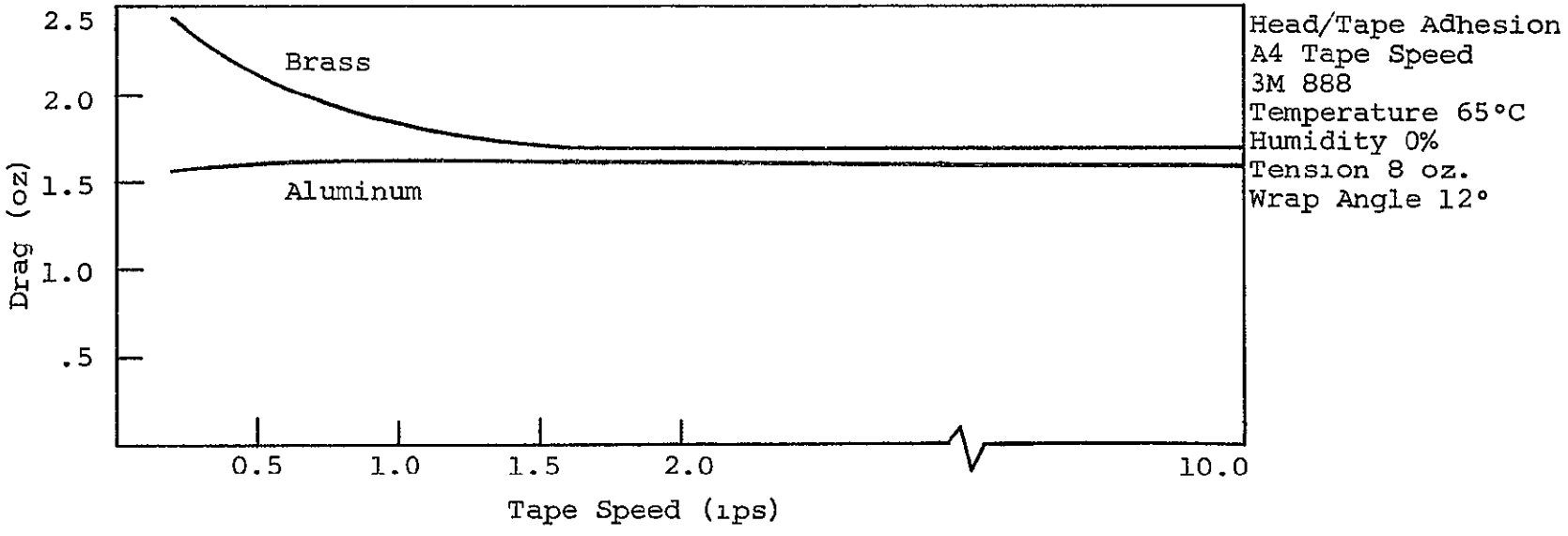

Fig. 33 EFFECT OF HEAD MATERIAL AT LOW SPEED

Increasing the ambient temperature resulted in more pronounced changes in drag at low speeds. For example, the results obtained with Bell and Howell W4 Tape, Fig. 34, showed that the trend of increasing drag at lower tape speeds was reversed at the lower ambient temperature.

The significance of brass heads and higher temperatures and the drag performance at low tape speeds suggested a possible chemical bonding related to the presence of oxygen in the atnosphere. Indeed, comparison of the data taken at various speeds with the Memorex 63L in air and nitrogen did verify a slight relationship with atmosphere. However, the change to an inert atmosphere was not sufficient to eliminate low speed effects, seen in Fig. 35. Further, changing the atmosphere had no affect on drag when it remained constant as the tape speed was lowered.

It was concluded that tape speeds as low as 0.2 ips could be utilized without degrading the adhesion performance, provided the head material was not brass. However, stick-slip was not one of the stated parameters of this program. Since stick-slip was observed at the higher ambient temperatures, tape speeds below 1 ips appeared to be unreliable in this respect.

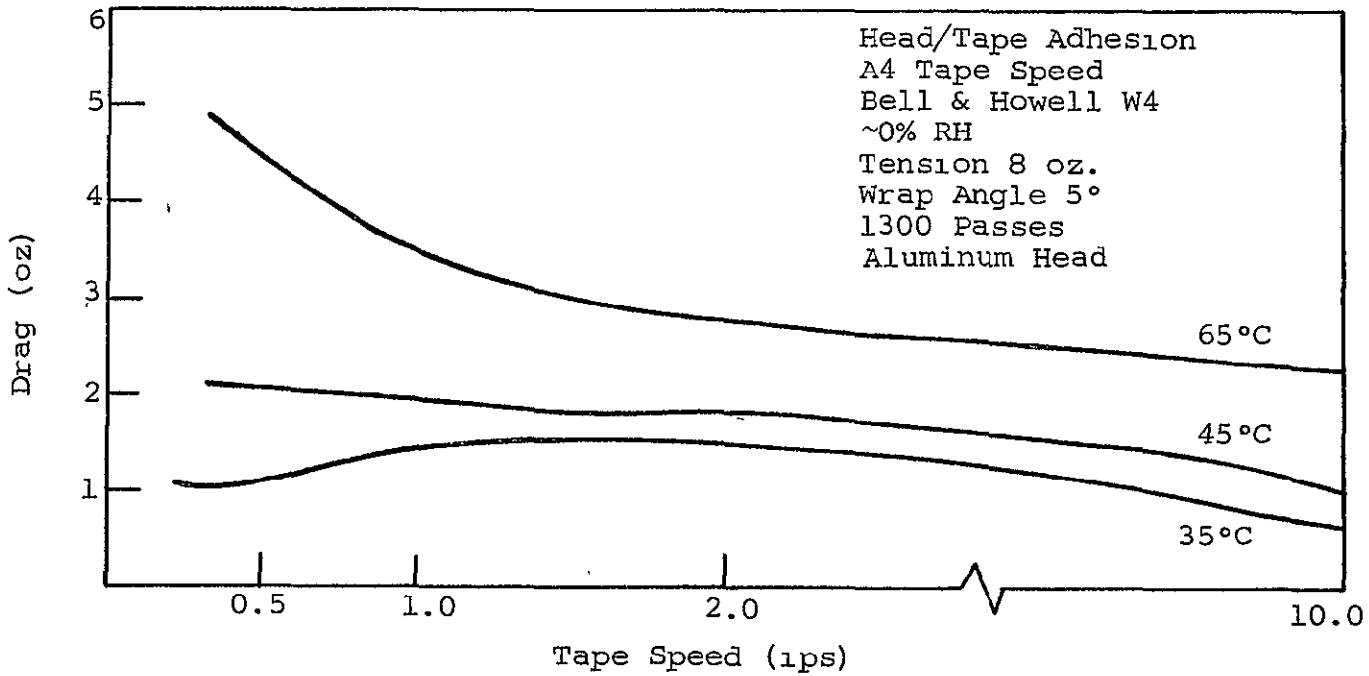

Fig. 34 VARIATION IN LOW SPEED DRAG WITH TEMPERATURE

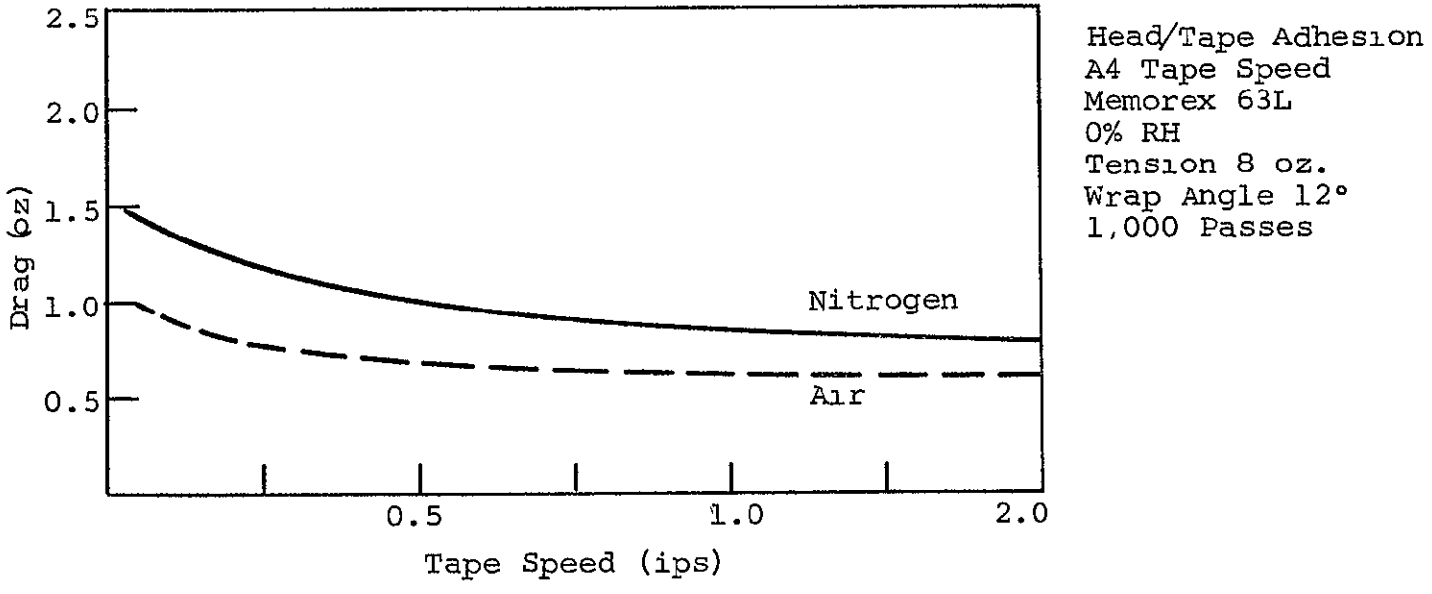

Fig. 35 VARIATION IN LOW SPEED DRAG WITH ATMOSPHERE

6. Bidirectional Operation

Both endless loop cartridges and reels have been used as storage mechanisms in satellite tape transports. One of the operational differences between these two configurations is that the tape in a cartridge slides through the tape pack, causing potential layer-to-layer friction or binding problems. These problems, discussed in detail by Stark[6], were not considered within the scope of the current head/tape interface program.

Another difference between the two configurations more pertinent to the interface was that tape in an endless loop transport passed over the heads in only direction. During Phase I since several reports concerning endless loop satellite recorders operating for a year or longer were received, the question of preference for single direction tape motion became important.

During the adhesion failure analysis tests, the occurrence of adhesion failures was accelerated when the procedures were changed from a single to bidirectional tape motion. Thus the hypothesis that single directiom tape motion was preferred.

Tests conducted with the 3M 888 and Memorex 63L tapes verified the expected degradation, resulting from bidirectional operation. These tests, run on the endless loop transports, consisted of reversing the tape direction every 20 passes for the first 1,000 passes, then every 1,000 passes for the remaining 9,000. Starting and running torque was monitored at each interval; corresponding tests were then run without reversing the tape direction. Motor calibration was obtained by removing the head. The results using the 3M 888 Tape, Fig. 36, indicated that the torque required to start and run the tape in the same direction was both lower and more consistent than when the direction was reversed. Also, continuous running torque was higher for the bidirectional case, although the difference was not as great. It should be noted that the tape

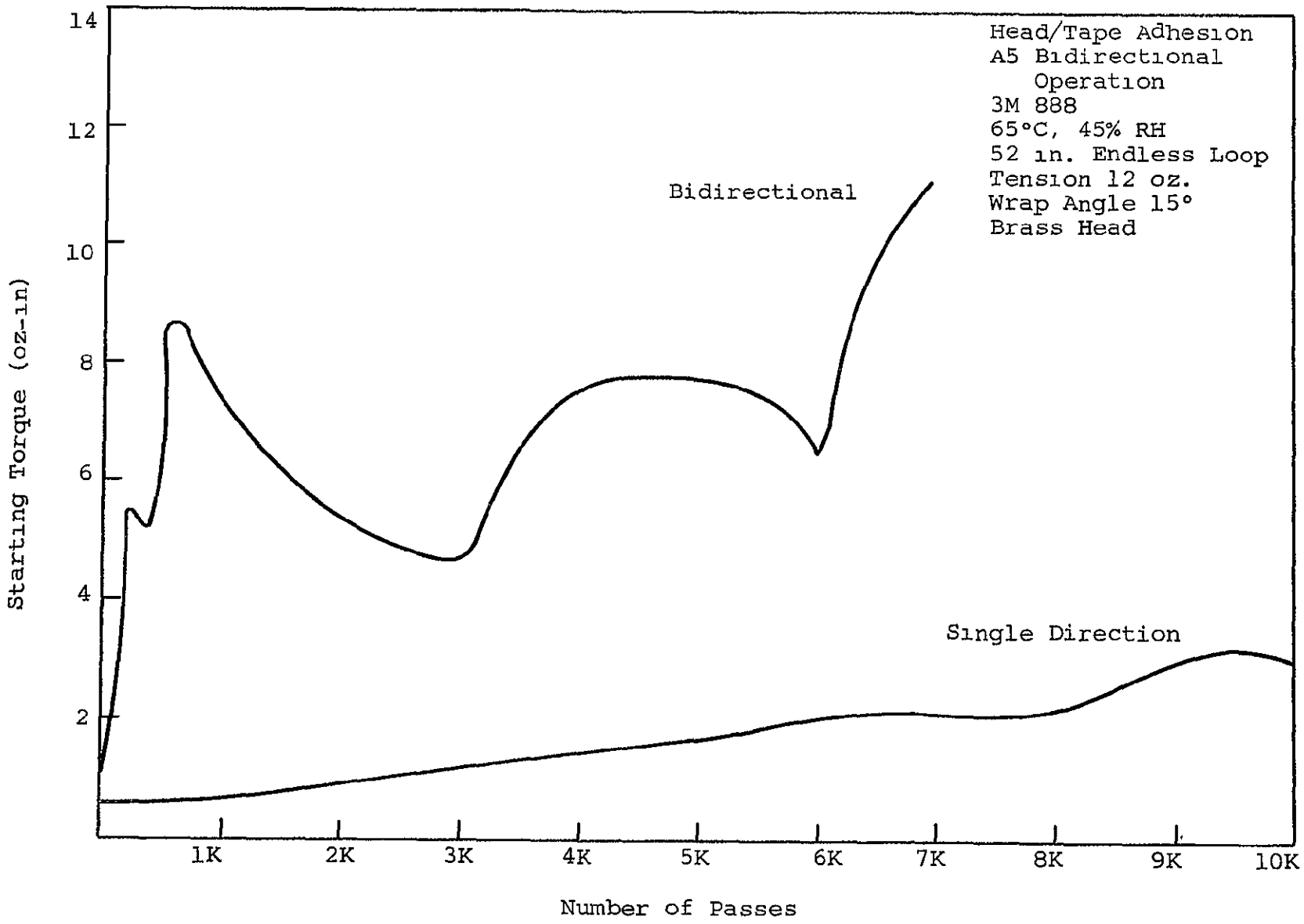

Fig. 36 EFFECT OF BIDIRECTIONAL OPERATION, 3M 888

surpassed the 10 ounce-inch failure definition when operated bidirectionally under the conditions shown.

Subsequent examination of the heads and tapes did not reveal a cause for the difference in performance. Both heads exhibited a fairly heavy brown discoloration, small accumulation of debris, and some scratching. Microscopic examination of the tapes did not reveal any observable differences.

An even stronger preference for single direction operation was exhibited by the Memorex 63L tape, shown in Fig. 37. In tests exhibited to those described above, the starting torque increased rapidly during the first 1,000 passes of bidirectional operation. At 1,000 passes, the tape physically broke at the splice, indicating approximately two pounds of applied force. However, the tape run in one direction only successfully completed 10,000 passes without exceeding 10 ounce-inch of required starting torque.

As with the 3M 888 tests, examination of the heads used for these tests did not reveal any significant differences. However, scanning electron microscope photographs of the tape surfaces, taken in stereo, provided a possible explanation. Numerous surface irregularities were observed protruding outward. These areas had an asymmetrical shape similar to a ramp, resulting in an easy and hard direction for each of the tapes. These ramps adversely affected both the starting and running torque during the bidirectional tests.

A recommendation to restrict tape motion to a single direction would have a serious impact on the reel-to-reel transport configuration often used in satellited. Such a recommendation cannot be justified without substantial verification of the head/tape interface performance, as well as analysis of the endless loop storage mechanism.

A preference for single direction tape motion was established during the program by conducting tests at high

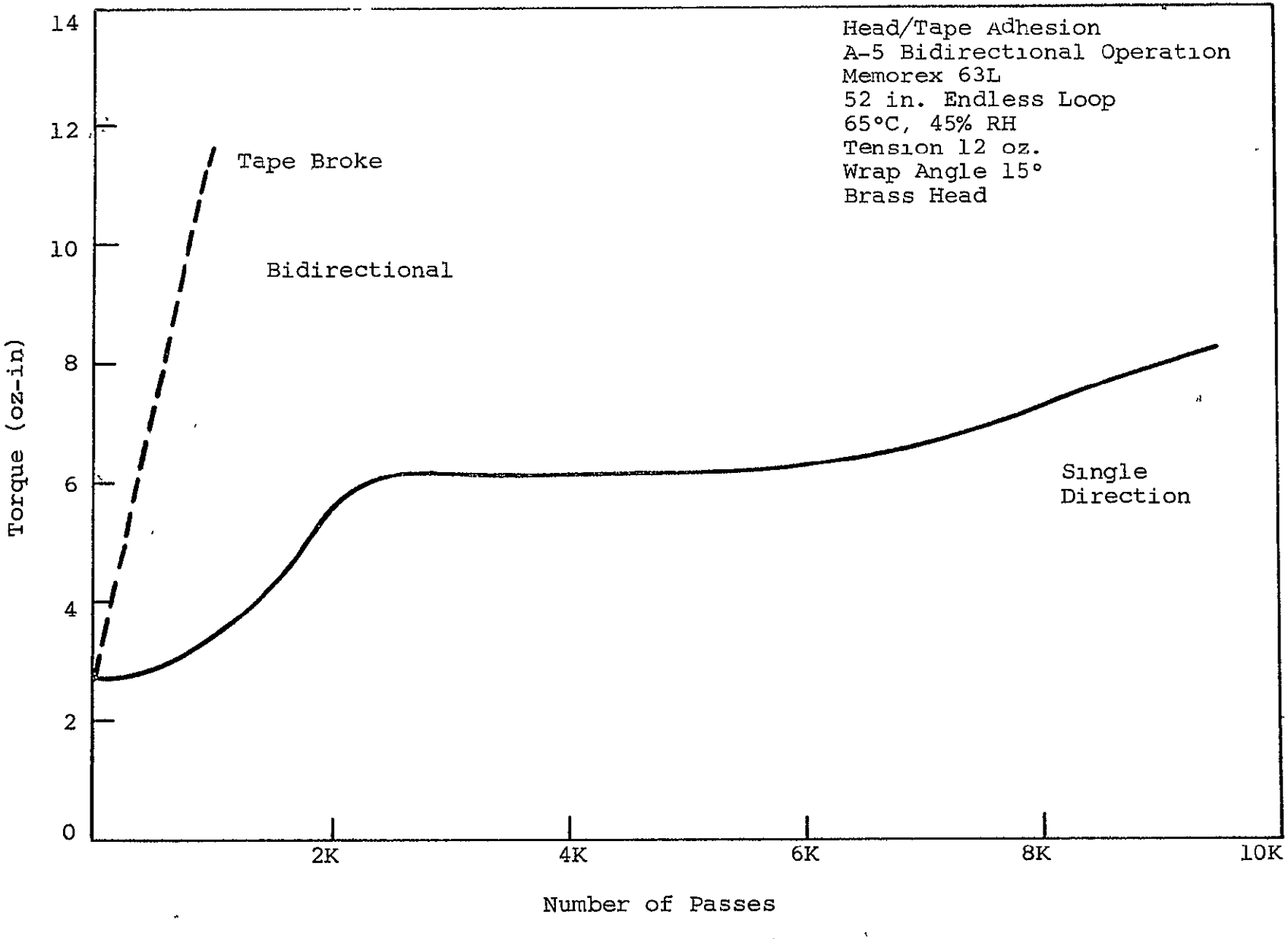

Fig. 37 EFFECT OF BIDIRECTIONAL OPERATION, MEMOREX 63L

temperature and humidity conditions of high tape tension and wrap angle. However, tapes and heads meeting the selection guidelines and used in accordance with the operation guidelines were repeatedly tested bidirectionally without failure.

7. Coating Application

The results of tests run on the endless loop test transports showed differences in the required torque to drive the tape in forward and reverse. This difference was mainly attributed to the single capstan drive configuration and to the tape tension when running in reverse. However, possibly the differences in the tape surface were also a contributing factor. Such differences could have resulted from various steps in the coating application, oxide dispersion, or surface polishing.

A series of tests was conducted on five tape types to determine if the tape itself had a directionality factor. These tests consisted of monitoring the starting and running torque at the beginning and end of 100 passes in the forward direction. The tapes were then physically turned around and the new torque values recorded. Since the direction of initial fabrication could not be assumed from the wind on the purchased reel, a corresponding set of tests was run with the opposite coating direction.

The tests were run initially at room ambient conditions, and no coating directionality could be verified. The minor differences observed were within the experimental measurement error. Therefore, the temperature was increased to 65°C, and a new set of tests was run. Again the data did not reveal significant differences, and it was concluded that the tapes did not exhibit a preferable direction due to manufacturing procedures.

8. Head Pressure

The problems relating to frictional drag and debris all result from the intimate contact required at the head/tape interface. This contact is necessary to fulfill the purpose of a satellite recorder, the storage, and the data recovery. The significant factor in establishing the required pressure is the well known 54-db per wavelength separation loss. In order to maximize the short wavelength reproduce head output, the tape-to-head spacing must be minimized. This can be done by increasing the tape tension and wrap angle or by decreasing the radius of the head profile. The testing objective in this area was the determination of the optimum combination of tension, wrap angle, and head radius to achieve the necessary head pressure.

The initial activity in this investigation was to derive the equations describing the relationships between head pressure and the drag related parameters. This was done by considering a small element of tape at the head/tape contact surface, shown in Fig. 38.

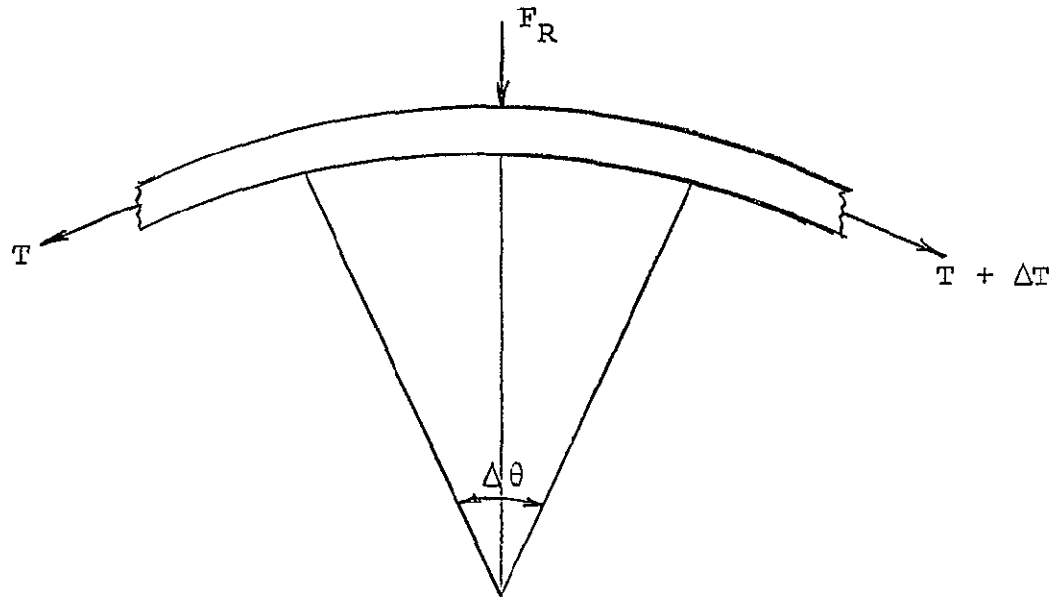

Fig. 38 INCREMENTAL HEAD AND TAPE CONTACT AREA

In this analysis: T = Tension

ΔT = Increase in tension

$\Delta\theta$ = Incremental wrap angle

ΔF_R = Radial force

ΔF_T = Tangential force

Resolving the radial and tangential forces yielded the following:

Radial:

$$\Delta F_R = T \sin \frac{\Delta\theta}{2} + (T + \Delta T) \sin \frac{\Delta\theta}{2}$$

$$= 2T \sin \frac{\Delta\theta}{2} + \Delta T \sin \frac{\Delta\theta}{2}$$

When ΔT and $\Delta\theta$ are small, $\sin \frac{\Delta\theta}{2} \simeq \frac{\Delta\theta}{2}$ and $\frac{\Delta\theta}{2} \Delta T \simeq 0$. Therefore, $\Delta F_R = T\Delta\theta$ .....(1).

Tangential:

$$\Delta F_T = (T = \Delta T) \cos \frac{\Delta T}{2} - T \cos \frac{\Delta T}{2}$$

When $\Delta\theta$ is small, $\cos \frac{\Delta T}{2} \simeq 1$. Therefore, $\Delta F_T = \Delta T$.

The coefficient of friction, μ, was defined as $\frac{\Delta F_T}{\Delta F_R}$ yielding:

$$\mu = \frac{\Delta T}{T\Delta\theta}$$

Rearranging this equation and integrating yields

$$\int_{T_0}^{T_1} \frac{dT}{T} = \mu \int_{0}^{\theta_T} d\theta$$

where T_0 = Incoming tension

θ_T = Total wrap angle

T_1 = Tension at θ_T

This integration results in the relationship

$$\frac{T_1}{T_0} = e^{\mu\theta T}$$

This expression was then substituted into the equation for radial force

$$\Delta F_R = T\Delta\theta = T_0 e^{\mu\theta}\,\Delta\theta$$

After integration, $F_{RT} = T_0\left[\frac{e\mu\theta}{\mu}\right]^{\theta_T}$

giving an expression for the total radial force

$$F_{RT} = \frac{T_0}{\mu}\,(e^{\mu\theta_T} - 1) \qquad \ldots\ldots\ldots(1)$$

The pressure then was computed as the total radial force divided by the contact area

$$P_R = \frac{T_0}{\mu r W \theta_T}\,(e^{\mu\theta_T} - 1) \qquad \ldots\ldots\ldots(2)$$

where r = head radius
w = tape width

Examination of the relationship for total radial force and head pressure lends considerable insight into the interaction of tension, wrap angle, and head radius. First, the drag force is related to the radial force by the coefficient of friction μ; therefore, drag $D = T_0(e^{\mu\theta} - 1)$. Since $e^{\mu\theta}$ roughly approximates $\mu\theta + 1$ for small values, the drag is nearly directly proportional to tension and wrap angle. However, making the same approximation in the expression for head pressure indicates that it is nearly independent of wrap angle. Thus, increasing the wrap angle changes both the total radial force and the contact area, resulting in approximately constant head pressure. Increased radial force beyond the immediate region of the head gap increases the frictional drag generated without improving the wavelength response. Therefore, additional head pressure should be obtained by changes in the head radius or tape tension rather than wrap angle.

A series of tests was conducted using various tensions, wrap angles, and radii to verify the mathematical relationships and determine the effects of each parameter on tape degradation. The levels of the independent variables were as follows:

Independent Variable	Level		
	A	B	C
Tension, ounces	4	8	12
Wrap Angle, degrees	2	5	8
Head Radius, inches	0.125	0.25	0.50

To reduce the number of required tests, one-third of the full factorial experimental design was run. The nine combinations were as follows:

Test No.	Tension	Wrap Angle	Head Radius
1	4	5	1/8
2	4	2	1/2
3	4	8	1/4
4	8	5	1/4
5	8	2	1/8
6	8	8	1/2
7	12	5	1/2
8	12	2	1/4
9	12	8	1/8

The tests were run at 45°C and nearly 0% relative humidity using aluminum dummy heads. 3M 871 tape was shuttled back and forth at 30 ips with drag measurements made periodically at several speeds. Head wear and debris accumulation was measured at the conclusion of 10,000 passes.

Typical data for these tests are shown in Table III. The results shown are for the center values of the independent variables, i.e., tension of 8 ounces, wrap angle of 15°, and head

Table III

SAMPLE TEST RESULTS, HEAD PRESSURE

3M 871, Aluminum Head No. 19, Test No. 4

Tension	8 oz.	Temperature	45°C
Wrap Angle	5°	Relative Humidity	0%
Head Radius-1/4 in.		VRC No. 2	

Measured Drag Force (oz.)

No. of Passes	Tape Speed (ips) 0.5	1.0	2.0	10	30
0	.534	.534	.56	.583	.583
200	.462	.487	.487	.512	.534
1200	.487	.487	.534	.56	.583
2480	.487	.56	.608	.631	.68
3730	.534	.534	.608	.68	.705
4930	.608	.688	.631	.705	.73
5340	.608	.608	.631	.68	.73
7700	.583	.68	.705	.73	.73
8950	.631	.68	.705	.752	.752
10,200	.652	.652	.705	.752	.752

Debris Accumulation: 116 μgram

Head Wear: Center 200 μin.
Edge 1.575 mil

radius of 0.250 inches. The first 200 passes was considered the breakin period, after which the heads were cleaned.

From the measurements of drag force, it was possible to compute a value for the coefficient of friction using the relationship $D = T_0(e^{\mu\theta} - 1)$. The average value of μ at 1 ips for the nine tests was 0.327 with a deviation of less than 15%. Considering the broad range of the independent variables examined, the direct relationship between drag and total radial force was excellently confirmed. Figure 39 shows that even the approximation, discussed above, relating the measured drag to the predetermined tension and wrap angle ($D\mu T\theta$) was verified. No relationship was seen between drag and the computed head pressure. For example, test 5 consisted of parameters yielding a low total radial force, but high head pressure. The drag was found to be low. Therefore, it was concluded that frictional drag could be predicted from the equation for total radial force and not be dependent upon head pressure.

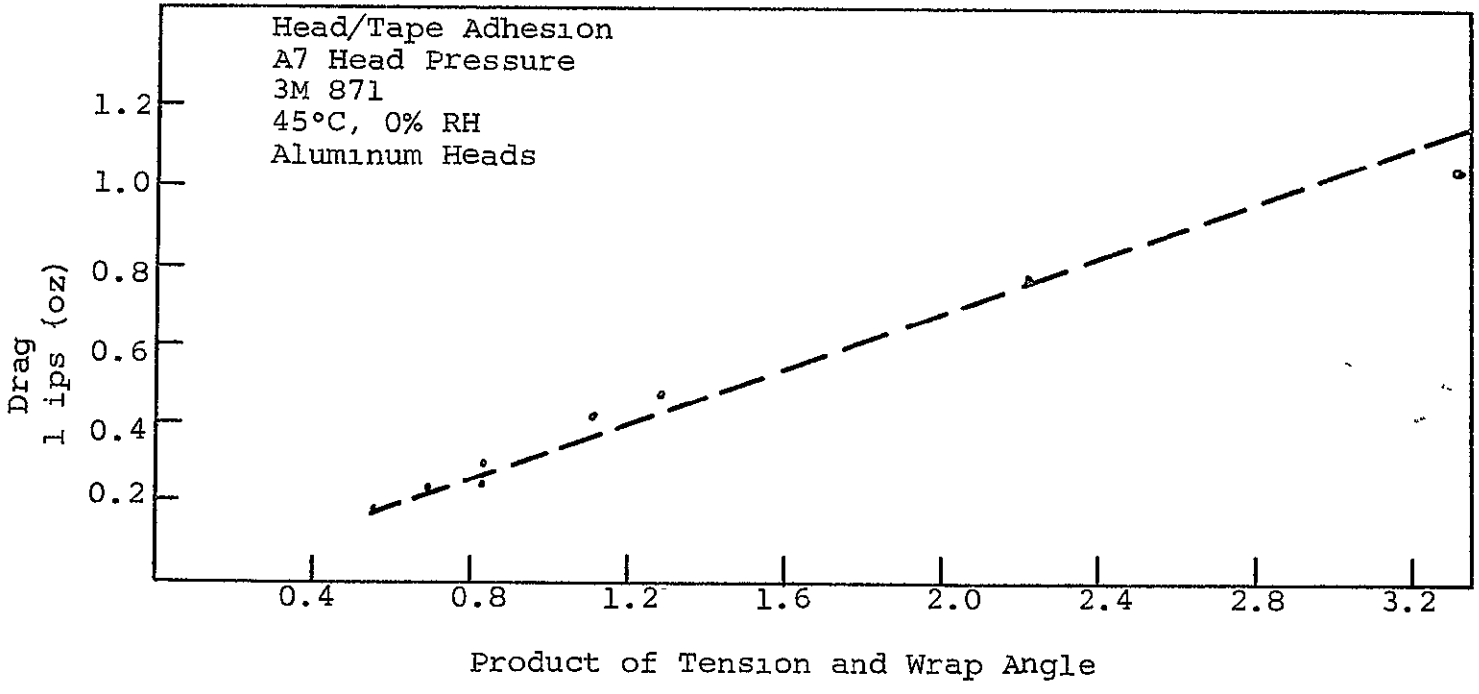

Fig. 39 APPROXIMATION OF TOTAL RADIAL FORCE

9. Tape Tension

In conjunction with the previous section relating frictional drag to radial force, it was also hypothesized that tape degradation increased more rapidly at higher tape tensions. Tape degradation was expressed in terms of the ratio of measured drag at the conclusion of 10,000 passes to the drag at 200 passes. At the 1 ips tape speed, this ratio ranged from 0.888 (drag was lower at 10,000 passes) to 1.753. A summary of the results is shown in Table IV.

The ratios computed for tape degradation could be roughly divided into three groups. These groups correlated more strongly with head radius than the other parameters, such as tension, radial force, pressure, or contact area. In general, the lowest ratios of final-to-initial drag were encountered with the 1/8-inch radius heads. The final test (12 oz, 8°, 1/8 in.) was an illustrative example, as it included the highest tension, radial force, and head pressure. However, the percent of increase in drag was one of the lowest observed.

Overall results of these tests clearly showed improved adhesion performance when small wrap angles and head radii were used. From the point of view of both initial drag and increases in drag, higher head pressure at the gap line should be obtained by increasing the tension, rather than the wrap angle. Constraints on the allowable tape tension are discussed in Section III.C, Mechanical Tape Handling.

Table IV

TENSION, WRAP ANGLE, HEAD RADIUS TESTS

Tape Tension (oz)	Wrap Angle (degrees)	Head Radius (in)	Radial Force (oz)	Head Pressure (oz/in^2)	Drag (200 Passes) (oz)	Drag (10,600 Passes) (oz)	Degradation Ratio
4	5	1/8	0.698	64	0.218	0.193	0.888
4	8	1/4	1.12	32	0.437	0.487	1.11
8	5	1/4	1.39	64	0.49	0.655	1.44
8	2	1/8	0.56	128	0.154	0.220	1.42
8	8	1/2	2.23	32	0.777	1.26	1.625
12	2	1/2	0.84	48	0.295	0.52	1.75
12	2	1/4	0.84	96	0.246	0.246	1.0
12	8	1/8	3.35	192	1.06	1.14	1.08

10. Tape Wear

Results of the majority of tests run during the program showed increasing frictional drag as the number of tape passes increased. The results were accentuated by operating at higher environmental temperatures and tape tensions, and also at a more rapid increase for some tapes than others. However, the general hypothesis that adhesion increased with tape wear was repeatedly verified.

One mechanism causing changes in the drag measurement was the accumulation of oxide/binder debris on the surface of the head. Therefore, debris alone, rather than changes to the tape, was considered the possible principal contributor to increased drag. A test was run using 3M 888 tape on the reel-to-reel transports at 65°C and 45% RH.

Conditions similar to the earlier endless loop tests were used, i.e., a brass head, 8 ounces of tape tension, and a 12° wrap angle. As was expected from the loop tests, an adhesion failure occurred in that the starting drag reached 14.5 ounces after 2247 passes. A strip chart recording of both the starting and running drag measurements is shown in Fig. 40. At this time the head was removed and replaced by a relapped head of identical dimensions and material.

After restoring the environmental conditions, the test was restarted and the frictional drag was found to be approximately the same when measured at the inception of the test. However, within 60 passes the drag had increased to 17 ounces, a figure higher than the first failure. The rate of degradation had clearly increased due to tape wear.

In other tests conducted to determine the effect of wear on the tape, comparative measurements of the surface finish were made for new and used tapes. These measurements were made using a Bendix Proficorder at low stylus pressures. Those tapes that

Head/Tape Adhesion
3M 888
A9 Tape Wear
65°C, 45% RH

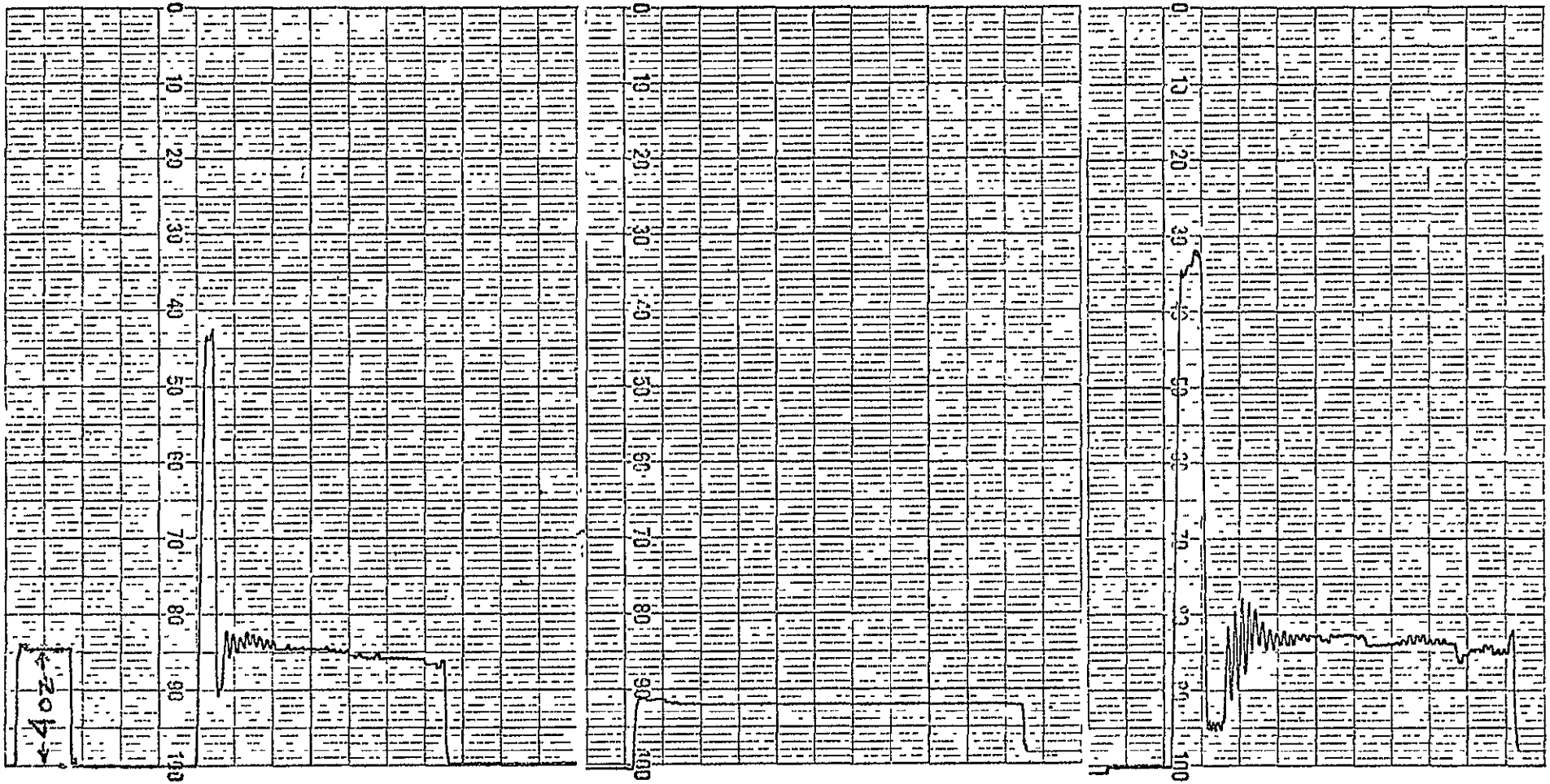

Start at 1 ips
2247 Passes
F_D = 14.5 oz.

Start at 1 ips
2248 Passes
Brass Head Replaced
F_D = 2 oz.

Start at 1 ips
60 Passes Over
New Head
F_D = 17 oz.

Fig. 40 RESULT OF TAPE WEAR, 3M 888

failed the endless loop adhesion tests exhibited substantial increases in surface roughness.

Figure 41 shows the strip chart recordings of surface finish for the new and used 3M 777 tape. Similar measurements are shown in Fig. 42 for the Memorex 63L. The used samples were taken from endless loops that failed during the 65°C, 45% RH temperature tests. After 9,000 passes with the 3M 777 and 3,900 passes with the Memorex 63L, both tape surfaces were considerably roughened.

The irregularities of the two used tape surfaces were somewhat different after use. The 3M 777 tape exhibited broad protrusions, almost belonging in the wavy category. The asperities in the Memorex tape, however, were much sharper and more frequent. These may have been the ramps discussed earlier on failure mechanisms. The short wavelength, microfinish amplitude did not change in wear with either tape.

The other possible effect of wear was a chemical change in the binder polymer. Indications of such a change were found for one tape, but not in the other. The results, discussed in Volume III, were obtained by comparing gas chromatograms of the new and used binders. Differences were found, but an attempt to analyze the change using a mass spectrometer was inconclusive due to lacking specific information of the original binder polymer.

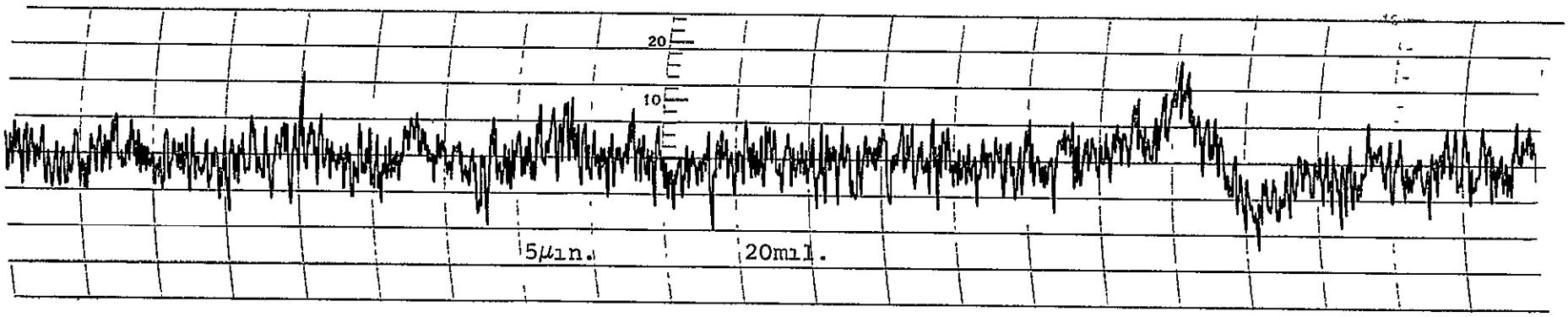

a. New Tape

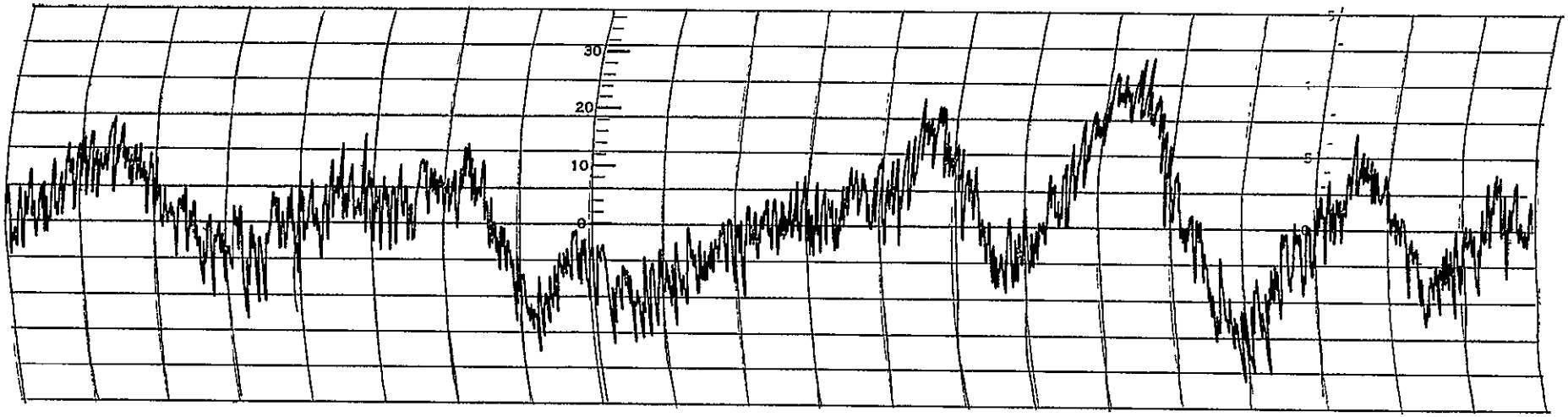

b. Tape Run 9,000 Passes

Fig. 41 DEGRADATION OF SURFACE FINISH WITH WEAR, 3M 777

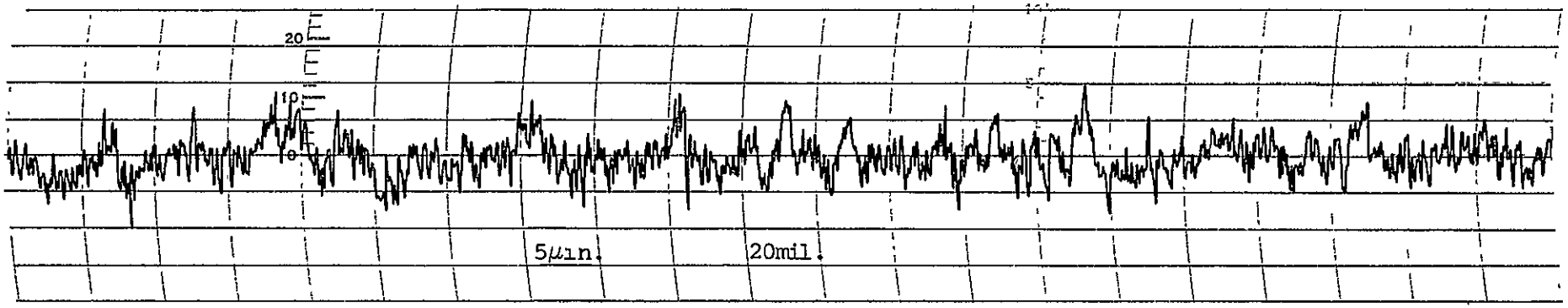

a. New Tape

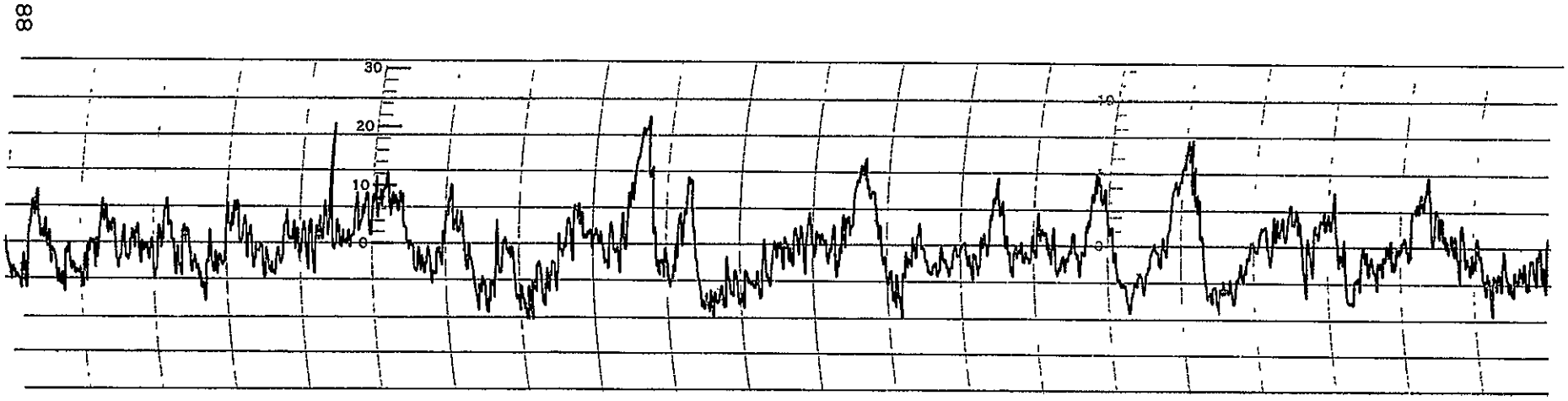

b. Tape Run 3,900 Passes

Fig. 42 DEGRADATION OF SURFACE FINISH WITH WEAR, MEMOREX 63L

11. Relaxation Time

The hypothesis that adhesion increased with a decrease in time between passes evolved from two reasons. First, considerable speculation, concerning a possibly high localized temperature rise at the interface, was encountered during Phase I. This heat, caused by frictional drag, would be dissipated with time. Secondly, chemical bonding was evidenced during the failure mechanism tests. Chemical changes, as indicated following tape wear, were potential precursors to this bonding. However, if these changes were reversible or could be neutralized, e.g., by oxidation, a minimum recovery time would be envisioned.

The measurement of local temperatures for very small, moving particles was considered a difficult task and not attempted during the program. Since a 20°C change in ambient temperature caused dramatic changes in drag, any friction generated heat was not the predominant temperature factor. One test was conducted, however, to eliminate very high partial temperatures from consideration. The DuPont Crolyn tape, containing chromium dioxide as the magnetic particulate media, was prerecorded and then run for 43,200 passes at 65°C. Because chromium dioxide has a Curie temperature of 127°C, those particles reaching that temperature would lose their magnetic properties. A 150-microinch wavelength was recorded to maintain a good signal to noise, and still retain most of the recorded information near the surface of the oxide.

The reproduced output after 43,000 passes at 65°C was 2.0 db below the initial value. The comparative result using a control tape at 20°C was also a 2.0 db reduction. Therefore, the signal loss was attributed to mechanical working effects, rather than temperature. Equipment limitations and possible substrate effects prevented the running of this test at temperatures closer to 127°C.

A test was also run on the endless loop transports when the time between passes was small. Two tape lengths were used,

48 inches and 64 inches, to change the revolution period at the same tape speed. The running torque, shown in Fig. 43 was found to be higher for the shorter tape loop, indicating that a time effect occurred at 65°C.

This effect was also observed using two tape speeds when a greater range of intervals could be attained. At 65°C a comparison of 1 and 30 ips (52 and 1.73 seconds per revolution, respectively), showed an increase of up to 2:1 in drag at the upper speed. However, the 52-second period resulted in drag similar to the 64-inch loop (2.13 seconds). No improvement was observed by increasing the time between passes from 2 to 52 seconds. At 45°C the effect was not observed.

Most transport configurations using a single head do not subject the tape to interfacial conditions within a two-second period. One possible condition is immediately following tape reversal, however, it is difficult to isolate the effects of bidirectional operation in this case. A more important condition is the multiple head recorder where the transit time between heads can be very short. The results of these tests indicate that using only one head both to record and playback is preferred. However, the effect was observed only at high temperature using large wrap angles, and was not found to be an important restriction under more reasonable conditions.

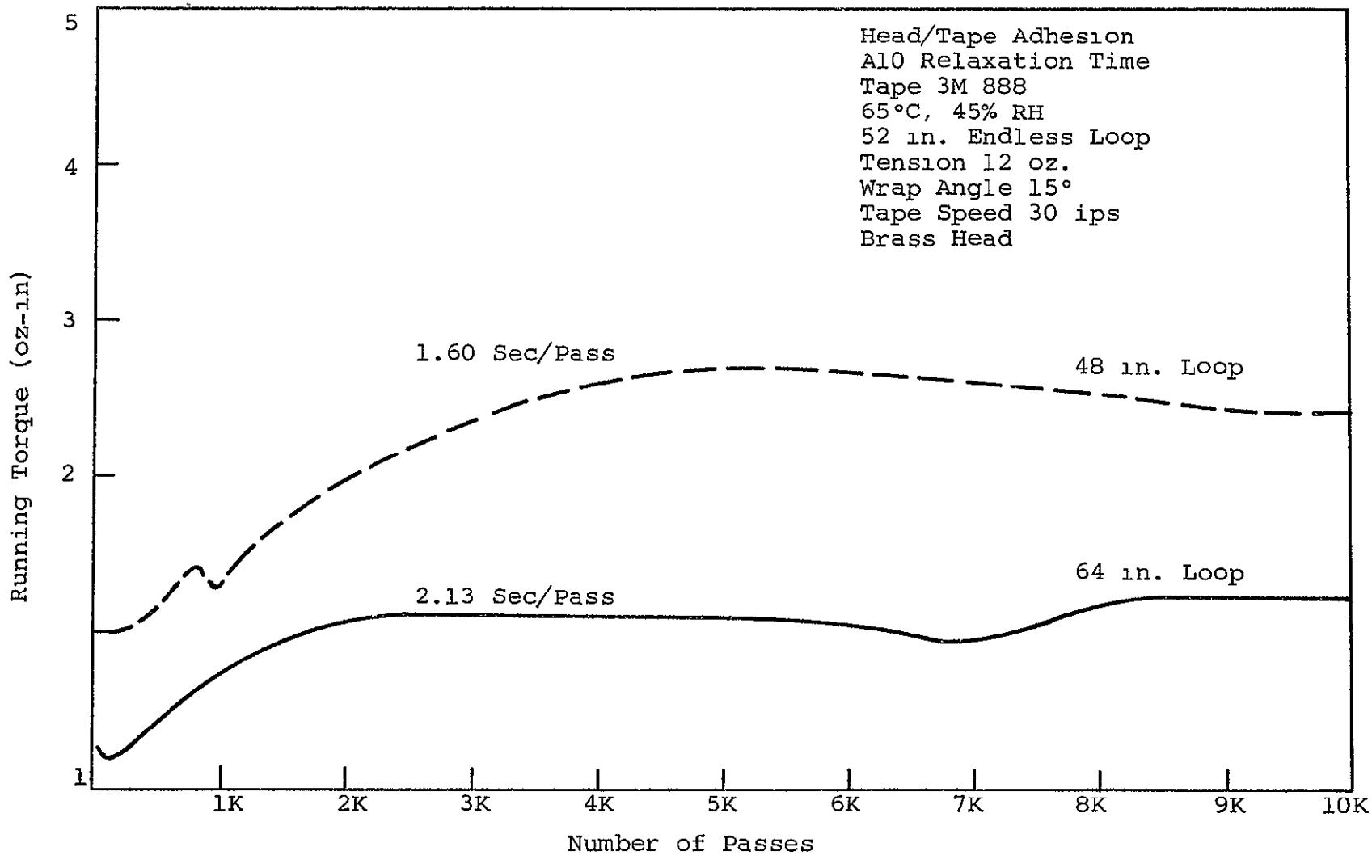

Fig. 43 EFFECT OF TIME BETWEEN PASSES

12. Tape Binder Formulation

Selecting magnetic tape for a satellite recorder has been accomplished without specific information, regarding either the chemistry or processing techniques used, from the tape manufacturer. This information has been unavailable because of the highly competitive nature of tape manufacturing and the adequate performance of tape produced for the high volume, terrestrial applications. However, prolonged, unattended use of the same tape types in satellites resulted in the problems that led to this program.

Early in Phase II the tape types selected for extensive testing throughout the program were submitted to chemists for analysis. Obtaining a complete chemical analysis of the cross-linked polymers used in tape binder systems was difficult. Such analyses often require prior data for comparison, such as with the infrared spectrograms. Further, the binder systems were found to be complex mixtures of several organic materials, requiring separation prior to identification. However, substantial information regarding the binders studied was determined thereby allowing good characterization of the tapes for tests to isolate the various chemical parameters. Details of the chemical analysis are reported in Volume III.

One result of the chemical investigations was the analysis of the basic polymer used in each of the tapes evaluated. A summary of these binders is in Table V. The binder polymers for several of the tapes were quite similar, particularly for different tape types produced by the same manufacturer. The polyurethanes found in the 3M tapes, for example, exhibited nearly identical infrared spectrograms. The chemical differences between the 3M tapes were found in additive contents. Further differences probably existed in coating or surface finishing techniques; however, these parameters were not easily recognizable in the final product.

Table V

I. R. IDENTIFICATION OF BINDER CONSTITUENTS

Tape	Binder Characterization (Absorption peaks)	Aromatic (aliphatic) Compt's (Absorption peaks)	Carbon - Oxygen (Absorption Frequencies)	Lubricant (Absorption Peaks)
3M 888	Polyurethane based (PUB) NH3300 cm^{-1} NH bend - CH stretch· 1535 cm^{-1} C=O amide stretch: 1700 cm^{-1}	Aromatic Components 825 cm^{-1} out-of-plane wag, 2 adjacent H 850 cm^{-1}· subst'd ring 3040, 3120 cm^{-1}: arom abs	Ester carbonyl, C=O 1730 cm^{-1} C-O stretch. 1230 CH_2-C=O 1420 C-C-O 1225	Organo-polysiloxane Si-O-Si 1020 and 1085 cm Si-CH_3 800 and 1270 cm^{-1}
3M 777	Polyurethane based NH 3300 cm^{-1} NH bend - CH stretch· 1535 cm^{-1}	Aromatic components: 825 cm^{-1} out-of-plane H-wag 850 cm^{-1} subst'd ring 3120, 3040 arom. abs.	Ester carbonyl 1730 cm^{-1} C-O stretching frequencies as in 3M 888 tape	Organo-polysiloxane As above. (present in lesser amount than 3M 888)
3M 351	Polyurethane based Absorption peaks similar to those above.	Aromatic components: Several bands in 3000 to 3200 cm^{-1} range.	Ester carbonyl, C=O 1730 cm^{-1} CH_2-C-C=O 1415 cm^{-1} C-C-O: 1225 cm^{-1}	Organo-polysiloxane Pronounced Si-O-Si 10 20 & 1085 cm^{-1} Si-CH_3 800 and 1270 (considerable amount)
Memorex 63L	Epoxide based Terminal OH: OH bend 1365 cm^{-1} OH wag 940 cm^{-1} H. .OH 3400 cm^{-1} Dimethyl-phenyl group 1380 cm^{-1}	Aromatic components 3040, 3065 and 1600 cm^{-1}	Ester carbonyl 1730 cm^{-1} Ether linkage· sym C-O-C 1290 cm^{-1} C-OH stretch 1100 cm^{-1}	Lubricity presumably afforded by aliphatic ester, extractable with n-hexane. Asymmetric C-O stretch : 1240, 1275 cm^{-1}
Memorex Quantum	Epoxide based OH bend, wag 1365, 940 cm^{-1} Broad H. OH 3400 cm^{-1}	Aromaticity: Several bands in 3000 to 3200 cm^{-1} range	Ester and ether absorption bands	n-hexabe - extractable aliphatic ester, similar to Memorex 63L
Memorex 79L	Polyurethane based NH stretch 3320 cm^{-1} (absence of epoxide-related OH bands) Amide overtones	Aromaticity 3030, 3120 cm^{-1} out-of-plane H-bending 810 cm^{-1}	Ester carbonyl: 1730 cm^{-1} CH_2-C-C=O 1415 cm^{-1} C-C-O 1225 cm^{-1}	Organo-polysiloxane SiO-Si 1020 and 1085 cm^{-1} Si-CH_3 1270, 800 cm^{-1}
DU PONT CROLYN	Polyamide based Amide I 1640 cm^{-1} Amide II 1540 cm^{-1} Overtone and combination bands 3280, 3180 cm^{-1}	Predominantly aliphatic Pronounced CH_2-wag in 1200 to 1400 cm^{-1} range Branched hydrocarbon i-propyl: 1375, 1385 cm^{-1}	C-O 1720 cm^{-1} comb. band C-O O=CN 630 cm^{-1} CH_2-C=O 1420 cm^{-1}	Lubrication presumably provided by long-chain aliphatic hydrocarbon 720 cm^{-1} CH_2-rock
RCA 617	Polyurethane based NH 3300 cm^{-1} NH bend - CH stretch 1535 cm^{-1} NH_2 1620 cm^{-1}	Aromaticity 3020, 1600 cm^{-1} Also contains: C-C trans 960 cm^{-1} C-Cl (?) 610 cm^{-1}	Ester carbonyl 1730 cm^{-1} CH_2-C=O 1420 cm^{-1} H .OH 3400 cm^{-1}	Organo-polysiloxane Si-O-Si 1020, 1080 cm^{-1} Si-CH_3 1270, 800 cm^{-1}

The initial hypothesis relating to the tape chemistry was that the epoxy based binder systems were more subject to adhesion problems than the polyurethanes available. However, examination of the data obtained with endless loops run only at high temperature partially supported this hypothesis. Comparing two epoxy tapes evaluated, Memorex 63L and Quantum, with the 3M polyurethane tapes, clearly indicated superior performance of the latter. Under conditions of 65°C and 15% RH neither of the epoxy tapes ran successfully for 10,000 passes. All four of the 3M tapes completed this test without exceeding 10 ounces/inches of required starting or running torque.

Two other polyurethane tapes included in the program did not always support the hypothesis as stated. The Memorex 79L provided a good basis for comparison because of the commonality of manufacturer (and presumably methodology) with the epoxy tapes. However, it was found that the differentiation between the Memorex tapes was more related to relative humidity than binder formulation. At 65°C and relative humidities of 30 and 45%, the 63L exhibited a longer life, while the opposite was true at 15%. Consequently, a clear distinction based upon binder polymer above could not be established.

A further cause to reject the hypothesis as stated was the polyurethane based RCA 617. The epoxy based tapes performed better than this tape through all combinations of temperature and humidity used.

It was concluded that knowledge of the basic binder polymer should not be a criterion for tape selection. This conclusion was based on the following. The program did not examine all other possible polymers. The only other alternative evaluated was the polyamide based DuPont Crolyn, and excluding a severe failure at 65°C and 45% RH, this tape exhibited performance similar to the 3M tapes. Further, it was anticipated that newer polymers could surpass the performance measured to date. More importantly, the

differences within the polyurethane tapes could be correlated with resultant adhesion performance. These differences, discussed in the following sections, enabled the selection process to be applied to an individual reel of tape. Finally, it was found that all three of the binder polymers evaluated could be utilized satisfactorily if operated within the proper constraints of environment, head pressure, and head material selection.

13. Lubricant Content

The problems of frictional drag at the head/tape interface have not been unique to satellite recorders, although limited available power has probably accentuated such problems. In order to minimize drag, lubricants have been added to the binder systems by the tape manufacturers. It was hypothesized and verified that this additive improved frictional performance.

Determining lubricant content was accomplished by weight analysis of the material extracted from the binder with N-hexane. Infrared analysis indicated that the lubricants used were often, but not always, organo polysilanes. The percent lubricant content, shown in Fig. 44, is a summary of the N-hexane extractables irrespective of the type of material.

The quantity of lubricant was one of the variables within the 3M binder systems that could be correlated with performance. For example, the two brands containing higher lubrication, 351 and 871, both ran successfully for 10,000 passes at 65°C and 45% RH. However, the 888 and 777, both containing less than 1.8% lubricant additive, exceeded the maximum starting torque established. At 45°C and 45% RH the 888 tape required exceeded 10 ounces/inches at the completion of 10,000 passes, while the 871 remained below 3.9 ounces/inches throughout the test.

The DuPont Crolyn contained a quantity of lubricant similar to 3M 888, and also exhibited substantially the same adhesion performance. Both tapes failed well before 10,000 passes at the highest temperature and humidity. The Crolyn, however, exceeded 10,000 passes throughout the remainder of the environmental conditions tested.

As previously mentioned, the comparative results for the Memorex tapes varied with relative humidity, and a clear correlation with lubricant content was not established. Although neither of the tapes completed the 65°C tests, this could only be attributed to lubricant content for the 63L.

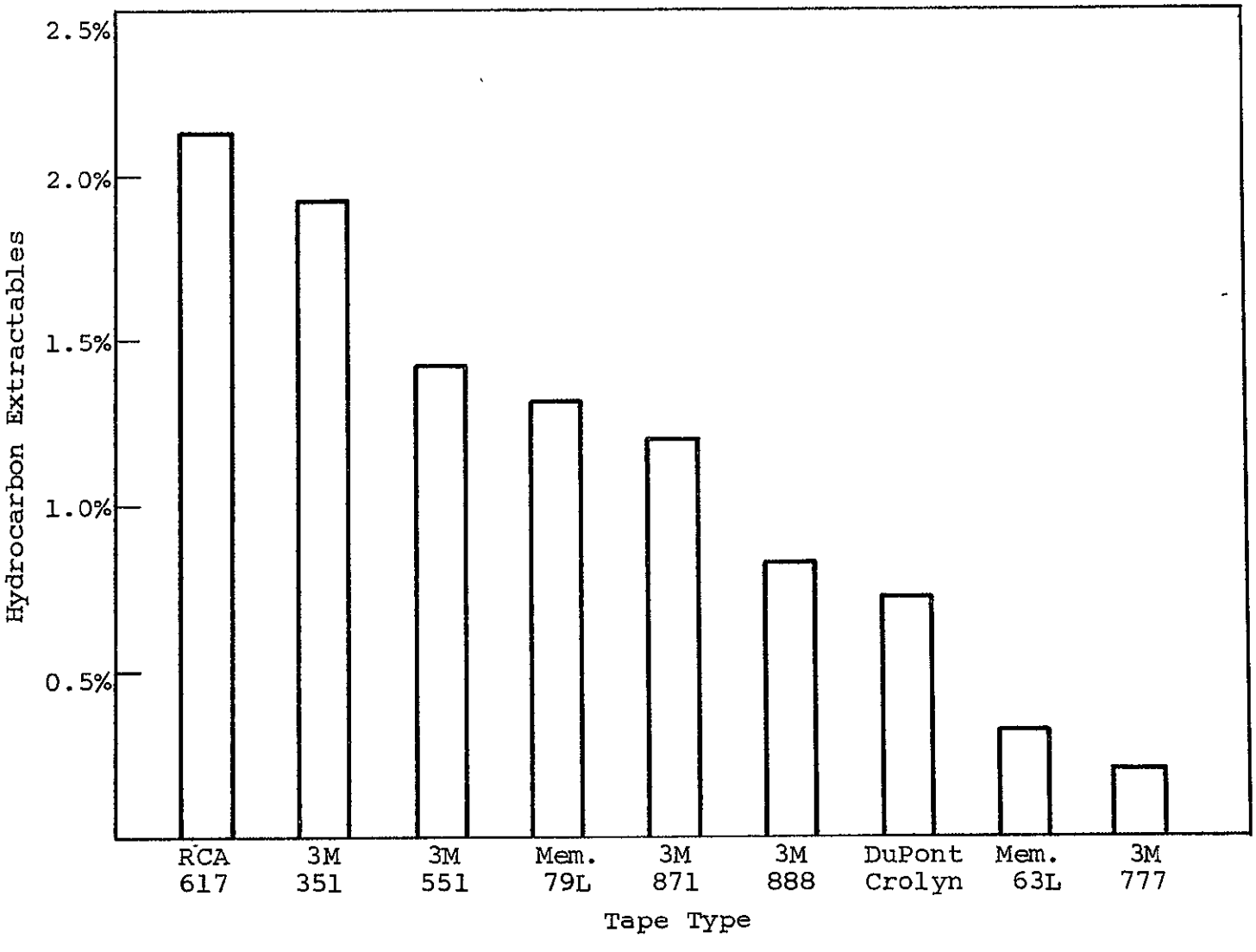

Fig. 44 COMPARISON OF N-HEXANE EXTRACTABLES

The RCA 617 was the major exception to the hypothesis that increased lubricant content improved frictional drag properties. Although this tape contained the highest quantity of lubricant, it also exhibited the poorest adhesion performance. However, the adhesion failures of the 617 were preceded by excessive debris, considered as the major effect of the high lubricant content. It was concluded that a minimum lubricant content was required for frictional performance. The effects of excessive lubricant will be discussed in Section III.B, Oxide/Binder Debris.

14. Halogen Content

Chlorine has generally been avoided in the binder systems of modern instrumentation tapes because of the potential formation of hydrochloric acid. This has been considered a danger in the storage of large quantities of magnetic tape. In addition, the chemical interaction of hydrochloric acid and brass would be detrimental to reliable head/tape performance.

None of the tapes evaluated during the chemical investigation included identifiable chlorine containing constituents. However, when a standard Beilstein test was performed for chlorine detection, three of the tapes showed a positive response. The presence of chlorine was then confirmed by other methods. The three tapes were RCA 617, Memorex 79L, and 3M 871. Several of the other tapes not included in the overall test program also exhibited a chlorine content. Whether the source of the chlorine was a component or coreactant of the binder system was not determined. One manufacturer, Graham Magnetics, indicated that a chlorine containing fungicide was added to their Epoch IV tape. However, the quantity was insufficient to yield a positive response to the test employed.

A comparison of the average required starting torques for the tapes with and without halogens is shown in Fig. 45. The curves summarize data measured at 45°C and 15% RH. At higher temperatures and humidities the curves were even more divergent. The data would have strongly supported a guideline restricting the presence of chlorine if the 3M 871 was not one of the tapes containing chlorine. However, the frictional performance of this tape was consistently satisfactory throughout the program. A possible explanation for this contrast was the source of the halogen; this could not be verified.

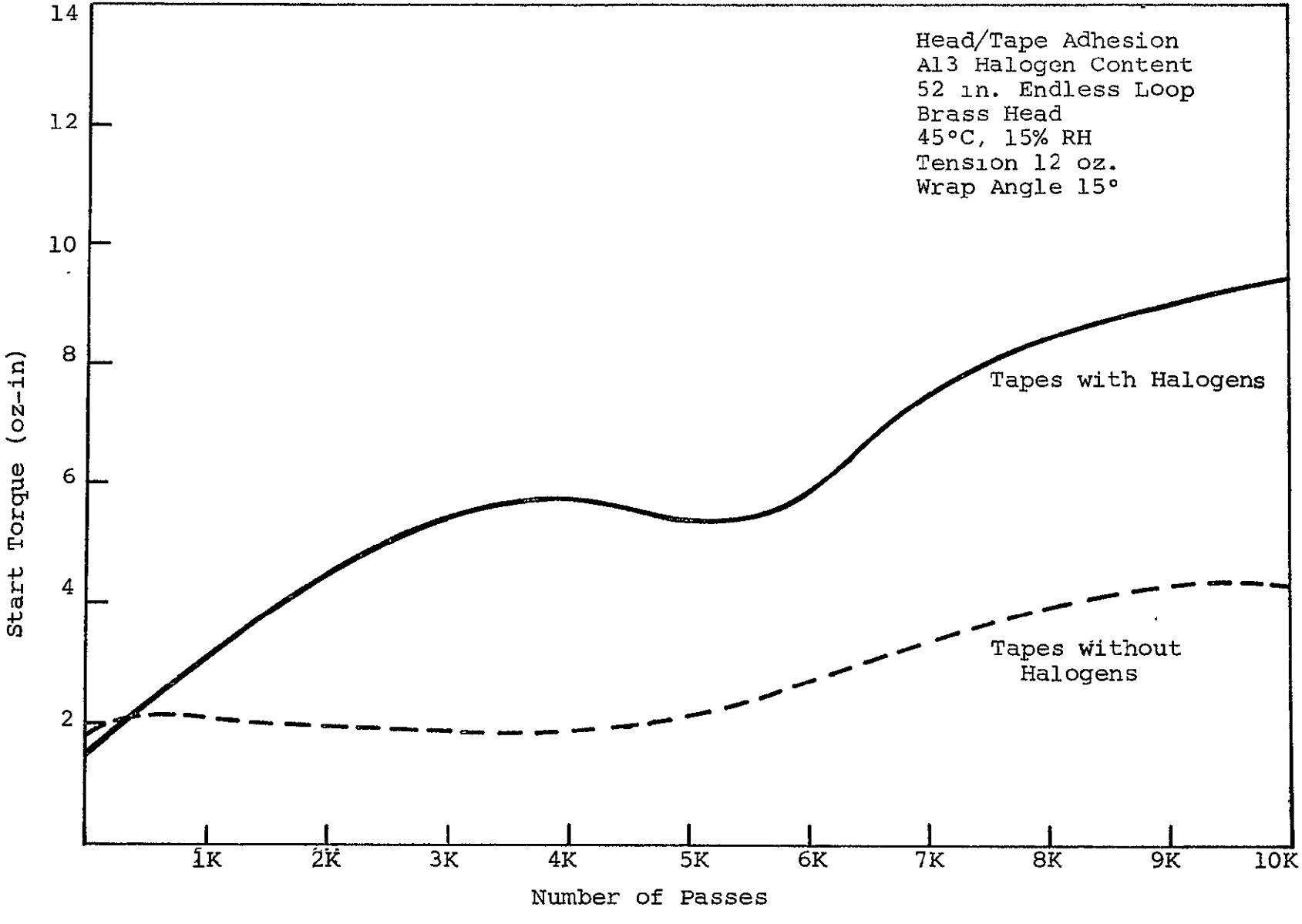

Fig. 45 EFFECT OF HALOGEN CONTENT

15. Oxide Loading

A substantial portion of the oxide/binder layer of modern tape is comprised of oxide. This presumably was done to maximize the magnetic performance of the tape. However, the possibility that an excessive quantity of oxide could adversely affect the frictional or debris properties of the tapes was considered.

The amount of oxide contained in each of the binder systems was determined by burning the organic materials and then weighing the residue. The resultant percentage by weight, Fig. 46, was comprised of the magnetic pigment and a very small quantity of silica, resulting from the silicone lubricants. However, no correlation was observed between this determination and lubricant content.

The degree of oxide loading was found to be approximately the same for all of the tapes evaluated. No direct relationship between oxide loading and adhesion was evident over the relatively narrow range measured for commercially available tapes.

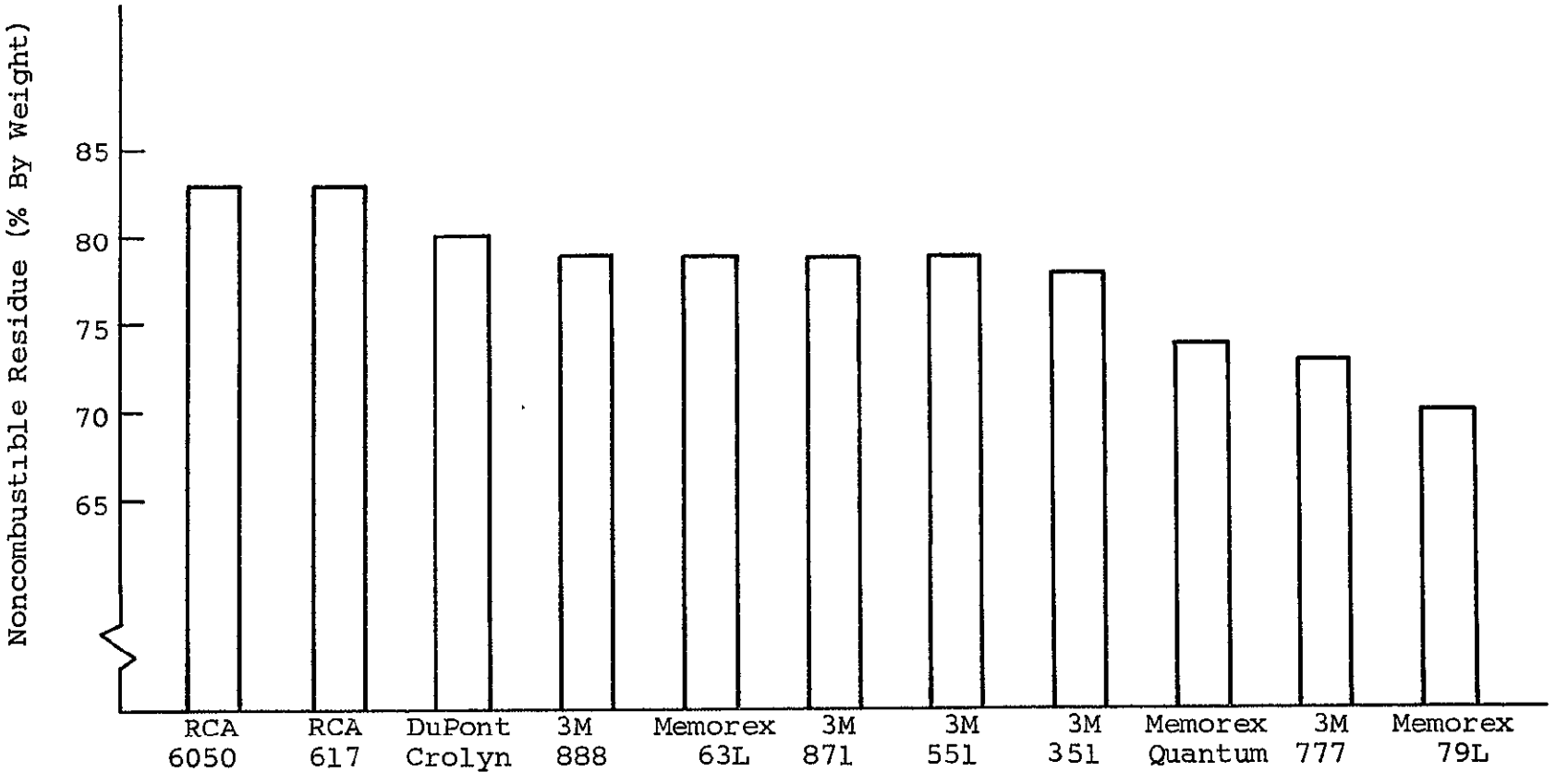

Fig. 46 OXIDE LOADING

16. Polymer Polarity

The polarity of a polymer is closely associated with the presence of certain functional groups, such as hydroxyl-, carboxyl- or amino-groups that are attached to the polymer backbone. These groups are likely to promote interaction with metal surfaces that could lead to the formation of chemical bonds at the sites of interaction. It was, therefore, hypothesized that highly polar type binders would be more susceptible to head/tape adhesion failures. Since the polar constituents in a tape binder would be more readily removed by polar solvents, the amount of extractable matter recovered from a tape in an elution process involving a combination of solvents was used as a measure of polarity of tape constituents.

The evaluation of the amount of extractable polar constituents from each of the tape coatings involved a complex process of fractionation. Using liquid chromatigraphic column techniques, various combinations of chloroform and methonol were used to separate the polar constituents. The procedures and results of this work are discussed in Volume III.

In order to assess the effect of polymer polarity on the adhesive characteristics of the various tapes, the results of tests run at 65°C and 15% RH were compared to the measured values of polarity irrespective of binder formulation. In Fig. 47, the required starting torque for each of the tapes following 1000 and 10,000 passes is plotted against the measured polarity for the tapes. The results showed that increasing polarity adversely affected the performance throughout the life of the tape. In addition, it was found that tapes having a value of polarity equivalent to 1.75% or more of extractable polar tape constituents did not successfully complete 10,000 passes at the environmental and operational conditions imposed.

Polymer polarity was concluded to be a significant indicator of the tape frictional characteristics. However, it was a difficult parameter to determine, and the procedures required were not considered practical for inclusion in the tape selection guidelines.

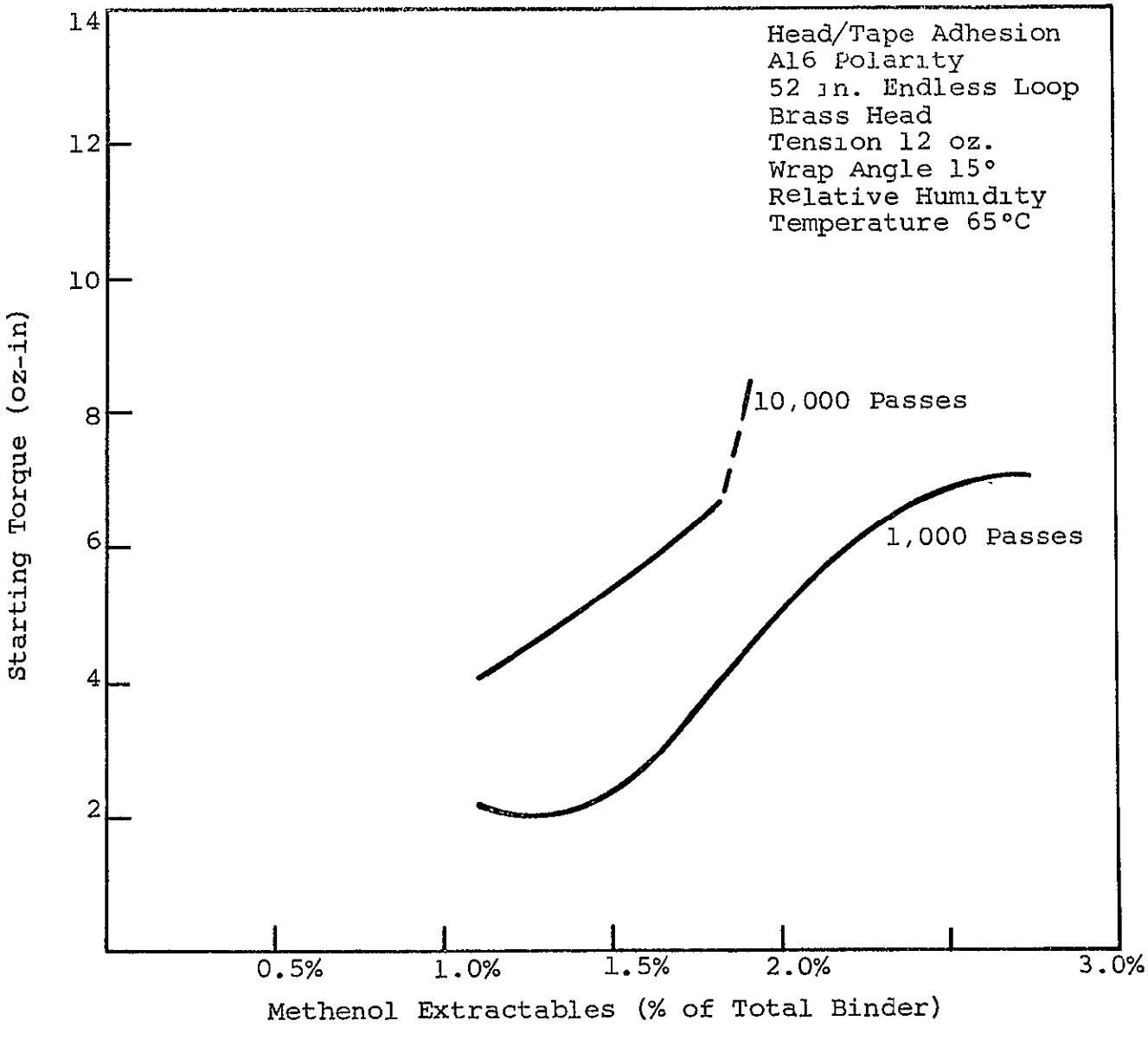

Fig. 47 EFFECT OF BINDER POLARITY

17. Resistivity

The resistivity of the binder/oxide layer of most commercially available tapes has been controlled by the addition of a conductive material such as carbon. This was done in recognition of possible static electricity problems resulting from operation in very dry environments. Since many satellite recorders have been operated in such environments, this parameter was considered potentially significant.

The surface resistance of the tapes examined during the program was measured using a Hewlett-Packard high resistance ohmmeter. A probe, shown in Fig. 48, was constructed of plexiglas and placed on the oxide side of the sample tape. The tape was pretensioned to 16 ounces, and a normal force of 8 ounces was applied. Measurements were taken at room temperature and two controlled humidities, 0% and 84% RH.

A summary of the surface resistivity measured for each of the tapes is shown in Table VI. A very wide range of values with several of the measurements being somewhat higher than the recommended maximum on the manufacturer's specification sheet, was obtained. However, measurements of different reels of tape having the same type designation showed a large variation in this parameter. For example, measurements of 135×10^7 were obtained for two reels of Memorex 79L.

During Phase I several reports of problems attributed to static electricity were received. However, static electricity was not determined to be the cause of any of the adhesion failures encountered during this program. Nearly all of the tapes exhibited superior performance at the lower humidities. The results of endless loop tests for the Memorex 79L, the tape possessing the highest resistivity measured, showed substantial reductions in drag as the humidity was decreased. Further, the Memorex 63L, also a highly resistive tape, was run in one

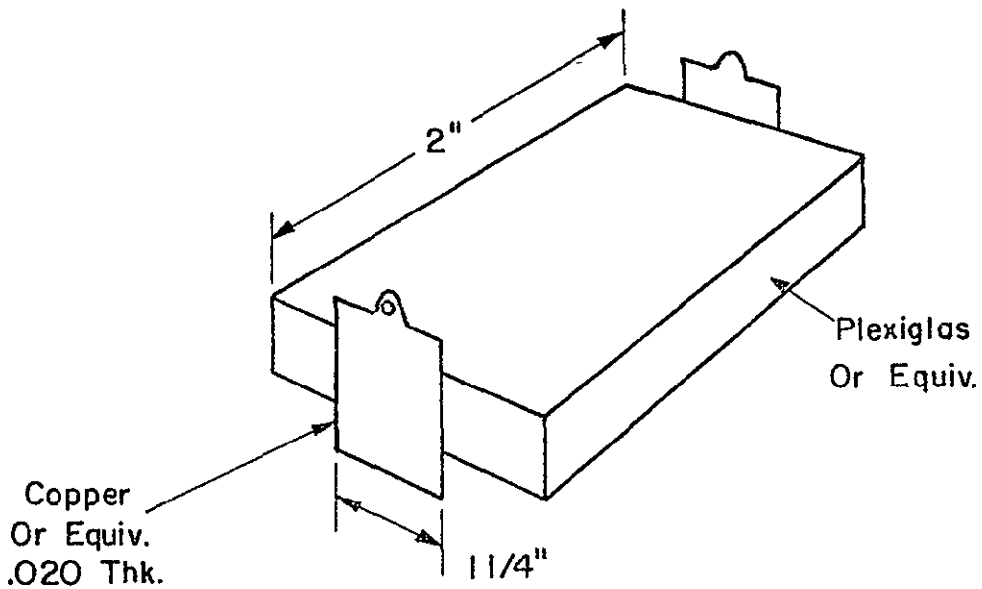

Fig. 48 RESISTIVITY TEST PROBE

Table VI

SURFACE RESISTIVITY

Tape Type	Resistivity 0% R.H.	Resistivity 84% R.H.
3M 351	$32.0 \times 10^7 \Omega$	$30.5 \times 10^7 \Omega$
3M 777	1.31×10^7	1.85×10^7
3M 871	1.85×10^7	2.38×10^7
3M 888	1.05×10^7	1.32×10^7
Memorex 63L	24×10^7	31.6×10^7
Memorex 79L	330×10^7	381×10^7
Memorex Quantum	3.2×10^7	4.2×10^7
RCA 617	0.22×10^7	2.88×10^7

direction only at 65°C and two humidities, 0% and 45%. Figure 49 shows the lower drag forces encountered at the low humidity.

The lack of firm evidence attributing increased drag to static electricity does not preclude the possibility of problems elsewhere throughout the transport, for example, in areas where high resistance protective coatings have been applied. Therefore, the maximum resistivity specified by the tape manufacturer was considered a valid constraint. The minimum limitation on this parameter is discussed in Section III.B, Oxide/Binder Debris.

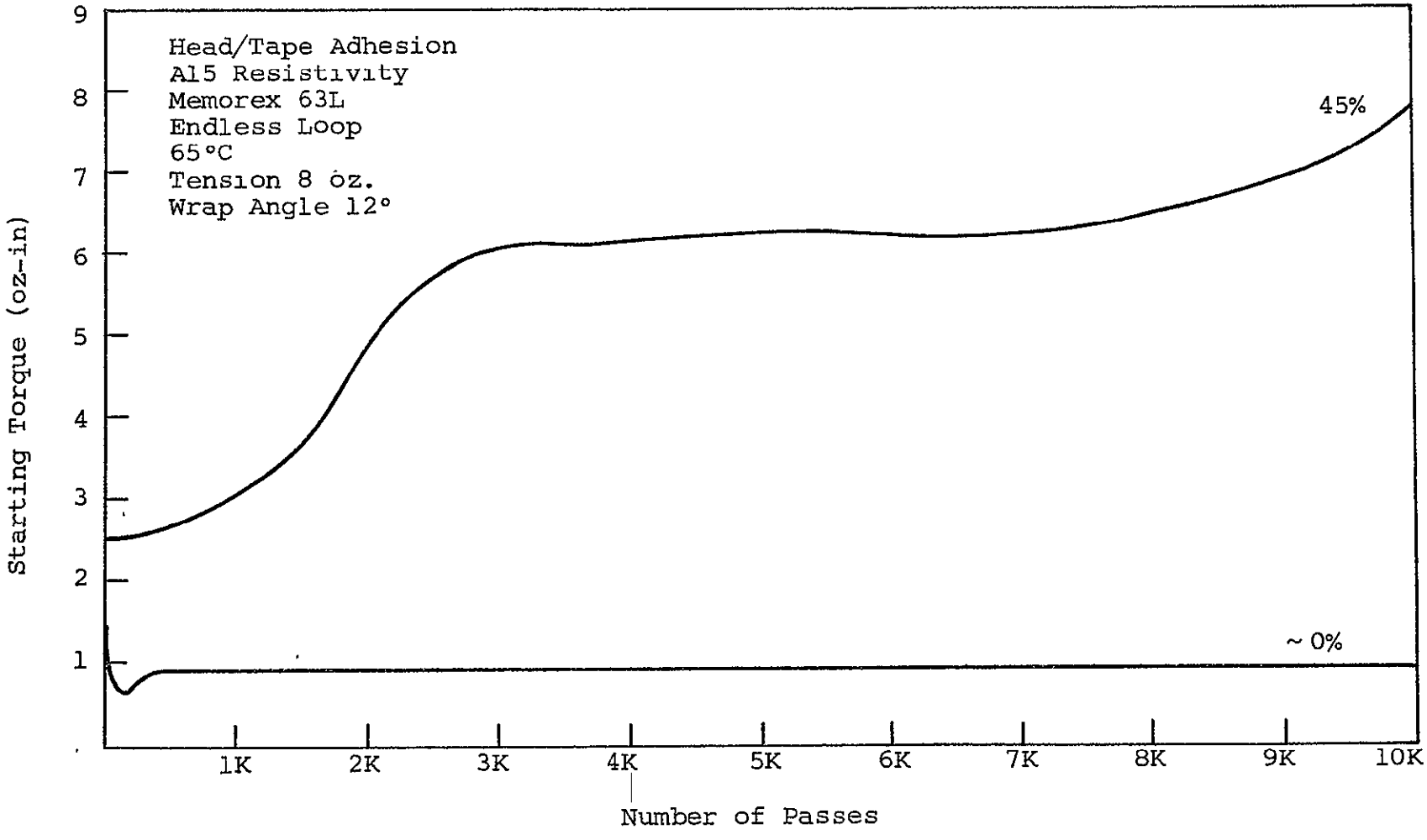

Fig. 49 EFFECT OF VERY LOW HUMIDITY, MEMOREX 63L

18. Oxide Orientation

One mechanism contributing to excessive drag for certain tapes was identified as a change in the surface finish that produced a direction sensitivity. As a possible explanation for the development of this surface condition, it was hypothesized that poor oxide orientation could result in a skewed particle alignment. The consequence of this would have been the exposure of particles after sufficient tape wear that tended to resist tape motion.

The procedure used to categorize orientation was to compare the squareness ratios measured for each of the tapes. A B-H magnetic loop tracer was used to obtain the data shown in Table VII. The variation between tapes was found to be very small. Further, reversing the tape samples did not alter any of the initial values measured. Since even the small variations measured did not correlate with the surface changes observed, it was concluded that the degree of oxide orientation achieved was relatively uniform and not a factor in the drag measurements.

Table VII

B-H LOOP SQUARENESS RATIO

Tape Type	Longitudinal	Transverse
3M 351	0.76	0.47
3M 777	0.76	0.42
3M 871	0.79	0.41
3M 888	0.76	0.46
Memorex 63L	0.72	0.50
Memorex 79L	0.78	0.43
Memorex Quantum	0.78	0.42
RCA 617	0.78	0.41

19. Oxide Dispersion

Dispersion of the magnetic particles within the binder system is significant in the determination of the magnetic performance of tape. In fact tape noise, resulting from a nonuniform oxide dispersion, has become a limiting factor in improving the signal-to-noise ratio of wideband, ground based recorders. This noise arises from the existence of oxide agglomerates or voids, either of which produce a nonuniform magnetic storage media. However, such irregularities could also cause changes in the tape surface, particularly after prolonged use. Therefore, it was hypothesized that the frictional characteristics of tape were related to oxide dispersion.

The characterization of oxide dispersion for each tape tested was obtained by comparing the reproduce level of a saturated signal to that obtained with a dc magnetized tape. To determine these parameters, a set of low-noise, unequalized reproduce electronics were used with a standard IRIG head. Each tape was recorded to saturation of 200 kHz and reproduced at 30 ips. After playback, the tapes were saturated in one direction only with a permanent magnet, thus allowing the determination of a signal to dc noise ratio for each tape.

The nine tapes evaluated were ranked on the basis of the preliminary broadband noise measurements, with 3M 888 being the best and Memorex 79L the poorest. A wave analyzer was then incorporated in the test setup to compare the spectra of the noise measurements. The wave analyzer was swept from dc to 20 kHz to dc as each of the tapes were run to identify the differences in the various spectra and increase the overall range of the measurements. Figure 50 shows the spectra for the 3M 888 and Memorex 79L.

Differences in the noise spectra of the various tapes led to the use of a narrowband filter to increase the range between the various tapes. Several center frequencies and noise

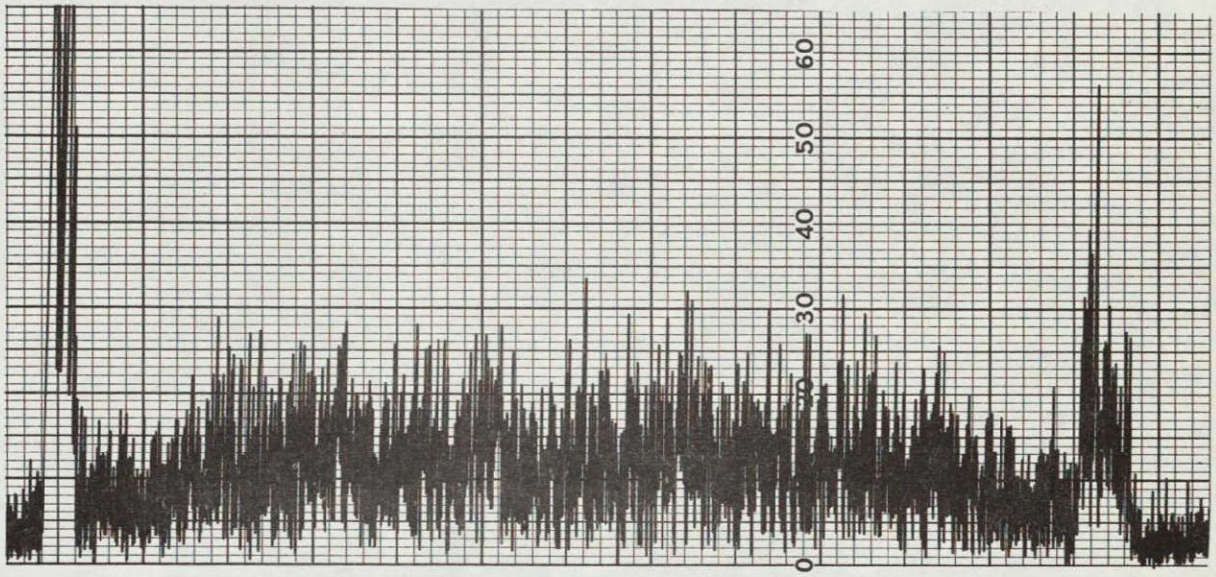

a. 3M 888

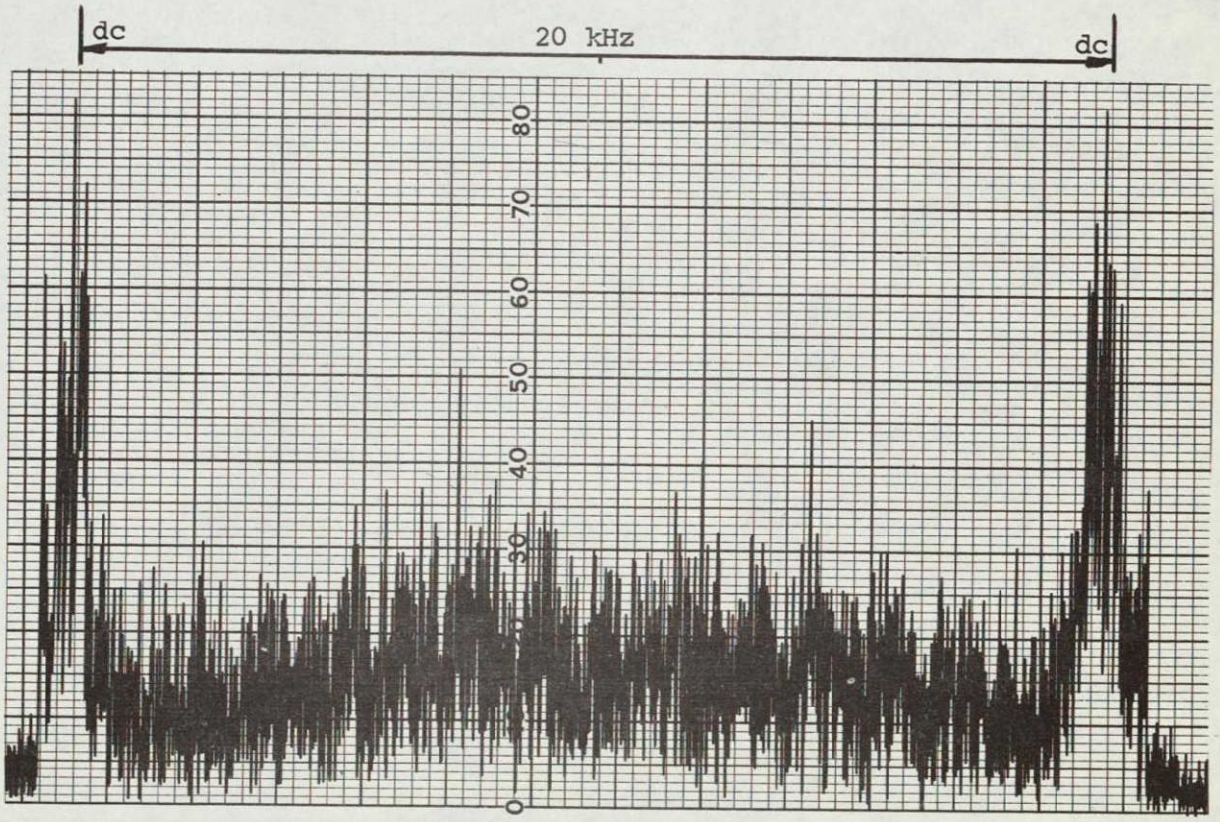

b. Memorex 79L

Fig. 50 TAPE NOISE SPECTRUM, DC TO 20 kHz TO DC

bandwidths were examined for inclusion as a tape selection guideline test. These are discussed in Volume III. The signal frequency selected for this test was 15 kHz with a noise bandwidth of 15 $\pm$ 5 kHz. Using these parameters, the tape noise was at least 10 db above the recorder system noise (measured with the tape separated from the head). Examining the results in Fig. 51 shows the lowest signal to dc noise ratio for the Memorex 63L and 79L tapes. Since these two tapes showed localized changes on the oxide surface, this test was considered to be a valid criterion for tape selection. An additional correlation of this parameter to oxide binder debris is discussed in Section III.B.

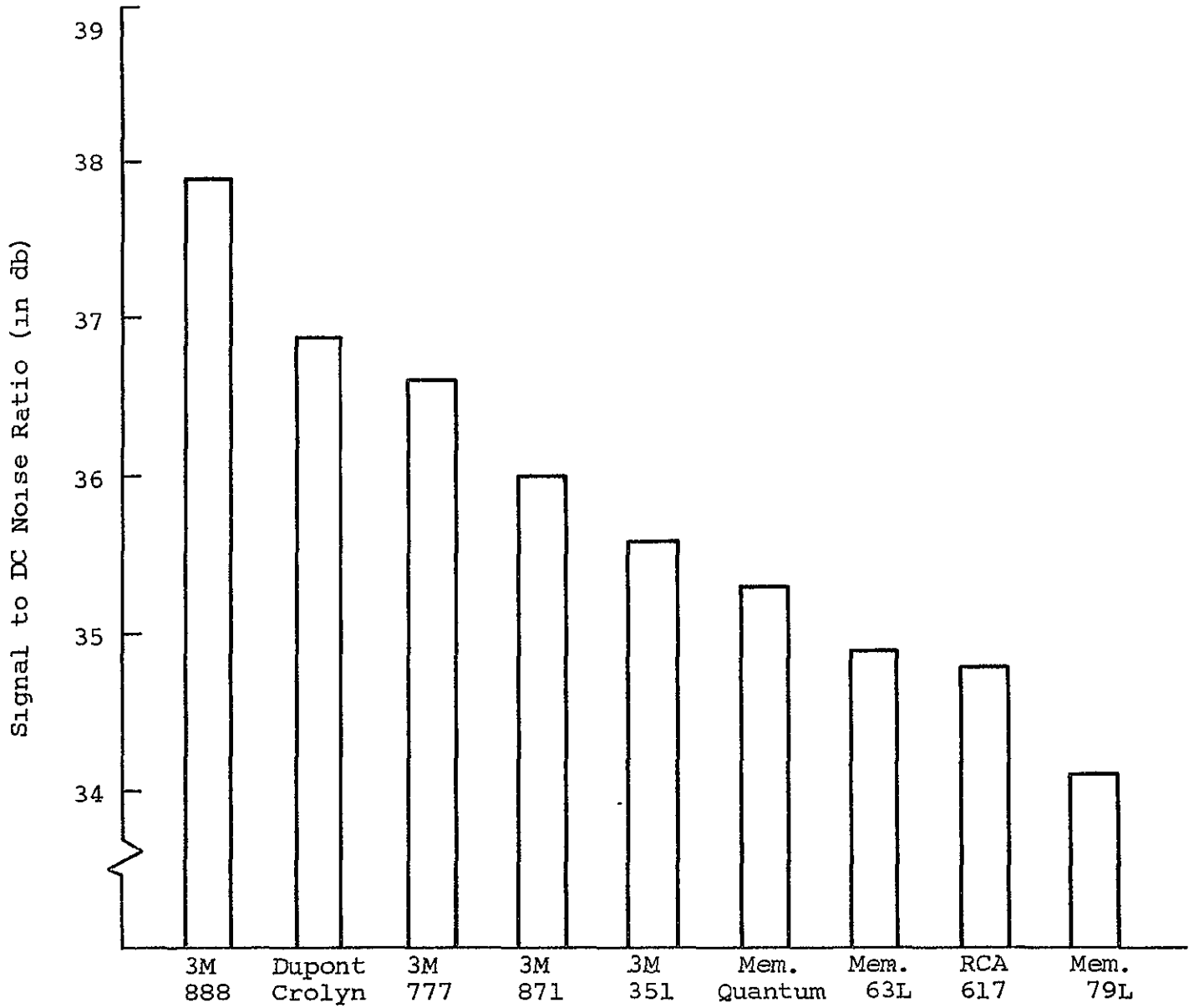

Fig. 51 COMPARISON OF SIGNAL TO TAPE NOISE RATIOS

20. Surface Finish

Several of the types of failures encountered during the testing program were related to tape surface finish. For example, it was shown in 10. Tape Wear that considerable degradation of the surface occured prior to frictional failure. The surface condition was also significant in drag increases resulting from bidirectional operation. In addition, the intimate contact of extremely smooth tape could have promoted chemical bonding of the head and tape. Because this one parameter had such a determining role in the ultimate tape performance, a possible correlation between the coefficient of friction and initial surface finish was investigated.

The surface roughness and waviness were measured using a Bendix Proficorder for each of the tapes included in the test program. Essentially no difference between tapes was observed in the waviness data. However, the results for surface roughness tabulated in Table VIII did exhibit a range from 4 microinches up to 20 microinches peak/valley.

Comparing these measurements with the data taken throughout the adhesion tests did not indicate any correlations. The smoothest tape measured, 3M 871, was one of the better tape types evaluated for adhesion. However, many of the remaining tapes had a similar quality finish. For example, the 3M 351 and Memorex 63L had nearly identical values for roughness although their adhesion properties differed considerably.

An additional consideration of the effects of surface finish was the possibility that the dc noise measurements obtained for each tape were representative of roughness rather than oxide dispersion. This did not generally appear to be verified. For example, the 3M 777, 3M 871, and Memorex Quantum, with roughness figures of 16, 4, and 10 microinches, possessed virtually identical signal to dc noise ratios. However, the roughness of the 851 could have contributed to its relatively

Table VIII

SURFACE ROUGHNESS

Tape Type	Finish µin P/V
3M 351	10
3M 551	8
3M 777	16
3M 851	20
3M 871	4
3M 888	6
Memorex 65L	11
Memorex 79L	14
Memorex Quantum	10
DuPont Crolyn	12

poor tape noise. This implies that a tape is required to have both uniform dispersion and a smooth surface finish to fulfill selection requirements, based upon a dc noise test.

21. Tape Hardness

Most models for the wear of sliding objects involve the hardness of the materials. Generally, the softer materials are worn by the harder materials. At the head/tape interface several materials are subject to wear. These include the magnetic and nonmagnetic portions of the head, as well as the oxide and binder of the tape. Because tape wear was determined to contribute to further frictional problems, it was hypothesized that adhesion increased with softer tape binders.

The measurement of surface hardness was accomplished on a Tukon Tester, Model A using a 22.5g load. The results of these tests, shown in Table IX, reveal that most tapes had a Knoop hardness number in the range of 12 to 14 and could not be differentiated because of their standard deviations. The RCA 617, considerably softer than the other tapes measured, tended to verify the original hypothesis because of its relatively poor adhesion performance. However, the two hardest tapes, Memorex 79L and 63L, did not exhibit superior frictional properties.

A comparison of the surface hardness of new and used tapes, Table X, showed a tendency for binder softening after use. However, the reduction in hardness was insufficient to permit isolation of the individual tapes.

The measurement of tape surface hardness was difficult because of the large quantity of hard magnetic oxide and the presence of a relatively soft substrate. Further, the data attained did not correlate well with the frictional properties of the tapes measured. Therefore, attempts to isolate this parameter were not continued.

Table IX

TAPE SURFACE HARDNESS

Tape Type	Knoop Hardness Number	Standard Deviation
Memorex 79L	18.29	± 1.9
Memorex 63L	15.98	± 1.9
3M 551	15.66	± 1.4
Memorex Quantum	13.93	± 2.6
3M 888	13.78	± 1.2
DuPont Crolyn	13.64	± 1.8
3M 351	12.94	± 1.3
3M 777	11.82	± 1.2
3M 871	11.69	± 1.2
RCA 617	8.80	± 0.75

Table X

DEGRADATION OF TAPE SURFACE HARDNESS

Tape Type	Unused Tape Hardness	Used Tape Hardness
Memorex 63L	15.98 ± 1.9	15.30 ± 1.6
Memorex Quantum	13.93 ± 2.6	12.14 ± 2.2
3M 888	13.78 ± 1.2	13.23 ± 2.2
DuPont Crolyn	13.64 ± 1.8	12.72 ± 1.6
3M 777	11.82 ± 1.2	11.21 ± 1.4
3M 871	11.69 ± 1.2	12.66 ± 2.0
RCA 617	8.80 ±0.75	7.26 ± 1.1

22. Head Material

During Phase I, reports were frequently received of satellite recorder manufacturers attempting to remedy an adhesion or debris problem by changing tape type. Often the heads were not changed until at least several tapes had been discarded. Undoubtedly, this order of corrective action was based partially on economics. However, until recently there were few commonly available heads constructed of materials other than brass or aluminum and used soft cores, e.g., permalloy. Brass or aluminum were commonly used as block materials for reasons such as:

- Availability
- Ease of machining and slitting
- Wear rates approximating permalloy
- Established lapping techniques

These heads were quite adequate for many ground based recorders where environments were comfortable and maintenance frequent. Problems began to occur, however, as higher operating temperatures were encountered with airborne recorders and longer head life was required for wideband instrumentation systems.

These demands initially resulted in heads being produced with mechanically harder magnetic core materials, such as Alfenol, Alfesil, and Sendust. Since the core material often comprises the majority of the contact area, there was less incentive to replace the block material. Recently, heads have been introduced with mechanically hard materials such as Havar in the contact area between tracks. For the reasons applicable to ground based recorders as well as the possibility of reduced chemical interaction with the tape, it was hypothesized that the hard core and block materials were preferable.

A preliminary evaluation of various head materials was performed on a static basis using one-inch diameter rods of typical head materials. The materials evaluated were brass,

aluminum, permalloy, chrome (plated), stainless steel, and teflon. Teflon was included because of its occasional use on stationary guides. Samples of each tape type were hung over the rods with 8 ounces of tension on each end. After soaking at elevated temperatures for 24 hours, the required breakaway force was measured with a spring scale. The average of the 3M tapes on the various head materials is shown in Fig. 52. The corresponding average of the Memorex tapes is shown in Fig. 53.

Brass was found to be the least desirable of the materials tested. The Memorex tape, in particular, tended to adhere to the brass rod. Some evidence of adhesion to stainless steel was observed at 85°C, but not at the lower temperatures. This was primarily due to the halogen containing Memorex 79L and 3M 871 tapes. These two tapes generally exhibited the highest breakaway forces throughout the tests. This effect was not observed with the RCA 617 tape, containing a halogen because it has a high lubricant content.

The Mylar substrate of 3M 888 was included in the static tests performed. In general, Mylar exhibited a lower tendency to adhere than any of the binder systems tested.

Subsequent tests on both the endless loop and reel-to-reel transports verified that other head materials were preferable to brass. Figure 54 plots the required starting torque versus number of tape passes for the 3M 888 with brass, aluminum, and alfesil dummy heads. This test was run in one direction only at 65°C and 45% RH. The starting torques were consistently lower when using either aluminum or alfesil rather than brass.

A similar comparison of brass and alfesil was conducted using the Memorex 63L tape at 65°C and 45% RH. The results, shown in Fig. 55, again show the preference for avoiding brass.

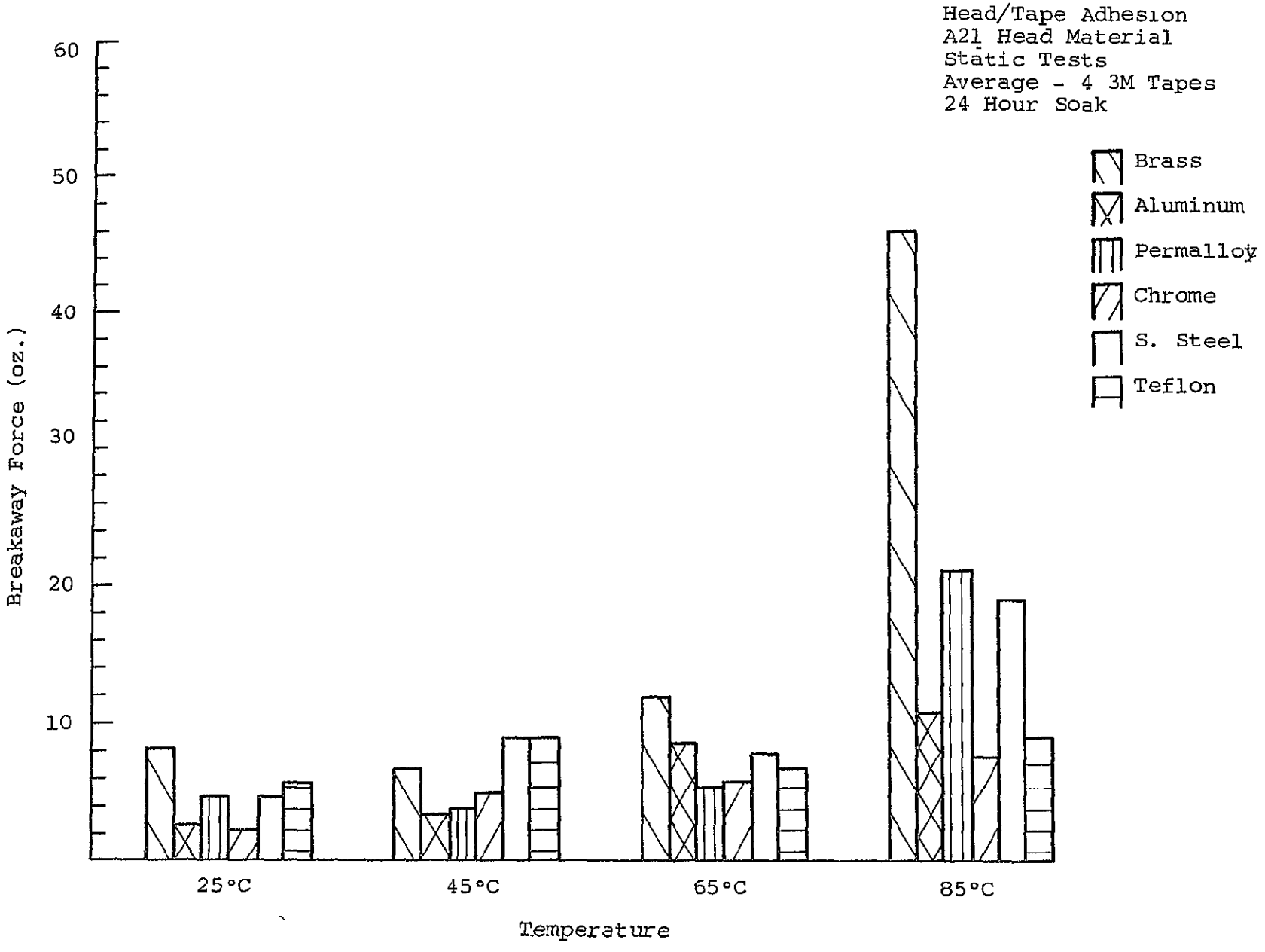

Fig. 52 STATIC COMPARISON OF HEAD MATERIALS, 3M TAPES

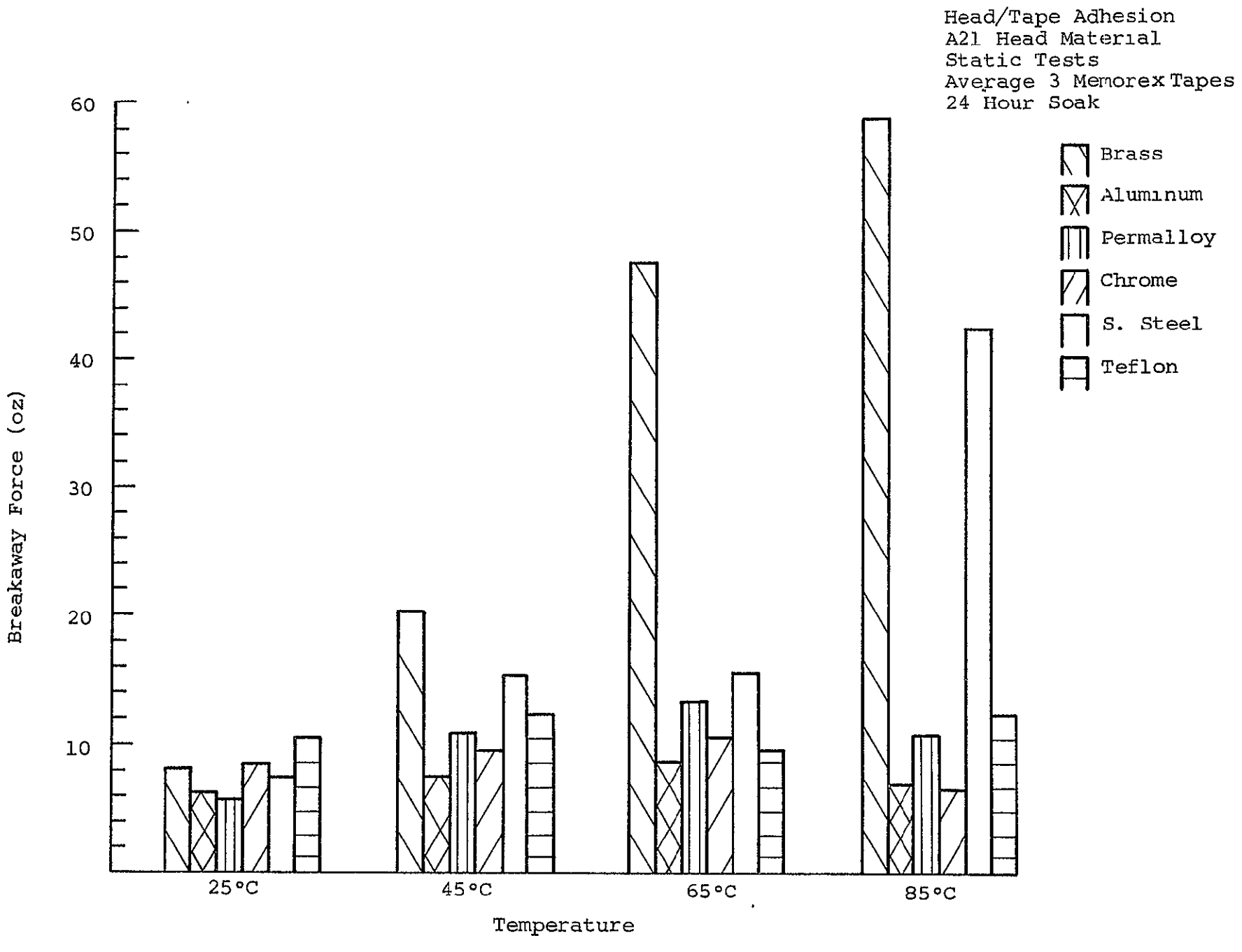

Fig. 53 STATIC COMPARISON OF HEAD MATERIALS, MEMOREX TAPES

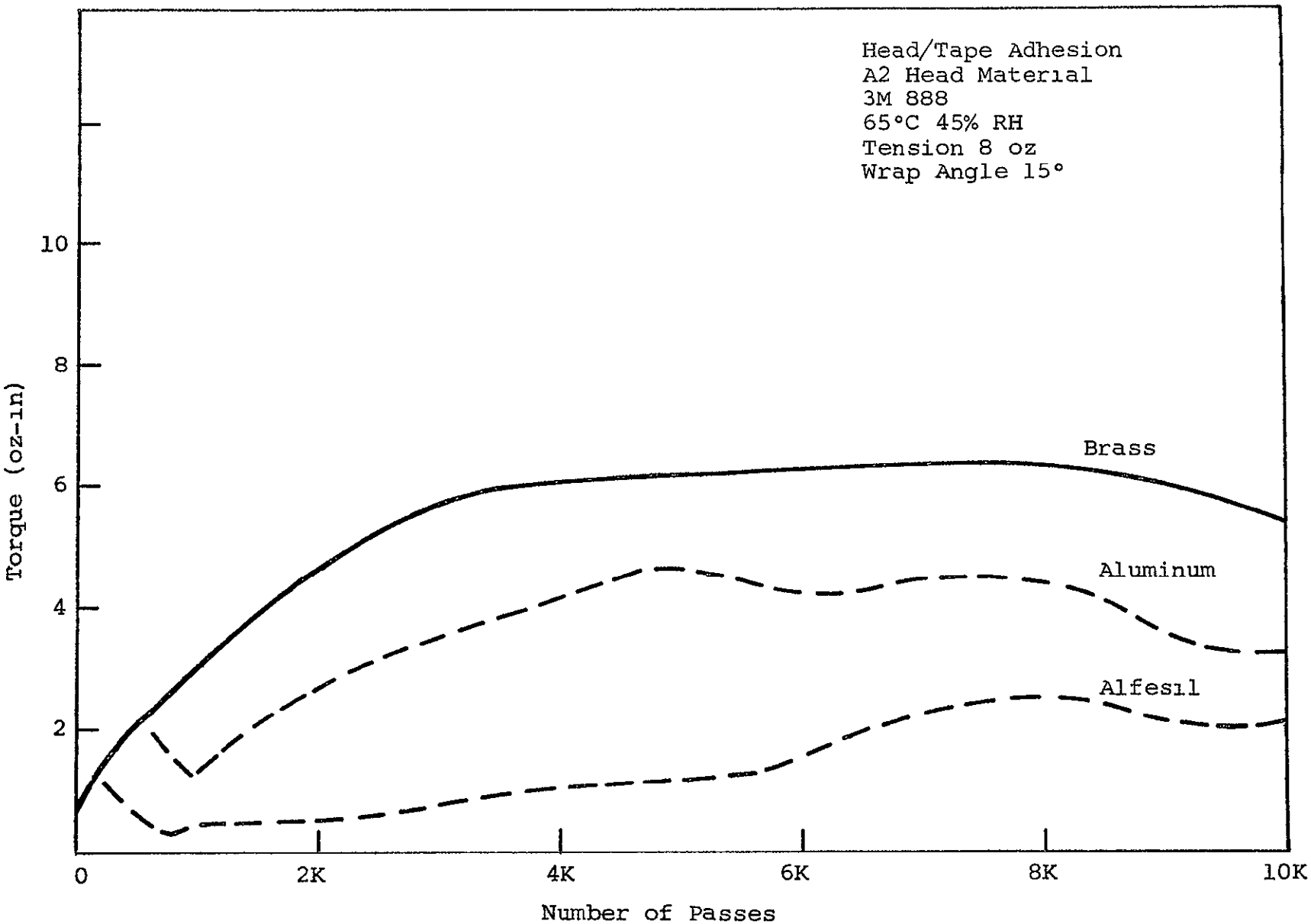

Fig. 54 EFFECT OF HEAD MATERIAL, 3M 888

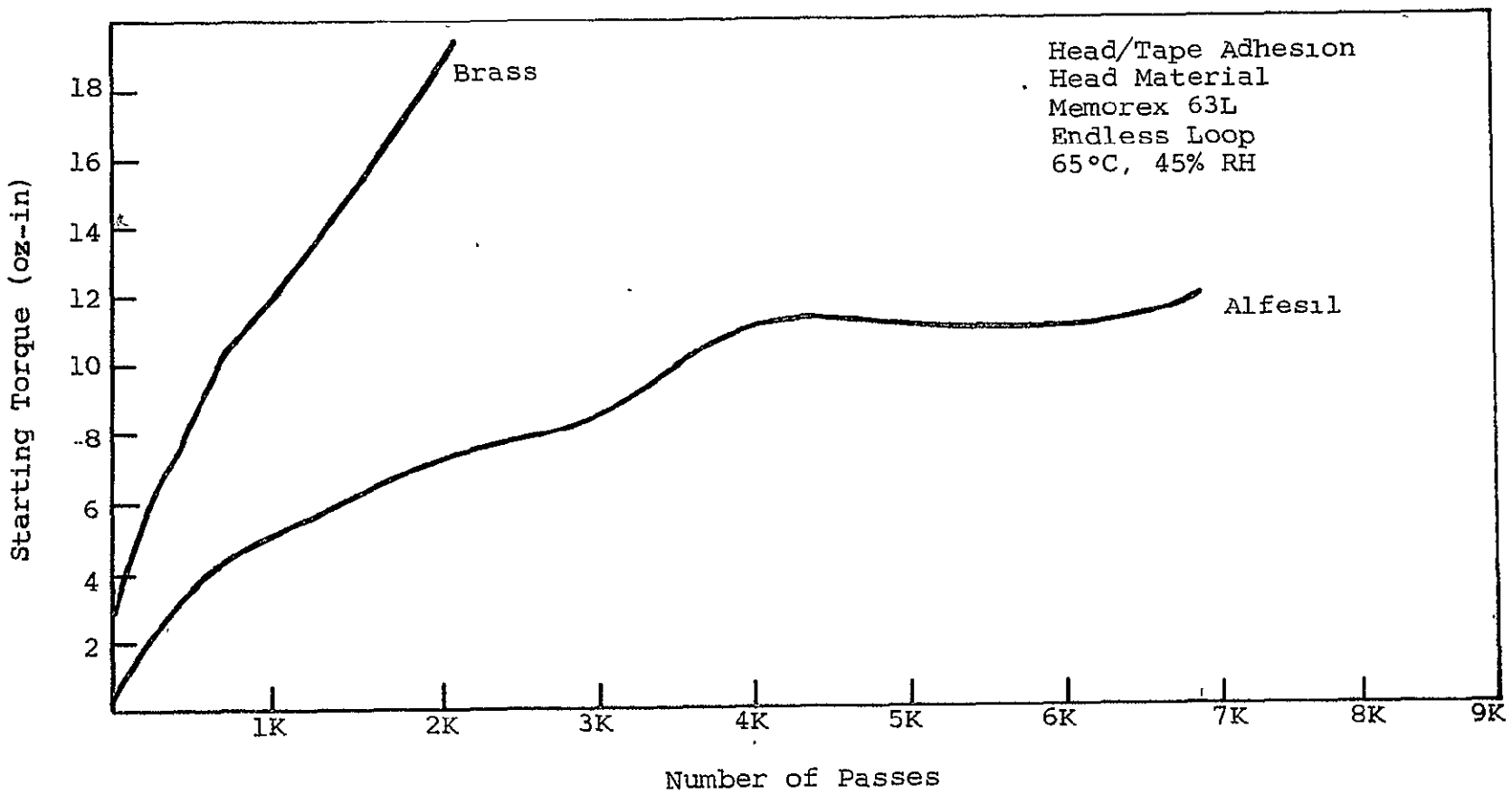

Fig. 55 COMPARISON OF BRASS AND ALFESIL, MEMOREX 63L

At low relative himidity, the harder head materials also exhibited lower friction than brass. Figure 56 plots starting torque versus usage for brass, havar, and alfesil. The temperature was 65°C; however, the humidity was essentially 0%. Using the 3M 888 tape, under these conditions, little difference was observed between havar and alfesil.

The results of a comparison between brass and aluminum using longer lengths of 3M 888 is shown in Fig. 57. This test was run on the reel-to-reel transport at 65°C and 45% RH. The two principal differences in the results using the two head materials were the required starting force and the debris. A comparison of the starting force after 3,500 passes is shown in Fig. 58. The drag at start was somewhat higher with the brass head, although the eventual running friction was approximately the same for both head materials. According to the Steinhorst[5] model for stick slip, this divergence of the static and dynamic coefficients of friction would explain the tape squeal encountered.

The choice of head material was concluded to be significant in determining the drag at the head/tape interface. Brass, in particular, should be avoided. In addition, the harder materials tested were found to be preferable.

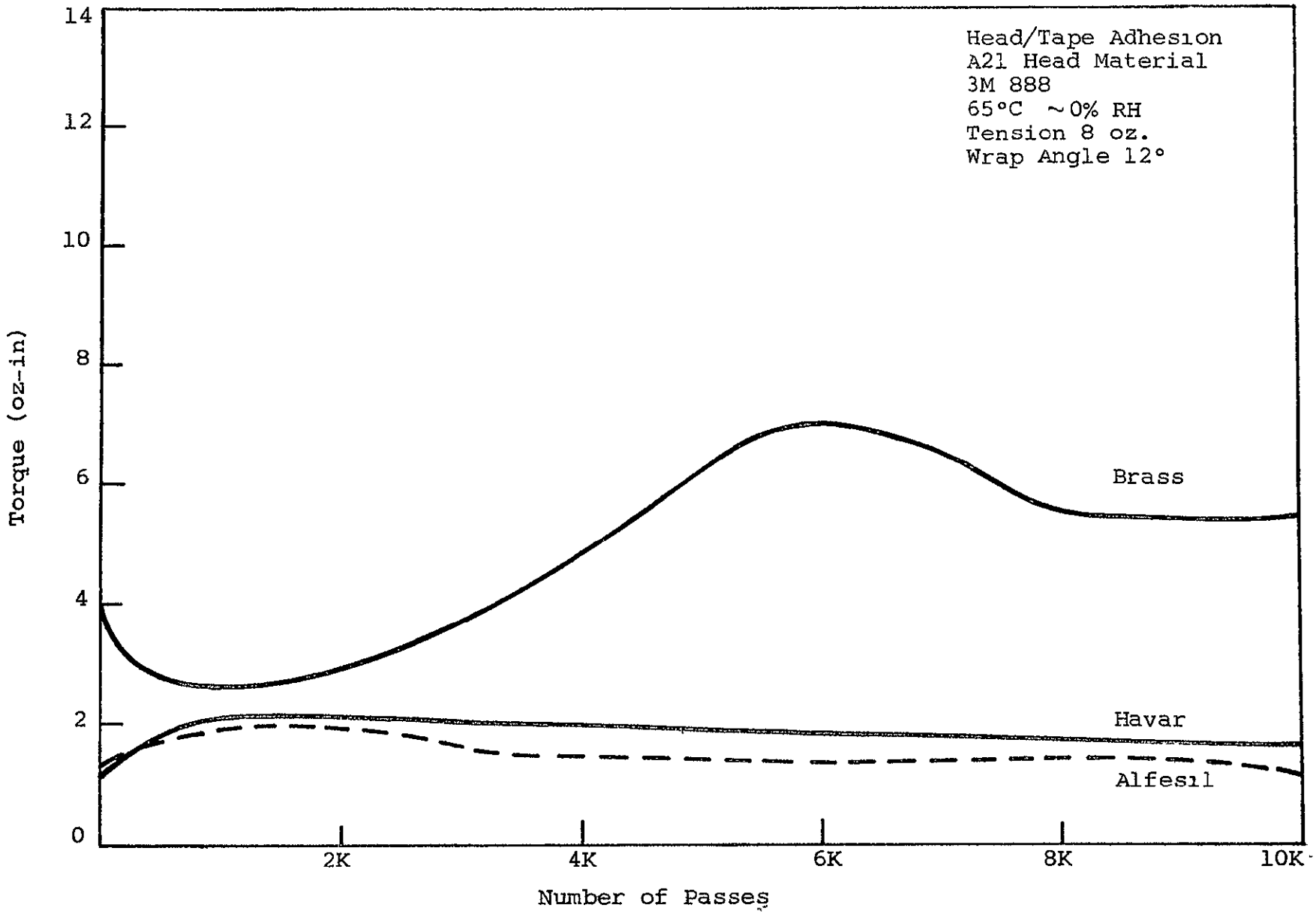

Fig. 56 EFFECT OF HEAD MATERIAL, 3M 888

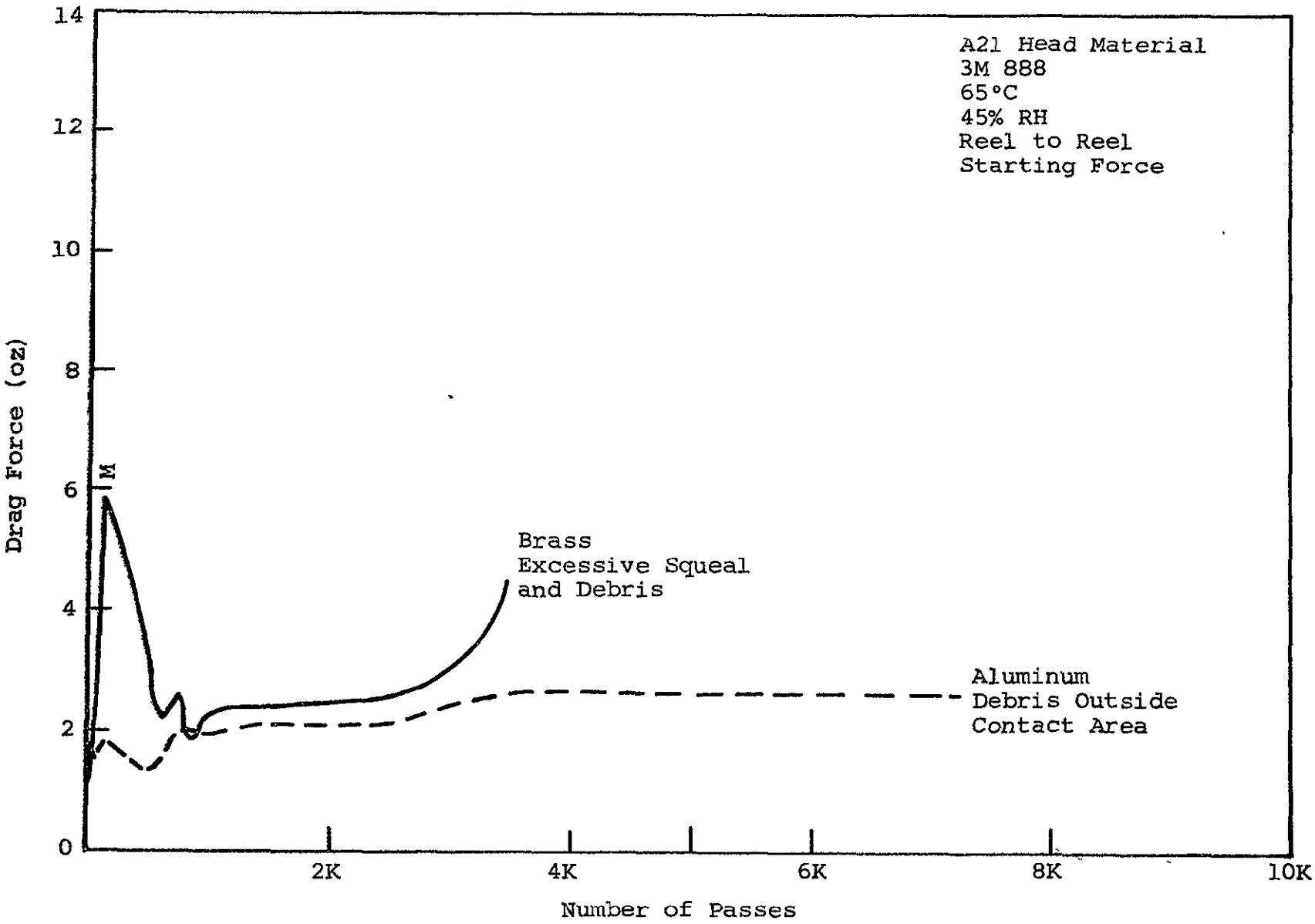

Fig. 57 COMPARISON OF BRASS AND ALUMINUM, 3M 888

Head/Tape Adhesion
A21 Head Material
3M 888, 3500 Passes
65°C, 45% RH
Wrap Angle 8°
Tape Tension 8 oz.
1 ips

Brass

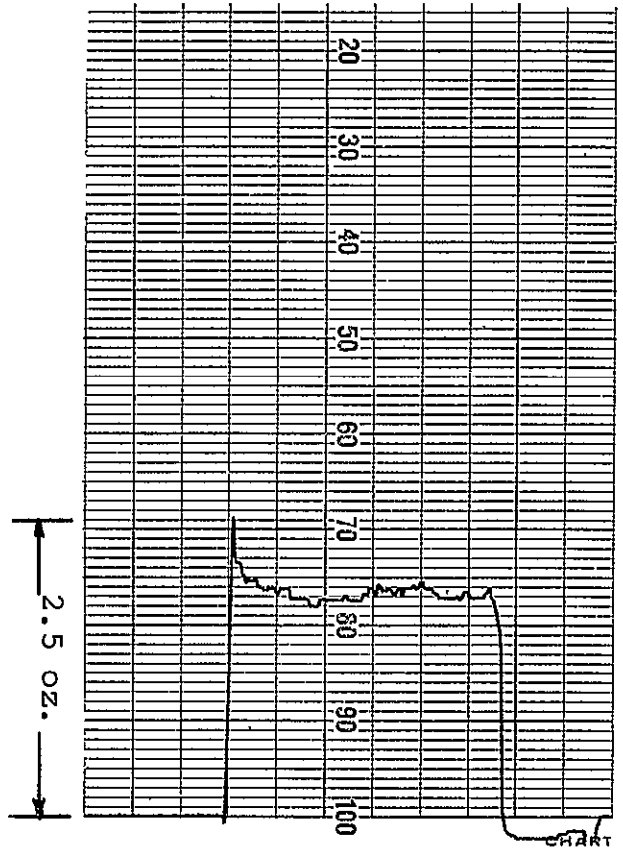

Aluminum

Fig. 5 COMPARISON OF BRASS AND ALUMINUM, 3M 888

23. Head Varnish

During Phase I a number of manufacturers reported evidence of a tan or brown stain on the surface of the heads following usage. This material, commonly referred to as head varnish, was considered responsible for short wavelength loss due to tape separation. However, its effect on frictional drag was unknown.

Throughout the test program similar discolorations were frequently found on the dummy heads after use. In order to evaluate the nature of these films, several of the heads were examined at high magnification using the scanning electronic microscope. Figure 59 is a photomicrograph of a brass head used in a test at 65°C and 30% RH with DuPont Crolyn tape. Magnification is 1000X, and the film was easily distinguished. However, when the same area of the head was examined using the backscatter mode of the SEM, the film was not at all evident (Fig. 60). Because the backscatter operating mode of the SEM is insensitive to materials with atomic numbers of less than 19, results such as these usually imply the presence of an organic film. However, the quantity of material involved was extremely small, and the possibility of insufficient sensitivity for any material still existed.

In an effort to identify the chemical nature of the film, several attempts were made to dissolve the material to allow infrared spectral analysis. However, none of the solvents used would dissolve the films produced by any of several tape types. The solvents used were:

- Methanol
- Acetone
- Methyl ethyl ketone
- Acetone
- N-Hexane
- Methylene chloride
- Dioxane
- Dimethyl sulfoxide
- Chloroform

Fig. 59 SURFACE OF BRASS HEAD WITH VARNISH (1000X)

Fig. 60 BACKSCATTER OF SURFACE SHOWN IN FIG. 59 (1000X)

Finally, a head containing the varnish was lapped with potassium bromide, allowing direct infrared evaluation without further transfer of the material. However, the quantity obtained was insufficient to achieve a spectral analysis. Therefore, the emphasis was redirected toward the investigation of the effects of the varnish on drag.

Initially several tests were concluded to determine if head varnish was continually produced throughout the life of the tape. A 200-kHz sine wave was recorded on an endless loop of Memorex 63L at 30 ips. The signal was then monitored as a large number of tape passes were compiled. It was found that the signal level had dropped 4 db within the first 2,000 passes, but then remained relatively constant for the succeeding 7,000 passes (Fig. 61). At this point the head was removed and re-lapped. The same recording was then replayed and the amplitude had increased 3 db. The test was continued for an additional 30,000 passes, during which time the amplitude slowly decreased. Separation loss calculations indicated a varnish thickness of slightly less than 10 microinches. This was deposited early in the test, although additional varnish accumulated throughout the remainder of the test. Similar results were observed using 3M 351 tape.

A test was also conducted to determine the effects of head varnish on drag. First, an endless loop of 3M 888 was run over a brass head for 10,000 passes at 65°C. A second tape was run over a different head to remove any initial abrasion. The second tape was then run on the head used for the initial test. The starting torques were essentially identical, Fig. 62. indicating that the former accumulation of head varnish did not affect the frictional drag properties. It was therefore concluded that the presence of head varnish affected only the short wavelength reproduce response of a recorder.

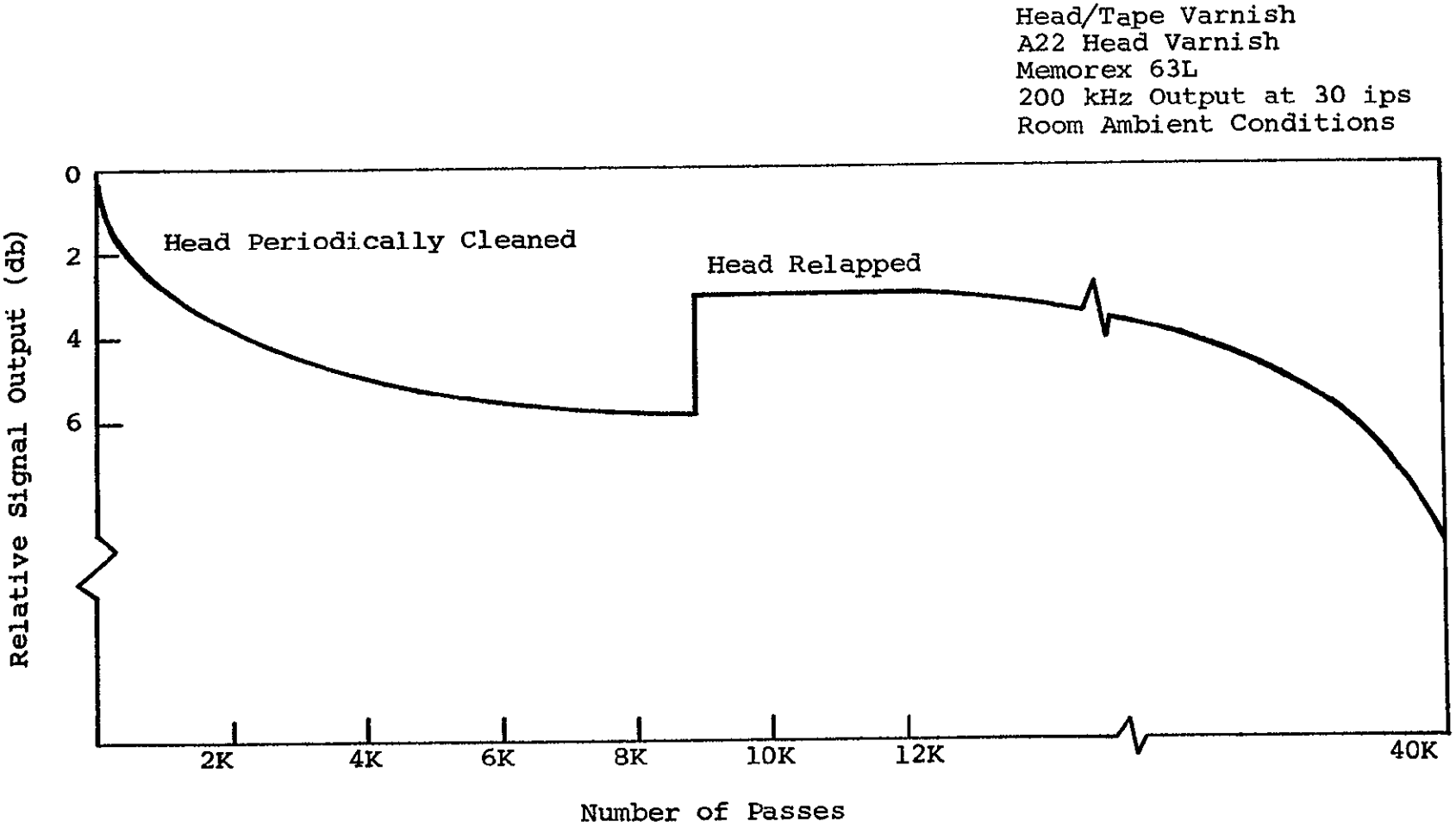

Fig. 61 EFFECT OF HEAD VARNISH ON REPRODUCE OUTPUT

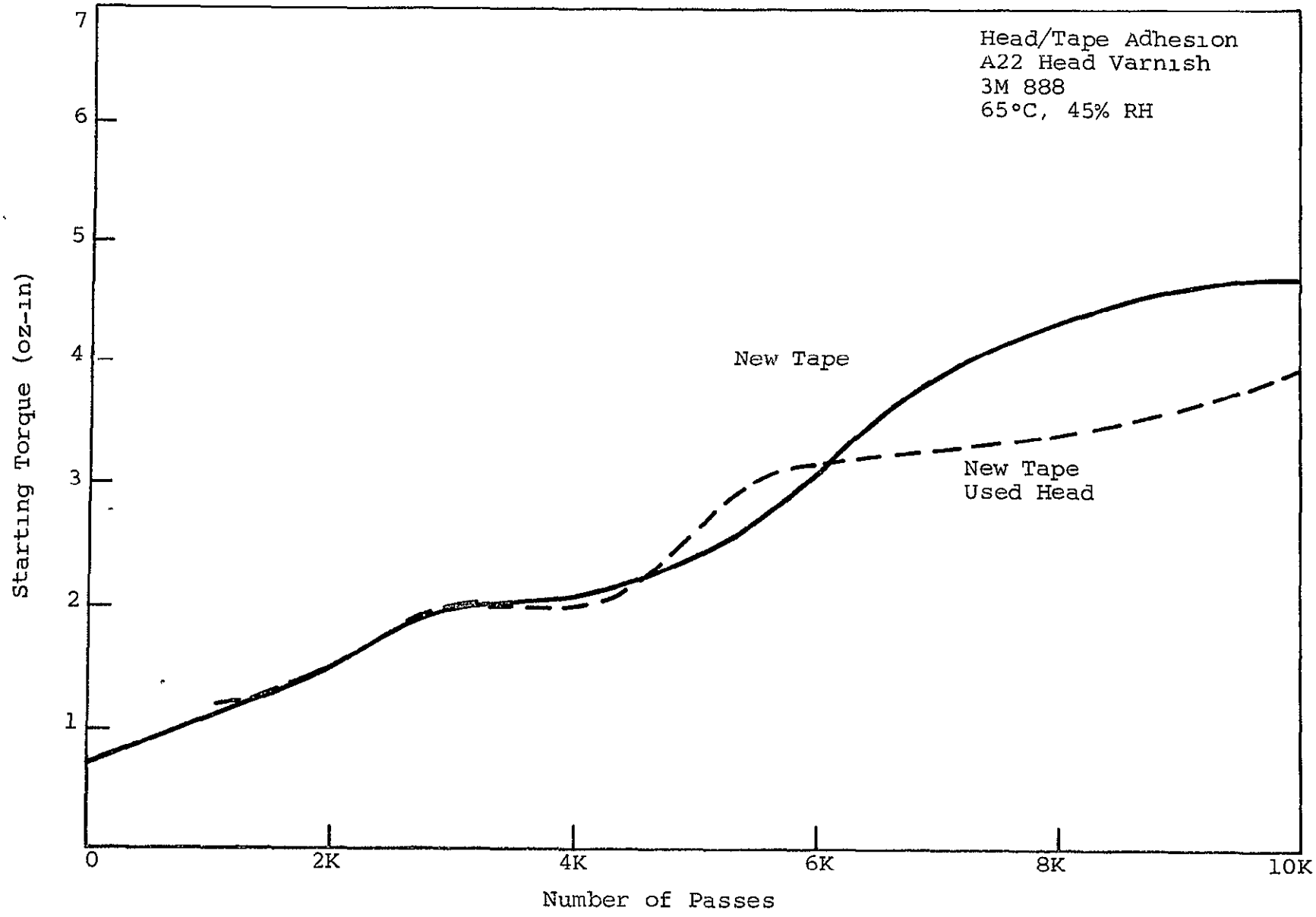

Fig. 62 PRESENCE OF HEAD VARNISH, 3M 888

B. Oxide/Binder Debris

The tendency of magnetic tape to produce debris as a result of extended use has been observed in all forms of magnetic recordings. Generally, this debris has not been a monumental problem with ground-based systems, where head cleaning has been incorporated as a daily maintenance procedure. However, debris in unattended satellite recorders has been a serious problem, exemplifying the need for stringent control of the head and tape parameters in these applications.

The formation of the debris has produced three particular failure modes in the magnetic recording process.

1. Although large amounts of debris fall to the surface of the transport, a certain quantity adheres to the soft oxide/binder surface of the magnetic tape. This material subsequently interferes with the reproduction of data and manifests itself as an increase in drop-outs in that specific area.

2. A buildup of this debris on the surface of a magnetic recording head has resulted in an overall spacing of the media from the head surface, resulting in a loss of signal amplitude at specific wavelengths.

3. A further problem has been associated with the interaction of the oxide/binder surface of the magnetic tape and the debris adhering to random areas of the contact surface of the recording head. Some interaction with the overall adhesion/stiction problem was noted.

In accordance with the overall philosophy of the test program, the initial thrust of the debris tests was directed towards the determination of failure mechanisms. Here the scanning electron microscope proved to be a valuable tool, as the surfaces of both heads and tapes could be readily viewed at high magnification. Therefore, most of the analysis of mechanisms leading to debris was accomplished by running tapes at various environments, followed by examination of the surfaces using the SEM.

The underlying cause of debris in a system involving sliding contact and friction is wear. Wear occurs when the material in the vicinity of the gross contact region is subjected to a stress system. When two surfaces are brought together, contact is made only at the tips of the microscopic irregularities on each surface, so that the total area of contact is much smaller than the apparent area of contact and depends primarily on the normal load and friction between the surfaces. When sliding takes place, these small areas will either shear brittly or deform plastically. Shearing occurs if the adhesion at these points is such that the junction strength is lower than either of the materials and the materials are brittle in nature. The areas deform plastically as the temperature during sliding becomes high enough or the material behaves ductily. In either case, there results in material movement away from the contact area. This mechanism is called gross plowing. If only surface asperities are involved, the mechanism is called local plowing.

Another way in which wear can occur is by transfer or exchange of material between the two contacting surfaces or surface galling. This transfer of material can produce a change in the geometry of either surface on a gross scale or a local scale. In either event, the stress system caused by the new geometry can produce plowing. When this type of wear occurs, debris is produced. The debris can then produce an abrasive action which is the final type of wear. If the abrasive action is caused by debris in oxide form, it is called fretting corrosion; otherwise it is called fretting.

The model states that wear can be reduced to a minimum or eliminated by keeping the stress in the vicinity of the region of contact below a certain value. The maximum shear stress theory of failure states that, if the maximum shear stress occurring in a body is greater than the shear strength of the material or greater than its yield strength, either rupture or plastic

flowing will occur. Thus, to eliminate gross plowing, the following condition must be observed.[7]

$$\tau_y > \tau_{max} \qquad \text{(B-1)}$$

where

τ_y = the yield point or failure stress of the weaker of the two materials in contact

τ_{max} = the maximum value of the shear stress developed.

Wear produced by material transfer and local plowing can be eliminated for one pass by keeping the stress below a certain fraction of the yield point in shear,

$$\tau_{max} < \alpha\tau_y \qquad \alpha < 1 \qquad \text{(B-2)}$$

One pass is defined as the relative displacement (s) sufficient just to unload the original contact region.

Wear produced by transfer, local plowing, fretting corrosion, and fretting can be eliminated for a given number of passes by keeping the stress below a fraction of the yield point in shear,

$$\tau_{max} < \beta\tau_y \qquad \beta \leq \alpha \text{, where } \alpha \text{ and } \beta \text{ are empirical constants} \qquad \text{(B-3)}$$

The contact stress problem between a sphere and a plane pressed together by a normal load is covered by the Hertz contact problem. If sliding is introduced into the Hertz contact stress problem, the two possible maximum shear stresses occurring for the sphere-plane geometry are:

$$\tau^s_{max} \approx 90\sqrt{\frac{1}{16}(1 - 2\nu)^2 + \mu^2} \qquad \text{(B-4)}$$

$$S_c = \left(\frac{6P}{\pi^3 \left[\frac{1 - \nu_1^2}{E_1} \right] + \left[\frac{1 - \nu_2^2}{E_2} \right] R^2} \right)^{1/3} \qquad \text{(B-5)}$$

$$\tau_{max}^{d} \approx 0.3190\ S_c \qquad \text{(B-6)}$$

where

μ = the coefficient of friction,

ν = Poisson's Ratio,

S_c = the maximum contact pressure as defined in the Hertz problem (B-5),

P = the normal load,

R = the radius of the sphere,

ν_1 = Poisson's Ratio for the material of the sphere

E_1 = Young's modulus for the material of the sphere and

ν_2 and E_2 = those for the material of the plane.

τ_{max}^{s} = maximum shear stress on the contact surface

τ_{max}^{d} = maximum shear stress beneath the contact surface

These expressions assume that the local coefficient of friction is equal to the coefficient of friction as measured and that the effect of the frictional force on the shear below the surface can be ignored. On the basis of this analysis Clinton, Sirico, and Pimbley[7] have developed an expression for the relative wear of ball and tape,

$$\frac{N_{ball}}{N_{tape}} = \frac{\tau_{yball}}{\tau_{ytape}} \qquad \text{(B-7)}$$

The most prevalent wear mechanism observed throughout the program was plowing. On the surface of heads, plowing resulted from the relatively hard magnetic particles run over the softer head materials. The tape surface was damaged by head discontinuities, oxide debris previously deposited, and dust. Figure 63 is an SEM photomicrograph of the surface of RCA 617 tape at a magnification of 3000X. This was a localized area of damage apparently resulting from a contaminant such as dirt. The surface damage resulting from either debris or asperities on the head was found to be essentially continuous along the tape length. Wear patterns such as shown in Fig. 64 for the DuPont Crolyn tape were typically found after tape usage. Similar patterns were frequently observed in the contact area of head surface. Figure 65 shows the brass portion of a brass and permalloy head after running 3M 888 tape. Again, this surface finish was representative of the soft metal heads following use.

The principal difference in the wear of head and tape surfaces was the relocation of the disturbed material. On the head surface, the material was simply displaced to either side of the wear line. On the tape surface, however, the binder was actually broken, and resultant debris was produced. An isolated area of damage on the surface of DuPont Crolyn is shown in Fig.66. Figure 66a magnifies a plow line in the direction of tape motion and clearly shows the resultant debris clinging to the tape surface. Such debris could eventually be deposited on the head or remain with the tape, although in either case a degradation in signal properties would result.

In addition to plowing, several other failure mechanisms were observed during the preliminary tests. Edge damage was encountered early in the program while running tape on an endless loop transport containing edge guides. Figure 67 is a SEM photomicrograph of the oxide surface of a Memorex special high temperature tape following this test. The damage encountered

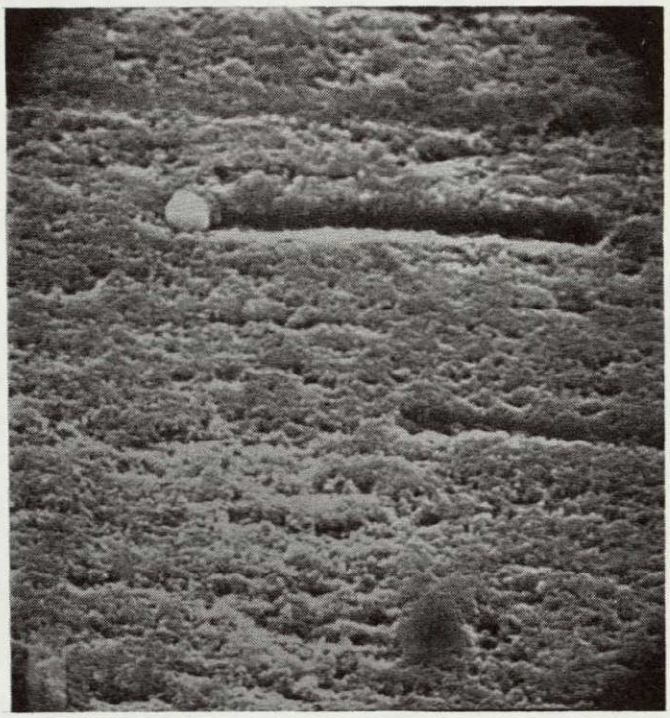

Fig. 63 LOCALIZED PLOWING OF RCA 617 TAPE (3000X)

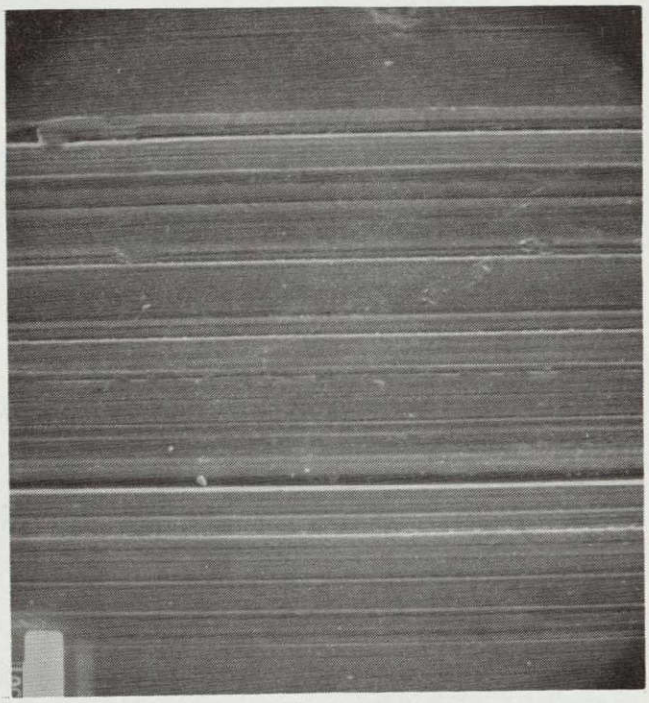

Fig. 64 USED TAPE SURFACE FINISH
DUPONT CROLYN (1000X)

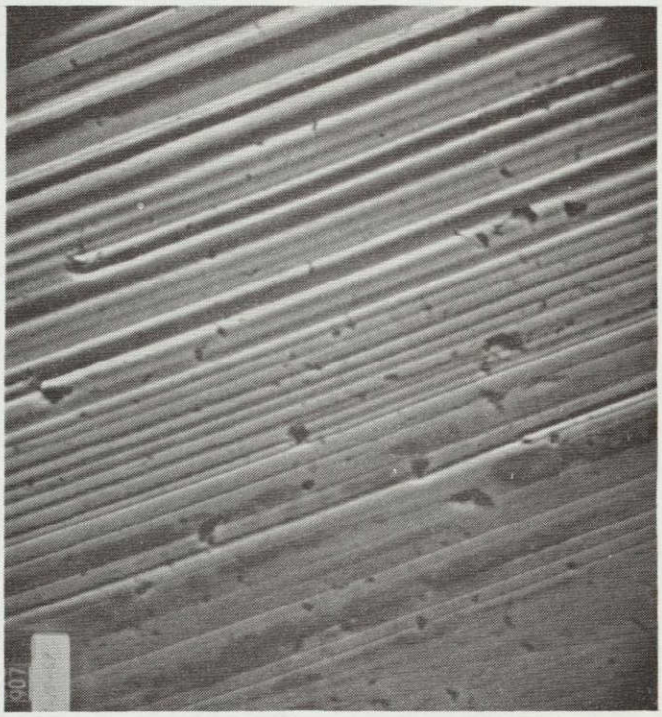

Fig. 65 BRASS HEAD SURFACE USED WITH 3M 888 (2000X)

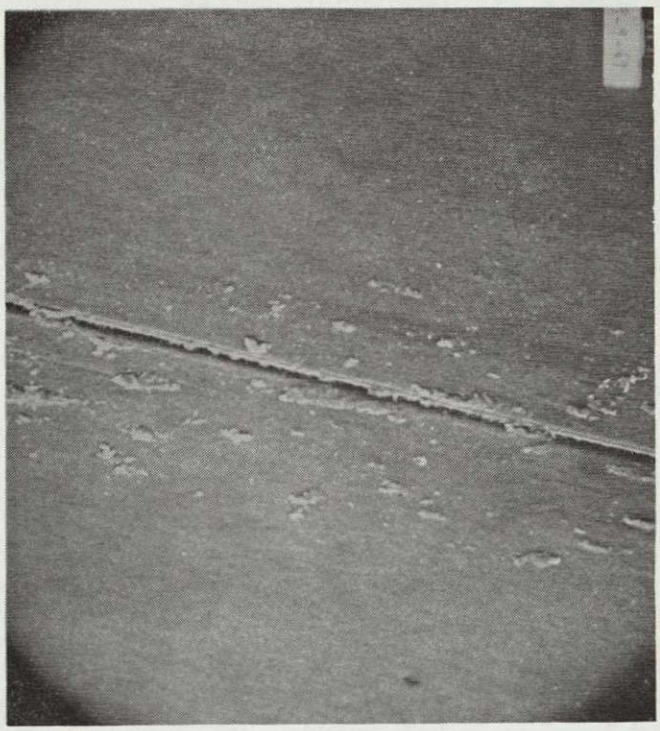

a. (300X)

b. (1000X)

Fig. 66 DISPLACEMENT OF TAPE BINDER AFTER WEAR

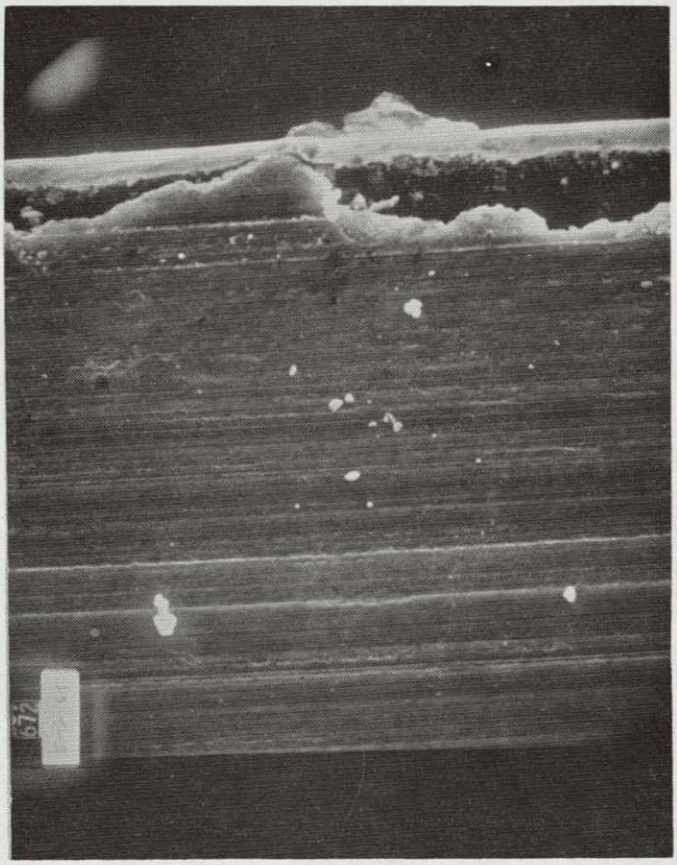

Edge of Mylar

Broken Edge of Binder

Fig. 67 EDGE DAMAGE ON OXIDE SURFACE (1000X)

was the result of insufficient adhesion of the binder to the mylar rather than surface effects.

The actual fracturing of an oxide binder layer was also observed on the special Memorex tape tested. The cracks shown in Fig. 68 developed while running the tape under only 8 ounces of tension. A large quantity of debris was generated during this test despite the room ambient environmental conditions. However, this was not a failure mechanism encountered with other tape types examined throughout the program.

Most of the debris resulting from the mechanisms described was a dry, powder-like material and usually brown in color due to the oxide. However, at high temperatures and humidities a substantially different type of debris was deposited on the heads. This material appeared to have been melted, as seen in Fig. 69. The photomicrographs were taken of a brass head following a test using 3M 888 at 65°C and 45% RH. Debris of this nature was usually located just before or after the actual contact area on the head, and was found to be extremely detrimental to the adhesion performance of the head and tape combination.

Having established a number of debris mechanisms, a series to tests was conducted to isolate certain specific tape and head parameters. As in the area of head-to-tape adhesion, a series of hypotheses was formulated and individually evaluated. A summary of the parameters studied and the hypotheses tested is shown in Figs. 70 and 71.

The general limitations of environmental and operational parameters used in the evaluation of head-to-tape adhesion were maintained throughout the debris tests. Both endless loop and reel-to-reel transport configurations were employed. However, the capability of quantizing debris was not as straightforward as the drag measurements for adhesion. The principal method finally employed was a measurement of the weight of debris accumulated on the heads. This was chosen because the most serious

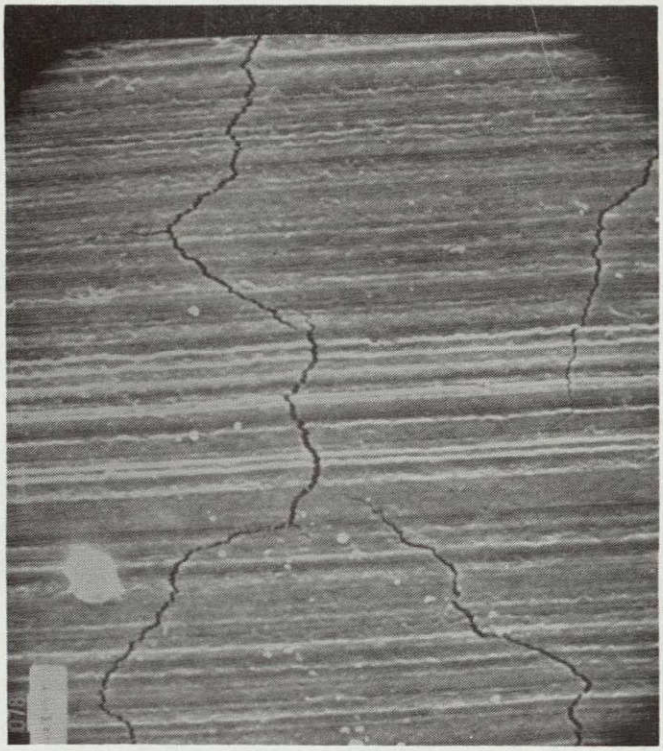

a. (3000X)

b. (10,000X)

Fig. 68 FRACTURING OF THE BINDER SYSTEM

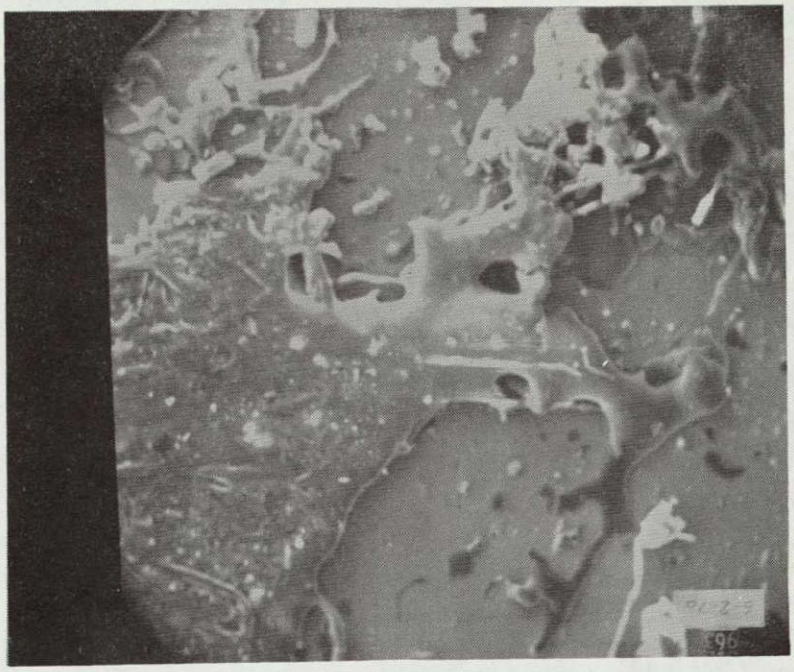

a. (100X)

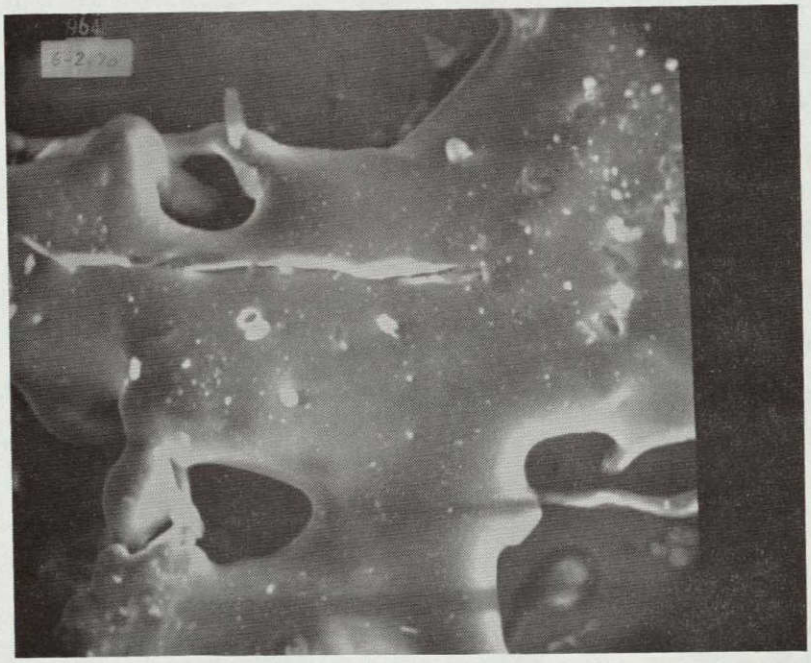

b. (300X)

Fig. 69 MELTED DEBRIS

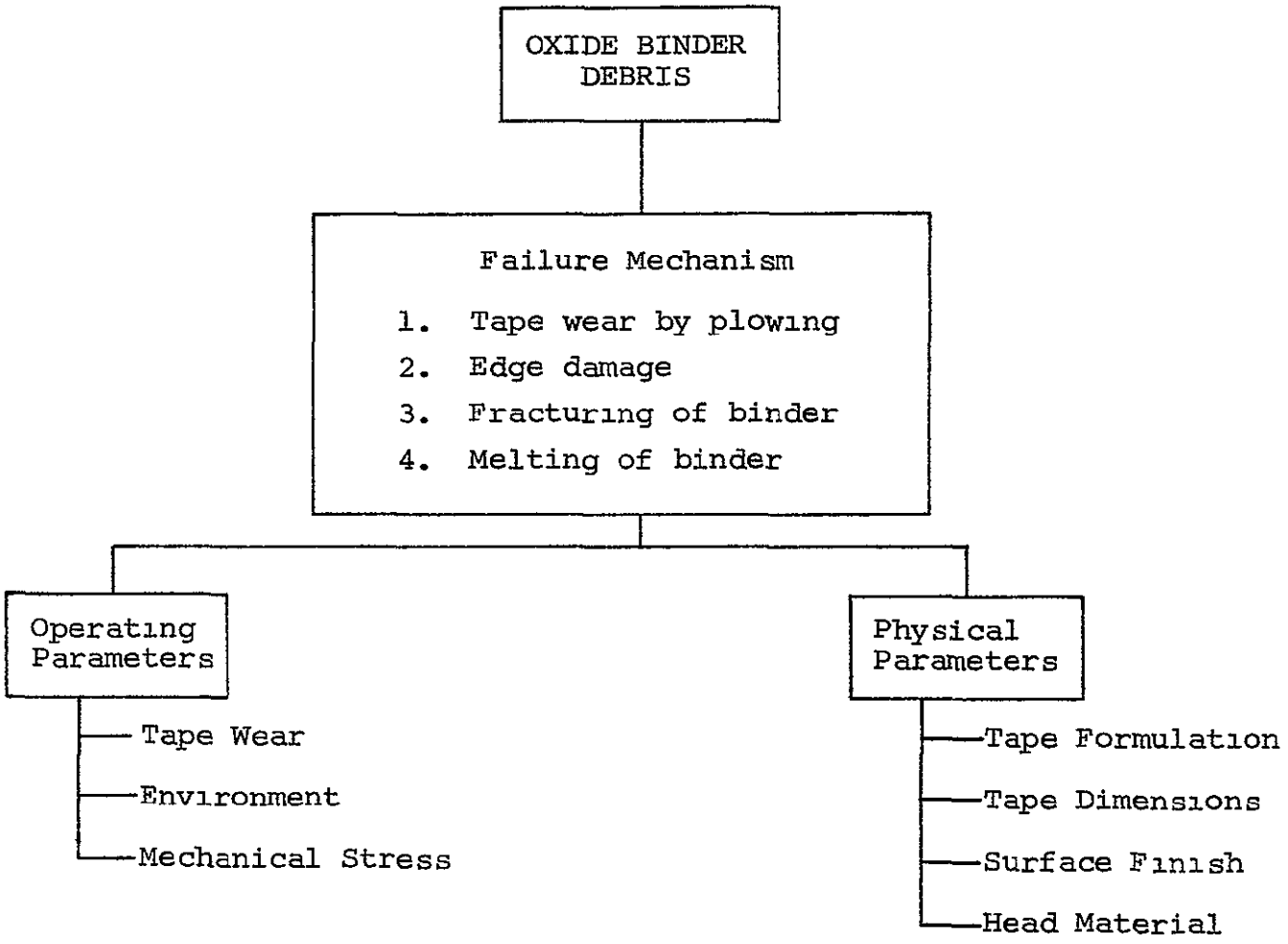

Fig. 70 OXIDE/BINDER DEBRIS FAILURE MODE ANALYSIS

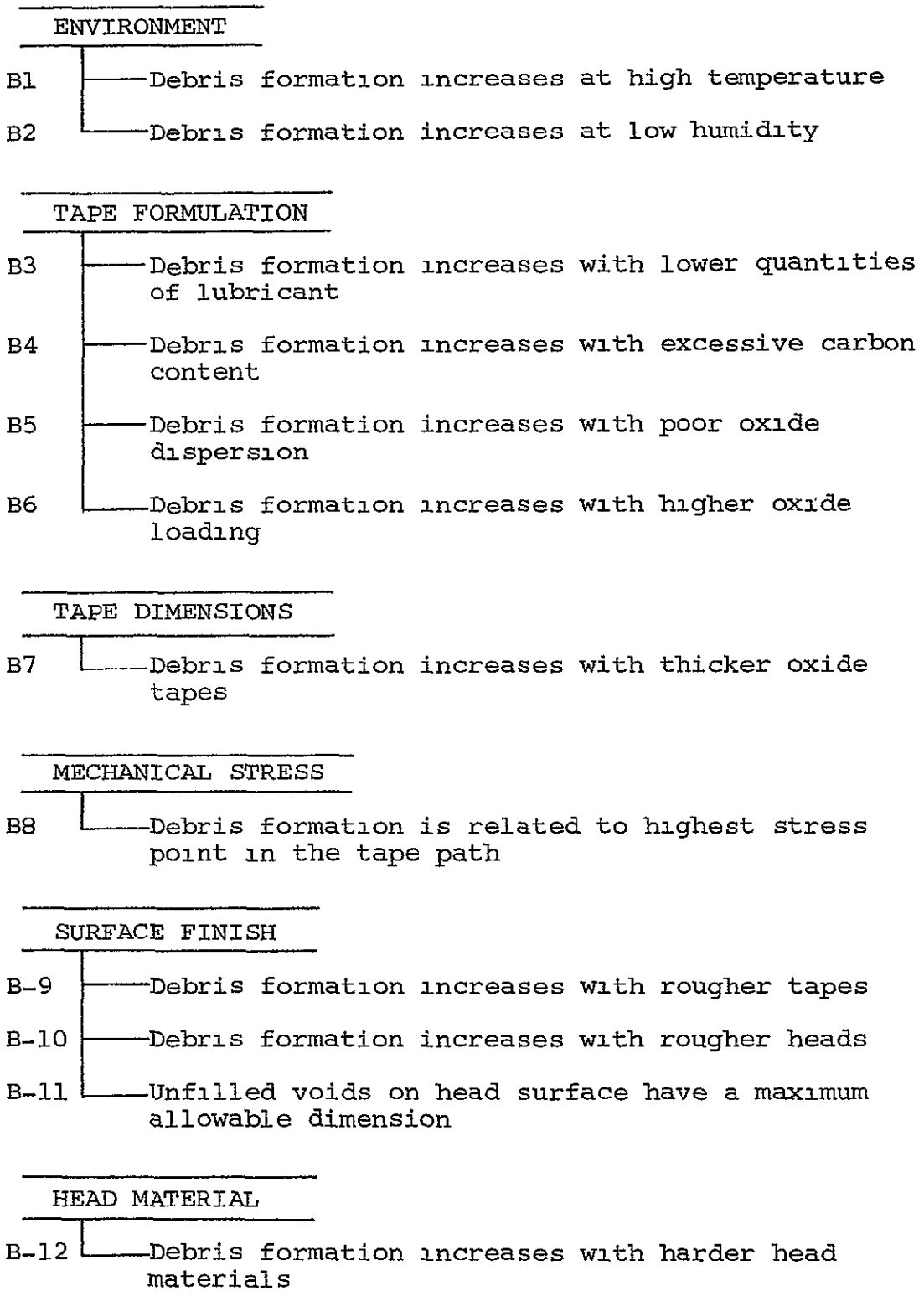

Fig. 71 OXIDE/BINDER DEBRIS HYPOTHESES INVESTIGATED

effects of debris, spacing of the entire tape from the head and increased friction, resulted from this accumulation.

1. Ambient Temperature

The preliminary tests conducted for failure mode analysis yielded two types of debris depending upon the environmental conditions. Specifically, debris produced at the higher temperatures resembled a melted material, while the debris found at room temperature was a powder, more nearly resembling that generated on typical ground-based systems. It was also noted that considerably larger quantities were generated at higher temperatures and humidities. Therefore, the hypothesis that the generation of debris increased was a logical outcome of these results. A series of tests was then established to verify the relationship between environment and debris.

The tests to isolate the parameter temperature were run on endless loop transports in an environmental chamber. The same eight tape types evaluated for frictional characteristics were used at temperatures of 65, 45, and 25°C. Each tape loop was run over an aluminum dummy head for over 49,000 passes at 30 ips. Tape tension was 8 ounces. At the conclusion of each test the head was removed, and the amount of debris deposited was carefully weighed using a precision balance accurate to within 10 micrograms and estimatable to 1 microgram.

The amount of debris collected at 65°C and approximately 0% relative humidity was found to be considerably greater than that collected at 45°C under the same conditions. Table XI, a comparison by tape type, indicates that all but one brand generated less debris at the lower temperature. However, this particular brand (3M 351) produced somewhat more debris that most of the remaining tapes. It was found that the generation of debris tended to be progressive, i.e., debris once deposited on a given area of the head caused further tape damage and a more rapid rate of accumulation (Fig. 72). Therefore, the trend reversal for

Table XI

OXIDE/BINDER DEBRIS VARIATION
WITH TEMPERATURE

Tape Type	Weight of Debris (μg)	
	65°C, 0% RH	45°C, 0% RH
RCA 617	2,000 (Est.)	1,457
3M 351	206	451
Memorex 79L	94	44
3M 871	57	47
Memorex Quantum	85	32
Memorex 63L	93	15
3M 888	65	17
3M 777	52	9

Fig. 72 LOCALIZED ACCUMULATION OF DEBRIS

this tape was not considered significant. A few tests were also conducted at 25°C; however, the small amount of debris produced was not reliably measurable.

The results of these tests, as well as the examination of heads from numerous other tests conducted throughout the program, confirmed the adverse effect of increased temperature on the formation of debris. A precise determination of why the increased temperature resulted in greater debris was not achieved. It was presumed from the indications of binder softening and from the wear model itself that the mechanical properties of the binder polymer were degraded at high temperature.

2. Relative Humidity

In conjunction with the endless loop tests to isolate the effects of temperature, an additional set of tests was run at 45°C to evaluate the effect of relative humidity. It had been hypothesized that the formation of debris would increase at low humidity, primarily due to possible drying effects of the binder system. However, the results of the head-to-tape adhesion tests indicated strong preference for operating at very low humidities. Further, head wear reportedly was reduced substantially at low humidity. Therefore, a possible conflict existed in optimizing this parameter.

The humidity tests were conducted in accordance with the same procedure discussed in the previous paragraph. The range of humidity examined was ~ 0% to 30% RH. The data obtained by weighing the debris accumulation did verify the hypothesis that low humidity operation accelerated the production of debris. As seen in Fig. 73, this was particularly true for the RCA 617 and 3M 351 tapes, the two tapes producing the highest quantities of debris at low humidity. The six remaining tape types (3M 888, 777, 871, and Memorex 63L, 79L, Quantum) produced small quantities of debris. Further, the average for the six tapes was reduced by only 20% when the humidity was increased to 30%.

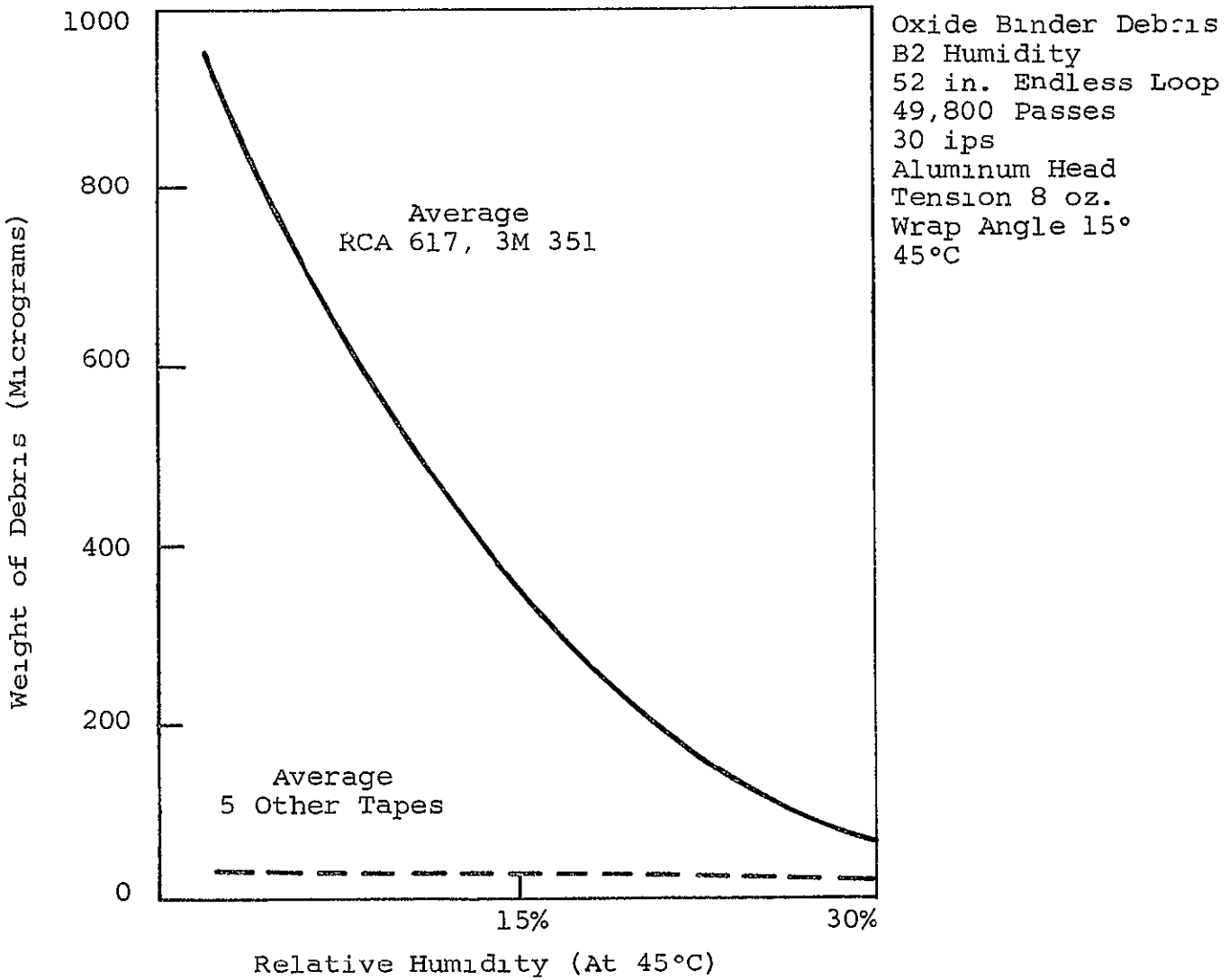

Fig. 73 EFFECT OF HUMIDITY

Relative humidities above 30% were not evaluated during these tests because of the poor adhesion results already obtained at 45% RH. However, a review of the adhesion data obtained at high temperature indicated greater quantities of debris at 45% RH than at 0% RH. Therefore, it was concluded that the debris accumulation shown in Fig. 73 does not continue to decrease with increasing humidity. Rather, a minimum could be expected around 15-30% RH. The increased quantities of debris at 45% RH were also observed after tests conducted on the reel-to-reel transport used longer lengths of tape.

3. Lubricant Content

The lubricants added to tape binders improved the frictional characteristics of the tape. It had been hypothesized that a reduction in frictional drag would also effect a reduction in debris. However, two tape types, RCA 617 and 3M 351, produced more debris than any of the others evaluated throughout the endless loop tests. It had already been determined that these tapes contained the highest quantities of lubricant.

The quantity of lubricant for each of the tape types tested was determined by the amount of material extracted from the binders with N-hexane. The relationship between these quantities and the debris generated at 45°C and 0% RH is shown in Fig. 74. The data clearly showed a trend of increasing debris as the quantity of lubricant was increased, and further that a maximum limitation existed beyond which the amount of accumulated debris increased rapidly. Therefore, it was concluded that the lubricant additive had a weakening effect on the binder polymer resulting in an overall loss of cohesion.

The abundance of lubricant found in the RCA 617 tape was apparently responsible for the generation of the large deposits of debris noted during the earlier head/tape adhesion tests. The tape, in turn, was adhering to its own debris, resulting in high frictional drag forces. It was for this reason that the RCA 617

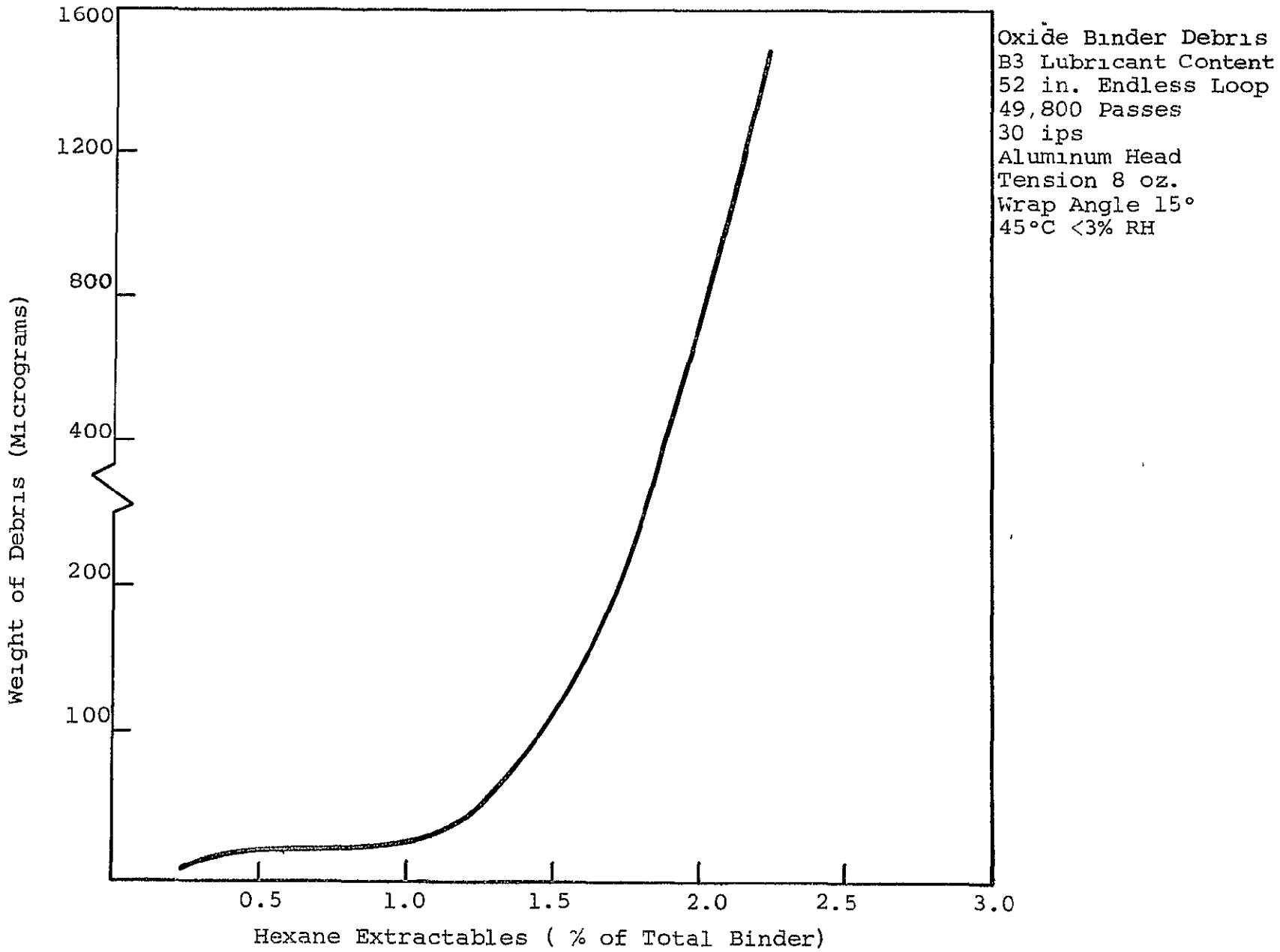

Fig. 74 EFFECT OF LUBRICANT CONTENT

did not comply with the earlier conclusion that increased quantities of lubricant reduced the coefficient friction for tape binders.

4. Carbon Content

As previously discussed, carbon has generally been added to tape binders to reduce the possibility of static electricity build-ups. However, as an additive to the basic polymer, it was conceivably a factor in further weakening the binder integrity. Therefore, it was hypothesized that debris formation increased with excessive carbon content.

An examination of the data obtained from the endless loop tests for debris did not confirm a correlation between low resistivity (i.e., in high carbon content) and the accumulation of debris. However, only one tape, RCA 617, measured less than 1.0×10^7 Ω/sq. Although this tape did produce large quantities of debris, this was primarily attributed to the quantity of lubricant. This judgment was based upon the magnetic properties of the resultant material, implying the presence of oxide.

Late in the program an additional tape, the Bell and Howell W4, was tested on a reel-to-reel transport. This tape possessed the lowest resistivity of any measured during the program, 0.165×10^7 Ω/sq. at 0% RH. When run at temperatures ranging from 35°C to 65°C, this tape produced very heavy black debris. This material was nonmagnetic and considered to be the result of excessive carbon in the binder system. Therefore, it was concluded that a minimum of resistivity of 0.5×10^7 Ω/sq. was adequate to avoid difficulties due to carbon debris.

5. Oxide Dispersion

The uniformity of the oxide dispersion for the tapes included in the program was discussed in III. A, Head/Tape Adhesion. It was found that a dc noise was sufficiently sensitive to detect irregularities that led to localized adhesion failures. Similarly, voids or agglomerates in the oxide layer were considered to be potential causes of debris due to localized reduction in cohesion.

The results of the dispersion test conducted showed the Memorex 63L and 79L to be the least uniformly dispersed of the nine tapes investigated. These two tapes also ranked poorly in the evaluation of debris produced. At 65°C only the lubricant rich RCA 617 and 3M 351 generated more debris. Conversely, the four tapes showing the highest signal-to-noise ratio (DuPont Crolyn, 3M 888, 551, and 777) also generated the least debris at 65°C. However, the test used to evaluate dispersion uniformity was not sufficiently sensitive to allow differentiation between these four tapes and a number of others exhibiting average signal to noise ratios. Therefore, it was concluded that the test was only applicable for the identification of the least uniformly dispersed tapes.

6. Oxide Loading

The hypothesis stating that debris increased percentage quantities of oxide could not be tested due to the lack of significant variation in oxide loading between tape types.

7. Tape Dimensions

Two basic tape thicknesses were evaluated during the program. The instrumentation and video tapes had nominally 1-mil substrates with an oxide thickness ranging from 0.17 to 0.54 mils. Two of the computer tapes had nominally 1.5 mil substrates with 0.55-mil oxide layers. The third computer tape had a thinner oxide because of significantly different magnetic

properties. In the mechanical tape handling analysis, Section III.C of this volume, the stress levels through the tape were found to vary with tape dimensions. This led to the hypothesis that greater quantities of debris would be produced by the thicker computer tapes.

An examination of the endless loop data showed that the 3M 777, a computer tape, produced the least amount of debris at each of the environments. Further, the Memorex computer tape, Quantum, generated the least debris of the tapes from that manufacturer. These results suggested some correlation between debris and substrate thickness. Within the tapes having the same 1-mil substrate, the 3M 871 had the thickest oxide layer. However, this tape was not one of the better tapes from the standpoint of oxide debris, apparently due to its relatively high lubricant content. Further, although the 3M 888 and 351 were dimensionally identical, the 351 consistently generated more debris.

Since the computer tapes contained the lowest quantities of lubricants, the isolation of thickness as a parameter was probably not actually achieved. Certainly the inconsistency between 3M 351 and 888 indicated a stronger correlation with lubricant content than tape dimensions. However, the mechanical stress analysis had predicted that the changes in stress would be greater with changes in backing rather than oxide thickness. Therefore, it was concluded that changes in the oxide layer thickness could not be considered a significant factor in the minimization of debris. Although the thicker substrate tapes did appear to generate less debris, it was not possible to isolate this result from the lower lubricant content common to these tapes. Since other means were available to reduce the stress levels in tape, an increase in substrate thickness was not considered a worthwhile technique to realize lower stress.

8. Mechanical Stress

The mechanical stressing of the tape on a transport can occur at any of the elements within the tape path. In certain areas, such as around capstans or rollers, this stress can be minimized. However, a minimum force must be maintained at the head to ensure faithful reproduction of the data stored. Therefore, an evaluation of the debris produced at various head pressures was calculated. This investigation was done in conjunction with the adhesion tests to isolate the effects of tension, wrap angle, and head radius. The 3M 871 tape was used on the reel-to-reel transports with aluminum dummy heads. Three levels for each of the independent variables were included.

The qualitative evaluation of debris was again determined by weighing the dummy heads before and after changing. However, some difficulty was encountered in accurately measuring the debris on the 0.5-inch radius heads because of the additional weight of the head itself which required the use of a less sensitive balance. Therefore, the 0.125- and 0.25-inch head data were used to isolate the effects of head pressure on debris.

A summary of the results obtained for the smaller radius heads is shown in Table XII. An examination of the data indicates that the debris accumulation did not correlate directly with the head pressure total radial force or tape tension. However, a relationship between debris and contact area (the product of r and θ) was observed. In general, it was found that the amount of debris generated increased as the contact area was enlarged, as indicated in Fig. 75.

The results did not indicate a higher formulation of debris while running with 12 ounces of tape tension, the highest tension used. However, the 12 ounces of tension was not producing abnormally high stress levels throughout the remainder of the transport tape path because of the 2-inch diameter rollers

Table XII

TENSION, WRAP ANGLE, AND HEAD RADIUS TESTS

Tape Tension (oz.)	Wrap Angle (degrees)	Head Radius (in.)	Radial Force (oz.)	Head Pressure ($oz./in.^2$)	Contact Area ($in.^2$)	Debris Accumulation (micrograms)
4	5	1/8	0.698	64	0.0218	84
4	8	1/4	1.12	32	0.0695	108
8	5	1/4	1.39	64	0.0436	90
8	2	1/8	0.56	128	0.0087	53
12	2	1/4	0.84	96	0.0175	75
12	8	1/8	3.35	192	0.0350	55

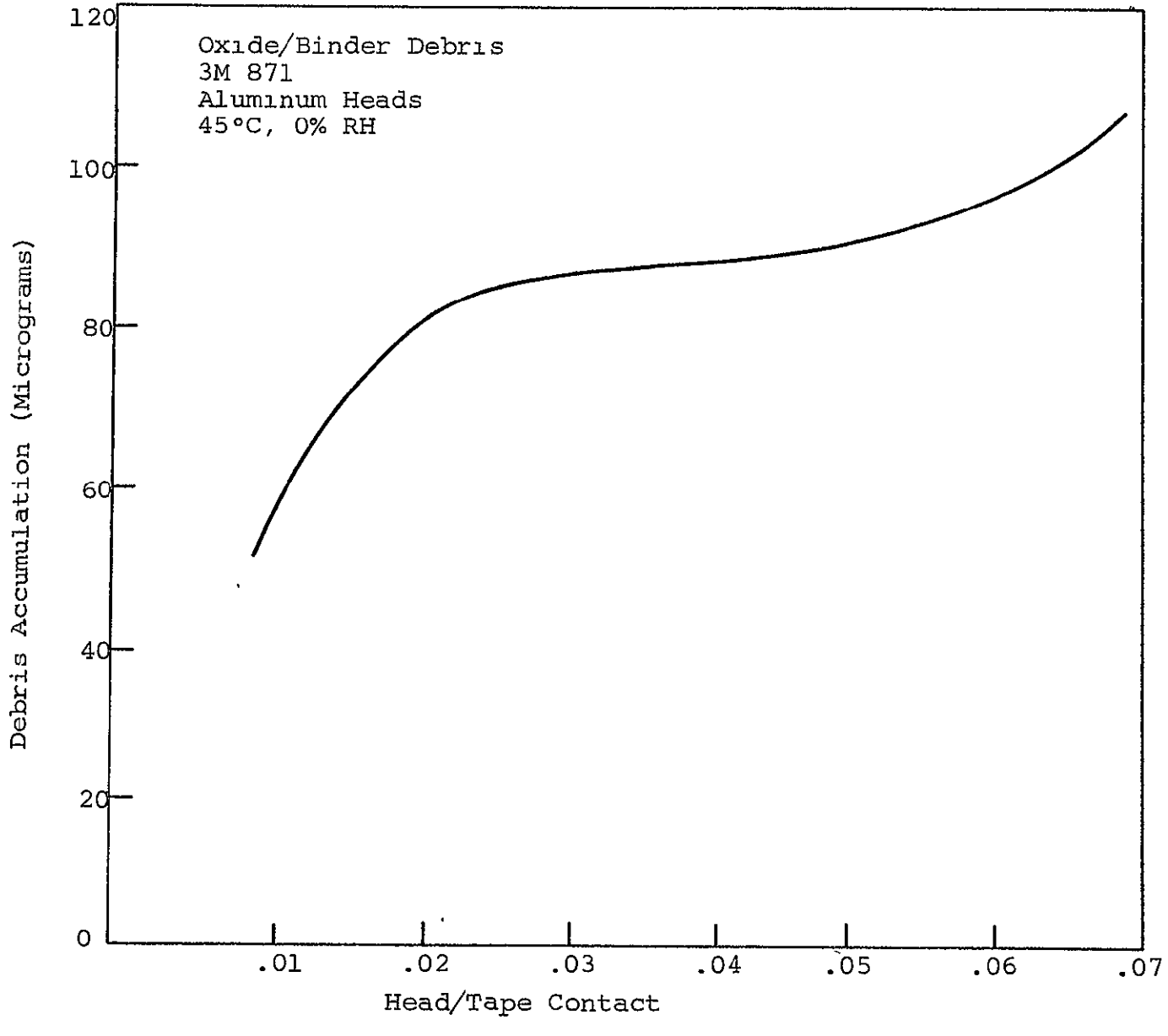

Fig. 75 RELATIONSHIP BETWEEN DEBRIS AND CONTACT AREA

and capstans used. Therefore, the tests did verify that reducing the stress levels in the tape by conservative mechanical design did prevent the buildup of excessive debris.

9. Tape Surface Finish

From the preliminary analysis of debris forming mechanisms, it was learned that tape wear resulting from plowing was nearly always present. The effect of this wear degraded the surface finish of most tapes, and numerous examples of rough, abraded tapes were examined microscopically. However, the surface irregularities inherent in the particulate media could conceivably accelerate the plowing mechanism. Therefore, it was hypothesized that the formation of debris increased with tapes having a rougher initial surface finish.

The surface roughness and waviness were measured for each of the tape types using a Bendix Proficorder. The roughness results, previously discussed in III.A, Head/Tape Adhesion, are shown in Table XIII. When compared to the data measuring debris accumulation at 65°C and 0% RH, no correlation was seen for the 3M tapes. A relationship between surface finish and debris was confirmed within the Memorex tapes at both 65 and 45°C; data are tabulated in Table XIV. However, the previously discussed interaction between surface finish and the dc noise test used for measuring oxide was still applicable. Since the noise test also isolated the Memorex 63L and 79L, it was considered an adequate and more convenient indicator of potential debris problems.

10. Head Surface Finish

Frequently during Phase I reports were received of satellite recorders losing the data from only one of several tracks due to oxide/binder debris. The localized buildup of debris on heads was also observed during the debris failure mode analysis tests. It was generally found that the surface finish of these

Table XIII

SURFACE FINISH

Tape Type	Peak/Valley (microinches)	Debris 65°C - 0% RH (mg)
3M 351	10	206
3M 777	16	52
3M 871	4	57
3M 888	6	65
Memorex 65L	11	93
Memorex 79L	14	94
Memorex Quantum	10	85
DuPont Crolyn	12	58

Table XIV

SURFACE FINISH, MEMOREX TAPES

Tape Type	Peak/Valley (microinches)	Debris 45°C-0%	Debris 45°C-30%
Memorex Quantum	10	15	12
Memorex 63L	11	17	20
Memorex 79L	14	32	58

heads, in the contact area preceding the debris deposits was badly worn or scratched. The result was an acceleration in the formation of additional debris.

A typical wear pattern for the dummy heads used throughout the testing program is shown in Fig. 76. Such measurements were obtained using a Bendix Proficorder. The surface on the far right of the figure is the unworn area of the head. The surface finishes of the worn contact area were found to be considerably rougher than the initial lapped surface. Also, the area of greatest normal wear was displaced from the edge of the actual contact area, as was expected due to the anti-elastic curvature of the tape under tensions. In addition to the normal wear, one deep scratch had developed, creating an area of excessive debris buildup. The head was also worn excessively on either side of the scratch. This was due to the effects of loose debris being pulled across the head with each successive pass. Worn head profiles resembling this figure were generally found with localized debris formations, such as shown in Fig. 77. Such accumulations of debris were observed at all environments and were not related to tape type. The condition clearly resulted from the head surface finish.

Three parameters determine the surface finish of a new head, the quality of lapping, the porosity of the material, and any voids or discontinuities between laminations or dissimilar metals. The lack of sufficiently smooth surface due to poor lapping can result in localized debris accumulations such as described above. The porosity was not considered during this program other than to select uniform materials for the dummy heads. The discontinuities, however, were significant in the ultimate generation of debris.

The construction of most conventional heads requires the use of both magnetic and nonmagnetic materials on the contact surface. The interface or junction between these materials

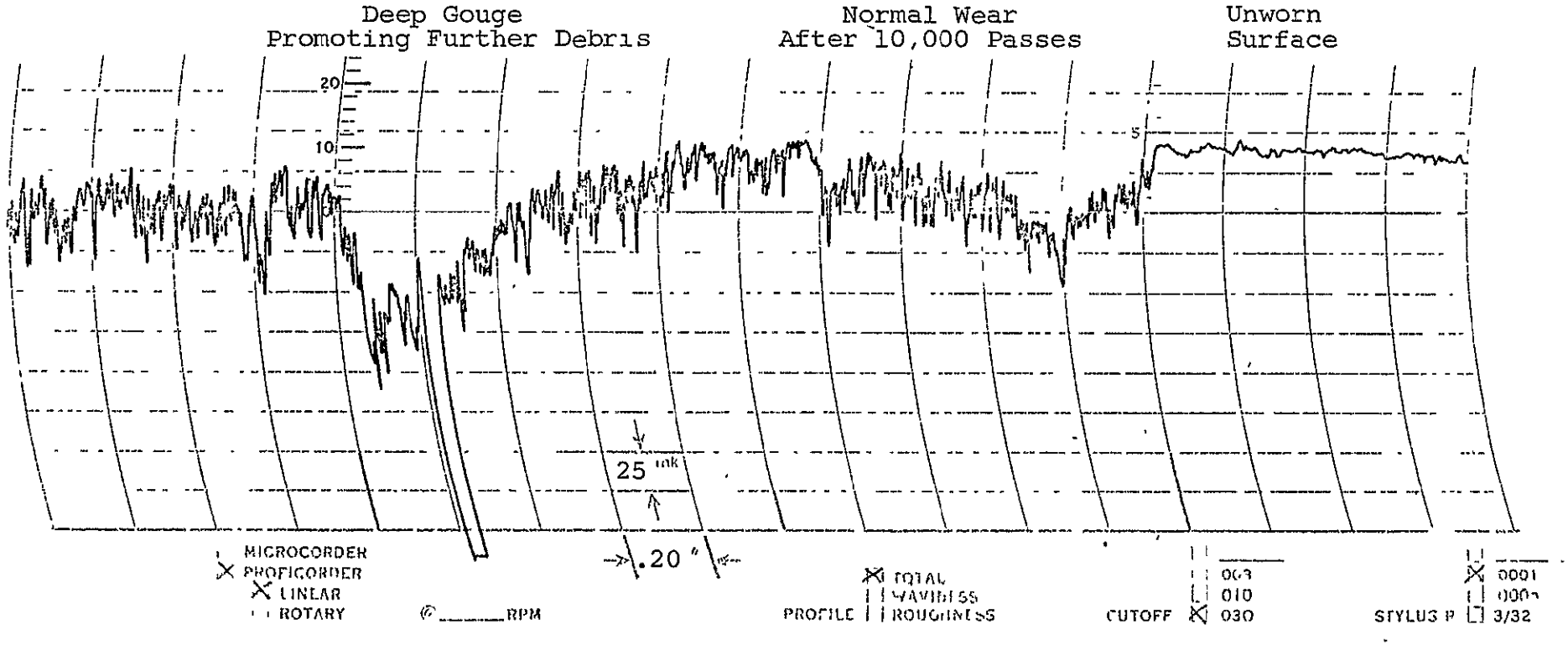

Fig. 76 SURFACE FINISH PROFILE

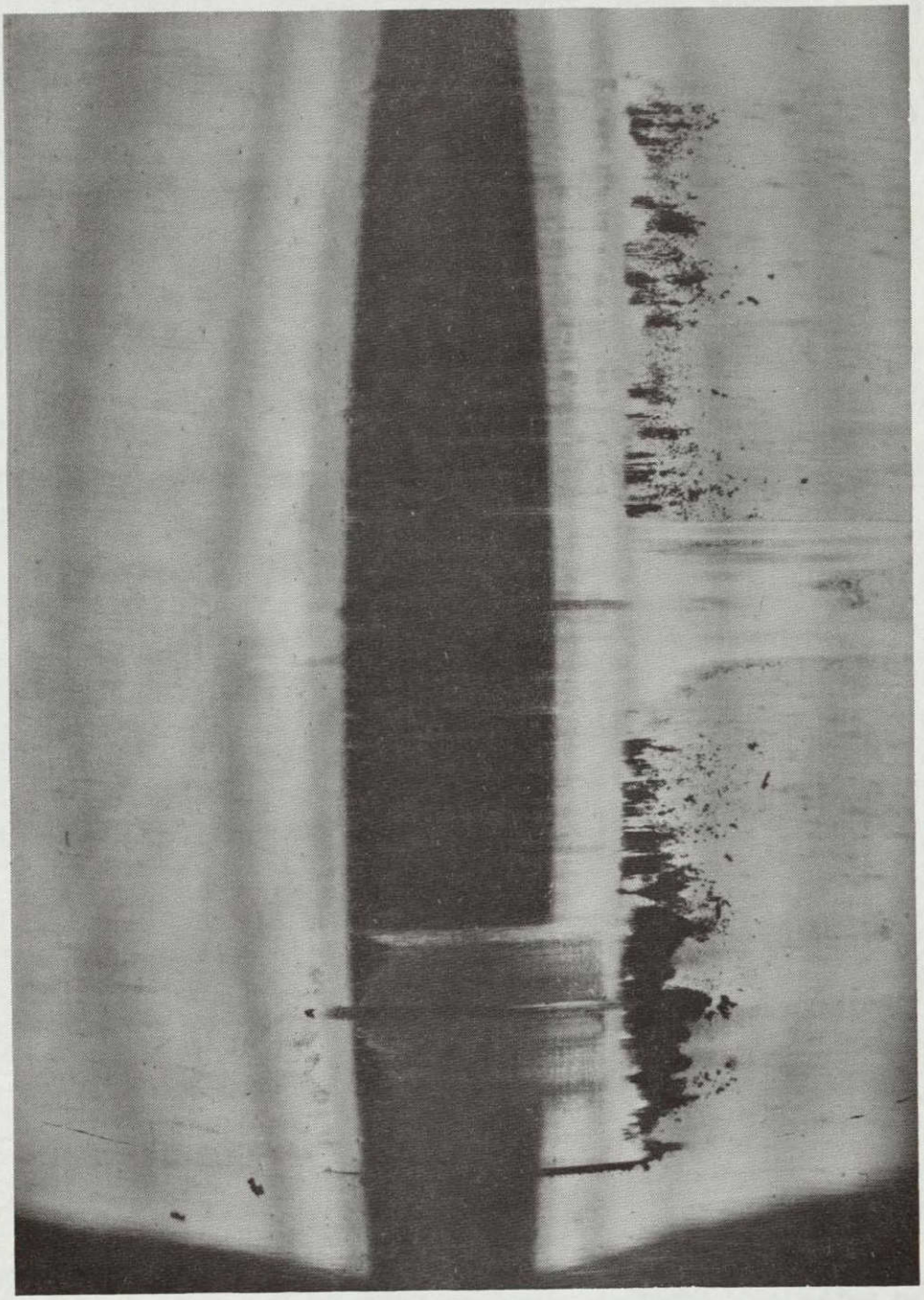

Fig. 77 LOCALIZED DEBRIS BUILDUP

was found to be a potential cause for the accumulation of debris. It was found that gaps between metals would become filled with oxide and binder, shown in Fig. 78. Further, the debris collected would build up to level above the surface of the head material, Fig. 79. Such buildups then continued to cause further tape wear.

Head designs using laminated core structures also expose discontinuities to the surface of the tape. Such lines or voids were investigated by constructing dummy head of brass with a laminated permalloy insert. It was found that debris was formed beyond the contact area corresponding to the voids between laminations, as shown in Fig. 80. The debris accumulations was often sufficient to produce significant buildups at the edge of the contact area (Fig. 81). These deposits were somewhat related to the dimensions of the void, although the progressive generation of debris tended to obscure the relationship between quantity and dimensions once a buildup was initiated. It was found that sufficiently small gaps at the junction between materials were not detrimental to the tape. Hence, it was concluded that a maximum dimension could be assigned to such areas of the head. Based upon the smallest discontinuity found that produced a deposit of debris, Fig. 82, the limitation of 50 microinches were established.

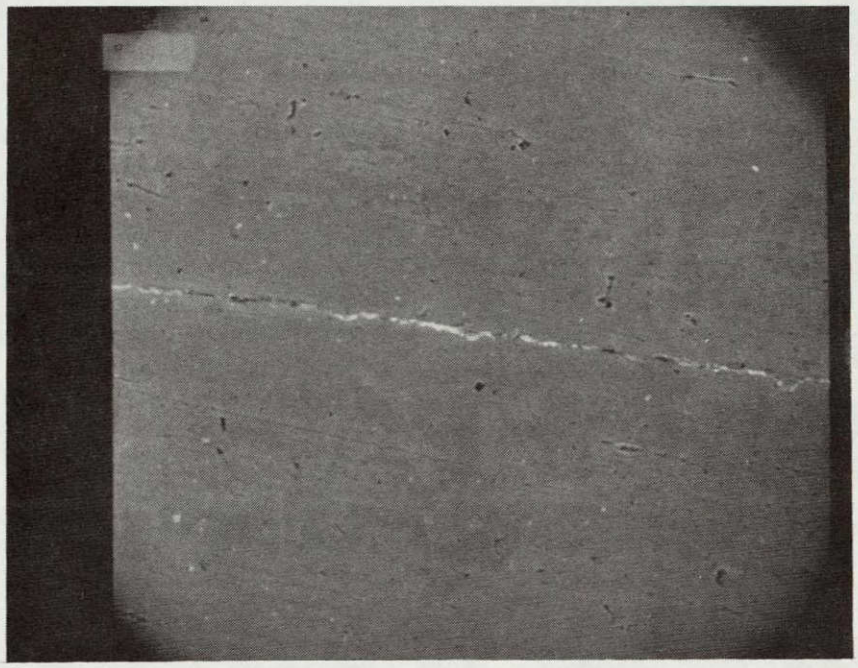

Fig. 78 DISCONTINUITY ON HEAD SURFACE (300X)

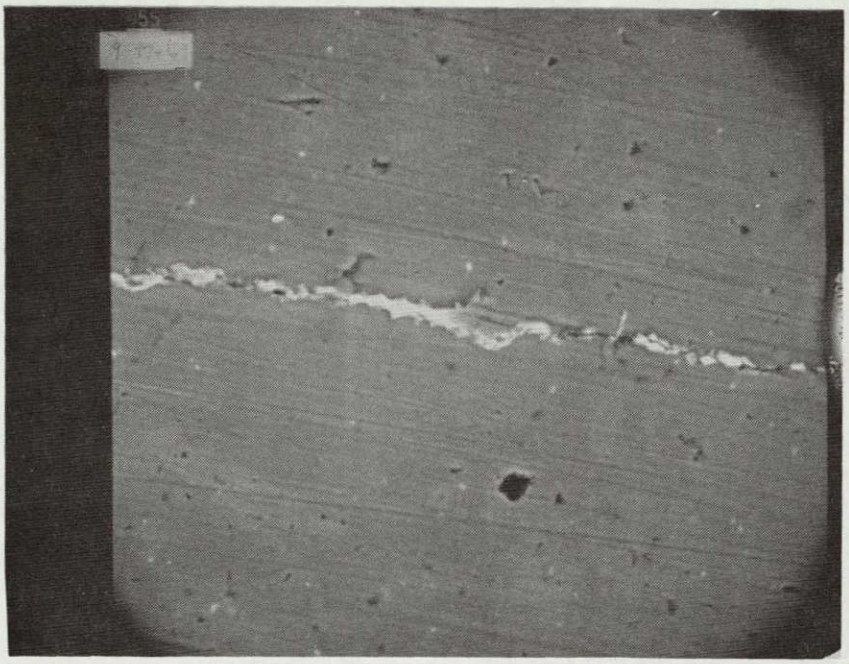

a. (1000X)

b. (3000X)

Fig. 79 DISCONTINUITY FILLED WITH DEBRIS

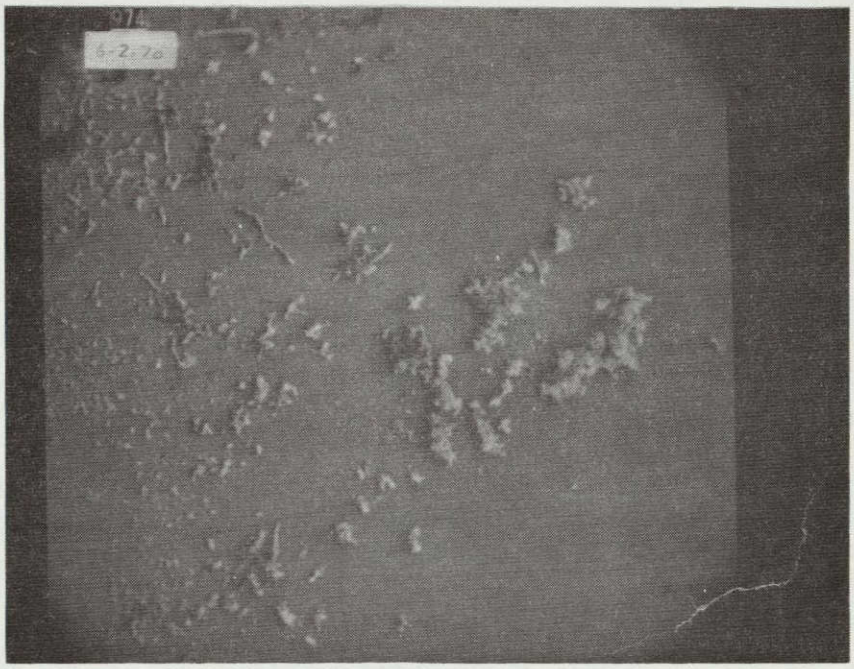

Fig. 80 DEBRIS FORMATION AT LAMINATIONS (100X)

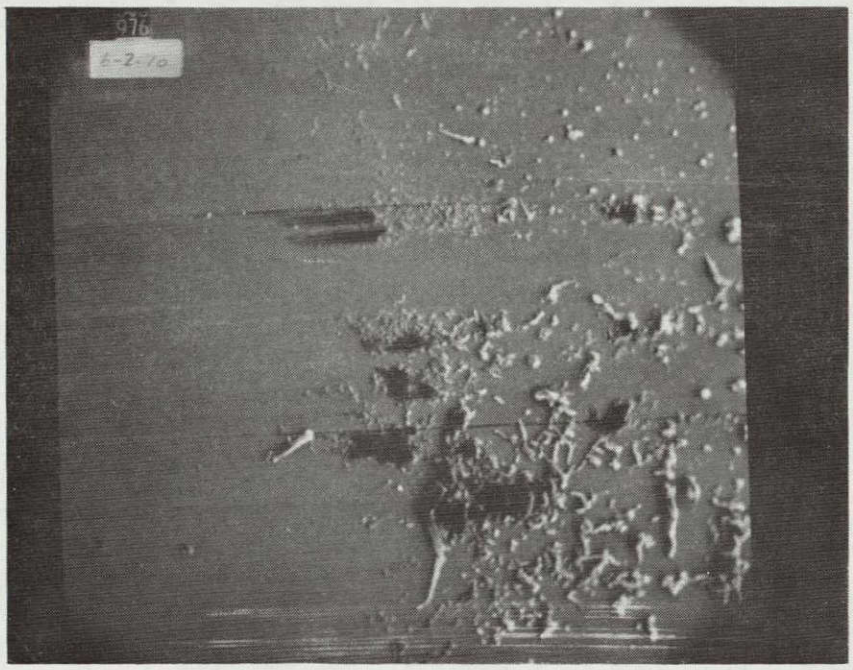

Fig. 81 DEBRIS BUILDUP DUE TO LAMINATIONS (60X)

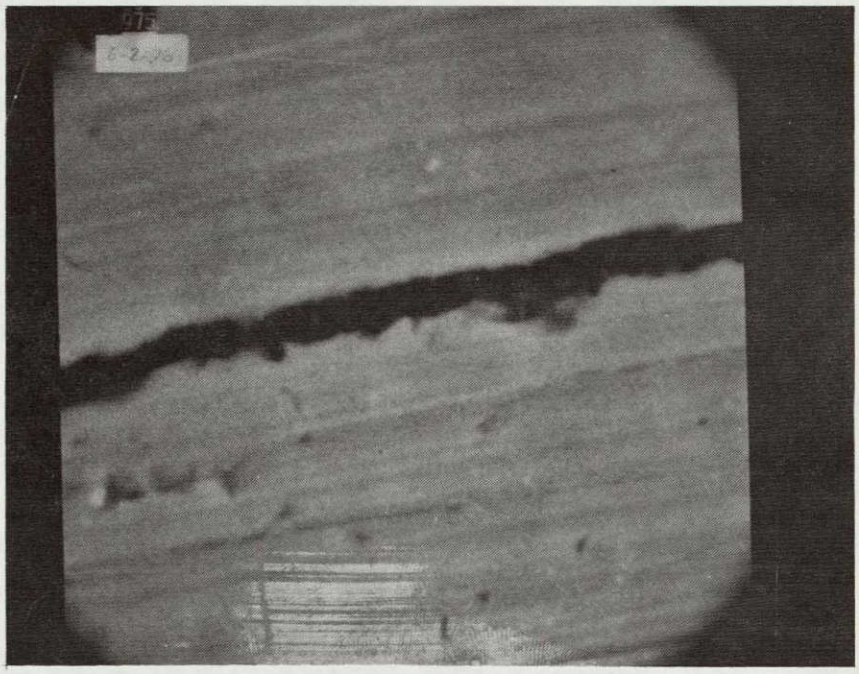

Fig. 82 SMALLEST DISCONTINUITY LOCATED CAUSING DEBRIS (6000X)

C. Mechanical Tape Handling

1. Introduction

The stresses and strains induced in magnetic tape due to mechanical handling have not been investigated to date despite the importance of being able to predict stresses in any rational design procedure. This section presents the analytical tools necessary for solving many of the commonly encountered tape transport problems.

Strength of materials procedures are used to determine the stresses in tape passing over a straight frictionless roller, tape passing over a canted frictionless roller, and tape passing over a crowned roller. A theory of elasticity solution is used to justify the strength approach to the crowned roller problem.

Two different types of canted rollers are considered. The first type is one in which the axes of adjacent rollers are non-parallel, but occupy the same plane. In this case, tape leaving one roller enters the canted roller at a non-normal entrance angle. The tape then proceeds around the canted roller in a helical path. Since the tape path is not perpendicular to the rollers axis of rotation, relative slippage and hence frictional effects are encountered. The study of this method of elevation alteration focuses upon the contact stresses (Section C-3) and the resulting frictional forces (Section C-4). The second type of canted idler is one where the axis of adjacent idlers are not parallel, but fall in parallel planes. This technique for elevation modification is based upon twisting or rotating the tape about its longitudinal center. Twisting causes the tape to enter the canted idler at a normal entrance angle. The tape progresses past the idler in a circular path without slippage. The additional stresses generated by twisting are evaluated in Section C-5.

To place the stresses calculated from the above models in proper perspective, the mechanical properties of magnetic tapes are discussed in Section C-7. Section C-8 is devoted to representing a computer program for evaluating stress levels for various tape-roller configurations. This computer program is comprehensive and represents the most effective procedure for investigating the stress levels resultant from a specific design. Further, the program readily permits parameter variations so that practical stress minimums can be realized.

The most singular result of this work is that with standard analytical tools; the stresses induced into tape by mechanical handling can be quantified. Additionally, the solutions developed here should represent the basis for a design strategy to minimize the stress levels in the oxide-binder system for any particular set of tape-roller configurations.

2. Stresses in Tape Passing Over Straight Roller

The purpose of this analysis is to determine the stresses in a magnetic tape as it passes over a straight roller as shown in Fig. 83.* The local tension in the tape is given by T, its width is W, the roller radius ρ, and the thickness of the tape t. Figure 84 is an enlarged detail of the bent tape showing that it is composed of two layers of thickness t_1 and t_2. The total thickness t is very small in comparison to the radius ρ. Point A is located at the outside of layer 1, point B is in layer 1 at its junction with layer 2, point C is in layer 2 at its junction with layer 1 and point D is at the outside of layer 2. The tape has internal forces and moment, T and M, and pressure between the roller and the tape, P. There are no shear forces since the radius of curvature

* Refer to p. 227 for LIST OF SYMBOLS.

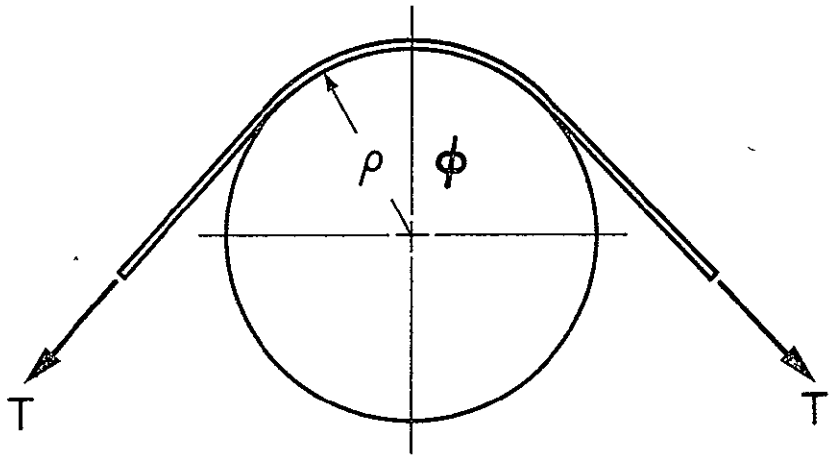

Fig. 83 TAPE-ROLLER SYSTEM

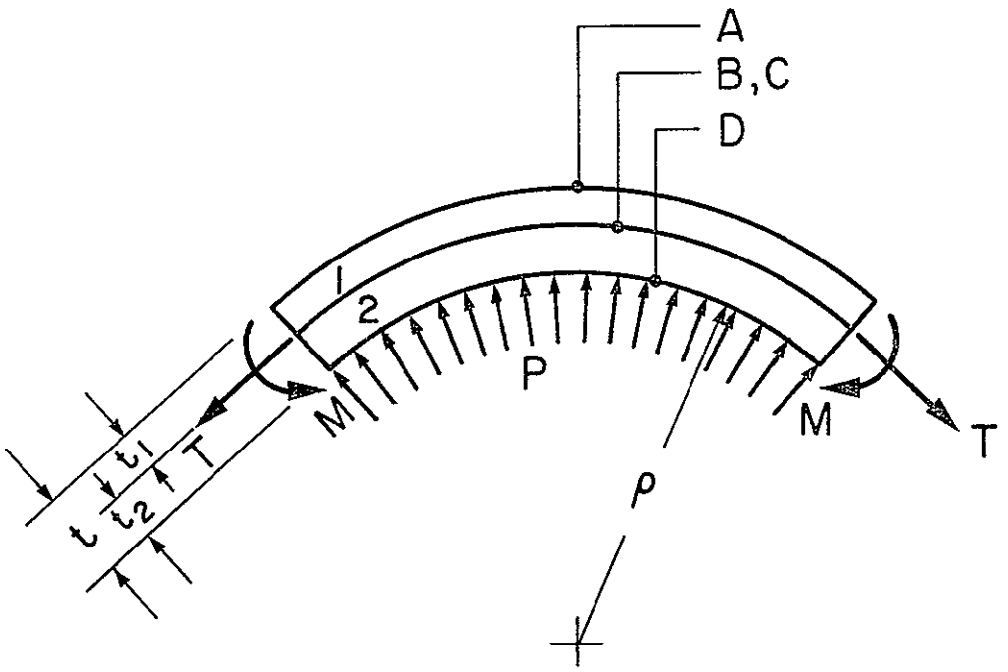

Fig. 84 DETAIL OF BENT TAPE

is constant. For a frictionless roller, the pressure between the tape and the roller is given by*

$$P = T/W\rho \tag{C-1}$$

Similarly, for the case of friction driving elements such as capstans, the pressure distribution from the point of initial contact to the exit point is

$$P(\varphi) = \frac{T_o e^{\mu \varphi}}{W\rho} \tag{C-2}$$

where φ is the total wrap angle.

Let us determine the pressure $P_B = P_C$ between the two layers. Since t is very small, the strains in layers 1 and 2 will be essentially constant over their thicknesses. These strains must be equal at the junction of the layers.

$$\varepsilon_1 = \varepsilon_2$$

Stress and strain are related by

$$\sigma = E\varepsilon \quad \text{or} \quad \varepsilon = \sigma/E \tag{C-3}$$

Therefore

$$\sigma_1/E_1 = \sigma_2/E_2 \tag{C-4}$$

---

*For development, see Appendix III.

where φ, the contact angle, is measured positive from the point of initial contact. Further, the local tension $T(\varphi)$ is given by

$$T(\varphi) = T_o e^{\mu\varphi} \tag{C-5}$$

with T_o being the incoming tension. Depending upon the specific case of interest, i.e., a free wheeling idler, $\mu = 0$, or the tape in contact with the head or driving elements, $\mu \neq 0$, values for T and P are selected from Equations (C-1), (C-2), and (C-5), respectively.

For a thin walled cylinder under pressure, the tangential stress is given by[8]

$$\sigma = \frac{(P_i - P_o)r}{t} \tag{C-6}$$

where P_i is the internal pressure, P_o is the external pressure, r is the cylinder radius and t is the wall thickness. The stresses at the junction are

$$\sigma_1 = \frac{P_B \rho}{t_1}$$

$$\sigma_2 = \frac{(P - P_B)\rho}{t_2} \tag{C-7}$$

Substituting into the strain equality Eq. (C-4) yields

$$\frac{P_B \rho}{t_1 E_1} = \frac{(P - P_B)\rho}{t_2 E_2}$$

Solving for P_B produces,

$$P \qquad P_B = P\, t_1E_1/(t_1E_1 + t_2E_2)$$

And since $P = \frac{T}{W\rho}$, the relationship for P_B becomes

$$P_B = T\, t_1E_1/W\rho(t_1E_1 + t_2E_2) \tag{C-8}$$

The tangential stresses (stresses along the tape length) in the two tape layers due to the tension (or equivalently due to the pressures) is obtained by substituting P_B of Eq. (C-8) into Eq. (C-7), e.g.,

$$\sigma_1 = \frac{P_B\rho}{t_1}$$

$$\sigma_1 = (T/W)\ E_1/(t_1E_1 + t_2E_2) \tag{C-9}$$

$$\sigma_2 = \frac{(P - P_B)\rho}{t_2} = \left[\frac{T}{W\rho} - \frac{Tt_1E_1}{W\rho(t_1E_1 + t_2E_2}\right] \frac{\rho}{t_2}$$

$$\sigma_2 = (T/W)\ E_2/(t_1E_1 + t_2E_2) \tag{C-10}$$

The radial compressive stresses (stresses in direction of tape thickness) at A, B, C, and D are equal to the pressures at these points.

$$\begin{aligned} \sigma_{rA} &= 0 \\ \sigma_{rB} &= -(T/W)t_1E_1/\rho(t_1E_1 + t_2E_2) \\ \sigma_{rC} &= -(T/W)t_1E_1/\rho(t_1E_1 + t_2E_2) \\ \sigma_{rD} &= -(T/W)/\rho \end{aligned} \tag{C-11}$$

The stresses along the tape length due to bending about the roller are given, in general, by[9]

$$\sigma_B = \frac{E}{1-\mu^2} \frac{Y}{\rho}$$

where y is measured from the effective centroid of the cross-section. The effective centroid is obtained using an equivalent single material cross-section for the layered cross-section. To obtain the equivalent stiffness, the width of one of the layers must be multiplied by the ratio of the moduli of elasticity. Figure 85 shows the equivalent cross-section.

The centroid of the equivalent cross-section is located at

$$\bar{Y} = \left[t_1^2 + (E_2/E_1)t_2^2 + 2(E_2/E_1)t_1t_2\right] \; /2 \; \left[t_1 + (E_2/E_1)t_2\right] \qquad \text{(C-12)}$$

The bending stresses at A, B, C, and D are

$$\sigma_{BA} = \frac{E_1}{1-\mu_1^2} \frac{\bar{Y}}{\rho}$$

$$\sigma_{BB} = \frac{E_1}{1-\mu_1^2} \frac{\bar{Y}-t_1}{\rho}$$

$$\sigma_{BC} = \frac{E_2}{1-\mu_2^2} \frac{\bar{Y}-t_1}{\rho}$$

$$\sigma_{BD} = \frac{E_2}{1-\mu_2^2} \frac{\bar{Y}-t_1-t_2}{\rho}$$

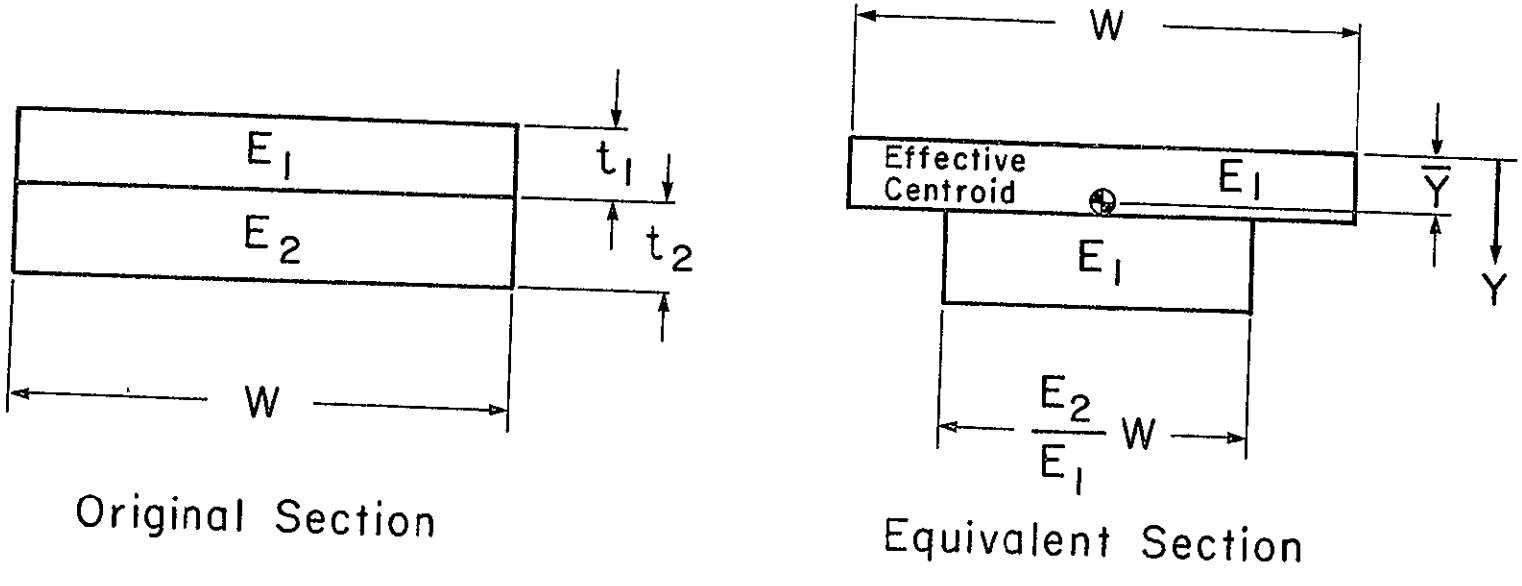

Fig. 85 EQUIVALENT CROSS-SECTIONS

Using the subscripts L, t and W to denote the directions along the length of the tape, across the thickness of the tape and across the width of the tape respectively, the principal stresses at A, B, C, and D are given by

$$\sigma_{LA} = \sigma_1 + \sigma_{BA}$$

$$\sigma_{tA} = 0 \qquad \text{(C-13)}$$

$$\sigma_{WA} = 0$$

$$\sigma_{LB} = \sigma_1 + \sigma_{BB}$$

$$\sigma_{tB} = \sigma_{rB} = -(T/W)t_1E_1/\rho(t_1E_1 + t_2E_2) \qquad \text{(C-14)}$$

$$\sigma_{WB} = 0$$

$$\sigma_{LC} = \sigma_2 + \sigma_{BC}$$

$$\sigma_{tC} = \sigma_{rC} = -(t/W)t_1E_1/\rho(t_1E_1 + t_2E_2) \qquad \text{(C-15)}$$

$$\sigma_{WC} = 0$$

$$\sigma_{LD} = \sigma_2 + \sigma_{BD}$$

$$\sigma_{tD} = \sigma_{rD} = -(T/W)/\rho \qquad \text{(C-16)}$$

$$\sigma_{WD} = 0$$

To investigate the significance of Eqs. (C-13) thru (C-16), a typical magnetic tape with the following physical characteristics was analyzed for the following cases:

a) Variation of Stress with Roller Diameter

b) Variation of Stress with Tape Tension

c) Variation of Stress with Mylar Backing Thickness

d) Variation of Stress with Oxide Coating Thickness

e) Variation of Stress with Mylar Backing Modulus of Elasticity

f) Variation of Stress with Oxide Coating Modulus of Elasticity

For the above cases, the maximum principal stress is σ_L; i.e., the stress along the tape length. The variation of this stress, calculated at the four positions A, B, C, and D is plotted for each case.

In all examples, stresses were calculated for the two cases of the oxide adjacent and exterior to the roller surface. In Figs. 86 and 87, a magnetic tape with a 0.92 mil back and a 0.21 mil coating was evaluated. Basically, it is seen that substantial stresses occur at roller diameters less than 0.5 inch. From a design point of view, the stresses in the oxide-binder system are low, under 400 psi in tensile, for roller diameters 1 inch and larger. In fact, for the case where the oxide is against the roller, the oxide-binder stresses are under 100 psi for the standard tape tension of 16 oz/in. and 1 inch roller diameter. Figure 87 illustrates the range of stresses as a linear function of tape tension. Again for the above case (oxide-roller contact), oxide-binder stresses are under 100 psi for a roller diameter of approximately 0.75 inch

Tape Tension - 16 oz/in. Width
Mylar Backing Thickness - 0.92 Mil
Oxide Coating Thickness - 0.21 Mil
Backing Modulus of Elasticity - 650,000 psi
Coating Modulus of Elasticity - 100,000 psi
Cant Angle of Roller - 0° (Straight)

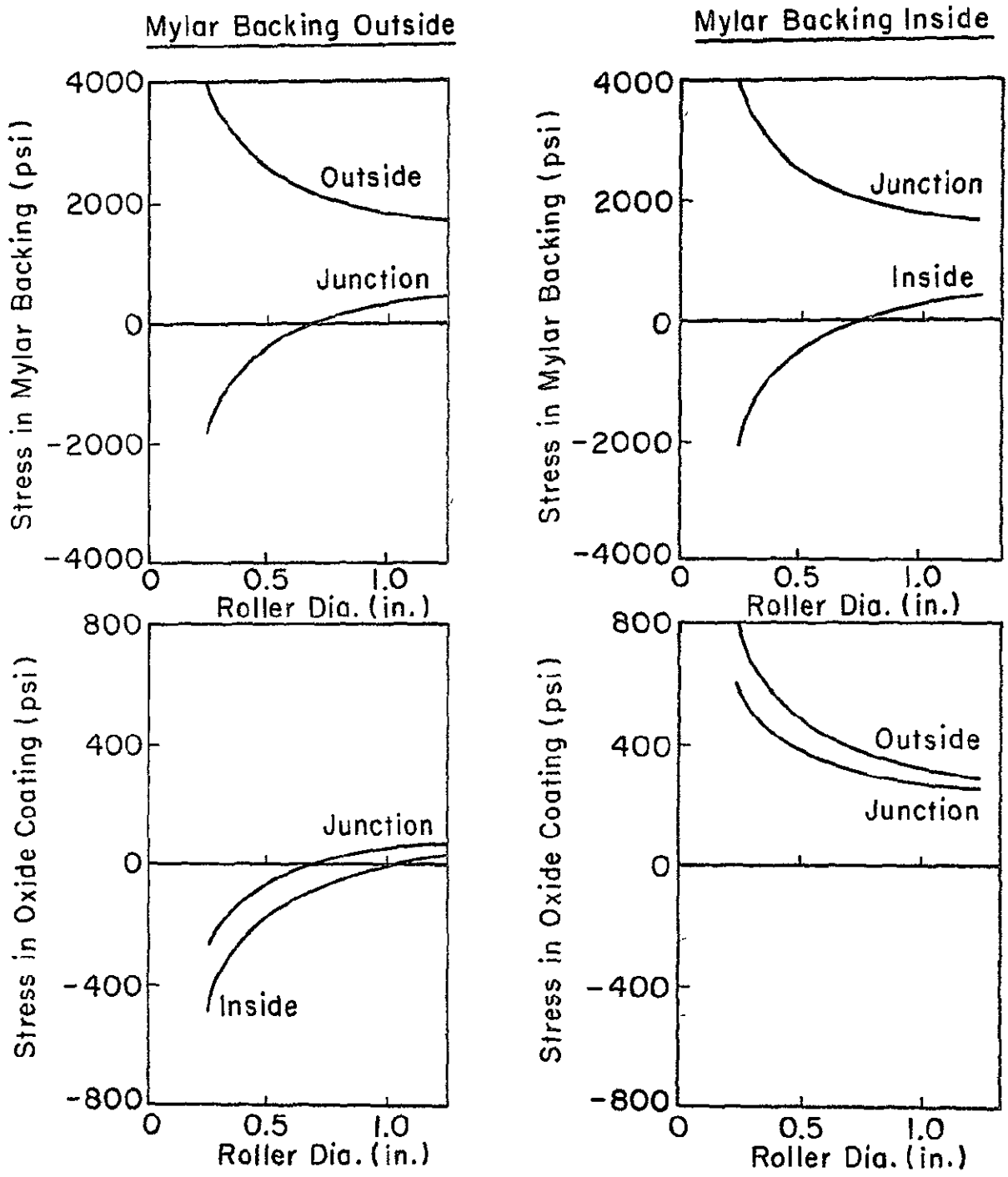

Fig. 86 VARIATION OF MAX STRESS WITH ROLLER DIAMETER

Roller Diameter - 0.75 in.
Mylar Backing Thickness - 0.92 Mil
Oxide Coating Thickness - 0.21 Mil
Backing Modulus of Elasticity - 650,000 psi
Coating Modulus of Elasticity - 100,000 psi
Cant Angle of Roller - 0° (Straight)

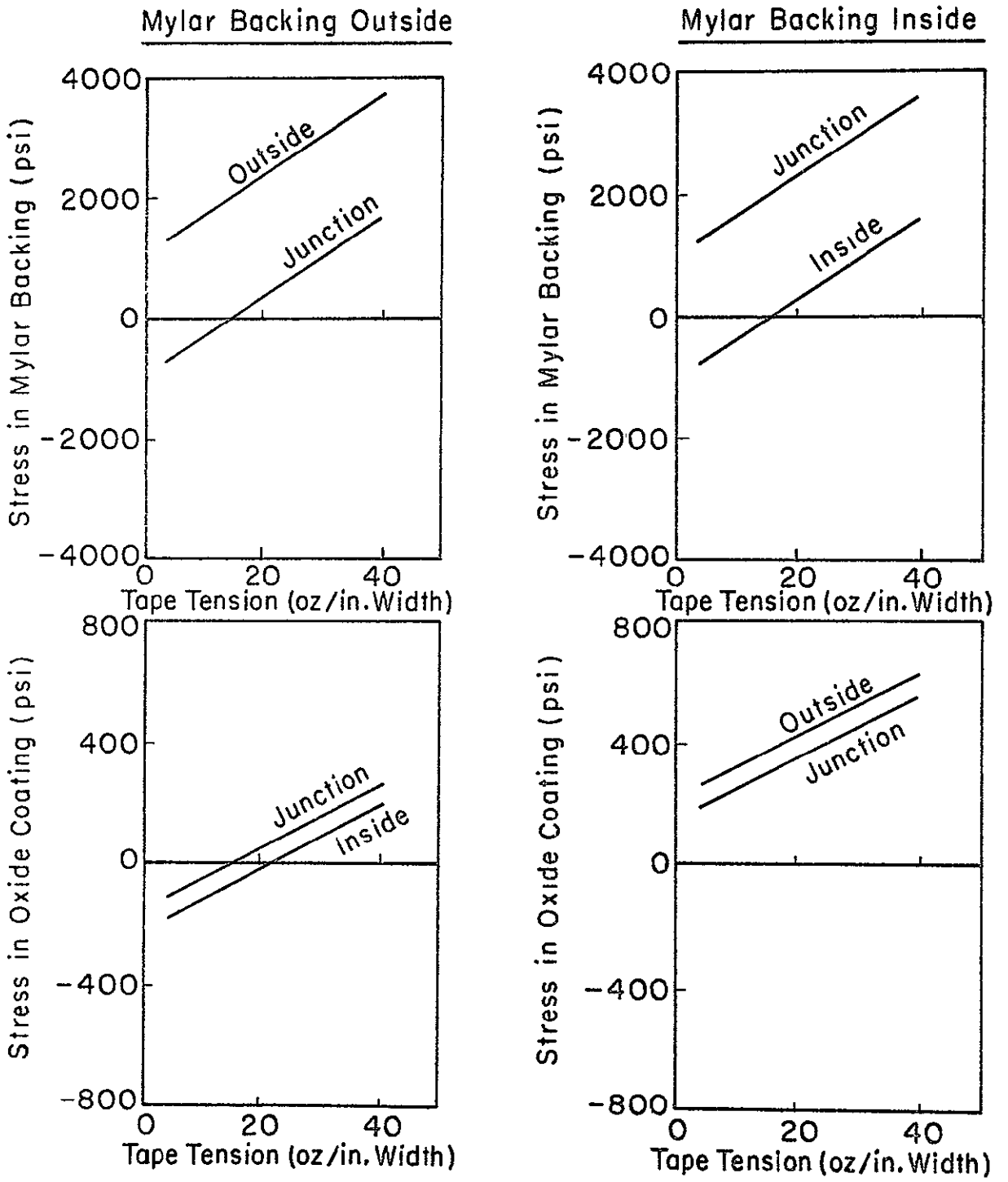

Fig. 87 VARIATION OF STRESS WITH TAPE TENSION

and tape tensions near 20 oz/in. Thus, it is obvious that, for a particular set of tape-roller configurations, the oxide stresses can be minimized at practical roller sizes and tape tensions.

Figure 88 illustrates the stress levels as a function of backing thickness. With the oxide against the roller, the binder stresses vanish for the following set of commonly encountered parameters.

Mylar Backing Thickness = 1 mil
Roller Diameter 0.75 in.
Oxide Coating Thickness 0.21
Tape Tension 16 oz/in.
Modulus of Elasticity (Backing) = 650,000 psi
Modulus of Elasticity (Coating) = 100,000 psi

Further, the stress throughout the coating is positive, under 100 psi, for coating thicknesses of 0.8 to 1 mil. In analyzing the stress variation for the other parameters, no particularly important dependence is observed. For example, Fig. 89 demonstrates that stresses in the mylar are independent of coating thickness. This situation is predictable because the oxide-binder system has a modulus of elasticity of almost an order of magnitude less than the backing. Figure 90 also shows the independence of the mylar stresses from the oxide-binder characteristics, and Fig. 91 shows the relative independence of stress with changes in the Mylar backing modulus of elasticity. Practically no mylar stress variation results from a factor of two change in the coating modulus of elasticity. Of course, the coating stresses, as expected from the stress-strain relationships, varies linearly with the coating modulus.

3. Stresses in Tape Passing Over Canted Frictionless Roller

The purpose of this analysis is to determine the stresses in a magnetic tape as it passes over a canted frictionless

Roller Diameter - 0.75 in.
Tape Tension - 16 oz/in. Width
Oxide Coating Thickness - 0.21 Mil
Backing Modulus of Elasticity - 650,000 psi
Coating Modulus of Elasticity - 100,000 psi
Cant Angle of Roller - 0° (Straight)

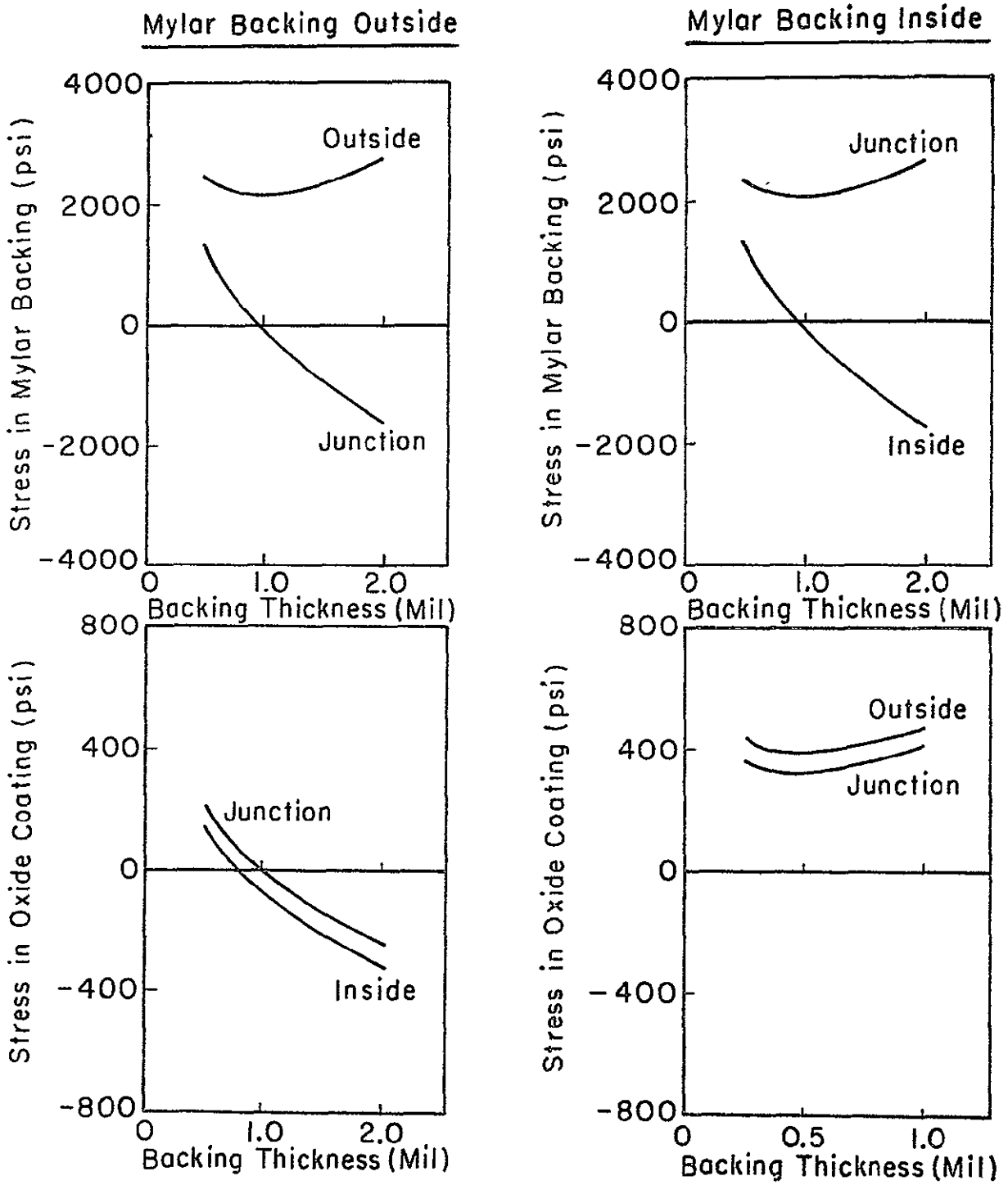

Fig. 88 VARIATION OF STRESS WITH MYLAR BACKING THICKNESS

Roller Diameter - 0.75 in.
Tape Tension - 16 oz/in. Width
Mylar Backing Thickness - 0.92 Mil
Backing Modulus of Elasticity - 650,000 psi
Coating Modulus of Elasticity - 100,000 psi
Cant Angle of Roller - 0° (Straight)

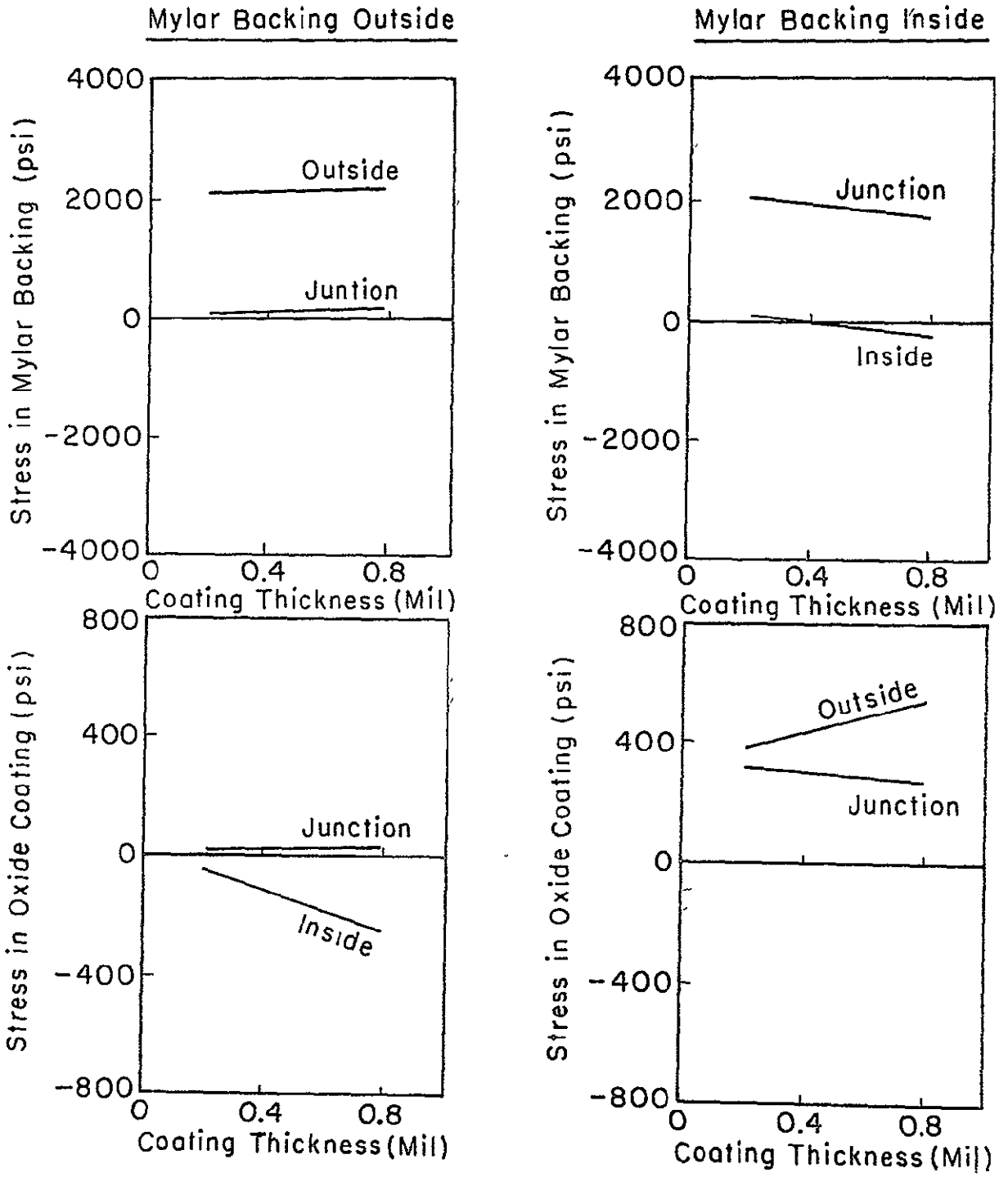

Fig. 89 VARIATION OF STRESS WITH OXIDE COATING THICKNESS

Roller Diameter - 0.75 in.
Tape Tension - 16 oz/in. Width
Mylar Backing Thickness - 0.92 Mil
Oxide Coating Thickness - 0.21 Mil
Backing Modulus of Elasticity - 650,000 psi
Cant Angle of Roller - 0° (Straight)

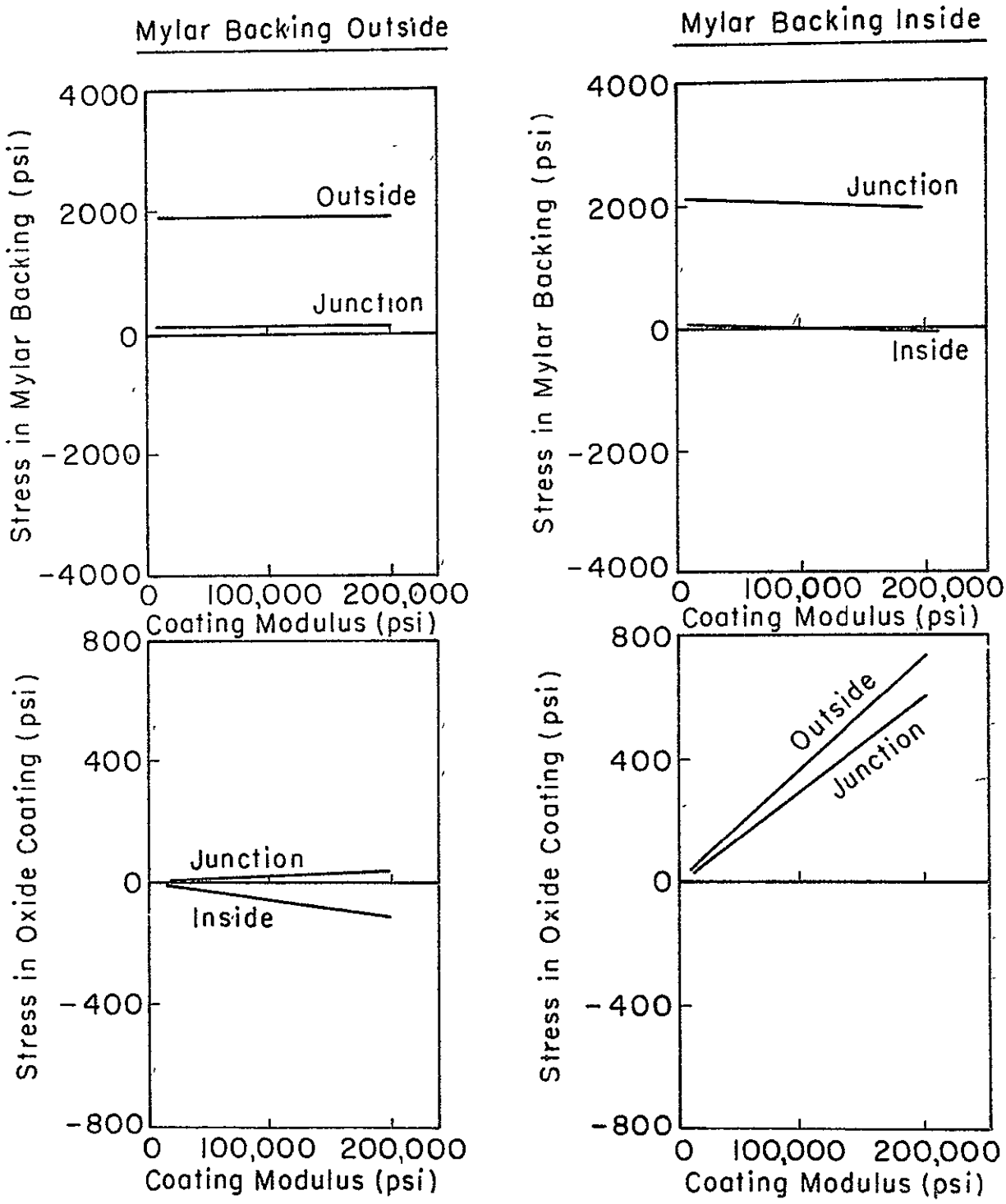

Fig. 90 VARIATION OF STRESS WITH OXIDE COATING MODULUS OF ELASTICITY

Roller Diameter - 0.75 in.
Tape Tension - 16 oz/in. Width
Mylar Backing Thickness - 0.92 Mil
Oxide Coating Thickness - 0.21 Mil
Coating Modulus of Elasticity - 100,000 psi
Cant Angle of Roller - 0° (Straight)

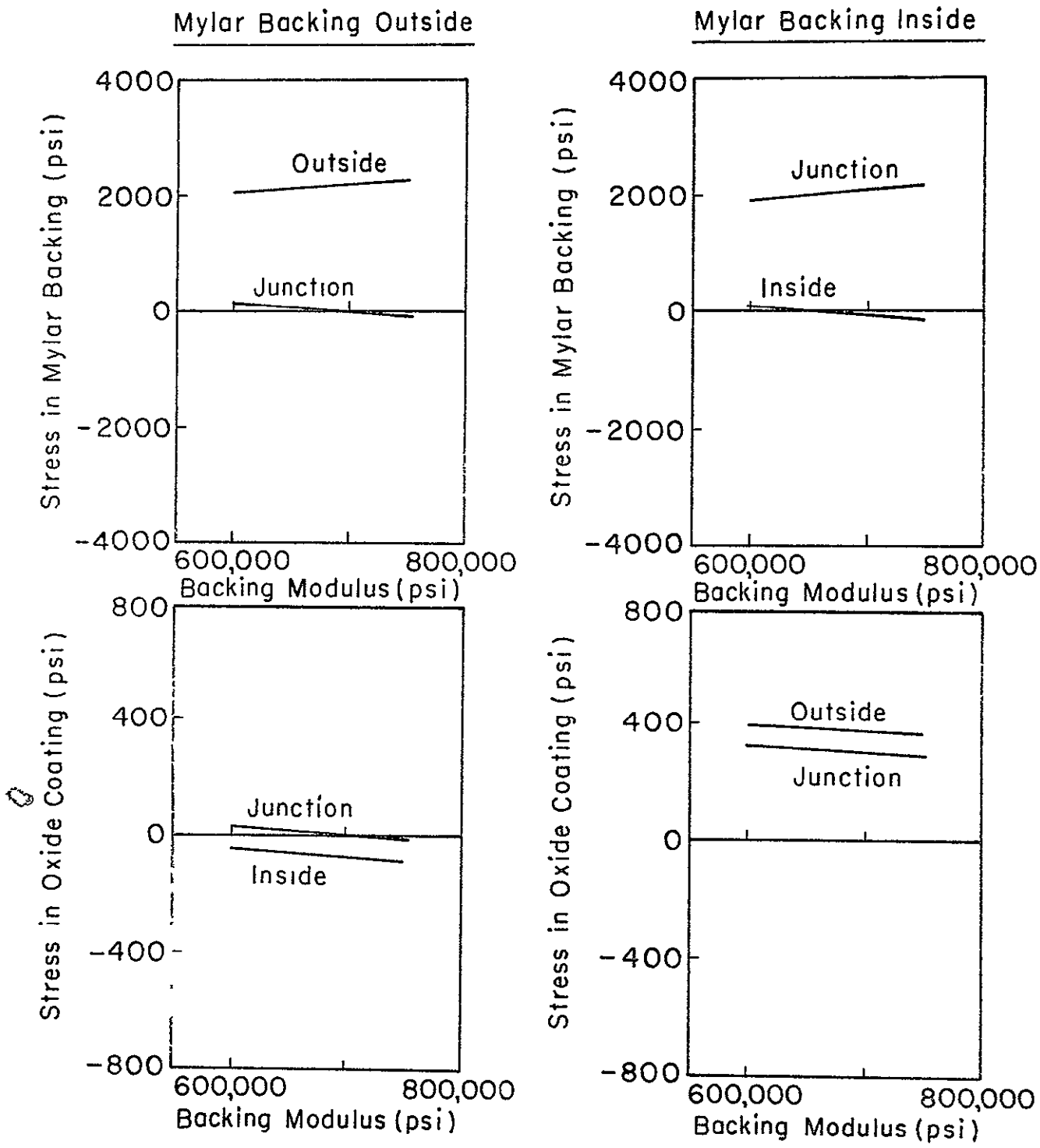

Fig. 91 VARIATION OF STRESS WITH MYLAR BACKING MODULUS OF ELASTICITY

roller as shown in Fig. 92. The cant angle is θ. The remaining nomenclature is the same as in C.2. The pressure between the tape and the roller is given by*

$$P = T \cos^2\theta / W\rho \tag{C-17}$$

The stress along the tape length in the two layers due to the tension (σ_1 and σ_2) and the radial compressive stresses (stresses in the direction of the tape thickness; σ_{rA}, σ_{rB}, σ_{rC}, and σ_{rD}) are the same as in Sec. C. 2 with (T/W) replaced by ($T \cos^2\theta / W$) for the compressive stresses.

$$\begin{aligned}
\sigma_1 &= (T/W)E_1/(t_1E_1 + t_2E_2) \\
\sigma_2 &= (T/W)E_2/(t_1E_1 + t_2E_2) \\
\sigma_{rA} &= 0 \\
\sigma_{rB} &= -(T \cos^2\theta / W)t_1E_1\rho(t_1E_1 + t_2E_2) \\
\sigma_{rC} &= -(T \cos^2\theta / W)t_1E_1/\rho(t_1E_1 + t_2E_2) \\
\sigma_{rD} &= -(T \cos^2\theta / W)/\rho
\end{aligned} \tag{C-18}$$

The stress due to bending is at the angle θ to the tape length. These bending stresses are given in C.2 as,

$$\sigma_{BA} = \frac{E_1}{1-\mu_1^2} \frac{\bar{Y}}{\rho}$$

*For development, see Appendix IV.

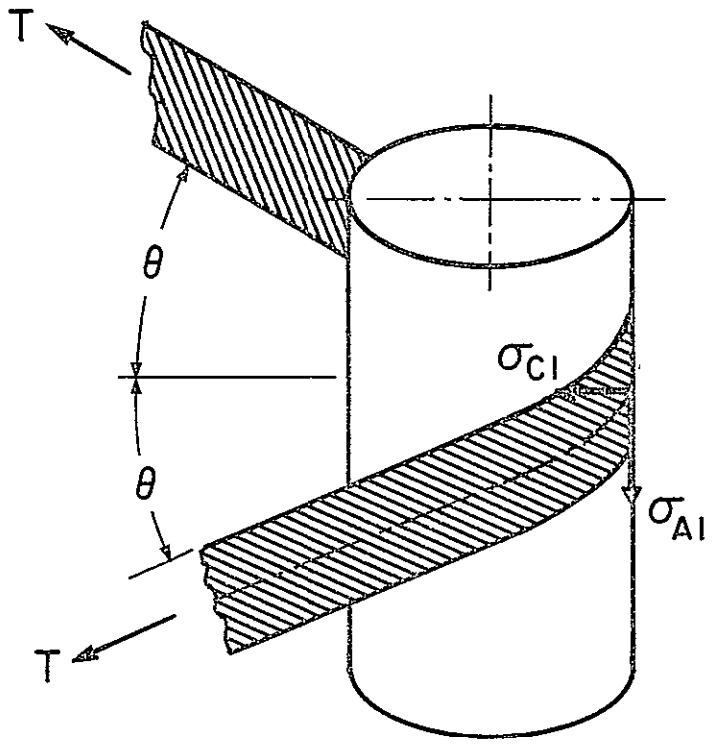

Fig. 92 CANTED ROLLER

$$\sigma_{BB} = \frac{E_1}{1-\mu_1^2} \frac{\bar{Y}-t_1}{\rho}$$

$$\sigma_{BC} = \frac{E_2}{1-\mu_2^2} \frac{\bar{Y}-t_1}{\rho}$$

$$\sigma_{BD} = \frac{E_2}{1-\mu_2^2} \frac{\bar{Y}-t_1-t_2}{\rho}$$

where

$$\bar{Y} = \left[t_1^2 + (E_2/E_1)t_2^2 + 2(E_2/E_1)t_1t_2\right] \; /2 \left[t_1 + (E_2/E_1)t_2\right]$$

The stresses due to tension are at the angle θ to those due to bending. The stress in the direction of the bending stresses due to tension are

$$\sigma_{C1} = \sigma_1 \cos^2\theta$$

$$\sigma_{C2} = \sigma_2 \cos^2\theta \qquad \text{(C-19)}$$

The stresses along the roller axis due to the tension are

$$\sigma_{A1} = \sigma_1 \sin^2\theta$$

$$\sigma_{A2} = \sigma_2 \sin^2\theta \qquad \text{(C-20)}$$

The shear stresses due to the tension in the directions above are*

$$\tau_1 = \sigma_1 \sin\theta \cos\theta$$

$$\tau_2 = \sigma_2 \sin\theta \cos\theta$$

Combining these stresses with the stresses due to bending yields a set of stress vectors in the normal and tangent directions of the roller, but skewed to the tape by the angle ϑ.

$$\sigma_{CA} = \sigma_{C1} + \sigma_{BA}$$

$$\sigma_{CB} = \sigma_{C1} + \sigma_{BB}$$

$$\sigma_{CC} = \sigma_{C2} + \sigma_{BC}$$

$$\sigma_{CD} = \sigma_{C2} + \sigma_{BD}$$

$$\sigma_{AA} = \sigma_{A1}$$

$$\sigma_{AB} = \sigma_{A1}$$

$$\sigma_{AC} = \sigma_{A2}$$

$$\sigma_{AD} = \sigma_{A2}$$

$$\tau_A = \tau_1$$

$$\tau_B = \tau_1$$

*For development, see Appendix V.

$$\tau_C = \tau_2$$

$$\tau_D = \tau_2$$

Using Mohr's circle, the principal stresses in the plane of the tape are given by

$$\sigma_{1A} = \frac{(\sigma_{CA} + \sigma_{AA})}{2} + \sqrt{(\sigma_{CA} - \sigma_{AA})^2/4 + \tau_A^2}$$

$$\sigma_{1B} = \frac{(\sigma_{CB} + \sigma_{AB})}{2} + \sqrt{(\sigma_{CB} - \sigma_{AB})^2/4 + \tau_C^2}$$

$$\sigma_{1C} = \frac{(\sigma_{CC} + \sigma_{AC})}{2} + \sqrt{(\sigma_{CC} - \sigma_{AC})^2/4 + \tau_C^2}$$

$$\sigma_{1D} = \frac{(\sigma_{CD} + \sigma_{AD})}{2} + \sqrt{(\sigma_{CD} - \sigma_{AD})^2/4 + \tau_D^2}$$

$$\sigma_{2A} = \frac{(\sigma_{CA} + \sigma_{AA})}{2} - \sqrt{(\sigma_{CA} - \sigma_{AA})^2/4 + \tau_A^2} \qquad \text{(C-21)}$$

$$\sigma_{2B} = \frac{(\sigma_{CB} + \sigma_{AB})}{2} - \sqrt{(\sigma_{CB} - \sigma_{AB})^2/4 + \tau_B^2}$$

$$\sigma_{2C} = \frac{(\sigma_{CC} + \sigma_{AC})}{2} - \sqrt{(\sigma_{CC} - \sigma_{AC})^2/4 + \tau_C^2}$$

$$\sigma_{2D} = \frac{(\sigma_{CD} + \sigma_{AD})}{2} - \sqrt{(\sigma_{CD} - \sigma_{AD})^2/4 + \tau_D^2}$$

Where σ_{1A}, σ_{1B}, σ_{1C}, and σ_{1D} are the maximum principal stresses, and σ_{2A}, σ_{2B}, σ_{2C}, and σ_{2D} are the minimum principal stresses in the plane of the tape. The third principal stress at the various positions are σ_{rA}, σ_{rB}, σ_{rC}, and σ_{rD}. The effect of cant angle on the magnitude of the contact stresses is illustrated in Fig. 93. No particular dependence is observed until cant angles approach 40°. At this point, it is well to reiterate that canted idlers, of the type considered here, require the tape to travel a helix path. For this type of configuration, the cant angles are usually 45°. Depending upon the tape-roller orientation, an increase in stress level of between 100 to 400 psi can be anticipated.

4. Tape Forces Due to Friction Effects from Canted Rollers where Tape Path and Roller Axes are not Perpendicular

As the tape travels, in a helical path, past a canted roller a tension increase is induced due to the relative slippage between the tape and roller surfaces. From Fig. 94, it is seen that the rotational speed of a free wheeling roller is

$$\omega = V_t \frac{\cos \alpha}{\rho}$$

where

ρ = roller radius

V_t = average tape velocity

α = roller cant angle

Similarly, the average slippage velocity is equal to

$$V_S = V_t \sin \alpha$$

Roller Diameter - 0.75 in.
Tape Tension - 16 oz/in. Width
Mylar Backing Thickness - 0.92 Mil
Oxide Coating Thickness - 0.21 Mil
Backing Modulus of Elasticity - 650,000 psi
Coating Modulus of Elasticity - 100,000 psi

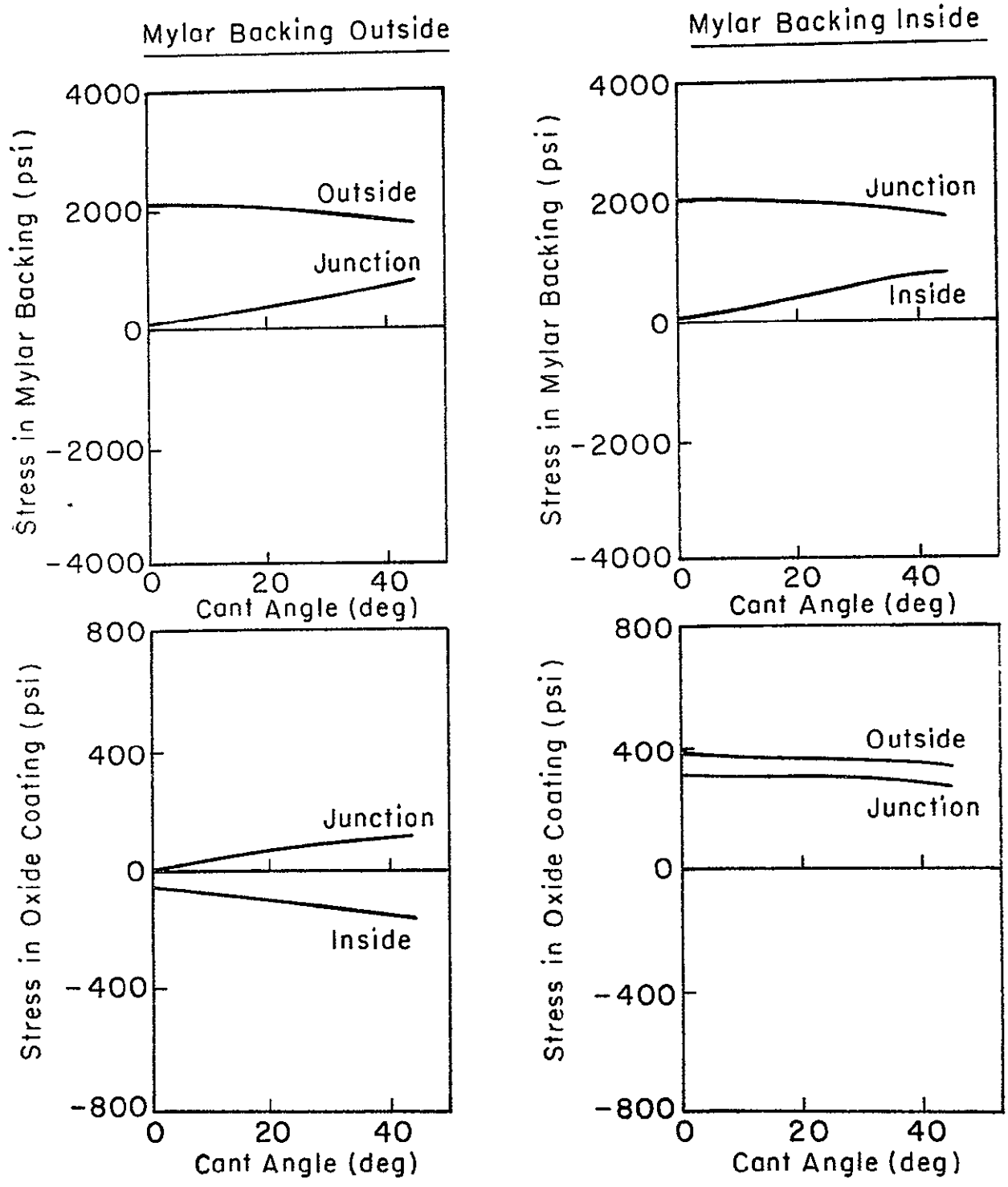

Fig. 93 VARIATION OF STRESS WITH CANT ANGLE OF ROLLER

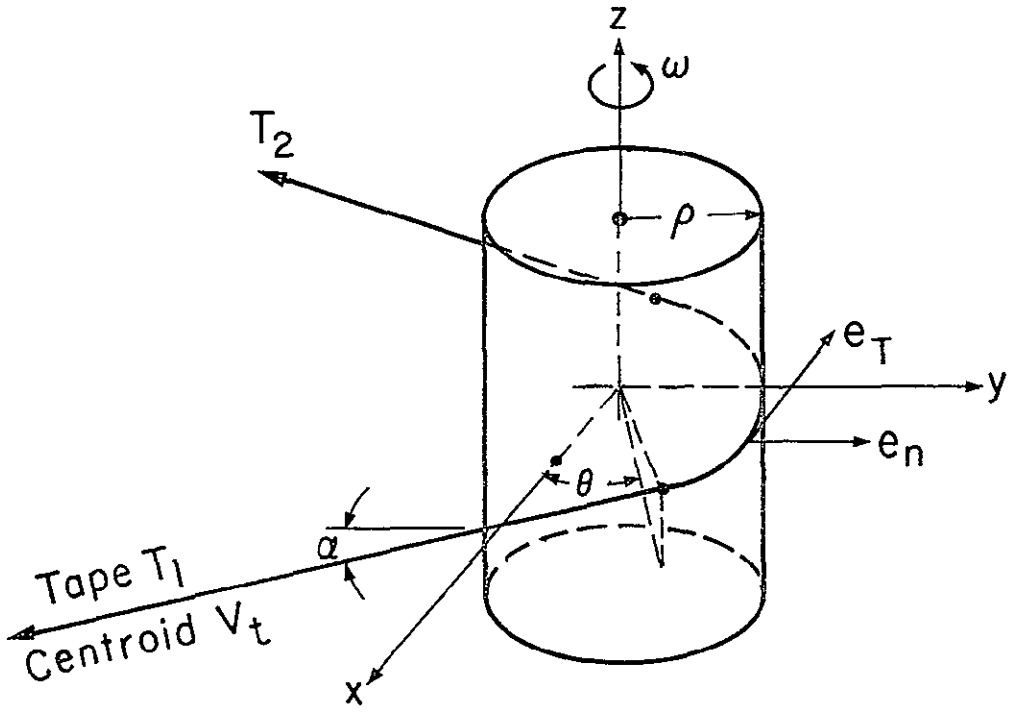

Fig. 94 TAPE TRAJECTORY PAST THE CANTED ROLLER

Since α is usually around $\frac{\pi}{4}$ radians, significant slippage levels can be realized. In order to quantify the influence slippage has on tape tension, the tape trajectory around the roller was defined as a basic screw helix, i.e.,

$$x = \rho \cos \theta$$

$$y = \rho \sin \theta$$

$$z = \rho (\tan \alpha)\, \theta$$

θ = x-y plane trajectory angle (see Fig. C-12)

The tangent and principal normal unit vectors are determined for each point in the trajectory as

$$\bar{e}_t = \frac{1}{\rho\sqrt{1+\tan^2\alpha}} = \left[-(\sin \vartheta)\,i + (\cos \vartheta)\,j + (\rho \tan \vartheta)\,k\right]$$

$$e_n = -(\cos \theta)\,i + (\sin \theta)\,j$$

where

i, j, k = cartesian unit triad

By summing forces on an incremental element which encompasses a small $\Delta\varphi$ angle, it is found that the local contact force δR, is equal to

$$\delta R = \frac{T\,\Delta\theta}{\sqrt{1+\tan^2\alpha}}$$

where T is the local tape tension. Noticing the tension increase resulting from friction, the local friction forces are obtained as

$$\Delta f = \mu \delta R \quad (\mu \approx \text{kinetic coefficient of friction})$$

and hence

$$\Delta f = \Delta T$$

or in the limit,

$$\frac{dT}{T} = \frac{\mu \, d\theta}{\sqrt{1+\tan^2 \alpha}}$$

Integrating the above yields

$$T_2/T_1 = e^{\bar{\mu} \, \theta_o} \qquad \text{(C-22)}$$

where

T_2 = exit tension

T_1 = entrance tension

θ_o = total x-y plane contact angle

$$\bar{\mu} = \frac{\mu}{1+\tan^2 \alpha}$$

It is of interest to note that, as the helix angle increases, the relative increase in T_2 diminishes because the normal pressure, R, is reduced.

5. Stresses Due to Tape Passing Between Two Nonparallel Rollers whose Axes are in Parallel Planes

This case, illustrated in Fig. 95, represents a situation where the elevation of the tape is altered by twisting the tape after it leaves one roller and enters a canted roller at an entrance orientation normal to the roller surface. The tape then proceeds in a circular path around the canted roller without slippage. The induced twisting causes the tape to rotate about its longitudinal center line, with the tape path at the outer edges being greater than at the center line. The increase in tape length is symmetric about the center line, and thus, the maximum strain occurs at the outer edges.

In analyzing the tape path, the outer edges have a length approximately equal to

$$\ell_o = \sqrt{\ell_c^2 + \left(\frac{W}{2}\right)^2 \tan^2 \vartheta}$$

where

ℓ_o = length of tape's outer edge

ℓ_c = length of tape centerline

W = tape width

ϑ = cant angle between rollers

The strain then becomes

$$\varepsilon = \frac{\ell_o - \ell_c}{\ell_c}$$

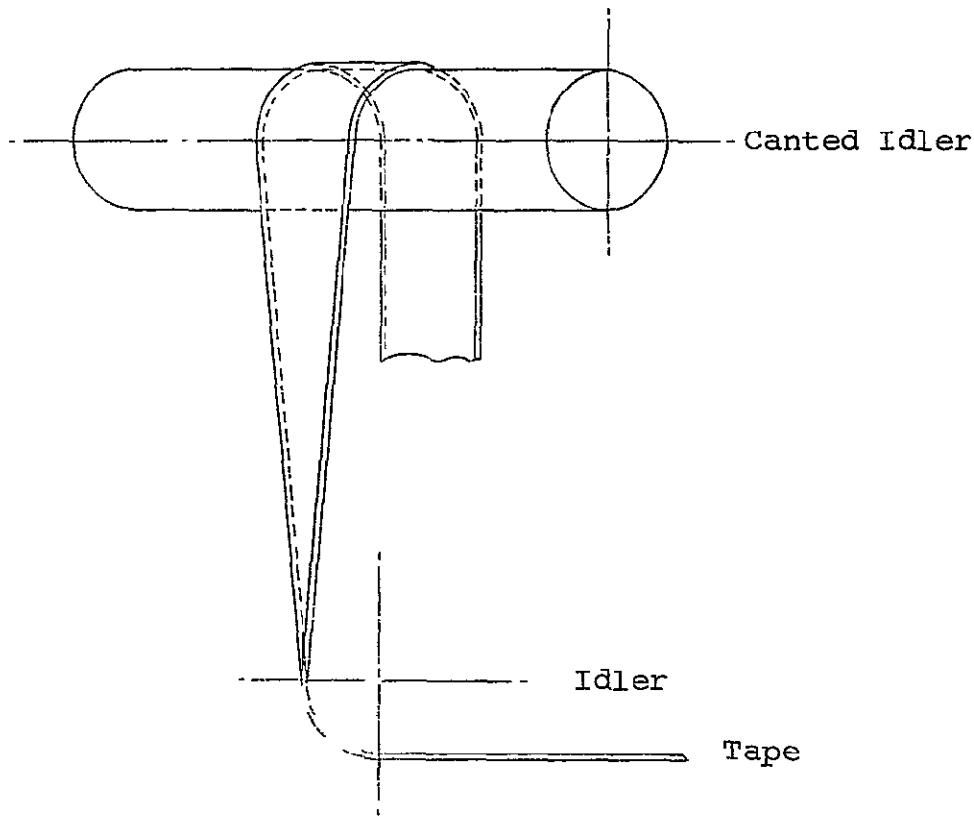

Fig. 95 TAPE ELEVATION CHANGE BY TWISTING

or

$$\varepsilon = \sqrt{1 + \left(\frac{W}{2\ell_c}\right)^2 \tan^2\theta} - 1$$

Using the standard stress-strain relationship yields the stress equation of

$$\sigma = E \left[\sqrt{1 + \frac{W}{2\ell_c}^2 \tan^2\theta} - 1 \right] \qquad \text{(C-23)}$$

As this equation demonstrates, at $\theta = 0$ (no cant angle between rollers),

$$\sigma = 0$$

but as $\theta \to 90°$, the stresses become unbounded. Of course, before this condition arises, the material plastically yields and permanent damage results. Figure 96 illustrates the dependence of stress upon the cant angle. As an example of the stresses encountered due to the twisting technique, the following set of commonly used parameters are considered.

$W = 0.5$ inch

$\ell_c = 4$ inches

$E = 650{,}000$ psi

$\theta = 20°$

For this case, the stress level reaches 2270 psi. To appreciate fully the impact of the twisting stress, the 2270 psi now must be superimposed upon the stress levels resulting from the tape passing over a cylindrical rollers as discussed in Sec. C.2.

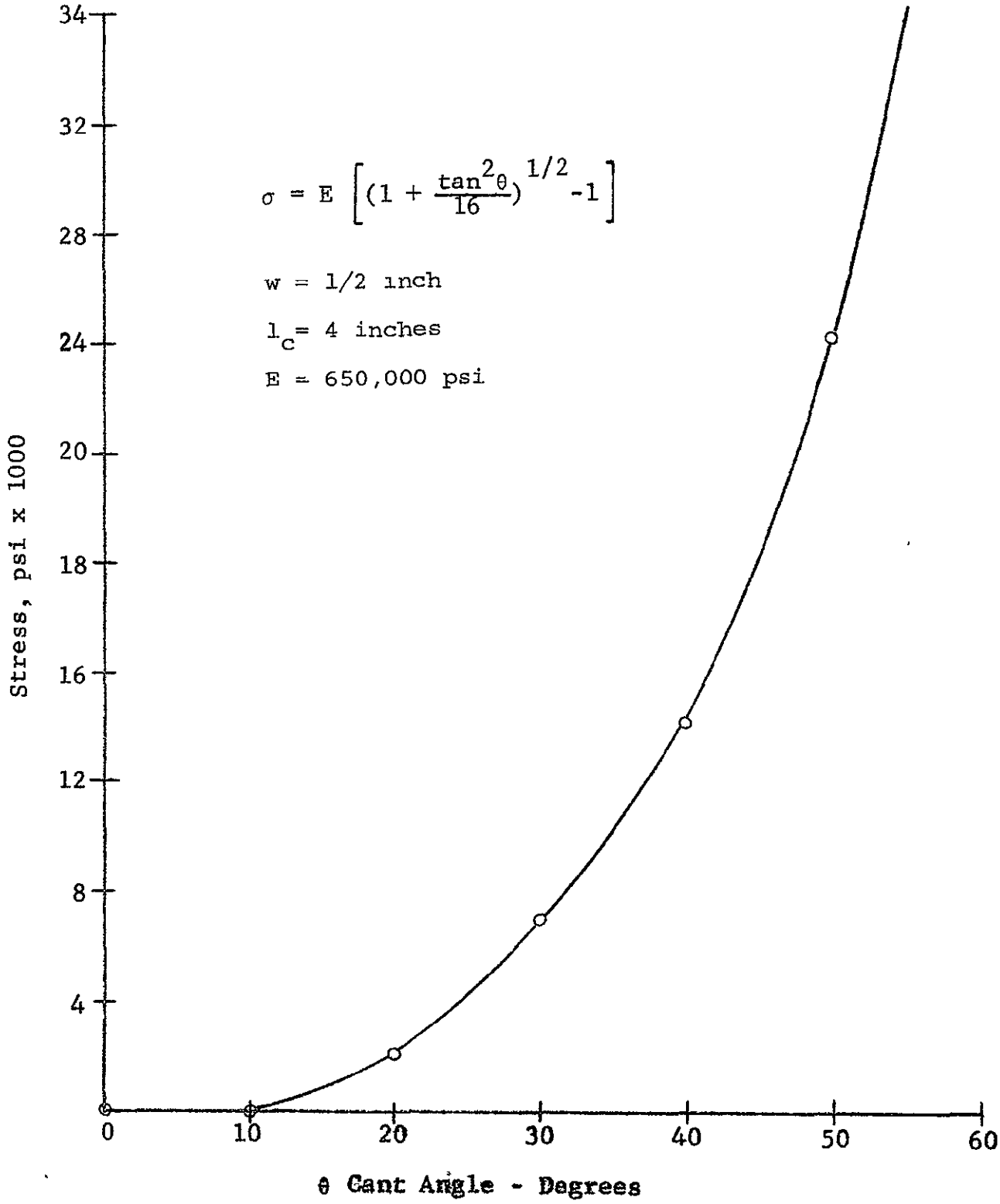

Fig. 96 TAPE STRESS RESULTING FROM ROLLER CANT ANGLE

6. Stresses in Tape Passing Over a Crowned Roller

The objective of this analysis is to determine the stress in a magnetic tape as it passes over a crowned roller as shown in Fig. 97. The crown radius is given by R, the maximum roller radius is ρ, and the total wrap angle is 2ϑ. The remaining nomenclautre is the same as in C.2. As the tape passes around the roller, longitudinal fibers near the center of the tape will be elongated more than those near the edge. For the purpose of analysis the tape will be assumed to pass around a straight roller to the crowned roller and onto a second straight roller as shown in Fig. 98. The straight rollers are at equal distances L from the crowned roller. Since the tape system is symmetric about the vertical centerline through the crowned roller, the analysis is amplified by investigating half of the total system. Let S be measured across the tape width as shown in Fig. C-15. Then the roller radius at any position S is given by

$$r = \rho - R\left[1 - \cos\left(\frac{S}{R}\right)\right] \qquad \text{(C-24)}$$

The length of tape in contact with the roller at any position S is given by

$$L_T = \varphi r = \varphi\left\{\rho - R\left[1 - \cos\left(\frac{S}{R}\right)\right]\right\}$$

At the outside edge of the tape

$$L_{TE} = \varphi\left\{\rho - R\left[1 - \cos\left(\frac{W}{2R}\right)\right]\right\}$$

The difference in the tape length at any position S will be

$$\delta = L_T - L_{TE} = \varphi\left\{\rho - R\left[1 - \cos\left(\frac{S}{R}\right)\right]\right\} - \varphi\left\{\rho - R\left[1 - \cos\left(\frac{W}{2R}\right)\right]\right\}$$

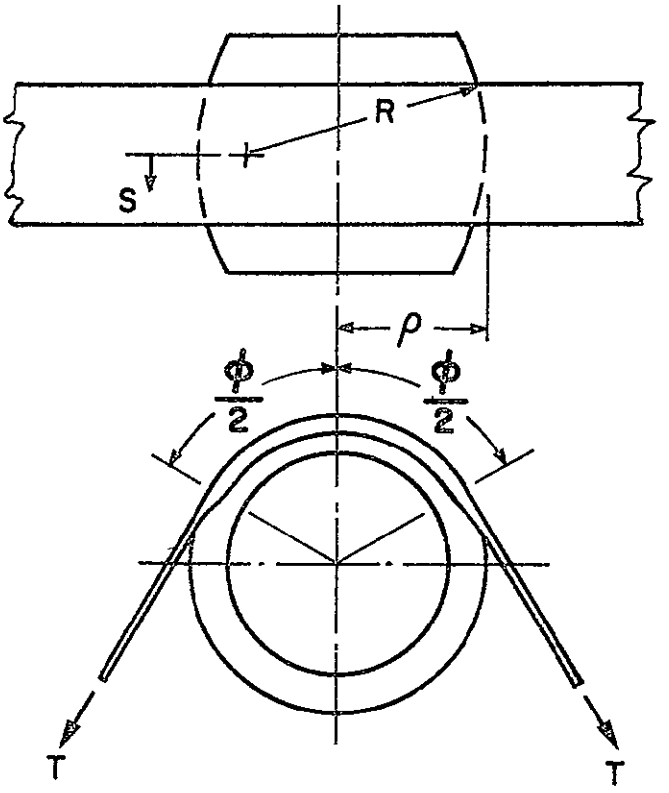

Fig. 97 CROWNED ROLLER CONFIGURATION

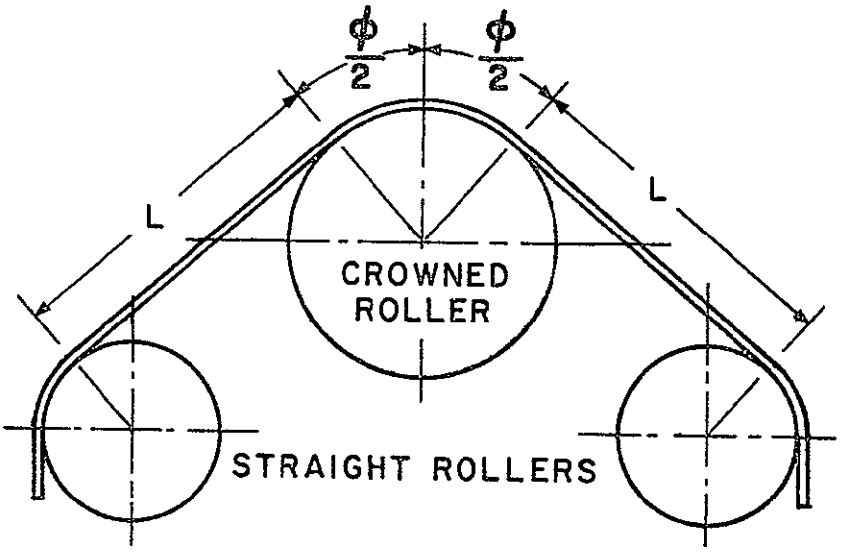

Fig. 98 TAPE-ROLLER SYSTEM

$$\delta = \varphi R \left[\cos\left(\frac{S}{R}\right) - \cos\left(\frac{W}{2R}\right)\right] \qquad \text{(C-25)}$$

As a first approximation to the stress distribution across the tape it is assumed that there is no effect from the tape upstream and downstream of the crowned roller. A two-dimensional elasticity solution has this assumption to be valid.* Under these assumptions, the strain distributor across the tape width is given by

$$\varepsilon = \delta/L_{TE} = \varphi R \left[\cos\left(\frac{S}{R}\right) - \cos\left(\frac{W}{2R}\right)\right] / \varphi \left\{\rho - R\left[1-\cos\left(\frac{W}{2R}\right)\right]\right\}$$

$$= R\left[\cos\left(\frac{S}{R}\right) - \cos\left(\frac{W}{2R}\right)\right] / \left\{\rho - R\left[1-\cos\left(\frac{W}{2R}\right)\right]\right\} \qquad \text{(C-26)}$$

The stress distribution will be

$$\sigma_L = E\varepsilon = ER\left[\cos\left(\frac{S}{R}\right) - \cos\left(\frac{W}{2R}\right)\right] / \left\{\rho - R\left[1-\cos\left(\frac{W}{2R}\right)\right]\right\} \qquad \text{(C-27)}$$

For layer 1

$$\sigma_{L1} = E_1 R\left[\cos\left(\frac{S}{R}\right) - \cos\left(\frac{W}{2R}\right)\right] / \left\{\rho - R\left[1-\cos\left(\frac{W}{2R}\right)\right]\right\} \qquad \text{(C-28)}$$

For layer 2

$$\sigma_{L2} = E_2 R\left[\cos\left(\frac{S}{R}\right) - \cos\left(\frac{W}{2R}\right)\right] / \left\{\rho - R\left[1-\cos\left(\frac{W}{2R}\right)\right]\right\} \qquad \text{(C-29)}$$

In using crowned rollers, it has been observed that the tape rarely makes full contact with the roller surface. To determine the local tension associated with a specific contact width,

---

* See Appendix VI.

the tension load is equated to the tape stresses by summing the forces across an incremental element, i.e.,

$$\Delta T = (\Sigma \sigma t)\ \Delta s$$

or in the limit

$$T_R = 2 \int_o^{\frac{w_o}{2}} (\sigma_{L1} t_1 + \sigma_{L2} t_2)\, dS$$

$$= \left[2\ (E_1 t_1 + E_2 t_2) R \Big/ \left\{\rho - R\left[1 - \cos\left(\frac{w_o}{2R}\right)\right]\right\}\right] \int_o^{W/2} \left[\cos\left(\frac{S}{R}\right) - \cos\left(\frac{w_o}{2R}\right)\right] ds$$

$$T_R = 2R\ (E_1 t_1 + E_2 t_2) \left[R \sin\left(\frac{w_o}{2R}\right) - \frac{w_o}{2} \cos\left(\frac{w_o}{2R}\right)\right] \Big/ \left\{\rho - R\left[1 - \cos\left(\frac{w_o}{2R}\right)\right]\right\} \qquad \text{(C-30)}$$

where w_o is the total tape width in contact. The stress, due to any excess tension after total tape width contact is achieved, will be given by (from C.2)

$$\sigma_1 = \left[(T - T_c)/W\right] E_1/(t_1 E_1 + t_2 E_2)$$

$$\sigma_2 = \left[(T - T_c)/W\right] E_2/(t_1 E_1 + t_2 E_2) \qquad \text{(C-31)}$$

T_c being the tension for total tape width contact w_o.

The stresses along the tape length due to bending around the roller are given by

$$\sigma_{BA} = \frac{E_1 \bar{Y}}{1 - \mu_1^2} \left(\frac{1}{\rho} + \frac{\mu_1}{R}\right)$$

$$\sigma_{BB} = \frac{E_1 (\bar{Y} - t_1)}{1 - \mu_1^2} \left(\frac{1}{\rho} + \frac{\mu_1}{R}\right)$$

$$\sigma_{BC} = \frac{E_2(\bar{Y}-t_1)}{1-\mu_2^2}\left(\frac{1}{\rho} + \frac{\mu_1}{R}\right)$$

$$\sigma_{BD} = \frac{E_2(\bar{Y}-t_1-t_2)}{1-\mu_2^2}\left(\frac{1}{\rho} + \frac{\mu_1}{R}\right) \qquad \text{(C-32)}$$

The stress in the direction of the tape width due to bending around the roller are given by

$$\sigma_{WA} = \frac{E_1\bar{Y}}{1-\mu_1^2}\left(\frac{1}{R} + \frac{\mu_1}{\rho}\right)$$

$$\sigma_{WB} = \frac{E_1(\bar{Y}-t_1)}{1-\mu_1^2}\left(\frac{1}{R} + \frac{\mu_1}{\rho}\right)$$

$$\sigma_{WC} = \frac{E_2(\bar{Y}-t_1)}{1-\mu_2^2}\left(\frac{1}{R} + \frac{\mu_2}{\rho}\right) \qquad \text{(C-33)}$$

$$\sigma_{WD} = \frac{E_2(\bar{Y}-t_1-t_2)}{1-\mu_2^2}\left(\frac{1}{R} + \frac{\mu_2}{\rho}\right)$$

These constitute the total stresses in the width direction. The total stresses in the direction of the tape length are

$$\sigma_{LA} = \sigma_{L1} + \sigma_1 + \sigma_{BA}$$

$$\sigma_{LB} = \sigma_{L1} + \sigma_1 + \sigma_{BB} \qquad \text{(C-34)}$$

$$\sigma_{LC} = \sigma_{L2} + \sigma_2 + \sigma_{BC}$$

$$\sigma_{LD} = \sigma_{L2} + \sigma_2 + \sigma_{BD} \qquad \text{(C-34)}$$

Figures 99 through 102 illustrate the dependence of the Eq. (C-34) stresses on the main tape-roller parameters, such as roller diameter, tape width, and crown radius. These curves were developed by using Eqs. (C-30) and (C-34). Equation (C-30) is used to determine the total contact width, since rarely does the tape contact the roller across its full width. Figures 99 and 100 illustrate the amount of tape width contact resulting from an applied tension. Two cases are presented; namely, the tension contact width variation for a roller diameter of 2 inches with crown roller radius varying from 1 inch to 4 inches, and the tension-contact width variation as a function of changing the roller diameter from 0.5 inch to 3.0 inches but maintaining the crown radius at 1.5 inch

It is seen that for both cases, conventional tape tensions of 8 to 16 oz. yield no more than 3/8 inch contact. As an example of a typical case, for a 2 inch diameter roller with a full crown radius of 1.5 inch, 8 ounces of tension results in approximately 0.25 inch contact width. To investigate the tape stresses further it is necessary to determine the average tape tension across the contact width. For the case described, i.e., T = 8 ounce and W = 0.25,

$$T/W = 32 \text{ oz/in.}$$

Inserting this number into Eq. (C-34) together with the roller and tape physical parameters, yield the stresses in the mylar and oxide layers. This analytical approach has been repeated several times to produce the mylar and oxide layer stresses distributions illustrated in Figs. 101 and 102.

Roller Diameter	2.0 in.
Mylar Backing Thickness	0.92 Mil
Oxide Coating Thickness	0.21 Mil
Backing Modulus of Elasticity –	650,000 psi
Coating Modulus of Elasticity –	100,000 psi
R = Crown Radius in Inches	

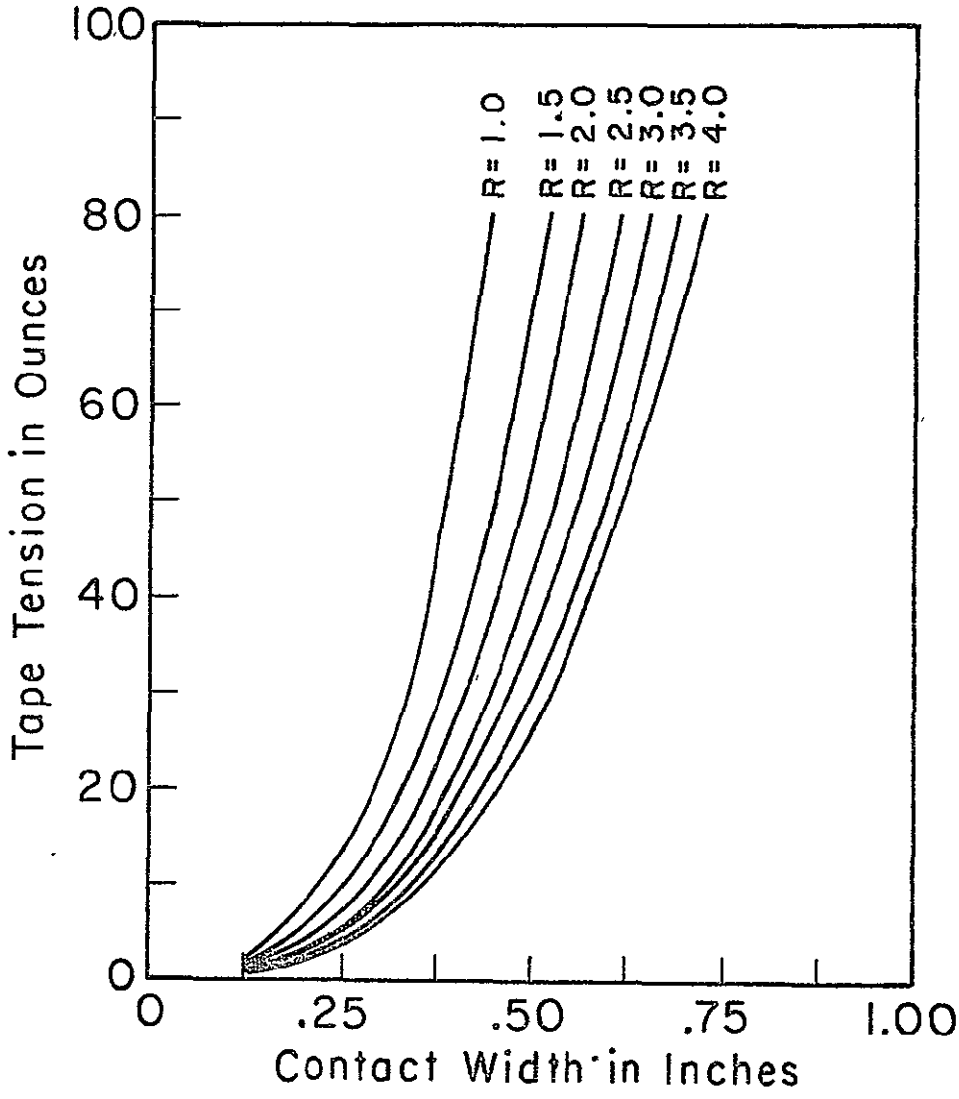

Fig. 99 TAPE TENSION VERSUS CONTACT WIDTH FOR A CROWNED ROLLER - VARIATION WITH CROWN RADIUS

Crown Radius 1.5 in.
Mylar Backing Thickness 0.92 Mil
Oxide Coating Thickness 0.21 Mil
Backing Modulus of Elasticity - 650,000 psi
Coating Modulus of Elasticity - 100,000 psi
D = Roller Diameter in Inches

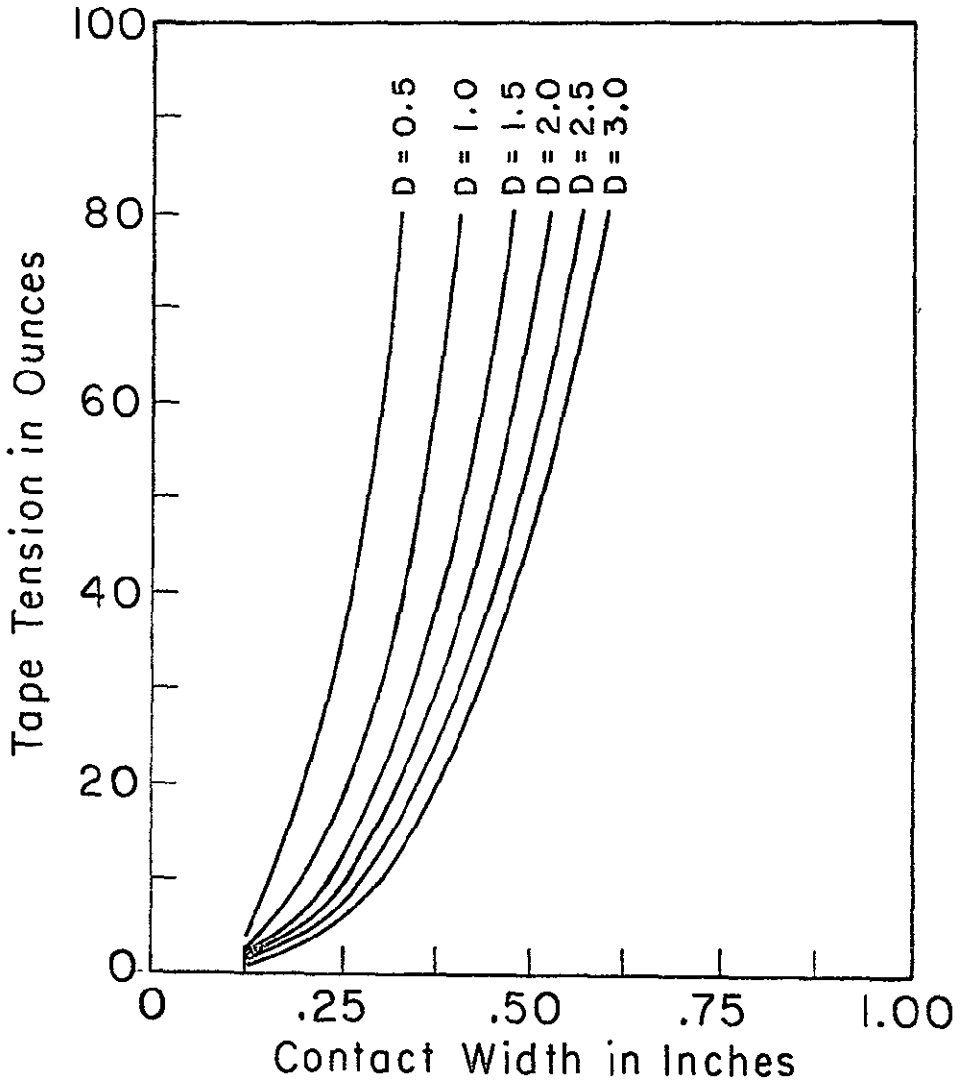

Fig. 100 TAPE TENSION VERSUS CONTACT WIDTH FOR A CROWNED ROLLER - VARIATION WITH ROLLER DIAMETER

Tape Tension - 16 oz/in Width
Mylar Backing Thickness - 0.92 Mil
Oxide Coating Thickness - 0.21 Mil
Backing Modulus of Elasticity - 650,000 psi
Coating Modulus of Elasticity - 100,000 psi
Tape Width - 0.50 in.
Crown Radius - 1.5 in.

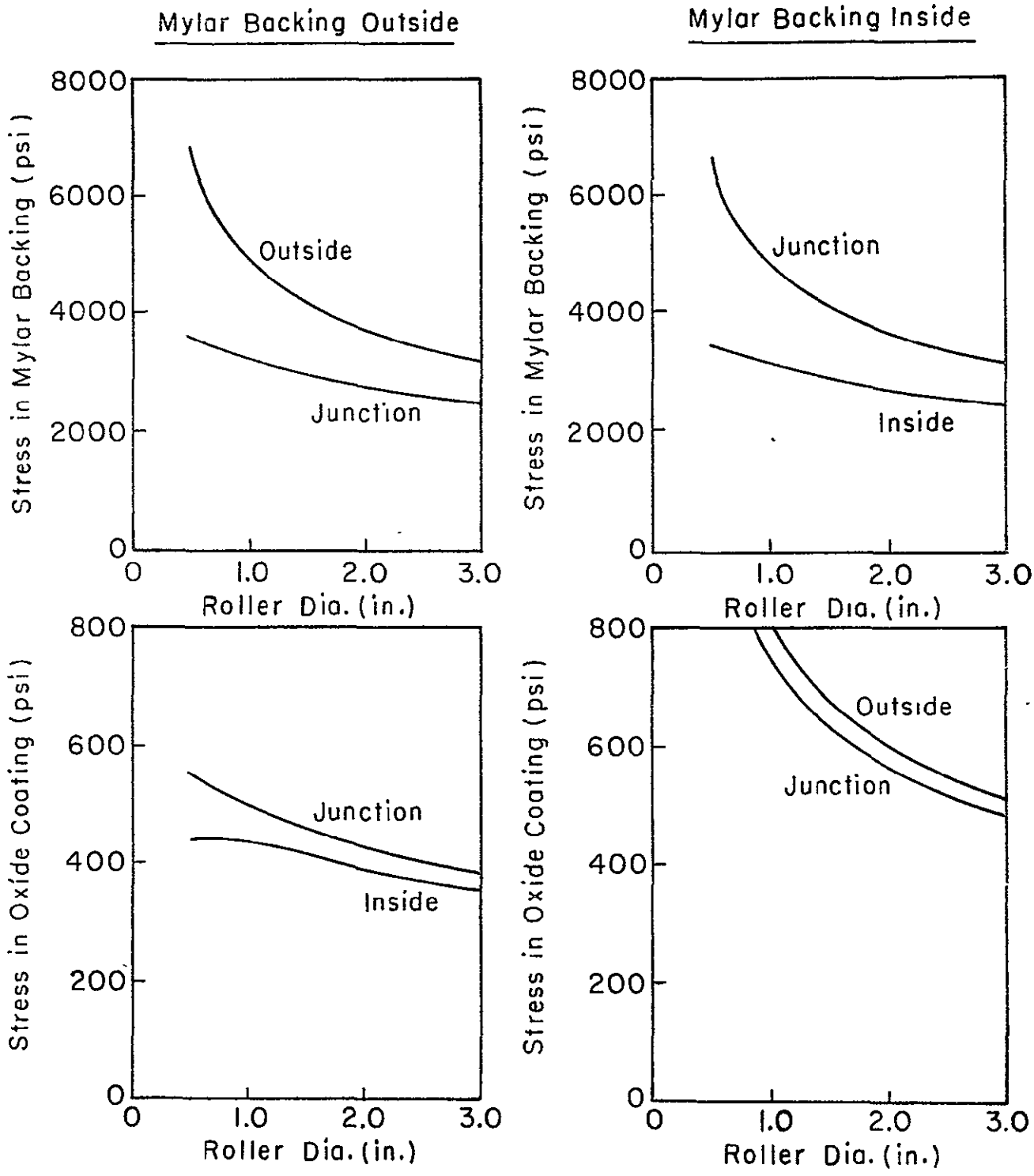

Fig. 101 MAXIMUM STRESS VERSUS CROWN IDLER DIAMETER

Roller Diameter - 2.0 in.
Tape Tension - 16 oz/in Width
Mylar Backing Thickness - 0.92 Mil
Oxide Coating Thickness - 0.21 Mil

Backing Modulus of Elasticity - 650,000 psi
Coating Modulus of Elasticity - 100,000 psi
Tape Width - 0.50 in.

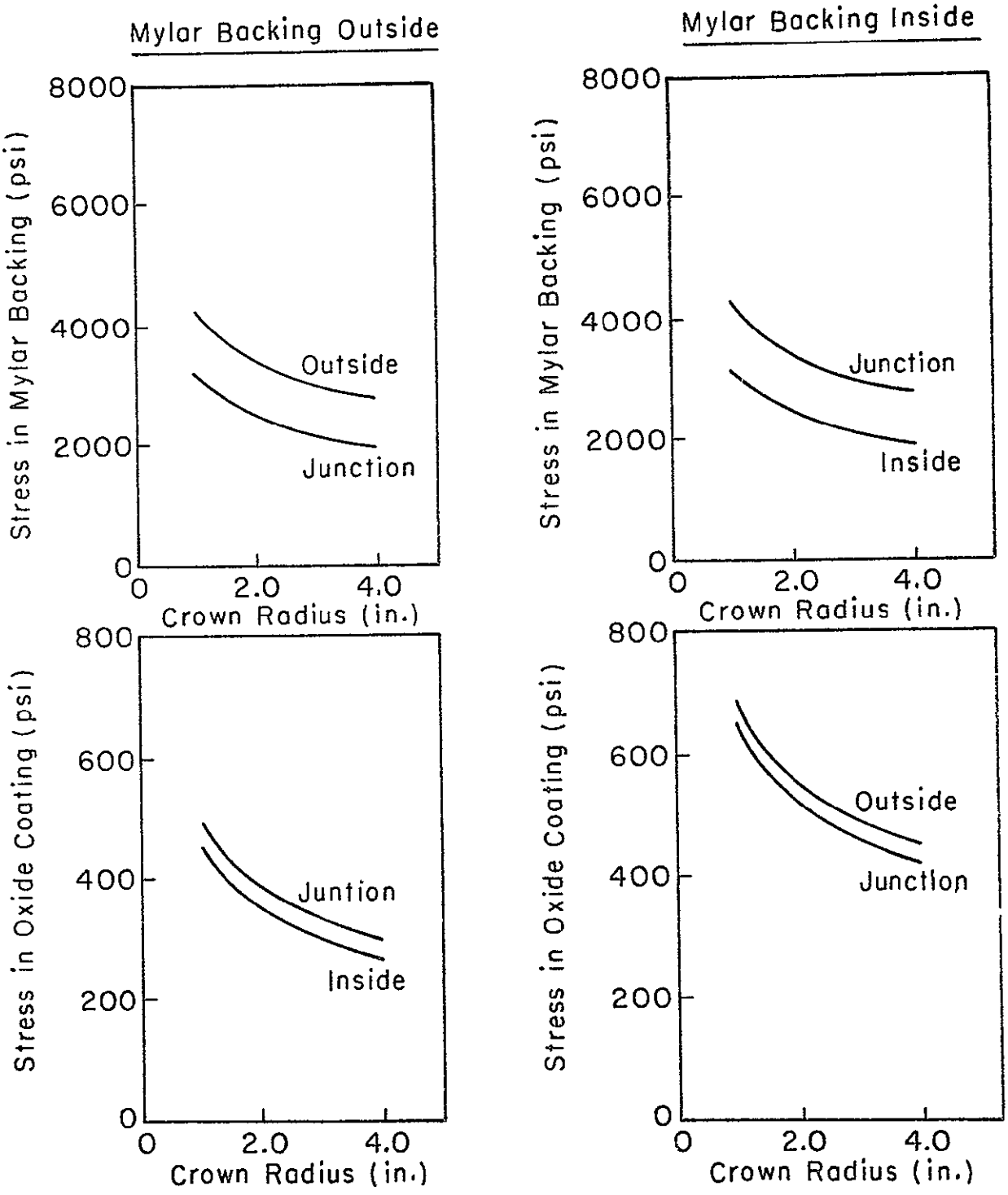

Fig. 102 MAXIMUM STRESS VERSUS CROWN RADIUS

7. Mechanical Properties of Tape

Stress-strain tests were conducted for several popular magnetic tapes to determine their yield point stresses and moduli of elasticity. The accuracy of the results was insufficient to calculate with confidence the properties of the oxide coatings, but it was concluded that the coating is much less stiff than the mylar backing (approximately one order of magnitude). The tests were performed on an Instron Tensile Tester that was operated at 0.05 inch/minute. At this speed, several tests were run to assure repeatability of results, and to assure that loading dynamics were not encountered. As a point of reference with other materials, a 0.2% offset point was designated as the yield point stress. The modulus of elasticity was obtained by graphically measuring the $\sigma - \varepsilon$ slope in the 0 - 3000 psi region. Figure 103 gives a typical stress-strain curve, and Table XV lists the yield point stress and modulus of elasticity for 10 different tapes.

In most cases, the 0.2% offset point falls within a local nonlinear region where the tape appears to lose stiffness and then recovers with a slightly increasing but nonlinear modulus of elasticity. This region appears to represent a significant variation in material properties. Generally, the yield stress point, which usually initiates this region, is within the range of 6000 to 9000 psi. To compare these values with operational experience, the work of Licht and White[10] on Mylar belts appear to support the position that stresses greater than 2500 psi should not be exceeded for long life. The obvious differences between belts and tapes are recognized, but nonetheless, many cases of tape failures have been identified at Mylar stresses in the region of 5000 psi. Hence, supported by data points for several different but allied applications, a conservative design strategy is one in which the backing stress levels are

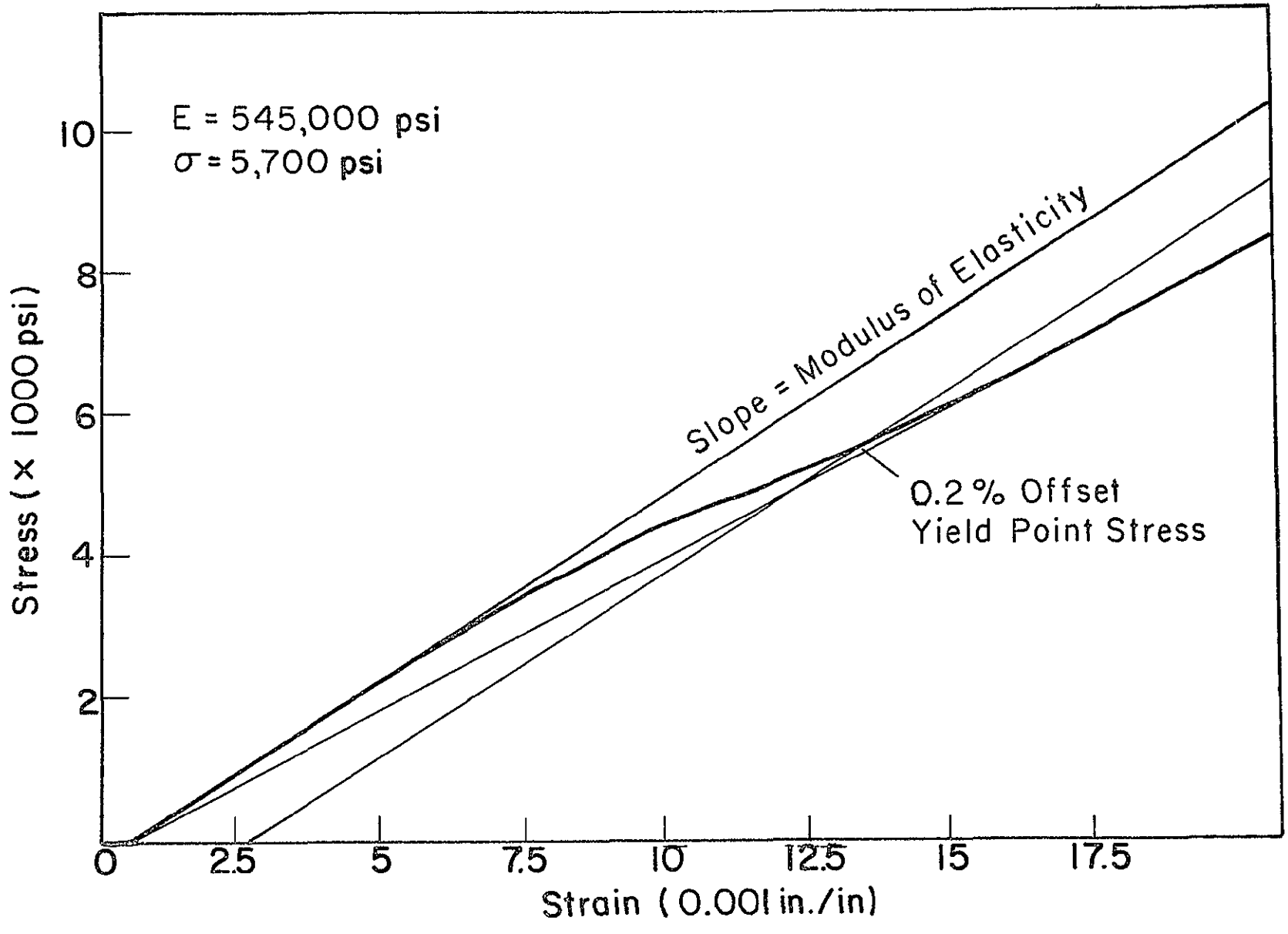

Fig. 103 TYPICAL MAGNETIC TAPE STRESS-STRAIN CURVE

Table XV

TAPE MATERIAL CHARACTERISTICS

Tape Type	Thickness		Average Modulus of Elasticity (psi)	Average 0.2% Offset Yield Point Stress (psi)
	Backing (mils)	Coating (mils)		
3M 871	0.92	0.32	520,000	6,600
3M 871	0.92	0.00	670,000	8,900
3M 888	0.92	0.21	600,000	7,400
3M 351	0.92	0.21	510,000	6,800
3M 777	1.42	0.55	500,000	4,200
2 mil Mylar Tape	2.00	0.00	720,000	8,900
Memorex 63L	0.93	0.17	650,000	6,900
Memorex 79L	0.93	0.17	580,000	7,100
Memorex Quantum	1.42	0.55	560,000	4,900
Memorex Quantum	1.42	0.00	710,000	6,800
RCA 617	0.91	0.41	440,000	5,800
RCA 617	0.91	0.00	640,000	9,000
DuPont Crolyn	1.42	0.20	540,000	6,200
DuPont Crolyn	1.42	0.00	640,000	6,400

maintained under 50% of the yield stress while minimizing the stresses in the oxide-binder system. To emphasize this latter point, the data in Fig. 86 illustrates that, for practical roller sizes, the oxide-binder stresses of under 200 psi are easily obtained.

8. Tape Stress Computer Program

The equations for the stresses in tape due to its interfacing with straight or crown rollers are programmed in Fortran V language for the Univac 1108 digital computer to facilitate the computation of stresses. Also included is a sub-routine for the case of a canted roller which causes the tape to traverse its circumference in a helix path. For the case where twisting or additional frictional forces are encountered, the resulting stresses should be added to those due to roller contact

Input Data for Tape Stress Computer Program

Card 1,3,5,.....,2N-1 (N is the number of data sets)

Columns	Item	Format	Units	Description
1	1	11	None	I=1 cylindrical roller-new page and heading desired I=2 cylindrical roller-no new page and heading desired I=3 crowned roller-new page and heading desired I=4 crowned roller-no new page and heading desired
2-11	T_1	F10.0	mils	thickness of outside tape layer (away from roller)
12-21	T_2	F10.0	mils	thickness of inside tape layer (next to roller)
22-31	E_1	F10.0	psi	modulus of elasticity of outside tape layer
32-41	E_2	F10.0	psi	modulus of elasticity of inside tape layer

Columns	Item	Format	Units	Description
42-51	μ_1	F10.0	None	Poisson's ratio for outside tape layer
52-61	μ_2	F10.0	None	Poisson's ratio for inside tape layer

Card 2,4,6,...,2N for I = 1 or 2 (see card 1 description)

Columns	Item	Format	Units	Description
1-10	θ	F10.0	deg.	cant angle of roller
11-20	T/W	F10.0	oz/in.	tape tension
21-30	D	F10.0	in.	roller diameter

Card 2,4,6,...,2N for I = 3 or 4 (see card 1 description)

Columns	Item	Format	Units	Description
1-10	T/W	F10.0	oz/in.	tape tension
11-20	D	F10.0	in.	maximum roller diameter
21-30	W	F10.0	in.	tape width
31-40	R	F10.0	in.	crown radius

The output data is self explanatory. The first line of output is a listing of the input data in the same units as the input. The second line gives the stresses in psi for I = 1 Or 2 (cylindrical roller). For I = 3 or 4 (crowned roller) the second line includes the total tension T, the tension required to maintain full width contact of the tape with the roller TR, and the stresses in the tape in psi. The nomenclature for the stresses is the same as that used elsewhere in this section.

Computer Program

```
    1 READ(5,2)I,T1,T2,E1,E2,P1,P2
    2 FORMAT(I1,6F10.0)
      GO TO (3,5,9,11),I
    3 WRITE(6,4)
    4 FORMAT(59H1PRINCIPAL STRESSES IN TAPE PASSING OVER CYLINDRICAL ROL
     1LER//)
    5 READ(5,6)ANGLE,TW,D
    6 FORMAT(3F10.0)
      WRITE(6,7)T1,T2,E1,E2,P1,P2,ANGLE,TW,D
    7 FORMAT(6H *  T1,4X2HT2,5X2HE1,8X2HE2,7X2HU1,4X2HU2,2X5HANGLE,2X3HT
     1W,5X1HD/2F6.2,2F10.0,2F6.2,F6.0,F7.1,F6.2//5X3HSLA,5X3HSTA,5X3HSW
     2A,5X3HSLB,5X3HSTB,5X3HSWB,5X3HSLC,5X3HSTC,5X3HSWC,5X3HSLD,5X3HSTD,
     35X3HSWD)
      TWL=TW/16.
      T1L=T1/1000.
      T2L=T2/1000.
      EL=E2*(1.-P1*P1)/(E1*(1.-P2*P2))
      R=D/2.
      A=ANGLE*.017453293
      TE=T1L*E1+T2L*E2
      S1=TWL*E1/TE
      S2=TWL*E2/TE
      Y=(T1L*T1L+EL*T2L*T2L+2.*EL*T1L*T2L)/(2.*(T1L+EL*T2L))
      SBA=E1*Y/((1.-P1*P1)*R)
      SBB=E1*(Y-T1L)/((1.-P1*P1)*R)
      SBC=E2*(Y-T1L)/((1.-P2*P2)*R)
      SBD=E2*(Y-T1L-T2L)/((1.-P2*P2)*R)
      Z1=S1*(COS(A))**2
      Z2=S1*(SIN(A))**2
      Z3=S1*SIN(A)*COS(A)
      Z4=Z1+SBA
      Z5=SQRT((Z4-Z2)**2/4.+Z3*Z3)
      SLA=(Z2+Z4)/2.+Z5
      STA=0.
      SWA=(Z2+Z4)/2.-Z5
      Z4=Z1+SBB
      Z5=SQRT((Z4-Z2)**2/4.+Z3*Z3)
      SLB=(Z2+Z4)/2.+Z5
      STB=-TWL*(COS(A))**2*T1L*E1/(R*TE)
      SWB=(Z2+Z4)/2.-Z5
      Z1=S2*(COS(A))**2
      Z2=S2*(SIN(A))**2
      Z3=S2*SIN(A)*COS(A)
      Z4=Z1+SBC
      Z5=SQRT((Z4-Z2)**2/4.+Z3*Z3)
      SLC=(Z2+Z4)/2.+Z5
      STC=STB
      SWC=(Z2+Z4)/2.-Z5
```

```
      Z4=Z1+SBD
      Z5=SQRT((Z4-Z2)**2/4.+Z3*Z3)
      SLD=(Z2+Z4)/2.+Z5
      STD=-TWL*(COS(A))**2/R
      STD=-TWL/R
      SWD=(Z2+Z4)/2.-Z5
      WRITE(6,8) SLA,STA,SWA,SLB,STB,SWB,SLC,STC,SWC,SLD,STD,SWD
    8 FORMAT(F9.0,11F8.0//)
      GO TO 1
    9 WRITE(6,10)
   10 FORMAT(55H1PRINCIPAL STRESSES IN TAPE PASSING OVER CROWNED ROLLER/
     1/)
   11 READ(5,12)TW,D,W,R
   12 FORMAT(4F10.0)
      WRITE(6,13)T1,T2,E1,E2,P1,P2,TW,D,W,R
   13 FORMAT(6H *  T1,4X2HT2,5X2HE1,8X2HE2,7X2HU1,4X2HU2,3X3HT/W,3X1HD,5
     1X1HW,5X1HR/2F6.2,2F10.0,2F6.2,F6.1,F6.2,F5.2,F7.2//5X1HT,6X2HTR,6X
     23HSAT,5X3HSAW,5X3HSBT,5X3HSBW,5X3HSCT,5X3HSCW,5X3HSDT,5X3HSDW)
      T1L=T1/1000.
      T2L=T2/1000.
      EL=E2*(1.-P1*P1)/(E1*(1.-P2*P2))
      TE=T1L*E1+T2L*E2
      Y=(T1L*T1L+EL*T2L*T2L+2.*EL*T1L*T2L)/(2.*(T1L+EL*T2L))
      SBA=(E1*Y/(1.-P1*P1))*(2./D+P1/R)
      SBB=(E1*(Y-T1L)/(1.-P1*P1))*(2./D+P1/R)
      SBC=(E2*(Y-T1L)/(1.-P2*P2))*(2./D+P2/R)
      SBD=(E2*(Y-T1L-T2L)/(1.-P2*P2))*(2./D+P2/R)
      ABC=R/(.5*D-R*(1.-COS(.5*W/R)))
      Q1=E1*(1.-COS(.5*W/R))*ABC
      Q2=E2*(1.-COS(.5*W/R))*ABC
      TR=(T1L*E1+T2L*E2)*2.*(R*SIN(.5*W/R)-.5*W*COS(.5*W/R))*ABC
      TWL=TW/16.-TR/W
      S1=TWL*P1/TE
      S2=TWL*E2/TE
      SLA=SBA+Q1+S1
      SLB=SBB+Q1+S1
      SLC=SBC+Q2+S2
      SLD=SBD+Q2+S2
      SWA=(E1*Y/(1.-P1*P1))*(1./R+2.*P1/D)
      SWB=(E1*(Y-T1L)/(1.-P1*P1))*(1./R+2.*P1/D)
      SWC=(E2*(Y-T1L)/(1.-P2*P2))*(1./R+2.*P2/D)
      SWD=(E2*(Y-T1L-T2L)/(1.-P2*P2))*(1./R+2.*P2/D)
      T=TW*W
      TR=TR*16.
      WRITE(6,14)T,TR,SLA,SWA,SLB,SWB,SLC,SWC,SLD,SWD
   14 FORMAT(F6.1,F9.1,F9.0,7F8.0//)
      GO TO 1
      END
```

Sample Output

PRINCIPAL STRESSES IN TAPE PASSING OVER CROWNED ROLLER

*	T1	T2	E1	E2	U1	U2	T/W	D	W	R
	,21	,92	100000,	650000,	,45	,45	28,0	2,00	,13	1,50

T	TR	SAT	SAW	SBT	SBW	SCT	SCW	SDT	SDW
3,5	1.1	452.	91.	398.	62.	2587.	401.	1612.	-436.

*	T1	T2	E1	E2	U1	U2	T/W	D	W	R
	,21	,92	100000,	650000.	,45	,45	28,0	2,00	,25	1,50

T	TR	SAT	SAW	SBT	SBW	SCT	SCW	SDT	SDW
7,0	8,6	563.	91.	529.	62.	3439.	401.	2464.	-436.

*	T1	T2	E1	E2	U1	U2	T/W	D	W	R
	,21	,92	100000.	650000.	,45	,45	28.0	2,00	,38	1,50

T	TR	SAT	SAW	SBT	SBW	SCT	SCW	SDT	SDW
10,5	29.3	784.	91.	750.	62.	4872.	401.	3897.	-436.

*	T1	T2	E1	E2	U1	U2	T/W	D	W	R
	,21	,92	100000.	650000.	,45	,45	28,0	2,00	,50	1,50

T	TR	SAT	SAW	SBT	SBW	SCT	SCW	SDT	SDW
14,0	70.0	1097.	91.	1063.	62.	6908.	401.	5933.	-436.

*	T1	T2	E1	E2	U1	U2	T/W	D	W	R
	,21	,92	100000.	650000.	,45	,45	28,0	2,00	,63	1,50

T	TR	SAT	SAW	SBT	SBW	SCT	SCW	SDT	SDW
17,5	138,2	1508.	91.	1474.	62.	9578.	401.	8604.	-436.

*	T1	T2	E1	E2	U1	U2	T/W	D	W	R
	,21	,92	100000.	650000.	,45	,45	28,0	2,00	,75	1,50

T	TR	SAT	SAW	SBT	SBW	SCT	SCW	SDT	SDW
21,0	242.0	2023.	91.	1988.	62.	12925.	401.	11950.	-436.

*	T1	T2	E1	E2	U1	U2	T/W	D	W	R
	,21	,92	100000.	650000.	,45	,45	28,0	2,00	,88	1,50

T	TR	SAT	SAW	SBT	SBW	SCT	SCW	SDT	SDW
24,5	390.2	2650.	91.	2616.	62.	17001.	401.	16026.	-436.

*	T1	T2	E1	E2	U1	U2	T/W	D	W	R
	,21	,92	100000.	650000.	,45	,45	28,0	2,00	1,00	1,50

T	TR	SAT	SAW	SBT	SBW	SCT	SCW	SDT	SDW
28,0	593.1	3400.	91.	3366.	62.	21876.	401.	20901.	-436.

LIST OF SYMBOLS

D = roller diameter (maximum diameter in the case of a crowned roller) (in.)

R = crown radius for crowned roller (in.)

ρ = roller radius $\frac{D}{2}$ (in.)

E_1 = modulus of elasticity of outside layer of tape (psi)

E_2 = modulus of elasticity of inside layer of tape (next to roller) (psi)

t_1 = thickness of outside layer of tape (in.)

t_2 = thickness of inside layer of tape (in.)

W_o = tape width in contact with crowned roller (in.)

W = total tape width (in.)

μ_1 = Poisson's ratio inside tape layer

μ_2 = Poisson's ratio outside tape layer

T = tape tension (oz)

T_R = tape tension for partial contact (oz) in crowned roller

T_C = tape tension for full crowned roller contact (oz)

σ = stress, psi

ε = strain In./in.

P = tape-roller contact pressure, psi

ϕ = total tape-roller wrap angle

θ = roller cant angle

D. Tape Pack Design

Presented in this section is a critical review of ASTIA Report No. AD 238 884L, entitled "Magnetic Tape Study."[11] Tape pack design is discussed with respect to environmental changes in temperature, humidity, shock, and vibration. Damage induced by these conditions occurs in the forms of edge crushing, axial crushing, axial slipping, tangential slipping and spoking. Tape pack damage is controlled and eliminated through proper selection of reel geometry for a given tape material. Spoking, a major failure mode, is eliminated by a design that avoids tangential compression of individual tape layers. The areas of tape pack design reviewed are:

- Reel flanges
- Hub slots
- Reel geometry
- Tape winding tension

It has been shown that uneven laying of tape on the reel, within the limits imposed by the flange separation distance, leads to the development of tape skews. These skews have amplitudes in excess of the limits predicted from purely geometrical considerations. In addition to the potential damage effect of excessive flange-to-flange spacing, the more obvious difficulty of reels with flanges bent, warped or having sharp edges exists.

The ASTIA report claims that typical reel flange holes tend to pump air into the reel and cause air entrainment in the tape pile (physically, this is difficult to justify). This effect tends to yield a distorted tape pile sensitive to temperature and humidity effects.

The experiments with a glass-flange reel showed that reels with no holes in the flanges produced a more solid tape pile than tapes wound under similar speed (15 in/sec) and tension conditions or any pierced flange standard or precision reel

types. It is further claimed that the existence of alternating open and closed flange areas adjacent to the tape pile face make the stored tape pack vulnerable to temperature humidity effects. However, it must be realized that the added inertia of this type flange may not be tolerable in lightweight recorders where limited power is available.

Because these results are questionable, some experiments were run on tape pack profiles at 30 and 240 in/sec with and without airflow. Figure 104 shows that, at 30 in/sec, the tape pack profile is similar for a reel wound with and without airflow (with and without flange holes). Figure 105 shows that a tape pack profile wound at 240 in/sec with airflow is more constant than the tape pack profile without airflow. Of course, these are wound at higher speeds than those used in the G.K.I. report.

The next area of interest in the design of tape packs is the hub. Moderate to high pressures are exerted by the tape on the hub, and any void will cause gradual, plastic extrusion of the tape. Depdending on particular hub slot design, the length of storage, and the winding tension pattern, as much as 300 feet of tape may be embossed. Since true concentricity of the tape roll is destroyed in the neighborhood of reel hub slots, stress concentrations are developed in the roll that lead to spoking and opening of voids throughout the entire roll during long-term storage or short-term temperature humidity cycling. Therefore, it is recommended that no hub slots be used. The configuration, shown in Fig. 106, eliminates this embossing problem.

The amount of tape contained in a tape pack is determined from the following relationships.

$$\ell = 2\pi N \ (2R_o - Nt)$$

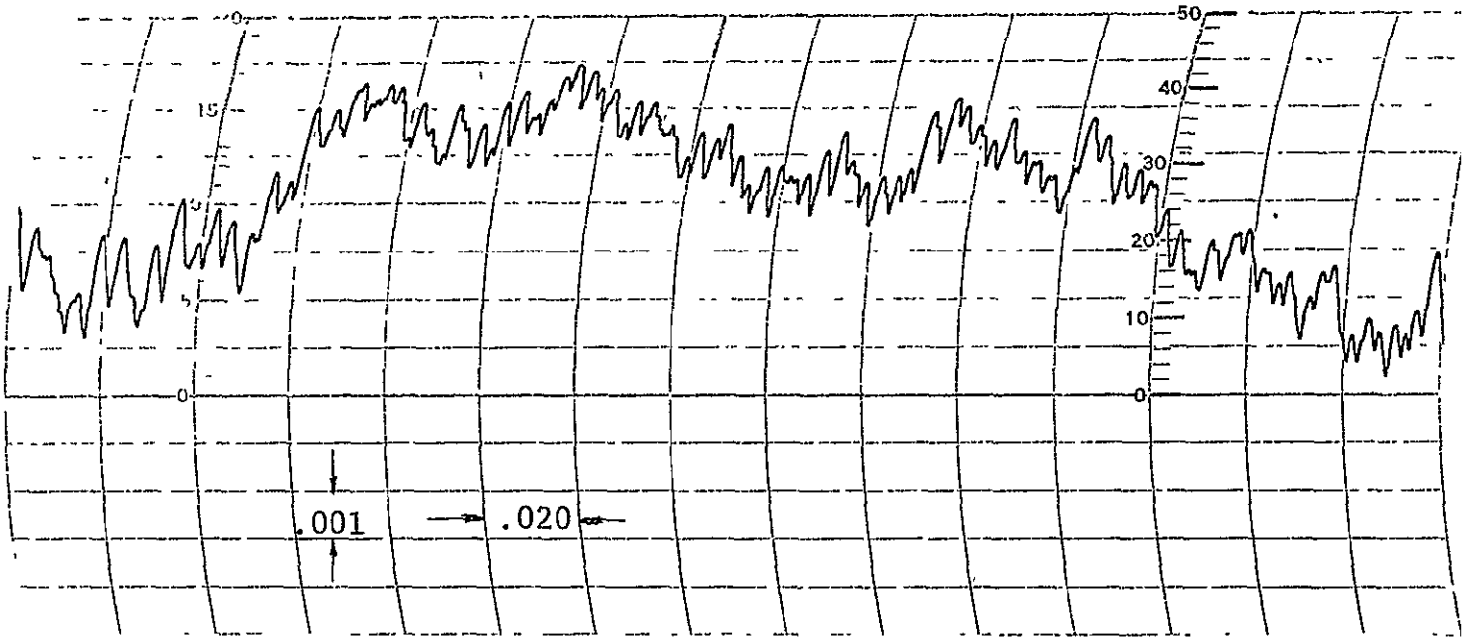

a. No Air Flow

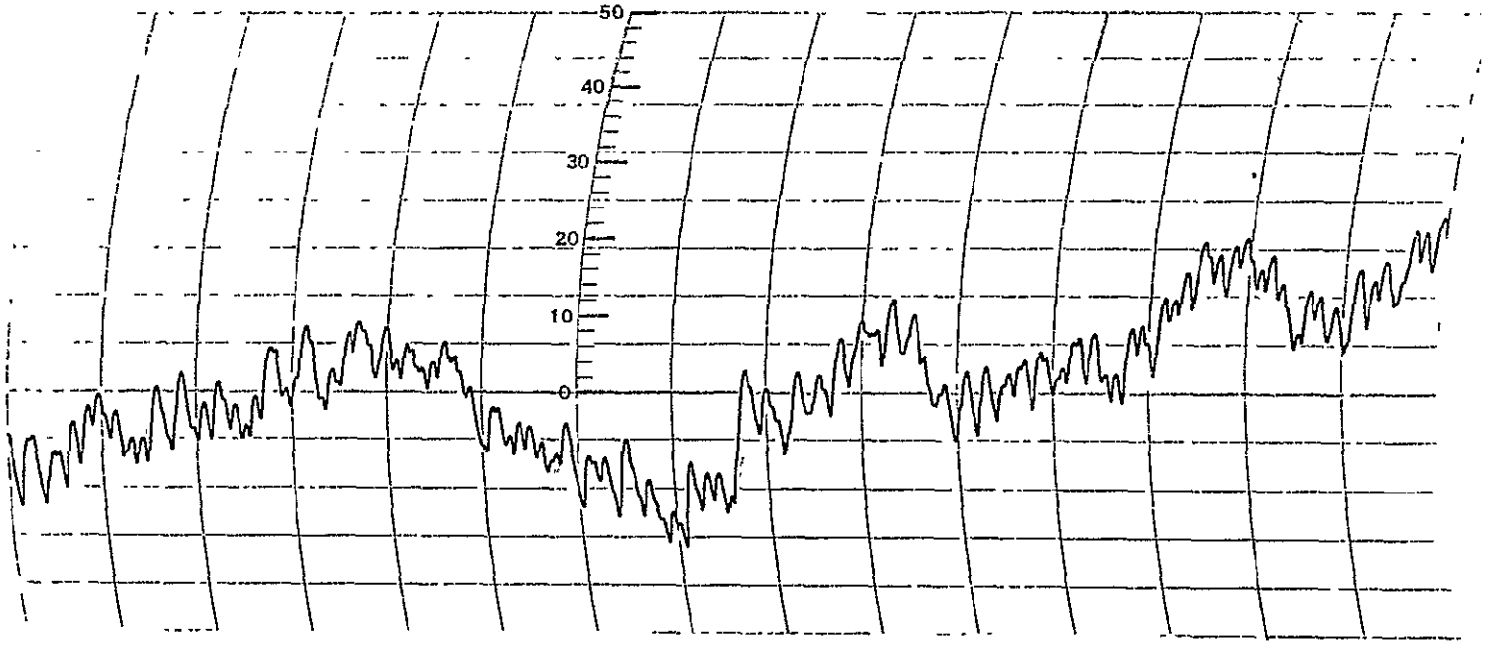

b. Air Flow Allowed

Fig. 104 TAPE PACK PROFILE 30 INCHES PER SECOND

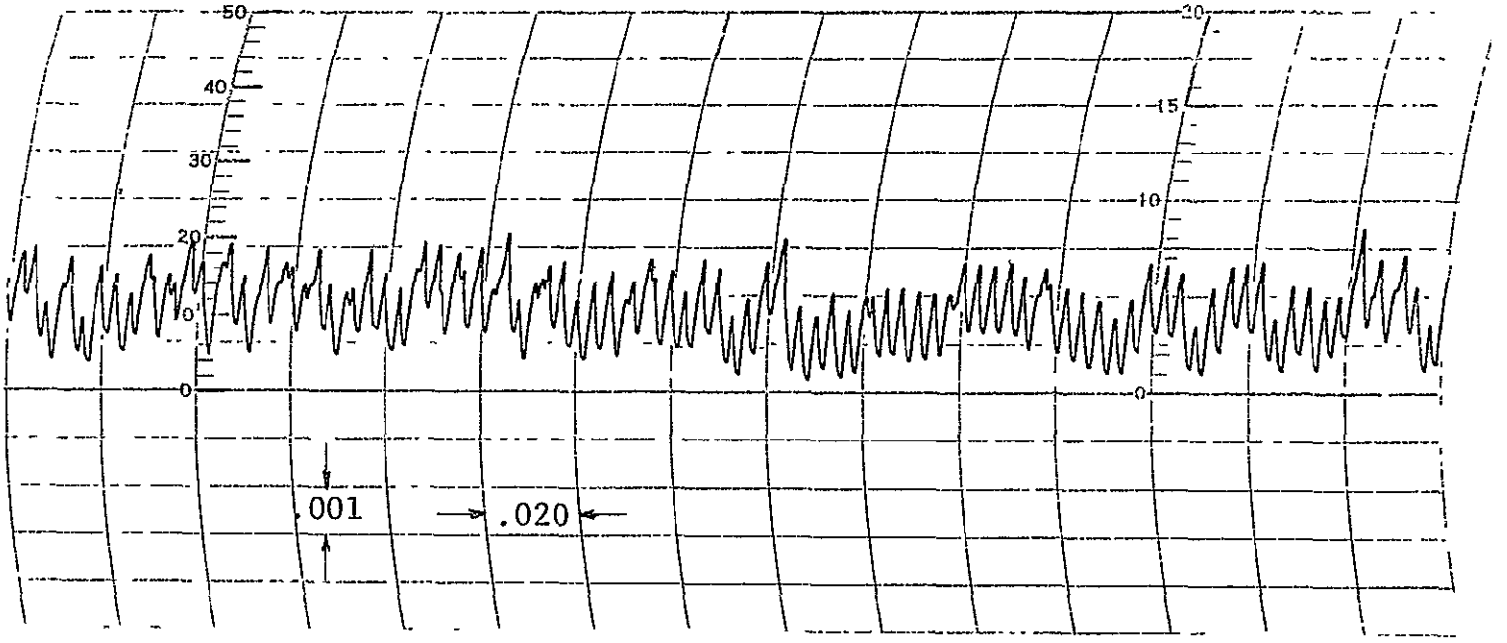

a. No Air Flow

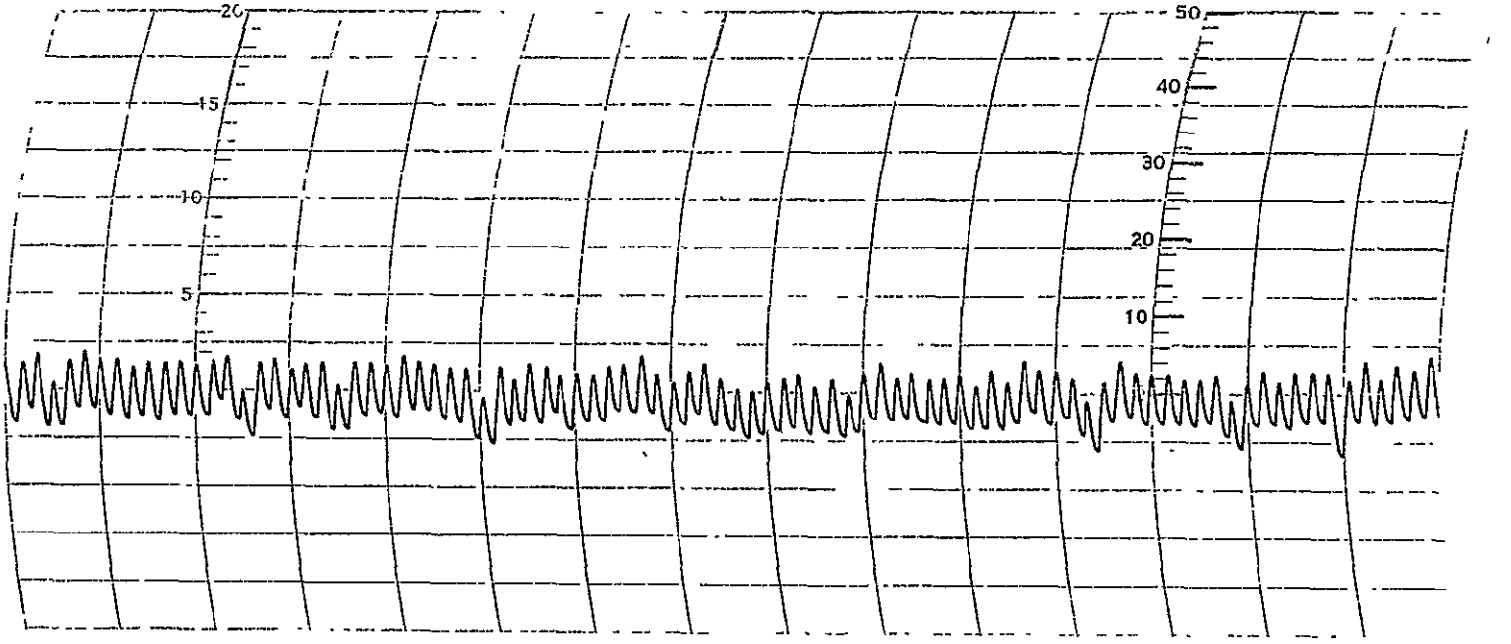

b. Air Flow Allowed

Fig. 105 TAPE PACK PROFILE 240 INCHES PER SECOND

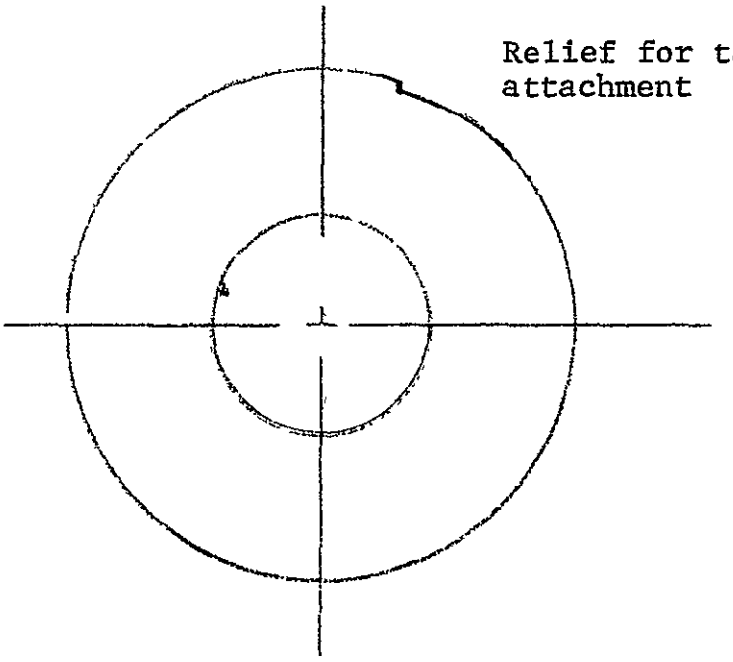

Fig. 106 REEL HUB CONFIGURATION

and

$$R_o = R_1 + Nt$$

where

ℓ = length of tape

N = number of tape layers

t = thickness of tape

R_o = outside of radius of tape pack

R_1 = inside radius of tape pack

The final topic discussed is the winding tension pattern governing tape pack behavior when subjected to common environmental effects. Tape rolls commonly suffere severe malfunction due to mechanical distortion, such as looseness, spoking, cinching, and axial displacement. This effect commonly occurs about one-third distance from the hub to the outer edge of the tape roll. This effect causes tape damage; however, temperature and humidity cycling, shock, and vibration amplify tape malfunction due to improper winding tension patterns.

For this reason an analysis of tape rolls was conducted to determine those reel geometry and winding tension patterns that would yield a tape roll devoid of a distorted area when the tape tension is negative. The following assumptions were made in formulating a mathematical model for the tape roll.

- The tape is evenly laid and the tape roll is homogenous
- No consideration is given to dynamic conditions of tape reel speed, tape velocity, etc.
- Changes in the tension pattern due to environmental effects are neglected.

- The tape roll was considered to be an axisymmetric disk made up on anisotropic material.
- The elastic limit of the tape introduces an upper limit on winding tension.

Through the use of this model, the basic properties of a desirable final tension pattern in a wound roll were developed. The final tension and pressure patterns in tape roll resulting from common winding practice (constant tension and torque) were derived and confirmed in practice. Then winding patterns designed to alleviate each of the basic causes of roll imperfections were derived. The following parameters and physical constants were used in this analysis.* Figure 107 shows a typical tape roll.

For design purposes, it follows from this analysis that the important parameters are

$$\beta/k = \frac{\text{hub compressibility}}{\text{longitudinal tape compliance}}$$

$$\alpha/k = \frac{\text{tape pile compressibility}}{\text{longitudinal tape compliance}}$$

R = outside radius of wound roll

The equilibrium equation for an infinitesimal segment of the tape roll is

$$T + P + r\frac{dP}{dr} = r \qquad \text{(D-1)}$$

The equations relating the material behavior, material constants α, λ, K, ρ, to stress T, P and strain u as a function of radial distance r are

*Refer to p. 242 for List of Symbols.

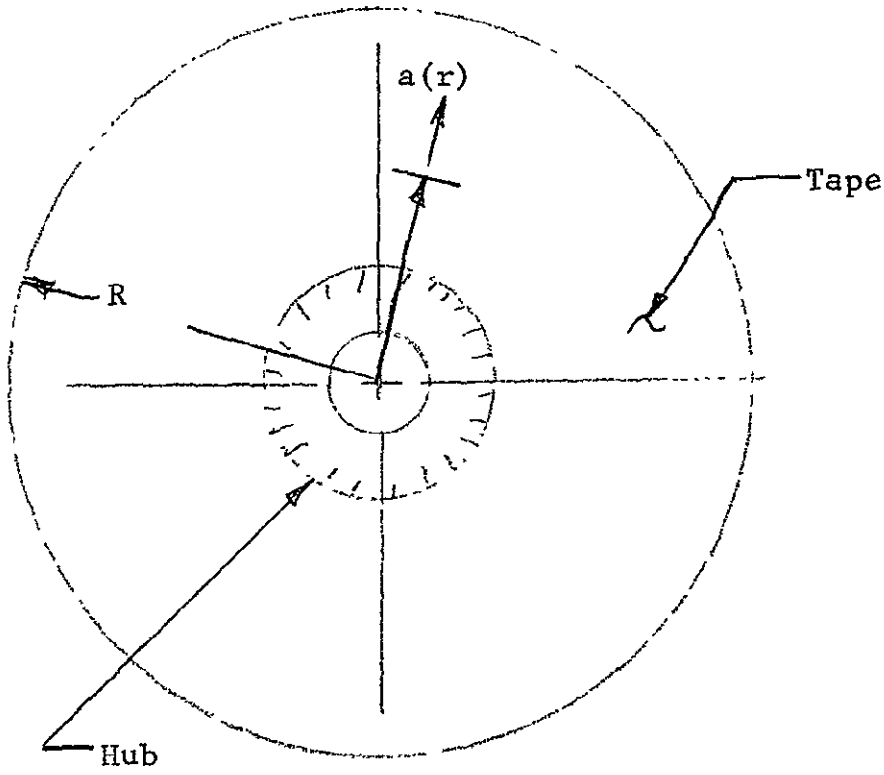

Fig. 107 TYPICAL TAPE ROLL

$$\frac{du}{dr} = \sigma P - \lambda KT \text{ -- radial strain} \qquad (D\text{-}2)$$

$$\frac{u}{r} = KT + \rho a P \text{ -- tangential strain} \qquad (D\text{-}3)$$

Algebraic combination of Eqs. (D-1), (D-2), and (D-3) yields a differential equation that describes the radial deformation as a function of material constants.

$$\frac{d^2u}{dr^2} + \frac{1}{r}(r + 2\delta)\frac{du}{dr} - \frac{1}{r^2}\frac{\alpha}{K}u = 0 \qquad (D\text{-}4)$$

In addition, the following relationships for pressure and tension are obtained.

$$P = \frac{1}{\alpha(\rho\lambda - 1)}\left[\frac{du}{dr} + \frac{\lambda u}{r}\right] \qquad (D\text{-}5)$$

$$T = \frac{1}{K(\rho\lambda - 1)}\left[\rho\frac{du}{dr} + \frac{u}{r}\right] \qquad (D\text{-}6)$$

For $|\alpha| < 0.1$, the general solution to differential equation (D-4) is

$$u = C_1 r^{\sqrt{\alpha/k - \alpha}} + C_2 r^{-\sqrt{\alpha/k - \alpha}}$$

where C_1 and C_2 are functions of the boundary conditions. On the outside boundary the pressure is P_f, and on the inside boundary, the deformation u of the tape roll matches the outside hub deformation.

Integrals are developed for the final tension T_f and a function of initial tension T_1 and the final pressure P_f.

$$T_1 = P_f$$

This relationship was integrated for constant tension winding, constant torque winding, and some varied tension winding profiles. These results were calculated and design data are plotted. All parameters are normalized for an inside hub radius of one. Design data are given for varied tape compressibility α, longitudinal compliance K, hub compressibility β, and tape roll diameter R for constant tension and constant torque winding. Figure 108 shows an example of the data for constant torque winding. The pressure profile for the same tape and hub properties is given in Fig. 109.

For any given final reel diameter R, the tension and pressure curves are higher for lower values of β/K and coverage to a single point as r approaches R. For large values of β/K (soft hub), the final tensions become negative near the hub inducing spoking. The change in tension per unit length of tape will also be very large near the hub. These undesirable tension pattern properties are manifested more in constant tension windings than in constant torque windings.

Figure 110 schematically shows the forces existing in a roll having a region of transition from positive to negative tension. Outside the transition, the inward pressure is small and the tension is large and positive. Inside the transition, the inward pressure is large and the tape tension is negative; the tape is under longitudinal compression. Since tape is subject to plastic flow, these forces will dissipate slowly after winding.

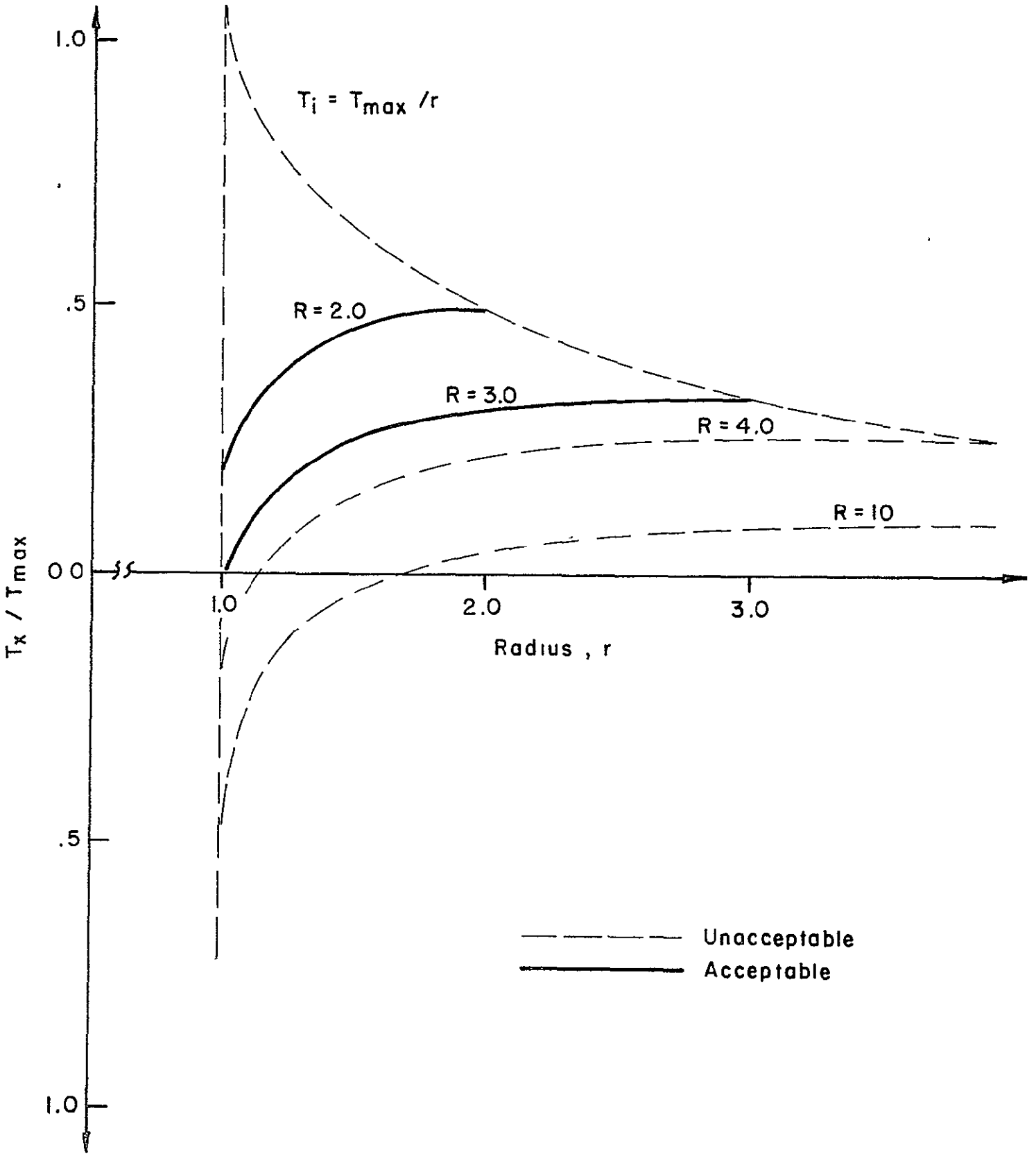

Fig. 108 FINAL TENSION PATTERNS FOR CONSTANT INITIAL WINDING TORQUE $T_i = T_{max}/r$, $\beta/K = 1.5$, $\alpha/K = 1.0$

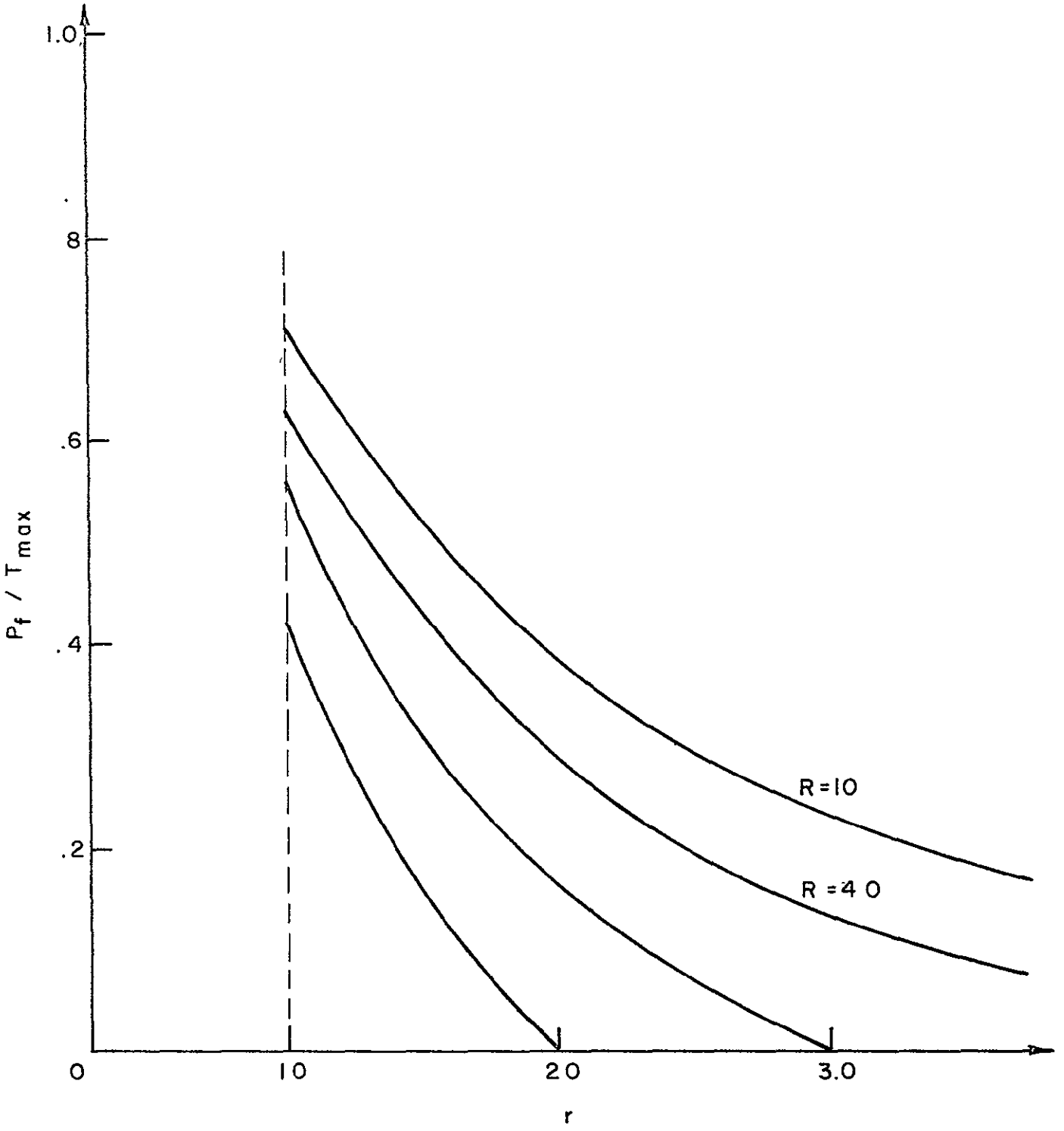

Fig. 109 FINAL PRESSURE PATTERNS FOR CONSTANT INITIAL WINDING TORQUE $T_i = T_{max}/r$, $\alpha/K = 1.0$, $\beta/K = 1.5$

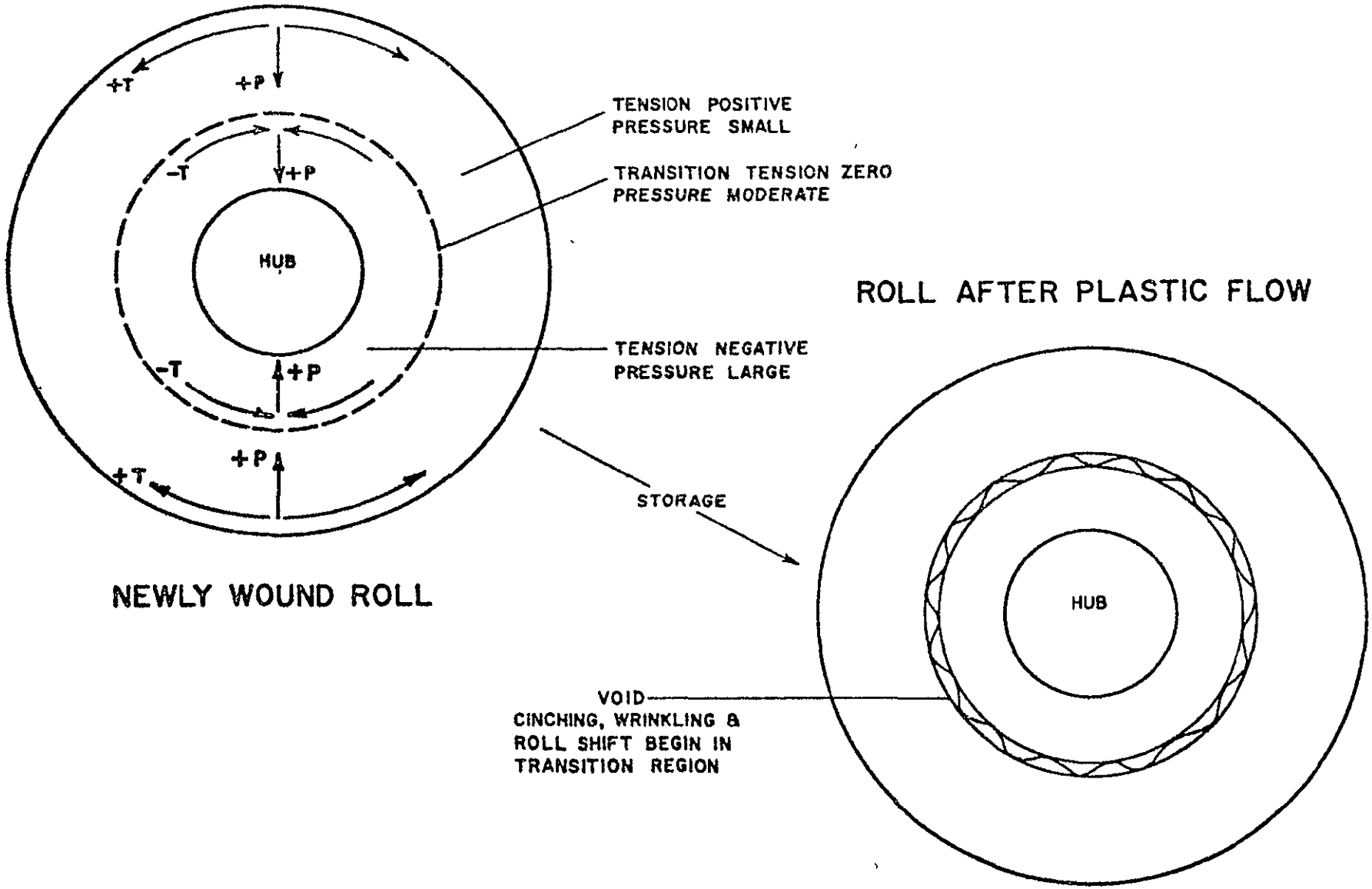

Fig. 110 STATIC FORCES ACTING IN A TAPE ROLL HAVING A NEGATIVE TENSION TRANSITION POINT

The tension and pressure patterns of Figs. 108 and 109 demonstrate the advantages of a large, comparatively incompressible hub. First, the more incompressible the hub of a roll, the higher the pressure throughout the roll; secondly, the more incompressible the hub of a roll, the more the roll will resist buckling or spoking and the more nearly it will retain its cylindrical symmetry; finally, the more incompressible the hub, the closer the final tension will be to the initial winding tension. Thus, the more incompressible the hub, the higher the final tension, and the more nearly constant.

It can be demonstrated that, if $\beta/k >> 2$, good final tension and pressure patterns cannot be achieved with any initial winding tension pattern. Hub compressibility for a given hub diameter is perhaps the most important single factor in determining the quality of a roll of magnetic tape (quality of the roll, not of the tape). Obviously, the minimum practical hub compressibility should be employed in quality reel design.

Using the developed winding theory, design data have been generated that allow the selection of reel design parameters that eliminate the negative tension region $\frac{T_t}{T_{max}}$ in tape rolls. It is these regions that leave the tape roll vulnerable to the environmental effects of shock and vibration and temperature humdity.

LIST OF SYMBOLS

σ - compressibility of the tape in a tape pile; decrease in tape thickness per unit tape thickness per unit pressure on tape surface

β - hub compressibility; decrease in hub radius per unit pressure on hub rim

σ - anisotrophy of Poisson's ratio; $(1/2)\ (\lambda-\rho\ \sigma/k)$

ε - maximum possible difference between linear hub expansion and tape expansion with temperature and humidity cycling

γ - coefficient of friction between adjacent layers of tape

K - longitudinal tape compliance; elongation of tape per unit length per unit tension per unit cross-sectional area

λ - Poisson's ratio; the ratio of transverse to longitudinal strain under longitudinal stress

ρ - Poisson's ratio; the ratio of longitudinal to transverse strain under transverse compression

$P(r)$ - radial pressure at any point r in the roll

r - variable of radial distance of wound roll

R - outside radius of wound roll

s - distance along the tape from the point r = 1 to r

t - tape thickness

T - tension per unit cross-sectional area; 1/t times the actual tension

T_f - final tension, tension per unit cross-section area of tape after roll is fully wound to the outside radius R

T_1 - initial or winding tension; tension per unit cross-section area of tape after roll is fully wound to the outside radius R

T_{max} - maximum allowable tension in the roll

u - change in the radial position r of a given section of tape under the application of external stresses

E. Head/Tape Dynamics

The objectives of this study were to find the local dynamic response of a magnetic tape moving past a stationary head and to find the local temperature distribution in the tape. This section discusses modeling of the problem for theoretical study. The problem was modeled so that local longitudinal motion could be obtained for varied head friction and geometry with tape tension excitation at the tape reels or capstans. The instantaneous local velocity and the head/tape friction force was used to determine thermal gradients in the head/tape regions.

In reviewing the technical literature two articles by Steinhorst[12,5] in German, were found that related to this problem. In the first article a dynamic elastic constant was obtained from his equations of motion. This constant, a function of the tapes longitudinal compliance and Poissons's ratio,

$$E_D = \frac{E_S(1-\upsilon)}{(1+\upsilon)\ (1-2\upsilon)} \qquad \text{(E-1)}$$

was measured by experimentally observing the natural vibration frequency f, of a tape of length ℓ, and density ρ,

$$E_D = 4\ell^2 f^2 \rho \qquad \text{(E-2)}$$

The second article was most interesting because it set up a design guideline to avoid stick-slip excitation of slowly moving tapes. Steinhorst found that, if the tape velocity was greater than V_{cr}, then stick-slip response (intense wow) can be avoided.

$$V_{cr} = \frac{(e^{\mu_h \gamma} - e^{\mu_g \gamma})\, B}{E_s b\ a} \sqrt{\frac{E_D}{\rho}} \qquad \text{(E-3)}$$

where

B = tape tension

a = tape thickness

b = tape width

μ_g = sliding friction coefficient

μ_h = static friction coefficient

γ = wrap angle

E_s = modules of elasticity

$\frac{E_D}{\rho}$ = sound velocity

ρ = average density

$E_D = E_s \frac{(1-\upsilon)}{(1-\upsilon)\ (1-2\upsilon)}$

υ = Poisson's ratio

$f = \frac{1}{2\ell} \sqrt{\frac{E_D}{\rho}}$ = tape natural frequency

Steinhorst gives examples of using this important formula, and in addition, a good discussion on the measurement of f, μ_g and μ_h.

Other literature on the longitudinal and lateral response of moving tapes, strings, and band saw blades to various external disturbances was reviewed. Three basic tapes of dynamic problems, all of which relate to the present head/tape dynamics problem, were solved in the articles reviewed.

(1) Natural frequencies and mode shapes

(2) Response of a tape, string, and band saw blade to external excitation

(3) Stability of a band saw blade excited by tension fluctuations

The latter two analyses provided guidelines for study of the head/tape problem. Both analyses provided a measure of tape performance. The response analysis provided performance specifications for wow and flutter, while the stability calculation, even though not observed, provided guidelines to problems such as stick-slip excitation. The model to be synthesized herein was selected to describe these types of phenomena.

A mathematical model of a tape-transport mechanical tape handling system, shown in Fig. 111 should simulate reels, guides, tape and capstans. The first natural frequency of the reel-tape system was far removed from the second natural frequency in most practical tape handling systems; this means that this model can be simplified to study the first natural frequency or the higher natural frequencies. The latter situation, with which we are concerned, implies large inertia of the reels acting like infinite impedance end connections to the tape. These end connections imparted a prescribed motion to the tape ends and by the mere fact that their impedance was large compared to that of the tape.

The tape was then modeled as a continuum (material with continuously distributed mass and elasticity) moving over a variable geometry head at an average velocity. This model was then used to study the head/tape interaction and its effect on local tape velocity and temperature distribution. This simple model was chosen because from it practical design data were obtained.

The actual model, illustrated in Fig. 112, shows the continuous tape modeled in three different parts. Parts 1 and 3 have no external loading but do have different inherent tension profiles that are a function of time and distance along the tape. Part 3 is loaded by the distributed friction forces caused by pressure of the head on the tape. This friction

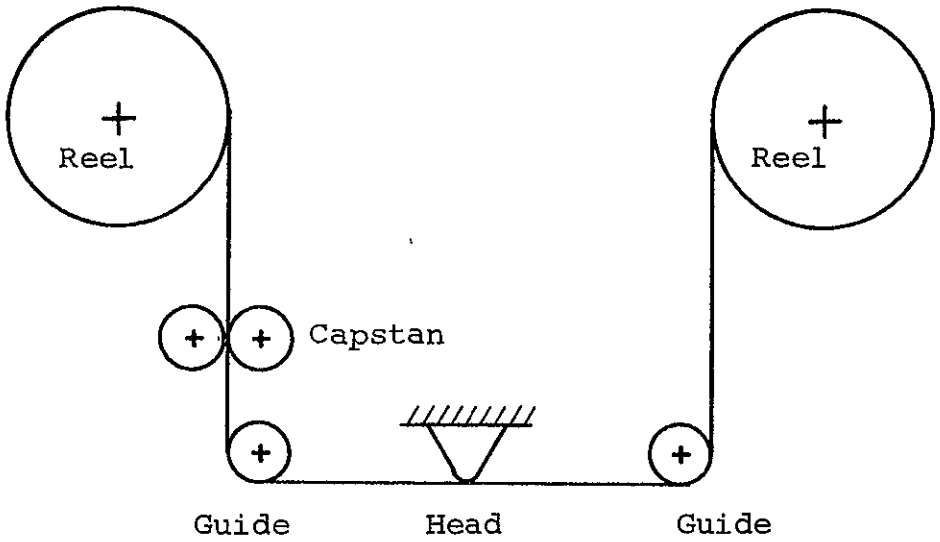

Fig. 111 TAPE HANDLING SYSTEM

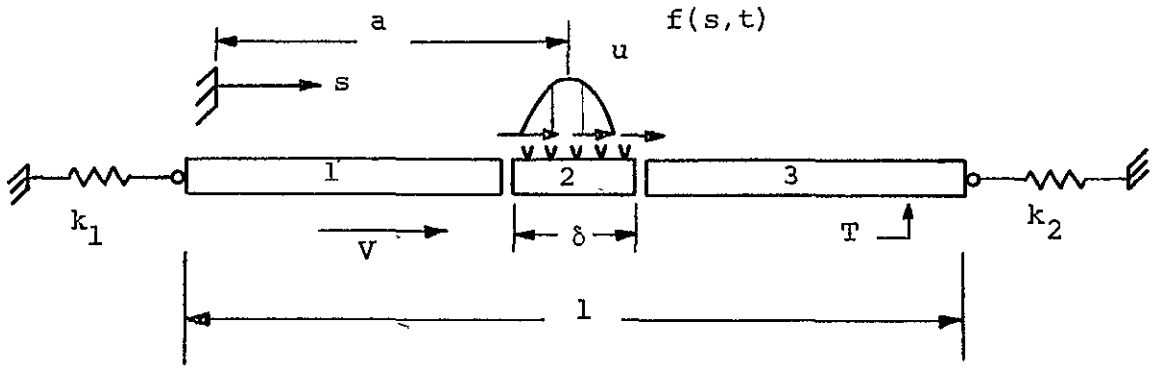

Fig. 112 ANALYTICAL MODEL OF HEAD/TAPE INTERACTION

pressure distribution is a function of the head geometry and the statistical constitution of the tape, although the latter effect will average out. The end conditions may or may not be modeled as elastic elements to simulate a condition of less than infinite impedance applied by the reels. Reel irregularities can be modeled as an external forcing function, i.e., the end point tensions are prescribed functions of time, usually some multiple of reel speed. This periodic disturbance can arise from bearing irregularities.

The equations of motion that describe this system are now developed. The equation of motion of the tape in the head area that describes the other two areas of the friction pressure is set equal to zero. The wrap angle of the tape on the head determines the length of the center tape section. For a head of constant radius, shown in Fig. 113, the tape length δ in the model where the friction force is applied equals

$$\delta = r\gamma \qquad \text{(E-4)}$$

where

r = head radius

γ = wrap angle

The friction force applied to the tape by head/tape interaction over the distance δ is a function of tape tension. The friction coefficient is a function of the tape speed. The difference in tensions T_1 and T_2 is a function of head frictional resistance (the reason why a stability problem such as stick-slip can occur) and tape motion, elasticity, and density.

To study this head/tape area an infinitesimal strip. length $rd\gamma$, of tape instantaneously moving over the head was

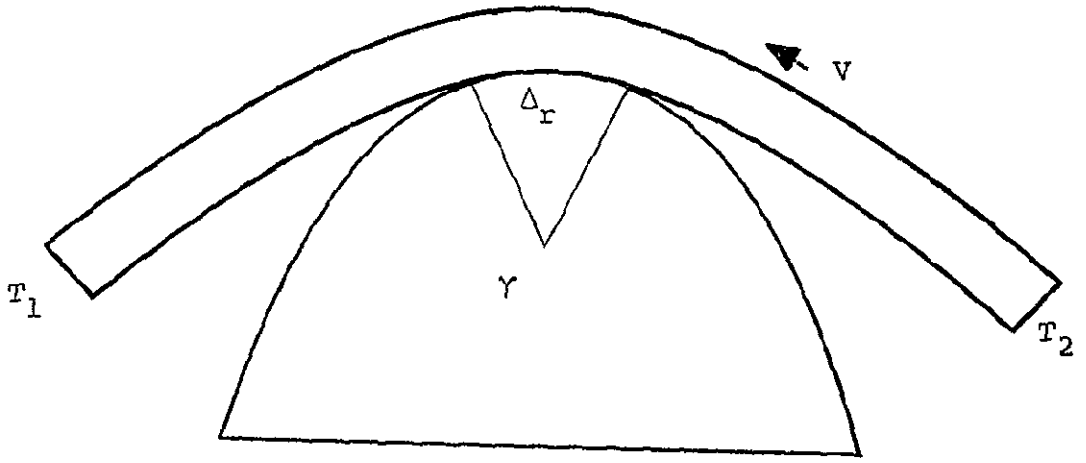

Fig. 113 HEAD/TAPE INTERACTION

used to derive the governing equations. The following relationships between the tension and normal pressure were used in this analysis.

$$T d\gamma = dN \qquad \text{(E-5)}$$

where

N = normal force on tape

The normal force on the tape was also related to the tension through the friction coefficient

$$dT = \mu \, dN \qquad \text{(E-6)}$$

For the element of tape shown in Fig. 114, the infinitesimal force on the tape was then

$$f(s) \, \mu \, dN \qquad \text{(E-7)}$$

where

f(s) = a factor that described the pressure profile

Using Equations (E-4), (E-5), (E-6), and (E-7), $f(s) \, \mu \, dN = \frac{T \mu ds(s)}{r}$ for a constant radius head.

The tape velocity at any point is given by instantaneous

$$v_1 = V + \frac{\partial u}{\partial t} + V \frac{\partial u}{\partial s} \qquad \text{(E-8)}$$

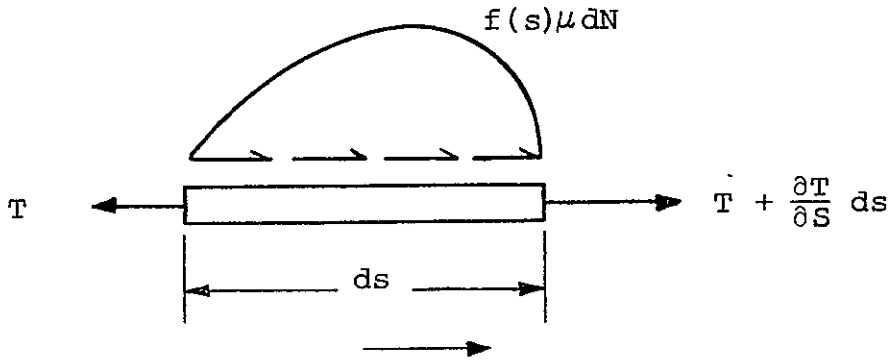

Fig. 114 INFINITESIMAL TAPE SELECTION

where

V = average tape velocity

$\frac{\partial u}{\partial t}$ = continuum local velocity caused by longitudinal displacement variations

$V \frac{\partial u}{\partial s}$ = local transport velocity

Newton's second law was used to sum forces on the strip, shown in Fig. 114, and the acceleration of the strip is the rate of change with respect to time of the instantaneous local velocity.

$$\frac{\partial Td_s}{\partial s} - \frac{T\mu f(s)ds}{r} = \frac{\partial V_i}{\partial t} \rho A ds \qquad \text{(E-9)}$$

$$\frac{\partial T}{\partial s} - \frac{T\mu f(s)}{r} = \rho AV \frac{\partial u}{\partial s \partial t} + \rho A \frac{\partial^2 u}{\partial t^2} \qquad \text{(E-10)}$$

where

u = tape displacement

s = continuum distance

t = time

ρ = density

A = tape area

V = average tape velocity

The tape tension at any point in the continuum can be written as[13]

$$T = T_o - \rho AV \left[\frac{\partial u}{\partial t} + V\left(1 + \frac{\partial u}{\partial x}\right)\right] + EA \frac{\partial u}{\partial x} \qquad \text{(E-11)}$$

where initial tension T_o, tension due to dynamic effects (second term), and elasticity (third term) were taken into account.

Finally, the equation of motion is

$$\rho A \frac{\partial^2 u}{\partial t^2} + 2\rho AV \frac{\partial^2 u}{\partial s \partial t} + (\rho AV^2 - EA) \frac{\partial^2 u}{\partial s^2} + \frac{\mu f(s)}{r} \left\{ T_o - \rho AV \left(V + \frac{\partial u}{\partial t} + \frac{c \partial u}{\partial s}\right) + EA \frac{\partial u}{\partial s} \right\} = 0 \qquad \text{(E-12)}$$

For dimensionless formulation, let

$$V = \frac{u}{a}$$

$$\tau = \frac{tV}{a} \qquad \text{(E-13)}$$

$$x = \frac{s}{a}$$

be dimensionless variables; and,

$$K = \frac{E}{\rho V^2}$$

$$F = \frac{\mu f(s) a}{r} \qquad \theta = \frac{T_o}{\rho AV^2} \qquad \text{(E-14)}$$

be dimensionless parameters.

Then,

$$\frac{\partial^2 U}{\partial \tau^2} + 2\frac{\partial^2 U}{\partial x \partial \tau} + (1 - K)\frac{\partial^2 U}{\partial x^2}$$

$$+ F\left\{\theta - \left(1 + \frac{\partial U}{\partial \tau} + \frac{\partial U}{\partial x}\right) + K\frac{\partial U}{\partial x}\right\} = 0 \qquad \text{(E-15)}$$

For parts one and three the same equations hold, except that $F = 0$.

This set of equations of motion was accompanied by appropriate boundary condition and continuity conditions at the interface of each continuum. Kinematic continuity was required at the interface of two tape parts, i.e.,

$$U_1(\ell_1 t) = U_2(0,t) \qquad \text{(E-16)}$$

continuity was also required at part force interfaces, i.e.,

$$T_1(t,\ell_1) = T_2(t,0) \qquad \text{(E-17)}$$

At the boundary either the longitudinal displacement u or the tension T was prescribed as a function of time. This was one manner of prescribing system external forcing phenomena, such as reel pulsations. In addition, μ the head/tape friction coefficient was a function of velocity and the system exhibited self-excitation (stick-slip) which was a form of instability. Steinhorst's stick-slip problem had shown this relationship with a V_{cr} which was a function of the tape head friction coefficients.

It is suggested that this model and background information be used to solve for the following head/tape interaction design data and guidelines.

1. System Natural Frequencies. This problem has been solved in varied forms; however, there is a need for general nondimensional results so that they can be used for all transports, irrespective of geometry and tape material characteristics. From this analysis, design curves would be generated to show regions of wow and flutter for various tape system parameters.

2. Tape Response to Environmental Phenomena. Due to reel, head, and capstan excitations the local response of the tape at the head is needed to determine design specifications for reels and other mechanical parts. This information would ensure transport component compatibility with tape system performance.

3. Tape Temperature Distribution. The local tape temperature gradients were found using the above local response to head, reel or capstan forcing functions and head/tape friction coefficients. This thermal information could yield additional design data on required tape characteristics.

4. Tape Instabilities. Better prediction of unstable tape performance (large wow) due to stick-slip excitation at the head and at the mechanical components would result from this investigation. Steinhorst's work is a start; however, this work should be extended to determine thermal gradients, tape damage, etc.

SECTION IV

DEVELOPMENT OF THE GUIDELINES

Throughout most of the head/tape interface program, concerted effort was placed upon isolating and individually examining the problem areas and applicable parameters. Even with this approach, a large number of interactions was uncovered. However, the eventual engineering application of the results obtained had to satisfy simultaneously the total requirements of a satellite recording system. Therefore, the final portion of the program consisted of the incoproration of all the significant results into a set of design or selection guidelines. These guidelines were developed on the basis of minimizing both frictional drag and debris. Verification of the guidelines was accomplished by selecting tape types not previously examined during the program, applying the guideline tests to predict performance, and then running tests to confirm the predictions. This section describes the development of the guideline tests and the verification results obtained.

A. Summary of the Experimental Test Program

The goal of the Head/Tape Interface Program was to establish a basis for selecting and using heads and tape to ensure a one-year period of unattended, reliable operation. This goal was achieved by first determining the types of problems occurring. The mechanisms causing these problems were then investigated, followed by exhaustive tests to relate the various chemical and physical factors involved to the degradation of performance.

The majority of the experimental testing program was directed toward the study of head-to-tape friction and oxide/binder debris. In both cases, several mechanisms were found to be contributing to the eventual problems. Chemical bonding, softening of the tape binder system, and changes in the tape surface finish were

all found to be responsible for increased frictional drag. In addition, the tape was also liable to adhere to debris accumulations on the head. These deposits of oxide/binder debris resulted from wear mechanisms such as plowing, excessive stress, edge damage, and inferior head surface finishes. Despite the number of mechanisms occurring, it was found that properly selected tapes and heads, used within well established operational and environmental constraints, could be reliably run for 10,000 passes without generating excessive friction or debris.

1. Significant Environmental Parameters

Three environmental factors -- temperature, relative humidity, and atmosphere -- were studied during the program. Of these temperature and humidity were found to be important parameters. Increasing the ambient temperature of the recorder from 20°C to 65°C accelerated both adhesion and debris problems. It was concluded that 10,000 passes could not be reliably obtained at temperatures above 45°C using currently marketed tapes and heads. Changes in relative humidity had opposing effects on adhesion and debris. While very low relative humidity was preferable in reducing frictional drag and adhesion, the generation of oxide/binder debris was minimized by increasing the humidity to around 30%. However, the effect of humidity was most significant at the higher temperatures. Therefore, establishing a maximum of 15% RH at the upper temperature was considered practical, even though an increase in humidity would be expected as the temperature was reduced.

2. Significant Tape Parameters

All three basic types of polymers used in the tapes examined performed adequately if used within the correct environmental and operational constraints. However, certain of the additives included in the binder systems had pronounced effects on the frictional drag and generation of debris. Further, it was felt that variations in these additive quantities accounted for many

of the performance differences reported for different reels of the same tape type. The most significant factor was the quantity of lubricant. Insufficient lubricant was detrimental to the frictional drag performance, while excessive lubricant caused the formation of oxide/binder debris. An acceptable range was determined to be 1.0 to 2.0% of the total binder system. Other significant additives were carbon and the unexplained presence of chlorine. The carbon, added to prevent buildup of static electricity, was found to be responsible for debris if used in excess. The presence of chlorine caused higher frictional drag, particularly when used with certain head materials (brass and stainless steel).

Tapes which exhibited excessive increases in drag or produced large quantities of debris generally had poor surface finishes by the conclusion of the tests. However, initial tape surface roughness measurements did not correlate with the performance obtained, but a measurement of tape noise was found to be useful in discriminating between candidate tapes. This measurement was capable of detecting either poor oxide dispersion or surface finish.

3. Significant Head Parameters

The choice of head material proved to be one of the most significant parameters in the determination of frictional drag and the generation of debris. For both considerations the harder head materials, including alfenol, alfesil, and havar, were superior because they were less subject to wear, and therefore, more nearly maintained their original lapped surface finish. Brass should be avoided. Aluminum heads did not exhibit the adhesion problems typical with brass. However, the surface of the aluminum heads was more readily abraded than the surfaces of the harder materials. Consequently, larger quantities of debris were generated.

The initial surface finish of the heads was particularly significant in formation of oxide/binder debris, irrespective of the tape type chosen. Voids or discontinuities as well as scratches resulting from imperfect lapping were found to be the basis for excessive tape wear and localized accumulations of debris.

4. Determination of Tension, Wrap Angle and Head Radius

The head-to-tape pressure, established by a combination of the tape tension, wrap angle, and the head radius, must be maintained at a sufficient value to record and playback adequately the shortest wavelength being considered. However, in establishing this head pressure it was found that the head-to-tape contact area should be minimized. Both tape degradation, as measured by increasing drag with number of passes, and debris accumulation were reduced when operating with small head radii and wrap angles. The factors limiting tape tension were the stress computed for the tape passing over various transport guidance elements and the design of the tape pack.

B. Development of the Guideline Tests

The results of the program indicated numerous significant factors in the selection and use of magnetic tape and heads. Those parameters describing the operational use were incorporated as design guidelines and no actual tests were required. However, the selection parameters required the development of procedures producing uniform results and sufficient sensitivity to discriminate between different reels of tape having the same brand designation. The following paragraphs detail the development of these procedures.

1. Thermal Stability

The severe degradation in performance for certain tape types at elevated temperatures indicated substantial differences in the

thermal stability of the binder polymers used. Such differences could be accurately determined by differential thermal or thermogravimetric analyses, either of which require extensive equipment. However, it was desirable to develop a thermal stability test requiring only simple fixtures and short lengths of tape.

The development of a thremal stability test was initiated by comparing the response of 3M 351 and Memorex Quantum tape to high temperature. This was done by placing 6-foot samples of the tapes over a polished copper rod attached to a soldering iron. With the mylar side against the rod, the condition of the oxide surface could be visually examined as the temperature was increased. Table XVI shows the behavior of the 3M 351 tape.

Table XVI

3M 351 Tape Behavior During Thermal Stability Test

Rod Temperature	Observed Effects
150 (°F)	No observed changed
200 (°F)	Conformance to radius of the rod
370 (°F)	Edge curl began
425 (°F)	Edge deformation
440 (°F)	Collapse of center section of the tape
	Severe deformation
650 (°F)	Smoke observed
720 (°F)	Loss of shine at top of rod
750 (°F)	Brown, viscous liquid developed
800 (°F)	Severe charring, blue-green coloration

When the test was repeated using the Memorex Quantum, very similar results were noted. Since most of the effects noted were attributed to the mylar rather than the binder systems, it was decided that a procedure resembling a blocking test was required.

Numerous tests were run with the oxide surface in contact with the heated rod. Throughout these tests the temperature, pressure, and exposure time were all varied with achieving the desired discrimination between the two tape types. However, when two samples of the Quantum tape were placed over the heated rod with the oxide surfaces facing each other, an adhesive bond was obtained. No adhesion was noted under the same conditions with the 3M 351. Although various temperatures and fixed pressures were tried, the results were obtained most reliably by pulling the two samples back and forth for a period of approximately five seconds. The temperature of the polished rod was stabilized at 340°F.

Each of the tape types evaluated during the program, as well as several others used for guideline verification were then subjected to the proposed test. The results are shown in Table XVII. It was concluded that this rather qualitative appraisal was actually a sensitive and expedient indicator of thermal stability. Consistent results were obtained with each tape type, and no occasions were encountered in which a tape type capable of reliable high temperature operation failed this test.

2. Lubricant Content

The quantity of lubricant contained in each of the tapes evaluated during the chemical analyses was obtained by a weight determination of the N-hexane extractables. However, for the guideline tests the less hazardous solvent benzene (C_6H_6) was chosen. Since the adhesion and debris performance of the various

Table XVII

THERMAL STABILITY TEST RESULTS

Tape Type	Observed Behavior
3M 351	No adhesion
3M 551	No adhesion
3M 777	No adhesion
3M 871	No adhesion
3M 888	No adhesion
Memorex 63L	No adhesion
Memorex 79L	Partial adhesion, same removal of oxide binder from both sides
Memorex Quantum	Adhesion with total removal of oxide binder from upper side
Graham Epoch IV	Adhesion, similar to Quantum
DuPont Crolyn	No adhesion
RCA 617	No adhesion
Ampex 771	No adhesion, but severe oxide crumbling
Bell and Howell W4	No adhesion

tapes had already been correlated to the N-hexane extractables, the development of this guideline procedure only involved assurance of the measurement accuracy and verification of the similarity between benzene and N-hexane.

The basic procedure used to determine the quantity of benzene extractables involved weighing a sample of the tape being tested, immersing the sample in benzene, and then reweighing the sample after thorough drying. An analytical balance, having a 100-microgram sensitivity, was determined to be sufficiently accurate, provided a large enough sample of tape was used. A three-foot length of 1/2-inch wide tape was found to be adequate.

Separation of the oxide/binder from the mylar substrate was found to be a difficult task with certain tape types. Therefore, the procedure developed included immersing the entire tape in benzene, but subtracting the weight of the mylar in establishing the percent lubricant content. Evaluation of the effects of benzene on uncoated mylar indicated a 0.05% weight loss. This was considered negligible in comparison to the lubricant quantities extracted from the binder systems.

The benzene extractables were then measured for each of the tapes considered during the program and expressed as a percentage of the oxide/binder layer. The results are shown in Table XVIII with the corresponding values for the previously reported N-hexane determination shown for comparison. It was found that the benzene extracted slightly more material in most cases, although the results for the two solvents were generally similar.

3. Oxide Dispersion

The oxide dispersion test developed during the program consisted of measuring the difference in output from a tape when recorded to saturation with a sine wave and with a permanent magnetic. This signal-to-dc-noise ratio was found to be

Table XVIII

LUBRICANT CONTENT

Tape Type	Lubricant Content (% by weight)	
	Benzene Determination	N-hexane Determination
3M 351	2.34	1.9
3M 551	1.46	1.4
3M 777	0.226	0.2
3M 871	1.46	1.2
3M 888	1.19	0.8
Memorex 63L	1.01	0.35
Memorex 79L	1.66	1.35
Memorex Quantum	0.71	
RCA 617	3.22 (coating detached)	
DuPont Crolyn	0.72	0.70

applicable in the selection of tapes that did not produce excessive quantities of debris. During the development of the guideline procedures, the test was re-evaluated in an effort to maximize the range of values measured. This was done by comparing the results obtained with 3M 888 and Memorex 79L over a number of bandwidths and center frequencies up to 1 MHz at 30 ips. However, it was found that the most effective bandwidth for discriminating between these two tapes was the 10-20 kHz originally selected.

When this test was applied to a number of tapes not previously tested, the range of signal-to-dc-noise ratios was considerably broadened (Table XIX). It was concluded that the selection of tapes initially investigated on the basis of previous use had inherently narrowed the variations in dispersion and/or surface finish.

C. Verification of the Guidelines

The guideline procedures for selection and use of magnetic tape was based upon a limited number of tapes extensively examined during the program. As confirmation of the validity of the procedures and limitations imposed, three additional tape types not previously evaluated were submitted to the guideline tests established. Tests were then conducted on the reel-to-reel transports to confirm the predicted performance of the tapes. The three tapes were 3M 551, Graham Magnetics Epoch IV, and Bell and Howell W4.

1. Tape Type 3M 551

The particular reel of 3M 551 tape purchased for this evaluation surpassed all the limitations imposed by the guideline tests. It was, therefore, expected that the tape would operate satisfactorily for a period of 10,000 passes. The results of the guideline tests are shown in Table XX.

Table XIX

EVALUATION OF SIGNAL-TO-DC-NOISE RATIO

Tape Type	15 kHz/dc Noise (db)
CEC W4	71.4
DuPont Crolyn	67.0
3M 888	66.1
3M 551	65.7
3M 777	65.5
3M 871	65.4
Memorex Quantum	65.4
RCA 617	64.9
3M 351	64.0
Memorex 79L	62.5
Memorex 63L	62.2
3M 851	61.4
Ampex 771	61.1
Graham Epoch IV	60.9

Table XX

EVALUATION OF 3M 551

Test	Result	Allowable Range
Thermal Stability	No adhesion	
Lubricant Content	1.46%	1.0 - 2.0%
Resistivity	37.5×10^7	$0.5 - 50 \times 10^7$
Chlorine Content	Negative	
Oxide Dispersion	66.1 db	63 db min.

The tape performance was evaluated on the reel-to-reel transport under the following conditions:

Temperature: 65°C
Relative Humidity: <3%
Tape Tension: 8 ounces
Wrap Angle: 5°
Head Material: Aluminum

The tape was shuttled at 30 ips for a total of 10,000 passes. Measurements of drag were periodically monitored at tape speeds ranging from 0.15 ips to 30 ips. The results at 1.0 ips show an initial drag of 1.03 ounces. This drag increased to 1.36 ounces at the conclusion of the 10,000 passes. This was considered exceptional performance in a 65°C ambient temperature. The head wear was found to be minimum, and the quantity of debris generated was insufficient to be measured. It was concluded that the guideline tests accurately predicted the satisfactory performance of this reel of tape.

2. Graham Magnetics Epoch IV

The Epoch IV tape produced by Graham Magnetics was chosen to verify the guideline tests because it was the product of a tape manufacturer not previously represented during the program. As such, it was anticipated that a greater diversity of binder polymers and coating techniques would be evaluated.

As seen in Table XXI the reel of Epoch IV tape evaluated did not pass the guideline tests for thermal stability, lubricant content, and oxide dispersion. In the lubricant content test, the binder became detached from the mylar substrate almost immediately after immersion in benzene. Although the oxide layer appeared to remain in tact, the measured quantity of lubricant could have been high because of material lost.

Table XXI

EVALUATION OF GRAHAM MAGNETICS EPOCH IV

Test	Result	Allowable Range
Thermal Stability	Adhesion with total removal of oxide from one side	No adhesion
Lubricant Content	2.86 (binder detached)	1.0 - 2.0%
Resistivity	2.5×10^7	$0.5 - 50 \times 10^7$
Chlorine Content	Negative	
Oxide Dispersion	60.9 db	63 db min

The tape was then run on a reel-to-reel transport using the same conditions applied during the 3M 551 test reported above. These were:

Temperature: 65°C
Relative Humidity: <3%
Tape Tension: 8 ounces
Wrap Angle: 5°
Head Material: Aluminum

The tape was shuttled at 30 ips, and periodic measurements of drag were performed at various tape speeds. At the conclusion of 1200 passes, small quantities of debris had accumulated on the leading and trailing edges of the contact area. However, by the completion of 2,100 passes the quantity of debris had increased, and the frictional drag had risen from 1.26 ounces to 2.20 ounces. The overall degradation continued, and by the end of 3,900 passes tape squeal had developed at the low speeds. In addition, very large quantities of debris had accumulated on both sides of the head-to-tape contact area. It was concluded that the guideline tests accurately predicted the unsatisfactory performance of this reel of tape.

3. Bell and Howell Type W4

The third tape evaluated in the guideline verification tests was the Bell and Howell W4. This allowed the inclusion of still another tape manufacturer in the overall program results. In addition, the tape was designed as an instrumentation tape, making it a potential candidate for future satellite applications.

As seen in Table XXII, the reel of W4 tape evaluated did not pass the guideline tests for lubricant content and surface resistivity. The results indicated excessive quantities of benzene extractables and carbon. Actually, the material extracted from the binder system with benzene had a distinct green-yellow

Table XXII

EVALUATION OF BELL AND HOWELL W4

Test	Result	Allowable Range
Thermal Stability	No adhesion	
Lubricant Content	4.78% (greenish extract)	1.0 - 2.0%
Resistivity	0.18×10^{7}	$0.5 - 50 \times 10^{7}$
Chlorine Content	Negative	
Oxide Dispersion	71.4 db	63 db min

color, and may well have been a low molecular weight material other than lubricant. The chemical nature of this extract was not determined. The results of these two guideline tests were considered indicators of potential oxide binder/debris problems.

The initial test conducted with the W4 tape was run at 65°C on a reel-to-reel transport using the same conditions previously incorporated for the other verification tests. Within the first 200 passes, considerable debris was deposited on the head. When the tape tension was removed, the tape remained attached to this debris. Since the first 200 passes were considered to be a break-in period, the head surface was cleaned and the test restored. However, by the conclusion of 2,900 passes extremely heavy, black debris had accumulated on the head, guides, and capstans. In addition, considerable tape squeal had developed. This was the result of adhesion to heavy debris accumulations. Therefore, it was concluded that the guideline tests had correctly indicated the debris failures encountered.

Further tests were run at 45°C and 35°C using the W4 tape and brass rather than aluminum heads. At 45°C heavy debris was noted after 1,200 passes, and after the completion of 2,340 passes the debris accumulation was sufficient to prevent tracking of the tape. A similar failure was observed following 3,100 passes at 35°C.

The results of these tests demonstrated the applicability of the guidelines to the selection of tapes to minimize frictional drag and debris accumulation. Moreover, the tests also confirmed the overall conclusion that commercially available heads and tapes, if properly used, can be expected to perform satisfactorily for a one-year period.

APPENDIX I

LIST OF VISITED ORGANIZATIONS

The organizations visited during the Phase I survey were:

Ampex Corporation
Redwood City, California

Applied Magnetics Corporation
Goleta, California

Astro-Science Corporation
El Monte, California

Beloit Corporation
Janesville, Wisconsin

Borg Warner
Santa Anna, California

DuPont de Nemours
Wilmington, Delaware

International Electro Magnetics
Palatine, Illinois

Jet Propulsion Laboratory
Pasadena, California

Kinelogic Corporation
Pasadena, California

Lash Laboratories
San Diego, California

Leach Corporation
Azusa, California

Lockheed Missile and Space
Sunnyvale, California

Minnesota Mining and Manufacturing
St. Paul, Minnesota

Minnesota Mining and Manufacturing
Mincom Division
Camarillo, California

Memorex
Santa Clara, California

NASA/Goddard Space Flight Center
Greenbelt, Maryland

North American Rockwell
Downy, California

Charles Pfizer and Company
Easton, Pennsylvania

Raymond Engineering
Middletown, Connecticut

RCA
Astro Electronics Division
Heightstown, New Jersey

RCA
Defense Electronics Division
Camden, New Jersey

RCA
Graphics Division

RCA
Magnetic Products Division
Indianapolis, Indiana

Spin Physics
San Diego, California

TRW
San Diego, California

U. S. Magnetic Tape Company
Huntley, Illinois

APPENDIX II

TEST EQUIPMENT

Two basic machines were used for the majority of the testing carried out during the program. An endless loop transport was used for accelerated testing, while a reel-to-reel machine was used to provide information on bread and debris problems.

A. Endless Loop Transport

The requirement to accumulate large numbers of tape passes in a short time dictated the need for an endless loop machine. Such a transport was designed and built at IITRI specifically for the program. The tape path of the endless loop transport was described by a single capstan, a crowned roller, suspended on an arm to establish tape tension, and two other idler rollers. The roller diameters (2 in.) and crowns (2 - 1/4 in.) were conservatively designed to minimize stress within the tape. In normal operation, only the Mylar side of the tape contacted the capstan or rollers.

The single capstan was mylar coupled to a servo-controlled dc motor. The motor, generator, and speed control were built by Electrocraft, Incorporated, Hopkins, Minnesota. The use of a dc motor and servo facilitated measurement of motor torque.

The endless loop transports were operated in an environmental chamber throughout most of the program, allowing control of both the temperature and relative humidity. In addition to environment, the following factors could be varied on these transports:

Parameter	Range
Tape Speed	0.1 - 120 ips
Tape Tension	0 - 20 ounces (1/2 inch tape)
Tape Width	1/4, 1/2, 1 inch
Tape Direction	forward or reverse
Wrap Angle	0 - 20° each side
Loop Length	48 - 64 inches
Available Torque	0 - 50 ounce-inch
Head Heigth & Azimuth	

B. Reel-to-Reel Transport

The reel-to-reel transports, were built for the NASA/Goddard Space Flight Center by the Video Recorder Corporation. They were designed with a tape path in which only the heads contacted the oxide side of the tape. Those guides and capstans contacting the mylar had diameters of at least two inches. As such, the designs were felt to be representative of conservatively designed satellite transports. While the endless loop transports were instrumented to measure motor torque, the reel-to-reel transports incorporated a cantilevered beam with strain gages to measure drag directly. The transports were housed in sealed containers, modified to allow thermal control. The atmosphere could also be selected. Other variable transport parameters were:

Tape Speed	0.1 - 120 ips
Tape Tension	0 - 20 oz (1/2 inch tape)
Wrap Angle	0 - 20° each side
Head Position	

Automatic bidirectional operation was also possible.

APPENDIX III

DEVELOPMENT OF CONTACT PRESSURE RESULTING FROM TAPE-ROLLER CONTACT

Figure 115 illustrates the basic parameters for a tape in contact with a freely rotating cylindrical roller. It is assumed that the tension, T, does not vary throughout the contact region. By summing the radial forces on an incremental section of tape, the average contact force, R, across this region is

$$R = 2T \sin \frac{\Delta\varphi}{2}$$

The increment contact area is

$$A = W\rho \ \Delta\varphi$$

And, the average pressure becomes

$$P = R/A$$

$$= \frac{2T \sin \Delta\varphi/2}{W\rho \Delta\varphi}$$

For $\Delta\varphi \ll 1$, $\sin \frac{\Delta\varphi}{2} = \Delta\varphi/2$ and

$$\boxed{P = \frac{T}{W\rho}}$$

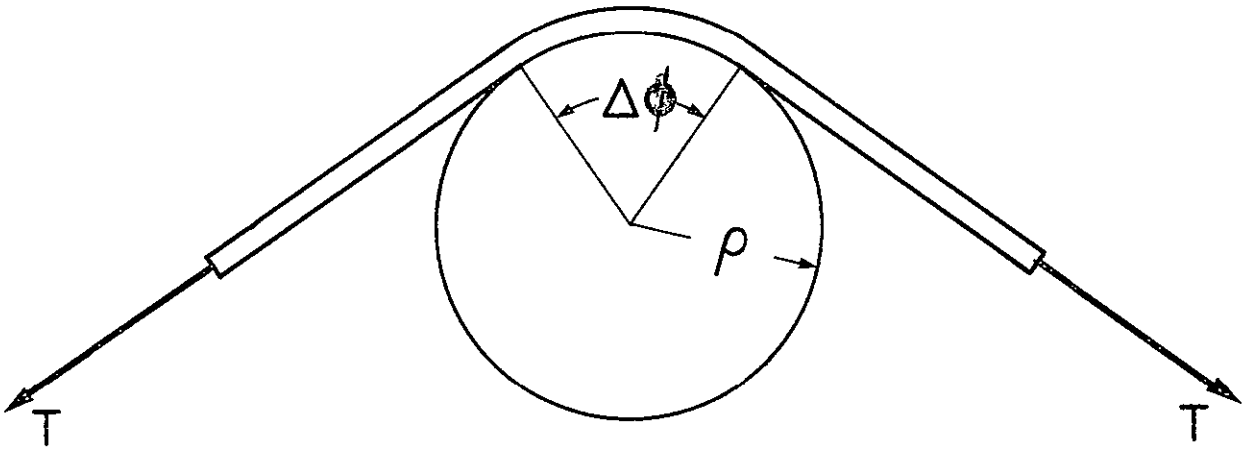

Fig. 115 TAPE-ROLLER PARAMETERS

APPENDIX IV

DEVELOPMENT OF CONTACT PRESSURE RESULTING FROM TAPE IN CONTACT WITH A CANTED ROLLER

Figure 116 illustrates a section of tape in contact with a canted roller where the tape is following a helix path. To determine the contact pressure, it is first essential to identify the tension component that is in the circumferential plane. This tension component is seen to be

$$\bar{T} = T \cos \theta$$

For an incremental element, the average radial force becomes

$$R = (2T \cos \theta) \sin \Delta\varphi/2$$

and the incremental contact area is

$$A = (W_\rho \Delta\varphi)/\cos \theta$$

Hence, the unit pressure becomes

$$P = \frac{R}{A}$$

or

$$P = \frac{T \cos^2 \theta}{W_\rho}$$

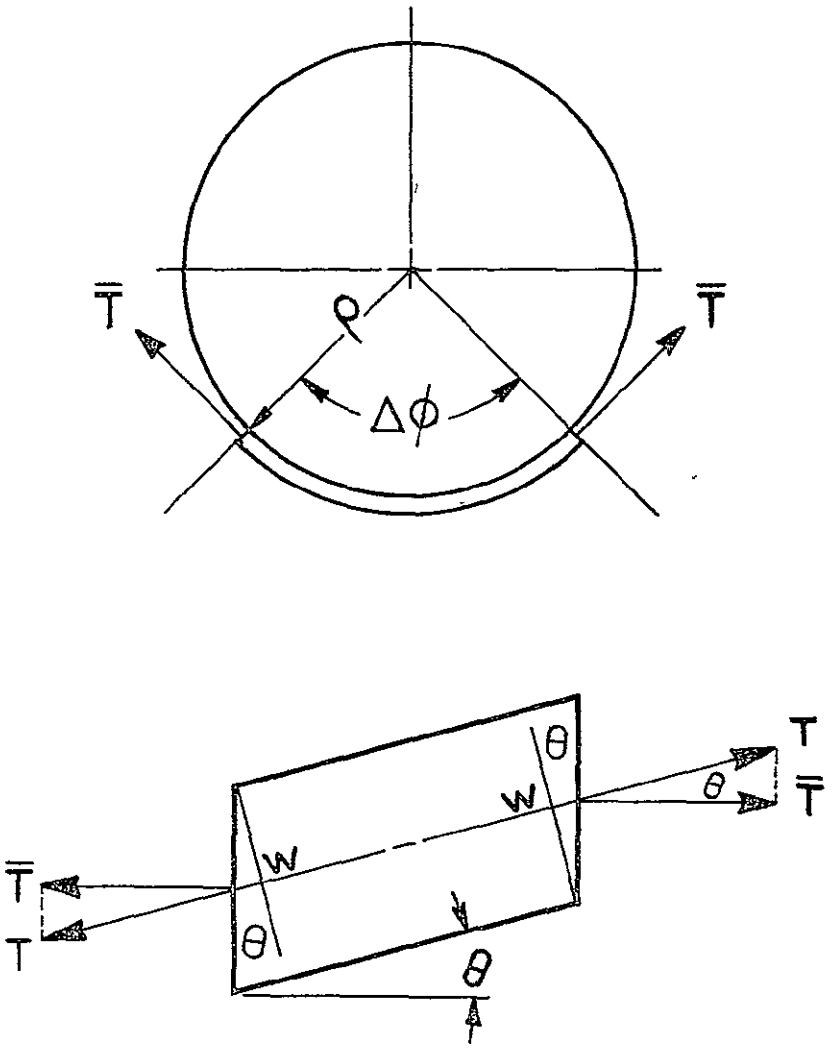

Fig. 116 TAPE ELEMENT IN CONTACT WITH A CANTED IDLER

APPENDIX V

STRESSES ALONG ROLLER MAJOR AXES

Figure 117 represents an incremental tape element in contact with a skewed roller. The stress, σ, is directed along the length dimension of the tape. The remaining stress components are defined as:

σ_c ~ stress in the direction of bending (in a plane normal to the roller axes)

σ_A ~ stresses along roller axes

τ_1 shear stresses due to bending stress

τ_2 ~ shear stress in axial direction

Summing forces along the radial plane yield

$$Wt\ \sigma_1 \cos\theta = \sigma_c t\ W/\cos\theta \quad \text{(bending)}$$

$$\sigma_c = \sigma_1 \cos^2\theta$$

$$\frac{W}{\cos\theta}\ t\ \tau_1 = \sigma_1\ (Wt)\ \sin\theta$$

$$\tau_1 = \sigma_1 \sin\theta \cos\theta \quad \text{(bending)}$$

Similarly, summing forces along the axial direction yield

$$Wt\ \sigma_1 \sin\theta = \sigma_A\ t\ W/\sin\theta$$

$$\sigma_A = \sigma_1 \sin^2\theta \quad \text{(axial)}$$

$$\frac{W}{\sin\theta}\ t\ \ \tau_2 = Wt\ \tau_1 \cos\theta$$

$$\tau_2 = \sigma_1 \sin\theta \cos\theta \quad \text{(axial)}$$

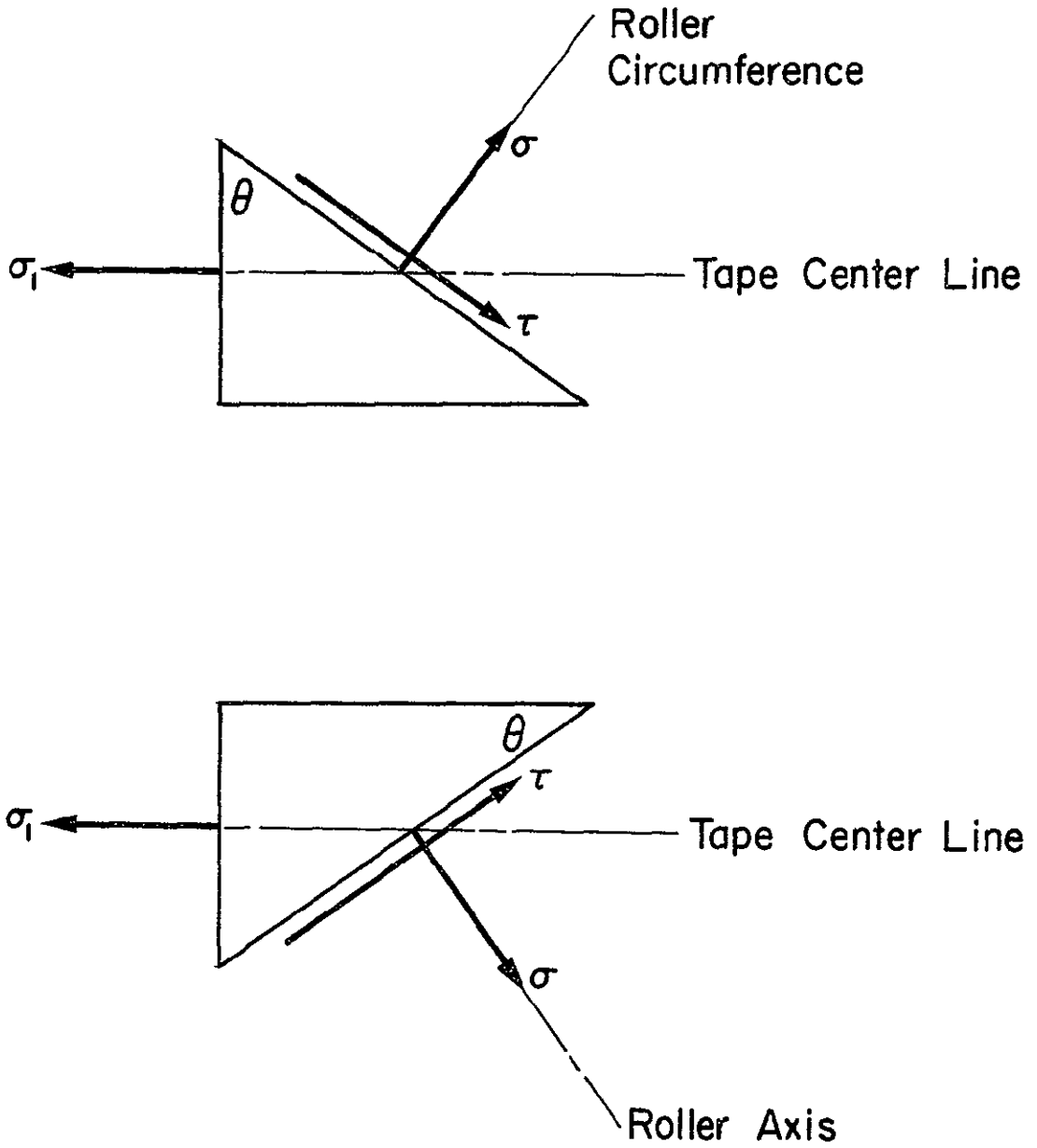

Fig. 117 TAPE ELEMENTS RELATING LONGITUDINAL TAPE STRESS WITH PRINCIPAL ROLLER

APPENDIX VI

EFFECTS OF TAPE NOT IN CONTACT WITH THE CROWNED ROLLER

The results of this analysis justify the assumptions of Section III.C.6 that there is no effect from the tape not in contact with the crowned roller and that there are no lateral stresses in the tape due to the non-uniform longitudinal strain distribution across the width of the tape. A section of the tape extending from the straight roller to the middle of the crowned roller was investigated. Only one half of the tape width is analyzed, since the contact area is symmetric about its centerline. The mathematical model is shown in Fig. 118 The field equations governing this plane stress problem are[14]

$$\left(\frac{2\lambda\mu}{\lambda+2\mu}+\mu\right)\left(\frac{\partial^2 u}{\partial x^2}+\frac{\partial^2 v}{\partial x\partial y}\right)+\mu\left(\frac{\partial^2 u}{\partial x^2}+\frac{\partial^2 u}{\partial y^2}\right)=0$$

$$\left(\frac{2\lambda\mu}{\lambda+2\mu}+\mu\right)\left(\frac{\partial^2 u}{\partial x\partial y}+\frac{\partial^2 v}{\partial y^2}\right)+\mu\left(\frac{\partial^2 v}{\partial x^2}+\frac{\partial^2 v}{\partial y^2}\right)=0$$

where λ and μ are the Lame' constants. The boundary conditions are

$$u = 0 \text{ for } x = 0$$

$$\tau = 0 \text{ for } x = 0$$

$$v = 0 \text{ for } y = 0$$

$$\tau = 0 \text{ for } y = 0$$

$$u = \varphi R \cos\frac{Y}{R}\left(\cos\frac{W}{2R}\right) \text{ for } x = L$$

$$\tau = 0 \text{ for } x = L$$

$$\sigma_Y = 0 \text{ for } Y = W/2$$

$$\tau = 0 \text{ for } Y = W/2$$

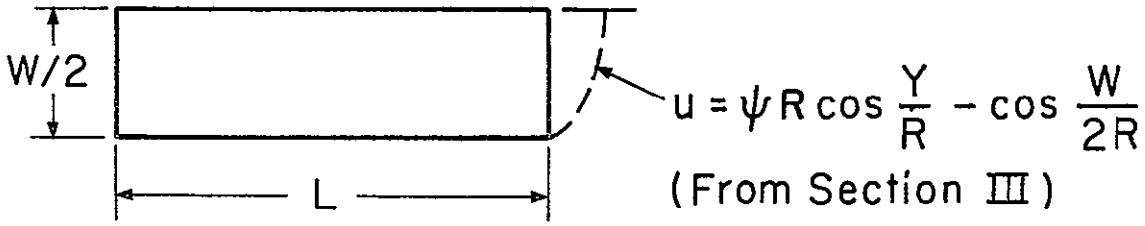

Fig. 118 MATHEMATICAL MODEL OF TAPE

Since no analytic solution could be easily obtained for this problem, the problem was solved numerically for a single set of tape and roller parameters using the finite differences technique. The results of this solution indicate that a reasonably accurate solution can be obtained using strength of materials techniques and the assumptions stated at the beginning of this discussion. For example, the numerical results demonstrate that the strain field due to the crown roller occurs predominately within the roller-tape contact region, and further the maximum lateral stresses are less than 10% of the longitudinal stresses.

APPENDIX VII

MAGNETIC TAPE EVALUATED

Throughout the program, a number of tape types produced by several manufacturers were evaluated. These tapes, listed below, were purchased and tested between 1 July 1967, and 31 December 1970. Lot or batch identification numbers are included, as variations in certain parameters may occur between reels or batches of the same tape type designation.

Manufacturer	Type Designation	Lot Number
Ampex	772	29G8306-4 (1 Reel Unknown)
Bell and Howell	W4	10027834
DuPont	Crolyn	8322711036102 8322711036119 (1 Reel Unknown)
Graham Magnetics	Epoch IV	8B20558B-15
IBM	500	0 6 07227 1
Memorex	63L	15092-A2-6A 15092-A1-17A
Memorex	79L	E59159-C2-5D ME56857-A1-5B
Memorex	Quantum	27E-HJ-3712C-A1- M30160-B3 (2 Reels)
3M	351	64748043029 64748043046
3M	551	67618-71-11-41 67618-71-12-41
3M	700	72727-99-000-37
3M	777	63904-390-1011 63904-390-1036
3M	851	65849-6-10-9
3M	871	69333-3-10-16 69333-6-20-19 74921-10-10-12 74768-5-11-9
3M	888	55512-46-10-17 67760-40-11-12 (1 Reel Unknown)
3M	8119	72347-01-10-41
3M	MTA 20294	70773-03-10-19
3M	MTA 20302	64883-1-2-2
3M	MTA 20478	75450-06-000-38
RCA	617	No Designation - Not A Commercial Tape

REFERENCES

1. Benn, G.S.L., "MM-71 Magnetic Head/Tape Stick-Slip Study," Final Report, Jet Propulsion Laboratory, Contract No. 952832, IIT Research Institute, Chicago, Illinois. To be published.

2. Schnurrman, R. and Warlow Davies, E., Proc. Phys. Soc. (London), 54, 18 (1942).

3. Hardy, W.B., Collected Works, Cambridge University Press, 1936.

4. Bowden, F.P. and D. Tabor, The Friction and Lubrication of Solids, Part II, Oxford at the Clarendon Press, 1964.

5. Steinhorst, W., "Elastic Longitudinal Vibration in Recording Tapes Especially With Stick-Slip Excitation," Feinwerktechnik, 70(4) 172 - 184, April 1966.

6. Stark, K.W., Techniques for the Design, Evaluation, and Analysis of Endless Loop Transports for Satellite Applications, NASA TN D-3391, May 1966.

7. Clinton, W.C., Sirico, J.L., Pimbley, W.T., "Wear of Thin Ferric Oxide Coatings Bonded to Mylar Tape," Wear, Vol. 8, No. 5, pp. 333-420 (Sept./Oct. 1965).

8. Timoshenko, S., Strength of Materials, Part II Advanced Theory and Problems, Van Nostand, New York, 1956.

9. Timoshenko, S., and Woinowsky-Krieger, S., Theory of Plates and Shells, 2nd Ed., McGraw-Hill, New York, 1959.

10. John H. Licht and Arthur White, Polyester Film Belts, NASA TN D-668, May 1961.

11. Magnetic Tape Study, ASTIA Report No. AD 238 884L, January 31, 1960.

12. Steinhorst, W., "Theoretical Observations of the Elastic Behavior of Recording Tapes," Feinwerkechnik, 70(3) 114-119, March 1966.

13. Thurman, A. L., and C. C. Mote, Jr., "Free, Periodic, Nonlinear Oscillation of an Axially Moving Strip," Trans. of ASME, Journal of Applied Mechanics, March 1969, p. 84.

14. Sokolnikoff, I.S., Mathematical Theory of Elasticity, McGraw-Hill, Chapter 5, Equations 67.3, 1956, p. 254.